

UC Irvine

UC Irvine Electronic Theses and Dissertations

Title

Developing Macrocyclic β -Hairpin Peptide Mimics to Elucidate the Structures of A β Oligomers in Alzheimer's Disease

Permalink

<https://escholarship.org/uc/item/74h4d7h1>

Author

Samdin, Tuan Dilshad

Publication Date

2021

Copyright Information

This work is made available under the terms of a Creative Commons Attribution License, available at <https://creativecommons.org/licenses/by/4.0/>

Peer reviewed|Thesis/dissertation

UNIVERSITY OF CALIFORNIA,
IRVINE

Developing Macrocyclic β -Hairpin Peptide Mimics to Elucidate the Structures of $A\beta$
Oligomers in Alzheimer's Disease

DISSERTATION

submitted in partial satisfaction of the requirements
for the degree of

DOCTOR OF PHILOSOPHY

in Chemistry

by

Tuan Dilshad Samdin

Dissertation Committee:
Professor James S. Nowick
Professor Jennifer A. Prescher
Professor Robert Spitale

2021

DEDICATION

To
my parents
my wife
my son
my friends

At my beginning,

“The story so far: In the beginning the Universe was created. This has made a lot of people very angry and been widely regarded as a bad move.”

Douglas Adams
The Restaurant at the End of the Universe

strolling through the middle,

“Life is pleasant. Death is peaceful. It’s the transition that’s troublesome.”

Isaac Asimov

Somewhere before the end.

“A day can really slip by when you’re deliberately avoiding what you’re supposed to do.”

Bill Watterson
Calvin and Hobbes

TABLE OF CONTENTS

LIST OF FIGURES	v
LIST OF TABLES	vii
LIST OF SCHEMES	viii
ACKNOWLEDGEMENTS	ix
CURRICULUM VITAE	x
ABSTRACT OF THE DISSERTATION	xiii
CHAPTER 1: Exploring Amyloid Oligomers with Peptide Model Systems	1
Introduction	1
The Fragment-Based Approach	5
Stabilized β -Hairpins	6
Computational Tools for Studying Amyloid Oligomers and Fibrils	13
Conclusion	15
Acknowledgements	15
Annotations	16
References	19
CHAPTER 2: Effects of N-Terminal Residues on the Assembly of Constrained β -Hairpin Peptides Derived from A β	29
Introduction	29
Results and Discussion	32
Synthesis of Peptide N+14	32
Oligomerization and Folding of Peptides 1 and N+14	33
Oligomerization and Folding of Shorter N-Terminally Extended Homologues	38
X-ray crystallographic structure of peptide N+1	45
Summary and Conclusion	47
References and Notes	50
Supporting Information	55
Table of Contents	55
Supporting Figures and Tables	57
Materials and Methods	69
Characterization Data	80

CHAPTER 3: A β -Barrel-Like Tetramer Formed by a Macrocyclic β -Hairpin Derived From A β	102
Introduction	102
Results	106
Design of Peptides 1a-i and 2a-d	106
Oligomerization of Peptides 1a-h and 2a-d	107
Folding of Peptides 1a-h and 2a-d	110
X-ray Crystallographic and REMD Studies of Peptide 2a	113
Reducing the Disulfide Bonds of Peptides 1a and 2a , and Oligomerization of Peptides 1i and 2c-d	118
Folding of Peptides 1i and 2c-d	119
Molecular Dynamics Simulations of a Crystallographically Derived Tetramer in a Lipid Membrane	121
Discussion and Conclusion	123
References	124
Supporting Information	127
Table of Contents	127
Supporting Figures and Tables	129
Materials and Methods	133
Characterization Data	145
 CHAPTER 4: Application of an α -Methyl Amino Acid in Crystallographic Studies of an A β Derived Peptide	 173
Introduction	173
Results and discussion	178
Oligomerization of Peptides 1-3	178
X-ray Crystallographic Studies of Peptide 3	179
Conclusion	181
References	182
Supporting Information	185
Table of Contents	185
Supporting Figures and Tables	186
Materials and Methods	189
Characterization Data	195

LIST OF FIGURES

1.1	Structures of fibrils and oligomers formed by amyloidogenic peptides	4
1.2	NMR structures of an A β β -hairpin and oligomer, and chemical structures of A β derived β -hairpins and macrocyclic β -hairpin peptide	10
1.3	X-ray crystallographic structures of oligomers formed by macrocyclic β -hairpin peptides derived from A β , β_2 -microglobulin, and α -synuclein	12
2.1	Extending the <i>N</i> -terminus of peptide 1 to include residues 1–14 as an <i>N</i> -terminal tail, giving peptide N+14 .	31
2.2	Synthesis of the <i>N</i> -terminally extended peptide, N+14 derived from A β_{1-36}	33
2.3	SDS-PAGE and circular dichroism spectra of peptides 1 , 2 , N+14 , and N+14Me	35
2.4	Chemical structure of peptide N+14Me .	37
2.5	Chemical structures of peptides N+1 , N+2 , N+12	39
2.6	CD spectra of peptides 1 and N+1 through N+14	40
2.7	Silver stained SDS-PAGE and folding of peptide 1 , peptides N+1 through N+14 , and trimers 1 and 2	41
2.8	Oligomer molecular weights vs. relative migration distance (R_f) of peptide 1 and peptides N+1 through N+14 by SDS-PAGE (semi-log plot)	42
2.9	Size exclusion chromatography traces of peptide 1 and select <i>N</i> -terminally extended peptides.	43
2.10	Oligomer molecular weights vs. elution volumes of peptide 1 and peptides N+1 through N+14 by SEC (semi-log plot)	44
2.11	X-ray crystallographic structure of the hexamer formed by peptide N+1 (PDB 6VU4)	47
2.S1	Western blot analysis of peptides N+8 , N+10 , N+12 , N+14 , and A β_{M1-42} using the 6E10 antibody	57
2.S2	The dimer subunit of the hexamer formed by peptide 1 and <i>N</i> -methylation of peptide 2	58
2.S3	Cytotoxicity of peptide 1 and the <i>N</i> -terminally extended homologues against SH-SY5Y cells, as assessed by an LDH release assay	59
2.S4	Chemical structure of covalently stabilized trimer 1	61
2.S5	Chemical structure of covalently stabilized trimer 2	62
2.S6	SEC traces of peptides N+12 and N+14	63

2.S7	SEC traces of peptides 1 , N+1 , N+2 , and N+4	63
2.S8	SEC traces of peptides N+6 , N+8 , and N+10	64
2.S9	SEC traces of peptides 2 and N+14_{Me}	64
2.S10	The trimer and dimer subunits within the X-ray crystallographic structure of the hexamer formed by peptide N+1	66
2.S11	X-ray crystallographic structures of the hexamers formed by peptides 1 (PDB 5W4H), N+1 (PDB 6VU4)	67
3.1	Structures of A β β -hairpins, and chemical structures and illustrations of peptides 1a-i and 2a-d	105
3.2	SDS-PAGE oligomerization and CD spectra of peptides 1a-h and 2a-b	112
3.3	X-ray crystallographic structure of twisted β -hairpin, antiparallel dimer, and β -barrel-like tetramer formed by peptide 2a	114
3.4	Illustration of the parallel and antiparallel β -sheet interactions present in the β -barrel-like tetramer formed by peptide 2a , RMED studies of peptide 2a , and β -barrel-like octamer and crystal lattice formed by peptide 2a	117
3.5	SDS-PAGE oligomerization and CD spectra of peptides 1a-b , 1i , and 2a-d	120
3.6	Molecular dynamics simulation of a crystallographically derived tetramer in a lipid membrane.	122
S3.1	Structures of A β oligomers and fibrils	129
S3.2	Time (ns) vs. RMSD of the Molecular dynamics simulation of a crystallographically derived tetramer in a lipid membrane	132
4.1	Chemical structures of macrocyclic β -hairpin peptides derived from A β ₁₇₋₂₃ and A β ₃₀₋₃₆	176
4.2	. X-ray crystallographic structure of a triangular trimer formed by peptide 1 , (PDB 4NW9)	176
4.3	Silver stained SDS-PAGE of peptides 1-3	178
4.4	X-ray crystallographic structure of monomer formed by peptides 1 and 3 and overlay.	179
4.5	X-ray crystallographic structure of a triangular trimer formed by peptide 3 and overlay with the trimer formed by peptide 1 , (PDB 4NW9)	180
4.6	X-ray crystallographic structure of the ball-shaped dodecamer formed by peptide 3	181

LIST OF TABLES

S2.1	Normalized absorbance values and calculated percent differences of circular dichroism samples relative to peptide 1	60
S2.2	Elution volumes of peptides 1 , 2 , N+1 through N+14 , and N+14_{Me} by size exclusion chromatography	65
S2.3	Crystallographic properties, crystallization conditions, data collection, and model refinement statistics for peptide N+1	68
S3.1	Crystallographic properties, crystallization conditions, data collection, and model refinement statistics for peptide 2a	130
S4.1	Crystallographic properties, crystallization conditions, data collection, and model refinement statistics for peptide 3	186

LIST OF SCHEMES

S2.1 Synthesis of the *N*-terminally extended peptide, **N+14** derived from $A\beta_{1-36}$

70

ACKNOWLEDGEMENTS

Thank you, James, for giving me a chance to chase my dream. A part of me always feared that I would never be able to define myself on my own terms. You have given me the opportunity to be curious and creative, the chance to disagree and fail, and the support and the environment I needed to grow and be bold. Your mentorship and kindness has helped me grow not only as a scientist, but as a person.

For my labmates and friends, thank you. There are times where it seemed as though every effort, experiment, and thought I had was doomed to end in failure. But you were always there to remind me that my beatings would only continue until my morale improved. So, despite having weeks if not months of work often crumble in failure, I knew that you would be right there with me as I tried again. And again. And again. Even when it was clear that all I had before me was a path filled with late, late nights and frustration in repairing instruments, you never allowed me to quit. Thank you, Nick, for teaching me SPPS and helping me take my first steps as an independent scientist. Thank you, Adam and Michał, for allowing me to annoy you with a hundred-and-one questions about X-ray crystallography. Thank you, Will, for keeping me grounded and giving me perspective when I felt lost and cast-off. And thank you, Sheng, Xing, Maj, Gretchen, and Chelsea for your friendship, the laughter, and the chance to share my “Tuansense”.

Thank you, Mom and Dad for your love and encouragement. I could not imagine a path to where I am today without the sacrifices you’ve made and the support you’ve given me. Thank you.

And lastly, to my wife and son. I cannot ever express how grateful I am for your love and patience. Pursuing a PhD was my choice, and with that choice I have been incredibly selfish. I’ve missed more than a few moments and milestones, so now I hope to build us a future where the only hard choices to be made, will be deciding who gets the last cookie.

CURRICULUM VITAE

Tuan Dilshad Samdin

Education

University of California, Irvine – James S. Nowick Laboratory

Ph.D. Candidate in Chemistry

Expected August 2021

University of California, Berkeley – Seung-Wuk Lee Laboratory

B.A. Molecular and Cell Biology

August 2016

Research Experience

Chemistry Department, UC Irvine - Graduate Researcher

August 2016 – present

- Led, mentored, and trained 5 undergraduate research assistants and collaborated with a team of 9 graduate students across 5 interdisciplinary projects to design, synthesize, and assess macrocyclic peptides capable of mimicking toxic proteins in Alzheimer's and other neurodegenerative diseases using: solid-phase peptide synthesis, microwave-assisted peptide synthesis (Liberty Blue), molecular cloning, bacterial transformation, protein expression, SDS-PAGE, western blot, FPLC, SEC, HPLC, mass spectrometry, CD, X-ray crystallography, and cytotoxicity assays
- Independently planned, managed, and executed 3 projects under strict funding timelines to meet deliverables, provided regular group updates through presentations and written reports
- Communicated my scientific results and research progress in 5 scientific publications, and at 6 regional and national scientific conferences to multidisciplinary audiences
- Optimized the group's synthetic workflow by writing and obtaining a grant for \$40,000 to purchase a microwave peptide synthesizer that subsequently increased crude product purity and yield, and reduced waste production and total synthesis time

Bioengineering Department, UC Berkeley - Undergraduate Researcher

August 2014 – May 2016

- Worked within a team of 6 interdisciplinary researchers with backgrounds in chemistry, biology, materials science, and bioengineering to design and optimize the production and chemical sensitivity of a novel bacteriophage-based biosensor for volatile organic compounds and environmental pollutants using: phage display, molecular cloning, PCR, bacterial transformation, bacterial culture, and AFM
- Presented our research to outside stakeholders, demonstrating how our biosensor could be paired with their smartwatch and smartphone products, resulting in two years of support for the laboratory
- Documented and maintained standard operating procedures for the safe and proper use of laboratory techniques, chemicals, and equipment
- Mentored and trained 3 undergraduate research assistants and 5 master's students in common laboratory techniques and use of equipment

Publications

- **Samdin, T. D.**; Guaglianone, G.; Kreutzer, A. G.; Freitas, J. A.; Wierzbicki, M.; *et.al.*; Nowick, J. S. A β -Barrel-Like Tetrameric Formed by a Macrocyclic β -Hairpin Peptide Derived from A β . **Manuscript in preparation**
- **Samdin, T. D.**; Kreutzer, A. G.; Nowick, J. S. Exploring Amyloid Oligomers with Peptide Model Systems. *Curr. Opin. Chem. Biol.* **2021**. *64*, 106–115
- Haerianardakani, S.; Kreutzer, A. G.; Salveson, P. J.; **Samdin, T. D.**; Nowick, J. S. Phenylalanine Mutation to Cyclohexylalanine Facilitates Triangular Trimer Formation by β -Hairpins Derived from A β . *J. Am. Chem. Soc.* **2020**, *142* (26), 20708–20716.

- Samdin, T. D.; Wierzbicki, M.; Kreutzer, A. G.; Howitz, W. J.; *et.al.*; Nowick, J. S. Effects of N-Terminal Residues on the Assembly of Constrained β -Hairpin Peptides Derived from A β . *J. Am. Chem. Soc.* **2020**, *142* (26), 11593–11601.
- Kreutzer, A. G.; Samdin, T. D.; Guaglianone, G.; Spencer, R. K.; Nowick, J. S. X-Ray Crystallography Reveals Parallel and Antiparallel β -Sheet Dimers of a β -Hairpin Derived from A β _{16–36} That Assemble to Form Different Tetramers X-Ray Crystallography Reveals Parallel and Antiparallel β -Sheet Dimers of a β -Hairpin Derived from A β _{16–36}. *ACS Chem. Neurosci.* **2020**, *11*, 2340–2347
- Lee, J. H.; Fan, B.; Samdin, T. D.; Monteiro, D. A.; Desai, M. S.; Scheideler, O.; Jin, H. E.; Kim, S.; Lee, S. W. Phage-Based Structural Color Sensors and Their Pattern Recognition Sensing System *ACS Nano* **2017**, *11*, 3632–3641.

Leadership Experience

Graduate Safety Team, UC Irvine – Fellow January 2020 – present

- Led a team of 6 graduate students to identify and address organizational and communication deficiencies between EH&S and more than 40 research laboratories in the Chemistry department
- Implemented and executed plan to update safety training protocols, transition the department to a new chemical inventory system, and create a database of standard operating procedures for the safe handling of hazardous chemicals
- Served as a liaison between graduate students and the department’s faculty and staff on matters related to laboratory safety and laboratory operations under Covid-19 restrictions

Business & Consulting for STEM Scientists Group, UC Irvine – Co-founder January 2020 – present

- Organized and led a group of 30 STEM graduate students seeking opportunities to transition from the benchtop to roles in business and consulting
- Networked with and recruited industry professionals to serve as speakers, held mock case interviews, and resume workshops for students

Chemistry TA Mentorship Program, UC Irvine August 2019 – present

- Mentored and trained 12 first-year graduate students on effective classroom management and teaching strategies as part of an ongoing effort to improve undergraduate learning experiences in Chemistry

Graduate Student Teaching Assistant, UC Irvine August 2016 – present

- Taught multiple undergraduate lectures and laboratories for the Chemistry, Pharmaceutical Sciences, and Biological Sciences departments
- Prepared weekly discussion lectures, worksheets, and study guides, and held weekly office hours for students

Berkeley Student Cooperative - Assistant Building Manager July 2014 – March 2016

- Managed a complex of 300 residents, maintained and oversaw a \$10,000/year community fund for resident events, apartment renovations, and community outreach and service projects
- Organized and held recruitment events for students from diverse and disadvantaged backgrounds including: low-income, first-generation, disabled, undocumented, and minority students of color seeking affordable and inclusive housing

Notations, Awards, and Fellowships

- Graduate Dean’s Dissertation Fellowship, University of California, Irvine \$5,000 2020
- Safety Fellow, Chemistry Department, University of California, Irvine 2020 – 2021
- Peptide Therapeutics Symposium Travel Grant Awardee – 6 out of 24 presenters 2019
- Ford Foundation Predoctoral Fellowship Honorable Mention – 350 applications out of 2000 2018
- Ford Foundation Predoctoral Fellowship Honorable Mention – 400 applications out of 2000 2017

- Amgen Scholar, Medicinal Chemistry and Pharmaceutical Sciences, UCI – 1 out of 15 candidates 2017
- Teagle Foundation Scholarship – \$40,000 distributed over 4 years 2012 – 2016

References

Professor James S. Nowick
Departments of Chemistry
and Pharmaceutical Sciences
University of California, Irvine

Professor Gregory A. Weiss
Departments of Chemistry, Pharmaceutical,
Sciences, and Molecular Biology and
Biochemistry
University of California, Irvine

Professor Jennifer A. Prescher
Departments of Chemistry, Pharmaceutical Sciences,
and Molecular Biology and Biochemistry
University of California, Irvine

Professor Robert Spitale
Department of Pharmaceutical Sciences
University of California, Irvine

ABSTRACT OF THE DISSERTATION

Developing Macrocyclic β -Hairpin Peptide Mimics to Elucidate the Structures of $A\beta$ Oligomers
in Alzheimer's Disease

By

Tuan D. Samdin

Doctor of Philosophy in Chemistry

University of California, Irvine

2021

Professor James S. Nowick

Chapter 1 provides a brief review on the application and use of peptide model systems to mimic the properties and structures of oligomers formed by amyloidogenic peptides and proteins. Oligomers formed by amyloidogenic peptides and proteins are noted for the significant heterogeneity they display in their stability, structure, and stoichiometry. Obtaining high-resolution structures of the oligomers formed by amyloidogenic peptides and proteins is crucial for advancing our knowledge of the molecular basis of the diseases these assemblies are associated with.

The assembly of amyloidogenic peptides and proteins such as the β -amyloid peptide ($A\beta$), α -synuclein, huntingtin, tau, and islet amyloid polypeptide (IAPP) into amyloid fibrils and oligomers is directly linked to amyloid diseases, such as Alzheimer's, Parkinson's, and

Huntington's diseases, frontotemporal dementias, and type II diabetes. Although amyloid oligomers have emerged as especially important in amyloid diseases, high-resolution structures of the oligomers formed by full-length amyloidogenic peptides and proteins have remained elusive. Investigations of oligomers assembled from fragments or stabilized β -hairpin segments of amyloidogenic peptides and proteins have allowed investigators to illuminate some of the structural, biophysical, and biological properties of amyloid oligomers. This chapter provides context for much of the work described in this dissertation and highlights recent advances in the study of amyloidogenic oligomers and challenges currently faced by the field.

To mimic and investigate the structures, biological, and biophysical properties of endogenous A β oligomers, the Nowick laboratory has developed macrocyclic β -hairpin peptides as model systems. These macrocyclic β -hairpin peptides comprise β -strand segments of residues that are derived from the full-length sequence of A β . To constrain the peptide to a macrocycle and stabilize a β -hairpin conformation, we use disulfide bridges and δ Orn turn units. To prevent the uncontrolled aggregation of these A β derived peptide our group typically incorporates an *N*-methyl group on one β -strand. In studying the assembly of these A β derived macrocyclic β -hairpin peptides, our laboratory has been able to report several crystallographic structures of dimers and trimers that further assemble to form tetramers, hexamers, octamers, and dodecamers. We believe that these unique structures reflect some of the immense variation and heterogeneity present in the structures of endogenous A β oligomers.

This thesis describes my efforts to build upon the archetypal macrocyclic β -hairpin model system developed by the Nowick laboratory to better mimic endogenous A β oligomers. In the course of my doctoral studies, I have developed and studied three new macrocyclic β -hairpin model systems. These model systems incorporate additional residues beyond the A β ₁₆₋₃₆ residue

segments typically studied by our laboratory and explore the incorporation of α -methyl groups in lieu of *N*-methyl groups to limit uncontrolled aggregation. These new macrocyclic β -hairpin model systems have also provided high-resolution insight into the unique ways in which A β β -hairpins can assemble to form oligomers.

Chapter 2 describes the synthesis, solution-phase biophysical studies, and X-ray crystallographic structures of hexamers formed by macrocyclic β -hairpin peptides derived from the central and *C*-terminal regions of A β , which bear “tails” derived from the *N*-terminus of A β . Soluble oligomers of A β , are thought to be the synaptotoxic species responsible for neurodegeneration in Alzheimer’s disease. Over the last 20 years, evidence has accumulated that implicates the *N*-terminus of A β as a region that may initiate the formation of damaging oligomeric species. Our laboratory has previously studied macrocyclic β -hairpin peptides derived from A β _{16–22} and A β _{30–36}, capable of forming hexamers that can be observed by X-ray crystallography and SDS-PAGE. To better mimic oligomers of full length A β , we use an orthogonal protecting group strategy during the synthesis to append residues from A β _{1–14} to the parent macrocyclic β -hairpin peptide **1**, which comprises A β _{16–22} and A β _{30–36}. The *N*-terminally extended peptides **N+1**, **N+2**, **N+4**, **N+6**, **N+8**, **N+10**, **N+12**, and **N+14** assemble to form dimers, trimers, and hexamers in solution-phase studies. X-ray crystallography reveals that peptide **N+1** assembles to form a hexamer that is composed of dimers and trimers. These observations are consistent with a model in which the assembly of A β oligomers is driven by hydrogen bonding and hydrophobic packing of the residues from the central and *C*-terminal regions, with the *N*-terminus of A β accommodated by the oligomers as an unstructured tail.

Chapter 3 describes the investigation of oligomers formed by macrocyclic β -hairpin peptides derived from A β _{12–40}. Peptides **1a–i** and **2a–d**, derived from residues 12–40, demonstrate

solution-phase and crystallographic assembly dependent on β -hairpin stability and intermolecular interactions mediated by N-terminal residues 12–14. Sodium dodecyl sulfate-polyacrylamide gel electrophoresis (SDS-PAGE) studies reveal that peptides **1a** and **1d** assemble to form octamers, peptides **1h** and **2a** assemble to form octamers and tetramers, and peptide **2d** assembles to form tetramers. X-ray crystallographic studies of peptide **2a** reveals the assembly of a β -barrel-like tetramer stabilized by edge-to-edge hydrogen bonding and hydrophobic packing. Additional evidence for the assembly of a β -barrel-like octamer is also present within the crystal lattice. Replica-exchange molecular dynamics (REMD) simulations show that this tetramer can accommodate residues 23–29 as a loop and additional residues from the N- and C-terminal region of A β . Molecular dynamics simulations reveal that this REMD modeled tetramer can disrupt a lipid membrane and facilitate water permeation in a pore-like fashion. These observations provide novel insight into the mechanisms by which endogenous A β oligomers may assemble and damage neuronal membranes in the Alzheimer's brain.

Chapter 4 describes studies of macrocyclic β -hairpin peptides comprising β -strands of A β residues 17–22 and 30–36. The incorporation of an *N*-methyl group on position 20, in peptides derived from 17–22 and 30–36, alters the hydrogen bonding edges and assembly of triangular trimers formed by these peptides. To better mimic the hydrogen bonding edges of β -hairpins formed by unmodified A β we investigated substitution of the *N*-methyl group on position 20 with an α -methyl group on position 19. The incorporation of α -methyl amino acids into macrocyclic β -hairpin peptides derived from presents an opportunity to study the structures of oligomers that may more closely resemble endogenous A β oligomers.

Chapter 1^a

Exploring Amyloid Oligomers with Peptide Model Systems

INTRODUCTION

The assembly and aggregation of peptides and proteins into fibrils and oligomers is a hallmark of amyloid diseases.[1–4] Amyloid diseases are diverse in their prevalence, presentation, and symptoms, encompassing neurodegenerative diseases, such as Alzheimer’s disease, Parkinson’s disease, Huntington’s disease, and Creutzfeldt-Jakob disease, as well as other diseases, such as type II diabetes and transthyretin amyloidosis.[4–8] Amyloid fibrils are common molecular assemblies associated with amyloid diseases, and are characterized by their insolubility, affinity for Congo red dye and thioflavin T (ThT), cross- β X-ray diffraction pattern, and extended networks of in-register parallel β -sheets.[9–14] The biophysical and structural properties of amyloid fibrils and their roles in disease have been studied extensively (**Figure 1.1 A–E**).[15–18] Yet, as investigations into amyloid fibrils have proceeded over the last four decades, evidence has increasingly pointed toward amyloid oligomers as the damaging species responsible for disease progression.

^a This chapter is adapted from Samdin, T.; Kreuzer, A. G.; Nowick, J. S. Exploring Amyloid Oligomers with Peptide Model Systems. *Curr. Opin. Chem. Biol.* **2021**, *64*, 106–115.

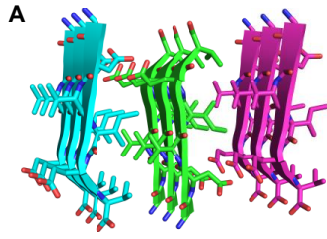
Some of the initial evidence for the presence of amyloid oligomers arose from solution-phase biophysical characterization of amyloid plaques isolated from Alzheimer's disease brains.[19,20] These early studies reported the presence of soluble assemblies of the β -amyloid peptide, $A\beta$, in addition to insoluble fibrils. The formation of these $A\beta$ assemblies and their relevance to disease pathology was supported by subsequent *in vitro* studies, which confirmed their assembly and neurotoxicity, and ultimately led to the formalization of the hypothesis that amyloid oligomers are causative agents in the neurodegeneration associated with Alzheimer's disease.[21–29]

Oligomers of $A\beta$ are soluble and heterogeneous — varying significantly in their structure, stability, and stoichiometry. Antiparallel β -sheets and β -hairpins are thought to be building blocks of many amyloid oligomers. Amyloid oligomers vary vastly in size, comprising as few as two or three, or as many as dozens or more molecules. Many of these features have been observed for oligomers formed by other amyloidogenic peptides and proteins, such as α -synuclein, polyglutamine, islet amyloid polypeptide (IAPP), and tau.[4,30–33]

Only one atomic-resolution structure of an oligomer formed by the full-length sequence of $A\beta_{42}$ has been reported thus far (**Figure 1.1 F**).[34] Carulla and co-workers reported the NMR-based structure of an $A\beta_{42}$ tetramer and provided additional evidence for its assembly into an octamer. The tetramer is a six-stranded antiparallel β -sheet comprising two β -hairpins of $A\beta_{42}$ surrounding two antiparallel β -strands of $A\beta_{42}$. Although the disease relevance of this oligomer has not yet been established, the tetramer represents the first high-resolution structure of an oligomer of full-length $A\beta$. In light of the large number of unique amyloid fibril structures reported and deposited in the Protein Data Bank (PDB), the lack of other high-resolution structures of amyloid oligomers represents an immense gap in our understanding of amyloid diseases.[15–18]

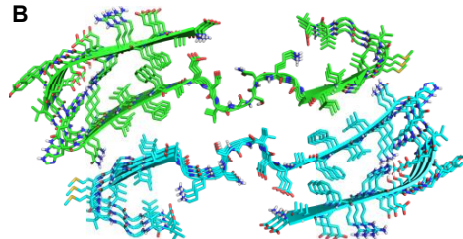
Peptide model systems derived from the sequences of amyloidogenic peptides and proteins have emerged as useful tools to investigate amyloid oligomers and bridge this gap in our understanding. These peptides are designed to mimic the biological and biophysical properties of native amyloid oligomers. Unlike native amyloid oligomers, the oligomers formed by these peptide model systems often have the added benefits of increased homogeneity and stability, facilitating high-resolution characterization of many of the oligomers that form. This review highlights recent investigations of peptide model systems that have helped advance our knowledge of amyloid oligomers.

Science, 2012, 191, 1228–1232



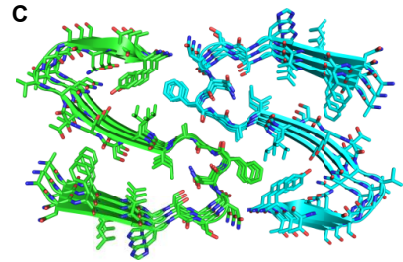
fibril steric zipper of α B crystallin_{95–100}
PDB 3SGS

Nat. Commun., 2019, 10, 1–8



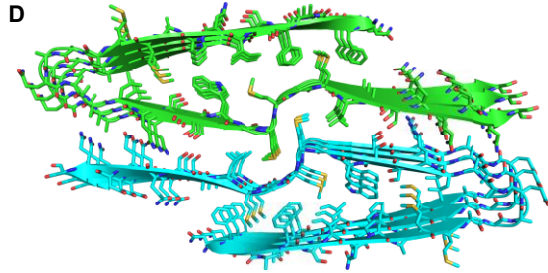
fibril of A β _{1–40}
PDB 6SHS

Nat. Struct. Mol. Biol., 2020, 27, 660–667



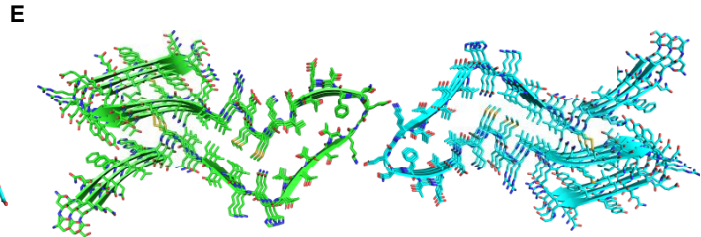
fibril of IAPP_{13–37}
PDB 6Y1A

Nat. Struct. Mol. Biol., 2020, 26, 619–627



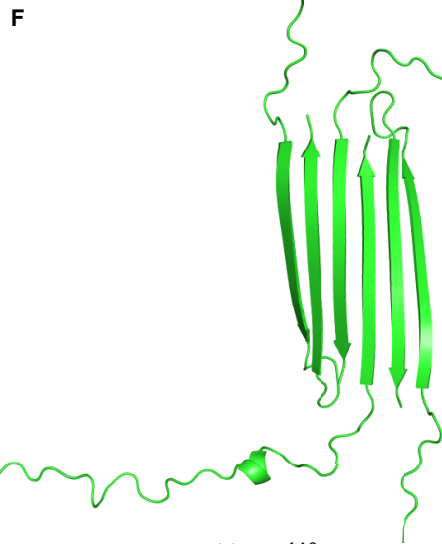
fibril of TDP-43_{311–360}
PDB 6N37

Nat. Struct. Mol. Biol., 2020, 27, 598–602

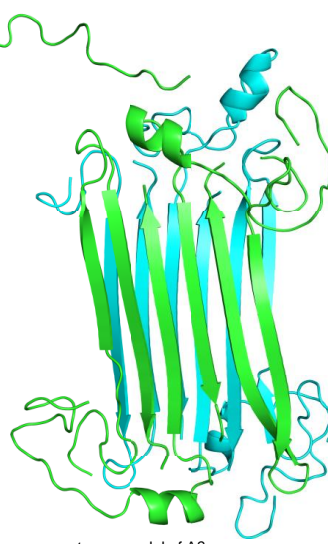


fibril of hPrP_{170–229}
PDB 6LNI

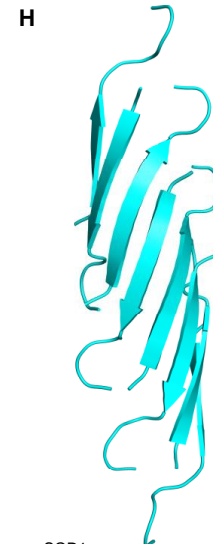
Nat. Commun., 2020, 11, 1–14



tetramer of A β _{1–42}
PDB 6RHY



octamer model of A β _{1–42}



SOD1_{28–38}
PDB 5IIW

Science, 2012, 191, 1228–1232



α B crystallin_{90–100}
PDB 3SGO

JACS, 2013, 135, 10202–10205



hPrP_{177–182} and hPrP_{211–216}
PDB 4E1I

Figure 1.1. Structures of fibrils and oligomers formed by amyloidogenic peptides. **A.** Fibril-like assembly of α B crystallin_{95–100}; X-ray crystallographic structure. **B–E.** Fibril-like assemblies of $A\beta_{1–40}$, IAPP_{13–37}, TDP-43_{311–360}, and hPRP_{170–229}; Cryo-EM structures. **F.** Tetramer and octamer formed by $A\beta_{1–42}$; NMR structure and NMR-based model. **G–I.** Oligomers of α B crystallin_{90–100}, SOD1_{28–38}, and hPRP_{177–182} crosslinked with hPRP_{211–216}; X-ray crystallographic structures.

THE FRAGMENT-BASED APPROACH

X-ray crystallographic investigations of short fragments of amyloidogenic peptides and proteins provide one strategy for studying the molecular interactions governing fibril and oligomer assembly at high resolution. Eisenberg and co-workers reported several high-resolution structures of fibril-forming peptides that are derived from amyloidogenic peptides and proteins.[35–37] Using this fragment-based approach, Eisenberg and co-workers determined the X-ray crystallographic structures of two oligomers composed of eleven-residue peptide fragments derived from α B crystallin and superoxide dismutase 1 (SOD1) (**Figure 1.1 G, H**).[38–40] The α B crystallin fragment assembles into a cylindrical barrel composed of six antiparallel β -strands, termed a cylindrin by the investigators (**Figure 1.1 G**). The SOD1 fragment assembles into a corkscrew-like arrangement of antiparallel β -strands (**Figure 1.1 H**). Surewicz and co-workers determined the structure of a hexamer composed of disulfide-linked antiparallel β -strands comprising two six-residue peptide fragments derived from human prion protein (**Figure 1.1 D**).[41] Intermolecular hydrogen bonding between antiparallel β -strands and the close packing of hydrophobic residues are common features that stabilize each of these oligomers.

These fragment-based models are significant, because oligomers of full-length amyloidogenic peptides and proteins are thought to be composed of antiparallel β -sheets and β -hairpins.[42–45] Structures of oligomers assembled from the fragments of amyloidogenic peptides and proteins can serve as models for naturally occurring disease-relevant oligomers formed by full-length amyloidogenic peptides and proteins. Oligomers of full-length amyloidogenic peptides and proteins have not yet yielded to X-ray crystallography or CryoEM. Although CryoEM has

emerged as a powerful tool in the structural biology of amyloid fibrils (**Figure 1.1 B–E**), thus far the oligomers of full-length amyloidogenic peptides and proteins have proven too small or too heterogenous for structural elucidation by CryoEM.[15–18,46,47]

STABILIZED β -HAIRPINS

β -Hairpins are building blocks of some of the oligomers formed by amyloidogenic peptides and proteins.[34,48,49] Model systems consisting of stabilized β -hairpins are valuable tools for studying amyloid oligomers, because they provide control of secondary and tertiary structure while allowing quaternary structure to form through self-assembly. Härd and co-workers demonstrated that three different amyloidogenic peptides and proteins can form β -hairpins and determined the structures of these β -hairpins. In 2008, Härd, Hoyer, and co-workers elucidated the NMR structure of a β -hairpin formed by A β ₄₀ by using an affibody to sequester and stabilize the β -hairpin (**Figure 1.2 A**).[42] In this β -hairpin, residues 17–23 and 30–36 of A β hydrogen bond to form an antiparallel β -sheet, while the intervening residues, 24–29, form a loop (**Figure 1.2 B**). The remaining *N*- and *C*-terminal residues are unstructured. Härd and co-workers also used affibodies to stabilize and determine the structures of β -hairpins formed by α -synuclein and IAPP.[43,44]

In further studies, Härd and co-workers investigated the biological, biophysical, and structural properties of oligomers formed by a covalently stabilized analogue of the A β β -hairpin that they previously reported.[45] In this analogue, Ala₂₁ and Ala₃₀ are mutated to cysteines to enable formation of a disulfide bridge (**Figure 1.2 C**). Oligomers formed by this disulfide-stabilized A β β -hairpin mimicked some of the characteristics of oligomers of unmodified A β — morphology by transmission electron microscopy (TEM), assembly by size-exclusion chromatography (SEC) and SDS-PAGE, and cytotoxicity toward neuronally derived SH-SY5Y cells. These oligomers were also recognized by oligomer-specific antibodies used to recognize native A β oligomers isolated from the brains of Alzheimer’s patients and transgenic mice. These

findings are significant, because they demonstrate that conformationally stabilized β -hairpin monomers of A β can assemble to form oligomers that recapitulate the properties of biologically relevant A β oligomers. Solid-state NMR spectroscopy revealed that a disulfide-stabilized β -hairpin comprising A β_{16-42} forms a barrel-shaped hexamer (**Figure 1.2 D**).[49] In this oligomer, a hydrophobic core forms at one end of the assembly by the packing of hydrophobic residues from the central and C-terminal regions of A β . Intermolecular antiparallel β -sheets form between A β_{34-36} and A β_{39-42} at one end of the barrel; the β -hairpin loops of each monomer comprise the other end of the barrel. This series of investigations of A β β -hairpins illustrates how stabilized β -hairpin peptides can be used to model and study the properties and structures of amyloid oligomers.[40,43,46]

Our laboratory has developed macrocyclic β -hairpin peptides as model systems to learn about the structure, and biological and biophysical properties of the oligomers formed by full-length amyloidogenic peptides and proteins.[50] The macrocyclic β -hairpin peptides consist of two peptide β -strands from the amyloidogenic peptide or protein that are constrained to a macrocycle by a δ -linked ornithine (δ Orn) turn unit and linked by a loop or a second δ Orn turn unit (**Figure 1.2 E–G**).[51] An *N*-methyl group on one of the β -strands prevents uncontrolled aggregation, and thus facilitates oligomer formation. X-ray crystallographic studies of macrocyclic β -hairpin peptides derived from sequences such as A β , β_2 -microglobulin, and α -synuclein have revealed the formation of dimers and trimers that further assemble to form tetramers, hexamers, octamers, nonamers, and dodecamers (**Figure 1.3**).[51–60] Wetzel and co-workers have developed β -hairpin model systems of polyglutamine derived peptides to better understand the role of polyglutamine folding and aggregation in Huntington's disease using D-Pro-Gly turn units and *N*-methyl amino acids.[61]

In our initial investigations of A β oligomers, we prepared and studied macrocyclic β -hairpin peptides derived from A β ₁₇₋₃₆. In 2014, we reported a macrocyclic β -hairpin peptide containing A β ₁₇₋₂₃ and A β ₃₀₋₃₆.^[51] X-ray crystallography revealed that this peptide assembles into trimers that further assemble to form a sandwich-like hexamer and a ball-shaped dodecamer (**Figure 1.2 E & Figure 1.3 A–C**). X-ray crystallographic studies of a homologous macrocyclic β -hairpin, incorporating the A β ₂₄₋₂₉ loop, revealed that the peptide assembles to form trimers that further assemble into ball-shaped dodecamers, and five dodecamers further assemble to form an annular pore (**Figure 1.2 G & Figure 1.3 G–I**).^[52] In subsequent studies, we covalently stabilized the trimers formed by the macrocyclic β -hairpin peptide containing A β ₁₇₋₂₃ and A β ₃₀₋₃₆ with disulfide-bridges (**Figure 1.2 H**).^[53] These covalently stabilized trimers assemble in solution, forming hexamers and dodecamers by SEC and SDS-PAGE. The covalent trimers are toxic to SH-SY5Y cells and are recognized by the amyloid oligomer-specific antibody A11, suggesting that they may recapitulate the topology of A β oligomers occurring in the Alzheimer’s brain.^[62] X-ray crystallography revealed that the trimers form a hexamer, a dodecamer, and an annular pore comprising six dodecamers (**Figure 1.3 D–F**). Recently, we found that incorporation of a cyclohexylalanine residue in place of a phenylalanine residue promotes folding of A β derived macrocyclic β -hairpins, further stabilizes trimers formed by the β -hairpins, and promotes formation of hexamers and dodecamers (**Figure 1.3 J–L**).^[56] We are now using antibodies generated against these synthetic A β oligomer mimics to probe biogenic A β oligomers from brain tissue.

We have also studied macrocyclic β -hairpin peptides derived from A β ₁₆₋₃₆, in which the β -strands adopt a different alignment than the β -hairpin peptides derived from A β ₁₇₋₃₆. These studies have revealed the assembly of toxic oligomers in both the crystal state and in solution, without the need for covalent stabilization through disulfide bridges.^[57] A macrocyclic β -hairpin containing

$A\beta_{16-22}$ and $A\beta_{30-36}$ assemble to form dimers and trimers that further assemble into hexamers that can be observed in SDS-PAGE and by X-ray crystallography (**Figure 1.2 E & Figure 1.3 M–O**). A related macrocyclic β -hairpin peptide containing $A\beta_{16-22}$ and $A\beta_{30-36}$ assembles in the crystal state to form trimers that further assemble into a dodecamer (**Figure 1.2 E & Figure 1.3 P–Q**).[58]

Current efforts in our laboratory seek to incorporate more residues from full-length $A\beta_{40}$ or $A\beta_{42}$ into our macrocyclic β -hairpin model systems, to better reflect oligomers formed by full-length $A\beta$. We recently incorporated $A\beta_{1-14}$ as an *N*-terminally extended "tail" to the hexamer-forming macrocycle comprising $A\beta_{16-22}$ and $A\beta_{30-36}$ (**Figure 1.2 F**). In studying a series of homologs bearing *N*-terminal tails, we found that residues from the *N*-terminus of $A\beta$ do not disrupt oligomer assembly and likely form an unstructured tail (**Figure 1.3 R**).[59] X-ray crystallographic studies of a macrocyclic β -hairpin peptide from $A\beta_{16-36}$ that incorporates the $A\beta_{23-29}$ loop revealed the assembly of parallel and antiparallel β -sheet dimers that further assemble to form a sandwich-like tetramer and a twisted β -sheet tetramer, with the latter packing to form an octamer (**Figure 1.2 G & Figure 1.3 S–W**).[60]

Collectively, our studies of β -hairpin peptides derived from $A\beta_{16-36}$, $A\beta_{17-36}$, and other amyloidogenic peptides and proteins have provided a multitude of distinct oligomer structures and revealed the unique ways in which β -hairpins can assemble to form compact oligomers stabilized by edge-to-edge hydrogen bonding and hydrophobic packing. Other laboratories have also reported various structures of $A\beta$ fibrils, oligomers, and monomer formed by β -hairpins with different β -strand alignments.[34,42,48,63] We believe our structures reflect some of the immense variation and heterogeneity in the structures of endogenous amyloid oligomers, because many behave like oligomers of full-length amyloidogenic peptides and proteins in biological and biophysical experiments.

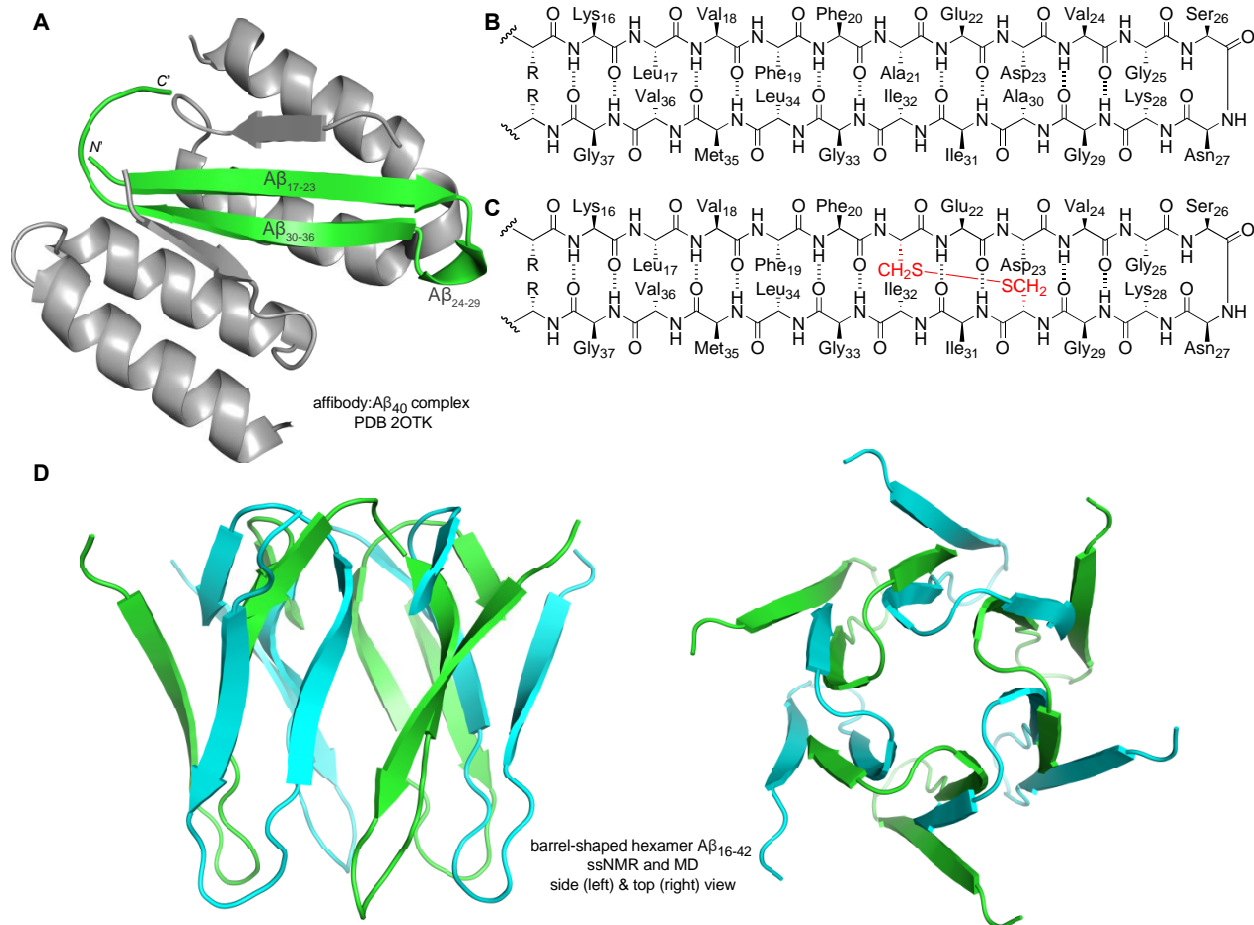
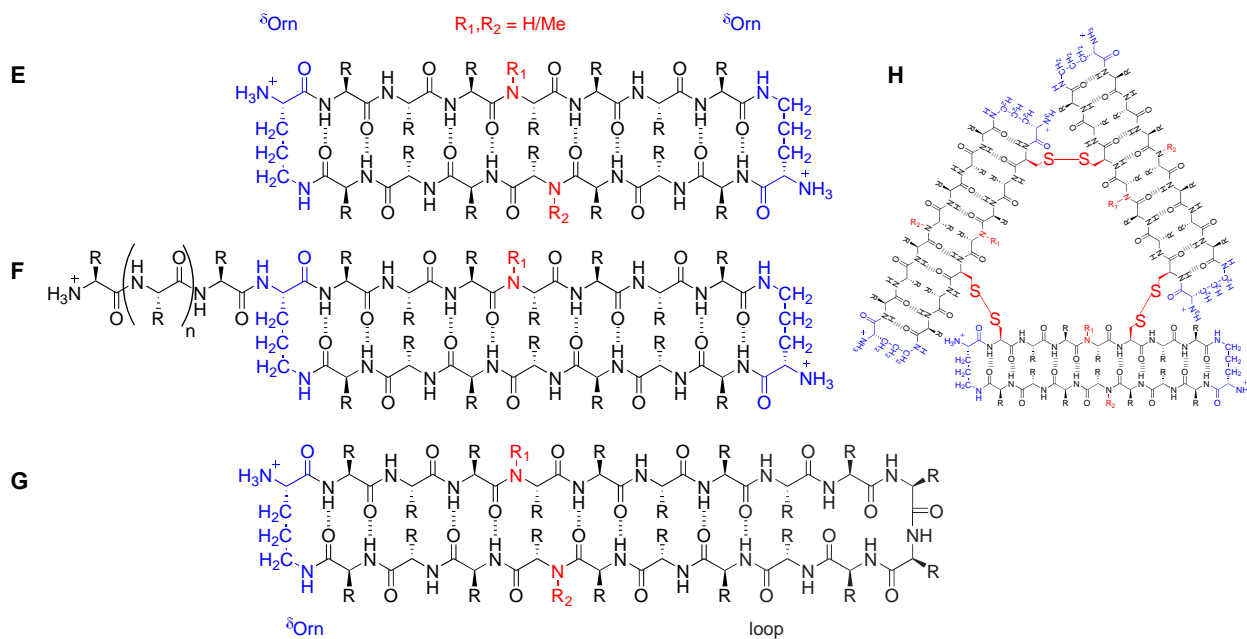
F. For a review see: *Acc. Chem. Res.*, 2018, 51, 706–718G. *JACS*, 2020, 142, 15593–11601H. *JACS*, 2016, 138, 4634–4642; *JACS*, 2020, 142, 20708–20716; and *ACS Chem. Neurosci.*, 2020, 11, 2340–2347

Figure 1.2. **A.** NMR structure of an A β ₄₀ β -hairpin stabilized by an affibody. **B.** Alignment of the A β ₄₀ β -hairpin. **C.** Disulfide stabilization of the A β ₄₀ β -hairpin. **D.** NMR-based model of a barrel-shaped hexamer formed by a disulfide stabilized A β ₁₆₋₄₀ β -hairpin. **E–H.** Macrocyclic β -hairpins and disulfide-stabilized β -hairpins derived from amyloidogenic peptides and proteins.

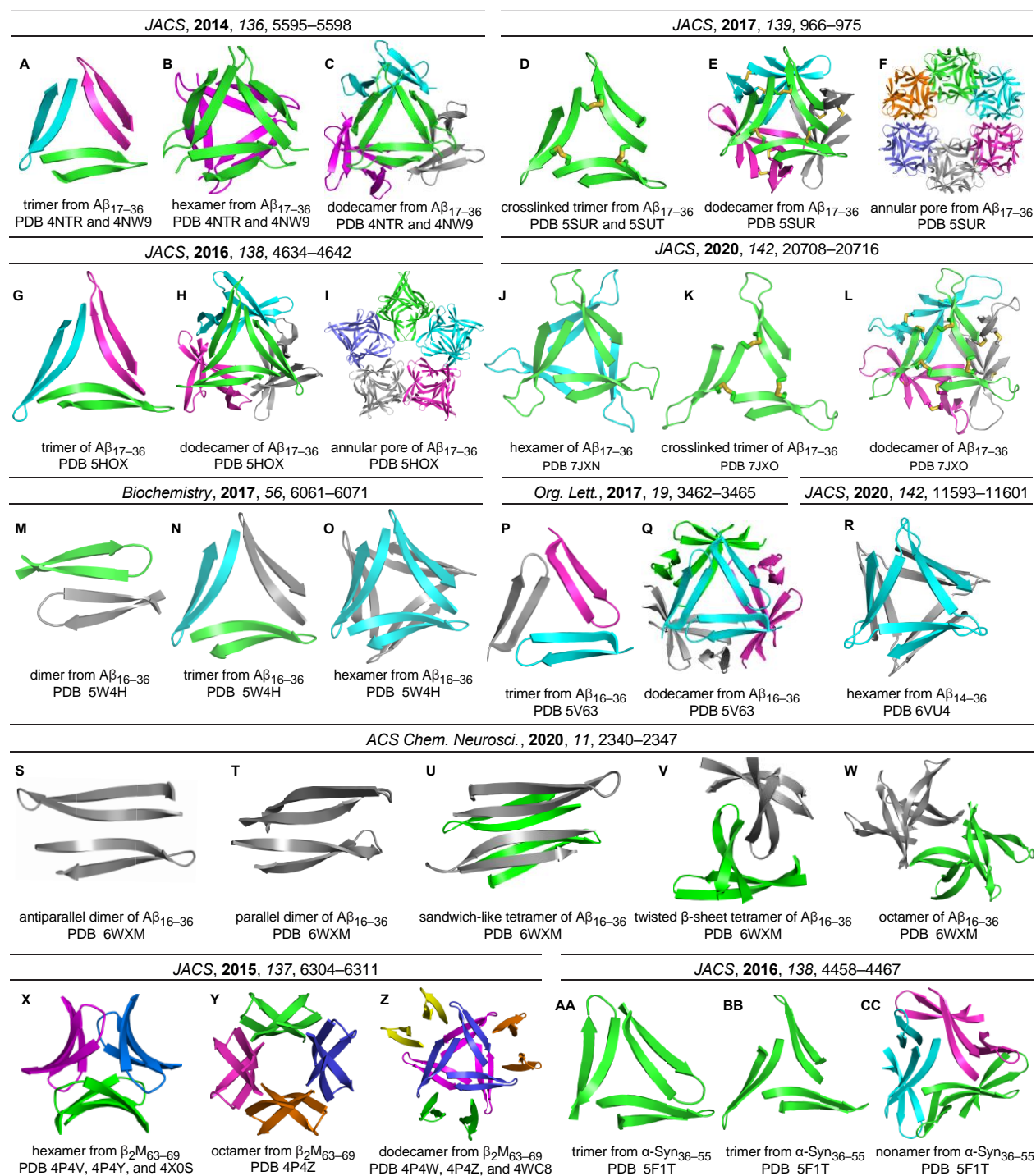


Figure 1.3. X-ray crystallographic structures of oligomers formed by macrocyclic β -hairpin peptides derived from A β , β_2 -microglobulin, and α -synuclein. **A–L.** Trimers, hexamers, dodecamers, and annular pores formed by macrocyclic β -hairpin peptides derived from A β_{17-36} . **M–W.** Dimers, trimers, tetramers, hexamers, octamer, and dodecamer derived from A β_{16-36} . **X–Z.** Hexamer, octamer, and dodecamer derived from β_2 -microglobulin. **AA–CC.** Trimers and nonamer derived from α -synuclein.

COMPUTATIONAL TOOLS FOR STUDYING AMYLOID OLIGOMERS AND FIBRILS

Molecular modeling can provide valuable insights into amyloid oligomer formation and structure by allowing the visualization, interpretation, and prediction of the conformations, motions, and interactions of the peptides and proteins involved.[4] These simulations allow observation of that which cannot be examined directly through experimentation and can complement experimental studies to provide deeper insights. For example, residues that had to be excluded from the peptide model systems to facilitate characterization by X-ray crystallography can be restored for study in molecular dynamics simulations. Okuno and co-workers thus used dissipative particle dynamics to restore $A\beta_{9-16}$ and $A\beta_{37-42}$ to a dodecamer-forming macrocyclic β -hairpin peptide comprising $A\beta_{17-36}$ (**Figure 1.3 H**).[52,64] The simulations revealed that residues $A\beta_{37-42}$ can pack to form a stabilizing hydrophobic core in the central cavity of the dodecamer. Our laboratory has similarly made use of replica-exchange molecular dynamics simulations to probe whether residues absent from the design of our macrocyclic β -hairpin peptides can be accommodated by the structures of the oligomers that form.[51,55,57,60]

The protein force fields used in molecular dynamics and other forms of molecular modeling were not developed for amyloid oligomers and have limited ability to accurately model the conformation, folding, and size of amyloidogenic peptides and proteins.[65–68] Shaw and co-workers used experimental NMR and SAXS data from amyloid oligomers to improve parameters for torsion angles, and protein and water van der Waals interactions, to produce a force field, *a99SB-disp*, that more accurately simulates disordered proteins such as $A\beta_{40}$. [69]

Improved algorithms for simulating the conformations of intrinsically disordered proteins and intrinsically disordered regions also promise to provide enhanced insights into amyloid oligomer formation. Recently, Petersson and co-workers reported the PyRosetta-based algorithms AbinitioVO and FastFloppyTail, which allow for the accurate prediction of protein structure across

a wide array of folds and degrees of order.[70] We anticipate that improvements in force fields and algorithms for predicting conformational ensembles will cross-fertilize other studies that use peptide model systems and full-length peptides and proteins and thus contribute to a better understanding of amyloid oligomers.

Molecular docking simulations have guided the development of ligands that bind amyloid oligomers that may ultimately lead to new imaging probes or drugs for Alzheimer's disease or other amyloid diseases. Thus, X-ray crystallographic structures of trimers and hexamers formed by macrocyclic β -hairpin peptides comprising $A\beta_{17-36}$ (**Figure 1.3 A, B, D, G**), have been used as targets for docking studies of triphenylmethane dyes, fluorescent probes, and therapeutic ligands for $A\beta$ oligomers.[71–74] Docking simulations of the triphenylmethane dye, crystal violet, with the structure of our covalently-stabilized trimer derived from $A\beta_{17-36}$ (**Figure 1.3 D**) produced a model for molecular recognition that guided structure-activity relationship studies.[71] Our laboratory is currently using the results of these computational and experimental studies to develop novel chemical probes for biogenic $A\beta$ oligomers.

Computational tools are also valuable in identifying amyloidogenic regions of peptides and proteins by identifying features that drive aggregation and assembly, such as hydrophobicity, β -sheet character, a prevalence of aromatic residues, and low-charge content.[75] A number of algorithms, computational tools, and databases have been developed to assess these characteristics for a given peptide or protein sequence.[76] Tools such as TANGO, WALTZ-DB 2.0, and Cordax assess and quantify the aggregation potential of a given sequence.[77–80] Results from this type of primary sequence analysis can supplement and direct structure activity relationship studies of amyloid fibrils and oligomers.[36–38,75] These tools further our understanding of the ever-growing “amyloidome,” which extends beyond disease and underlies many normal cellular, bacterial, and fungal processes.[81]

CONCLUSION

The amyloid state of peptides and proteins is an active and fascinating frontier of peptide and protein science for chemical and structural biologists alike. The ever-growing ties between amyloidogenic peptides and proteins and cellular function and disease inspires curiosity, and the resistance of these peptides and proteins to characterization using conventional techniques and tools drives innovation. Until the high-resolution observation of oligomers of full-length amyloidogenic peptides and proteins becomes widely feasible, peptide model systems that approximate and mimic endogenous oligomers will remain one of the best tools for dissecting their structural, biological, and biophysical properties. The growing understanding of amyloid oligomers provided by these studies will further our knowledge of amyloid diseases and bolster efforts to develop diagnostics and drugs.

ACKNOWLEDGEMENTS: We thank the National Institutes of Health (Grants GM097562 and AG062296) and the National Science Foundation (Grant CHE-1808096) for funding. T.D.S. is grateful to the University of California, Irvine for funding through the Graduate Dean's Dissertation Year Fellowship. We thank Professor Natàlia Carulla and Dr. Eduard Puig for providing the coordinates of their octamer model (Figure 1.1 F), and Professor Torleif Härd and Professor Christofer Lendel for providing the coordinates of their hexamer model (Figure 1.2 D). We thank Denise Bui for designing and creating the TOC graphic.

ANNOTATIONS

3**. Ke PC, Zhou R, Serpell LC, Riek R, Knowles TPJ, Lashuel HA, Gazit E, Hamley IW, Davis TP, Fändrich M, et al.: **Half a century of amyloids: Past, present and future.** *Chem Soc Rev* 2020, **49**:5473–5509.

This review highlights investigations of pathological, functional, and artificial amyloids in disease, structural biology, microbiology, and engineering. Significant attention is given to structural and biophysical characterization of amyloid fibrils and their assembly.

4**. Nguyen PH, Ramamoorthy A, Sahoo BR, Zheng J, Faller P, Straub JE, Dominguez L, Shea J-E, Dokholyan N V., Simone A De, et al.: **Amyloid oligomers: A joint experimental/computational perspective on Alzheimer’s disease, Parkinson’s disease, type II diabetes and amyotrophic lateral sclerosis.** *Chem Rev* 2021, doi:10.1021/acs.chemrev.0c01122.

This review examines *in vitro*, *in vivo*, computational, and pharmacological studies of oligomers formed by A β , tau, α -synuclein, IAPP, and superoxide dismutase 1 in Alzheimer’s disease, Parkinson’s disease, type II diabetes, and amyotrophic lateral sclerosis. The authors highlight how empirical observations of amyloid oligomers have led to and supplemented computational studies of oligomer formation and interactions.

25*. Cline EN, Bicca MA, Viola KL, Klein WL: **The amyloid- β oligomer hypothesis: Beginning of the third decade.** *J Alzheimer’s Dis* 2018, **64**:S567–S610.

This review summarizes evidence for the roles of A β oligomers in neurodegeneration and synaptotoxicity in Alzheimer’s disease. The authors highlight *in vitro*, *in vivo*, and clinical evidence that points to A β oligomers as the damaging species in Alzheimer’s disease.

34**. Ciudad S, Puig E, Botzanowski T, Meigooni M, Arango AS, Do J, Mayzel M, Bayoumi

M, Chaignepain S, Maglia G, et al.: **A β (1-42) tetramer and octamer structures reveal edge conductivity pores as a mechanism for membrane damage.** *Nat Commun* 2020, **11**:1–14.

This paper reports the first atomic-resolution structure of a tetramer formed by full-length A β ₄₂ and provides additional evidence for the formation of an octamer. The structure of the tetramer is the only structure of an oligomer of full-length A β that has been deposited in the Protein Data Bank (PDB).

39*. Sangwan S, Zhao A, Adams KL, Jayson CK, Sawaya MR, Guenther EL, Eisenberg DS: **Atomic structure of a toxic , oligomeric segment of SOD1 linked to amyotrophic lateral sclerosis (ALS).** *Proc Natl Acad Sci USA* 2017, **114**:8770–8775.

This paper reports the structure, biophysical, and biological properties of a corkscrew-like oligomer formed by an eleven-residue peptide fragment derived from SOD1.

50**. Kreutzer AG, Nowick JS: **Elucidating the structures of amyloid oligomers with macrocyclic β -hairpin peptides: Insights into Alzheimer’s disease and other amyloid diseases.** *Acc Chem Res* 2018, **51**:706–718.

This review highlights the use of macrocyclic β -hairpin peptides by the Nowick laboratory to mimic and study the structures, and biophysical and biological properties of oligomers formed by amyloidogenic peptides and proteins. X-ray crystallographic studies of these macrocyclic β -hairpin peptides have revealed the formation of dimers and trimers that further assemble to form tetramers, hexamers, octamers, nonamers, and dodecamers.

56*. Haerianardakani S, Kreutzer AG, Salveson PJ, Samdin TD, Guaglianone GE, Nowick JS: **Phenylalanine mutation to cyclohexylalanine facilitates triangular trimer formation by β -hairpins derived from A β .** *J Am Chem Soc* 2020, **142**:20708–20716.

This paper reports the X-ray crystallographic structures and solution phase behavior of trimers, hexamers, and dodecamers formed by macrocyclic β -hairpin peptides derived from $A\beta_{17-36}$. Substitution of cyclohexylalanine for phenylalanine facilitates the formation of trimers and their covalent stabilization through disulfide crosslinks.

59*. Samdin TD, Wierzbicki M, Kreutzer AG, Howitz WJ, Valenzuela M, Smith A, Sahrai V, Truex NL, Klun M, Nowick JS: **Effects of N-terminal residues on the assembly of constrained β -hairpin peptides derived from $A\beta$** . *J Am Chem Soc* 2020, **142**:11593–11601.

This paper reports the incorporation of $A\beta$ residues 1–14 as an *N*-terminal “tail” appended to a macrocyclic β -hairpin peptide derived from $A\beta_{16-36}$ that forms a hexamer. The tailed-macrocyclic β -hairpin peptides are synthesized using an orthogonal protecting group strategy that allows incorporation of the *N*-terminal residues, and are characterized by SDS-PAGE and X-ray crystallography.

69*. Robustelli P, Piana S, Shaw DE: **Developing a molecular dynamics force field for both folded and disordered protein states**. *Proc Natl Acad Sci U S A* 2018, **115**:E4758–E4766.

This paper describes the development of the *a99SB-disp* force field, which overcomes limitations of current protein force fields in accurately modeling amyloidogenic peptides and proteins in molecular dynamics simulations.

71*. Salveson PJ, Haerianardakani S, Thuy-boun A, Yoo S, Kreutzer AG, Demeler B, Nowick JS: **Repurposing triphenylmethane dyes to bind to trimers derived from $A\beta$** . *J Am Chem Soc* 2018, **140**:11745–11754.

This paper reports the development of triphenylmethane dyes as ligands for trimers derived from $A\beta$. Detailed studies of the interactions of crystal violet and other triphenylmethane dyes with C3 symmetric trimers derived from $A\beta_{17-36}$ are described.

REFERENCES

1. Knowles TPJ, Vendruscolo M, Dobson CM: **The amyloid state and its association with protein misfolding diseases.** *Nat Rev Mol Cell Biol* 2014, **15**:384–396.
2. Chiti F, Dobson CM: **Protein misfolding, amyloid formation, and human disease: A summary of progress over the last decade.** *Annu Rev Biochem* 2017, **86**:27–68.
3. Ke PC, Zhou R, Serpell LC, Riek R, Knowles TPJ, Lashuel HA, Gazit E, Hamley IW, Davis TP, Fändrich M, et al.: **Half a century of amyloids: Past, present and future.** *Chem Soc Rev* 2020, **49**:5473–5509.
4. Nguyen PH, Ramamoorthy A, Sahoo BR, Zheng J, Faller P, Straub JE, Dominguez L, Shea J-E, Dokholyan N V., Simone A De, et al.: **Amyloid Oligomers: A Joint Experimental/Computational Perspective on Alzheimer’s Disease, Parkinson’s Disease, Type II Diabetes and Amyotrophic Lateral Sclerosis.** *Chem Rev* 2021, doi:10.1021/acs.chemrev.0c01122.
5. Eisenberg D, Jucker M: **The amyloid state of proteins in human diseases.** *Cell* 2012, **148**:1188–1203.
6. Iadanza MG, Jackson MP, Hewitt EW, Ranson NA, Radford SE: **A new era for understanding amyloid structures and disease.** *Nat Rev Mol Cell Biol* 2018, **19**:755–773.
7. Dobson CM, Knowles TPJ, Vendruscolo M: **The amyloid phenomenon and its significance in biology and medicine.** *Cold Spring Harb Perspect Biol* 2020, **12**:pii: a033878.
8. Ruberg FL, Berk JL: **Transthyretin (TTR) cardiac amyloidosis.** *Circulation* 2012, **126**:1286–1300.
9. Li D, Liu C: **Structural diversity of amyloid fibrils and advances in their structure**

determination. *Biochemistry* 2020, **59**:639–646.

10. Fitzpatrick AW, Saibil HR: **Cryo-EM of amyloid fibrils and cellular aggregates.** *Curr Opin Struct Biol* 2019, **58**:34–42.

11. Lu JX, Qiang W, Yau WM, Schwieters CD, Meredith SC, Tycko R: **Molecular structure of β -amyloid fibrils in Alzheimer's disease brain tissue.** *Cell* 2013, **154**:1257–1268.

12. Eisenberg DS, Sawaya MR: **Structural studies of amyloid proteins at the molecular level.** *Annu Rev Biochem* 2017, **86**:69–95.

13. Yakupova EI, Bobyleva LG, Vikhlyantsev IM, Bobylev AG: **Congo Red and amyloids: History and relationship.** *Biosci Rep* 2019, **39**:BSR20181415.

14. Xue C, Lin TY, Chang D, Guo Z: **Thioflavin T as an amyloid dye: Fibril quantification, optimal concentration and effect on aggregation.** *R Soc Open Sci* 2017, **4**:160696.

15. Kollmer M, Close W, Funk L, Rasmussen J, Bsoul A, Schierhorn A, Schmidt M, Sigurdson CJ, Jucker M, Fändrich M: **Cryo-EM structure and polymorphism of A β amyloid fibrils purified from Alzheimer's brain tissue.** *Nat Commun* 2019, **10**:1–8.

16. Röder C, Kupreichyk T, Gremer L, Schäfer LU, Pothula KR, Ravelli RBG, Willbold D, Hoyer W, Schröder GF: **Cryo-EM structure of islet amyloid polypeptide fibrils reveals similarities with amyloid- β fibrils.** *Nat Struct Mol Biol* 2020, **27**:660–667.

17. Cao Q, Boyer DR, Sawaya MR, Ge P, Eisenberg DS: **Cryo-EM structures of four polymorphic TDP-43 amyloid cores.** *Nat Struct Mol Biol* 2019, **26**:619–627.

18. Wang LQ, Zhao K, Yuan HY, Wang Q, Guan Z, Tao J, Li XN, Sun Y, Yi CW, Chen J, et al.: **Cryo-EM structure of an amyloid fibril formed by full-length human prion protein.** *Nat Struct Mol Biol* 2020, **27**:598–602.

19. Masters CL, Simms G, Weinman NA, Multhaup G, McDonald BL, Beyreuther K: **Amyloid plaque core protein in Alzheimer disease and Down syndrome.** *Proc Natl Acad Sci USA* 1985, **82**:4245–4249.
20. Selkoe DJ, Abraham CR, Podlisny MB, Duffy LK: **Isolation of low-molecular-weight proteins from amyloid plaque fibers in Alzheimer's disease.** *J Neurochem* 1986, **46**:1820–1834.
21. Burdick D, Soreghan B, Kwon M, Kosmoski J, Knauer M, Henschen A, Yates J, Cotman C, Glabe C: **Assembly and aggregation properties of synthetic Alzheimer's A4/β amyloid peptide analogs.** *J Biol Chem* 1992, **267**:546–554.
22. Podlisny MB, Ostaszewski BL, Squazzo SL, Koo EH, Rydell RE, Teplow DB, Selkoe DJ: **Aggregation of secreted amyloid β-protein into sodium dodecyl sulfate-stable oligomers in cell culture.** *J Biol Chem* 1995, **270**:9564–9570.
23. Podlisny MB, Walsh DM, Amarante P, Ostaszewski BL, Stimson ER, Maggio JE, Teplow DB, Selkoe DJ: **Oligomerization of endogenous and synthetic amyloid β-protein at nanomolar levels in cell culture and stabilization of monomer by Congo red.** *Biochemistry* 1998, **37**:3602–3611.
24. Lambert MP, Barlow AK, Chromy BA, Edwards C, Freed R, Liosatos M, Morgan TE, Rozovsky I, Trommer B, Viola KL, et al.: **Diffusible, nonfibrillar ligands derived from Aβ1-42 are potent central nervous system neurotoxins.** *Proc Natl Acad Sci USA* 1998, **95**:6448–6453.
25. Cline EN, Bicca MA, Viola KL, Klein WL: **The amyloid-β oligomer hypothesis: Beginning of the third decade.** *J Alzheimer's Dis* 2018, **64**:S567–S610.
26. Ferreira ST, Lourenco M V., Oliveira MM, De Felice FG: **Soluble amyloid-β oligomers**

as synaptotoxins leading to cognitive impairment in Alzheimer's disease. *Front Cell Neurosci* 2015, **9**:1–17.

27. Benilova I, Karran E, De Strooper B: **The toxic A β oligomer and Alzheimer's disease: an emperor in need of clothes.** *Nat Neurosci* 2012, **15**:349–357.

28. Selkoe DJ, Hardy J: **The amyloid hypothesis of Alzheimer's disease at 25 years.** *EMBO Mol Med* 2016, **8**:595–608.

29. Kulenkampff K, Perez MW, Sormanni P, Habchi J, Vendruscolo M: **Quantifying misfolded protein oligomers as drug targets and biomarkers in Alzheimer and Parkinson diseases.** *Nat Rev Chem* 2021, doi:10.1038/s41570-021-00254-9.

30. Bengoa-Vergniory N, Roberts RF, Wade-Martins R, Alegre-Abarrategui J: **Alpha-synuclein oligomers: A new hope.** *Acta Neuropathol* 2017, **134**:819–838.

31. Hoffner G, Djian P: **Monomeric, oligomeric and polymeric proteins in huntington disease and other diseases of polyglutamine expansion.** *Brain Sci* 2014, **4**:91–122.

32. Jeong HR, An SSA: **Causative factors for formation of toxic islet amyloid polypeptide oligomer in type 2 diabetes mellitus.** *Clin Interv Aging* 2015, **10**:1873–1879.

33. Shafiei SS, Guerrero-Muñoz MJ, Castillo-Carranza DL: **Tau oligomers: Cytotoxicity, propagation, and mitochondrial damage.** *Front Aging Neurosci* 2017, **9**:1–9.

34. Ciudad S, Puig E, Botzanowski T, Meigooni M, Arango AS, Do J, Mayzel M, Bayoumi M, Chaignepain S, Maglia G, et al.: **A β (1-42) tetramer and octamer structures reveal edge conductivity pores as a mechanism for membrane damage.** *Nat Commun* 2020, **11**:1–14.

35. Nelson R, Sawaya MR, Balbirnie M, Madsen AØ, Riekkel C, Grothe R, Eisenberg D: **Structure of the cross- β spine of amyloid-like fibrils.** *Nature* 2005, **435**:773–778.

36. Sawaya MR, Sambashivan S, Nelson R, Ivanova MI, Sievers SA, Apostol MI, Thompson MJ, Balbirnie M, Wiltzius JJW, McFarlane HT, et al.: **Atomic structures of amyloid cross- β -spines reveal varied steric zippers.** *Nature* 2007, **447**:453–457.
37. Hughes MP, Sawaya MR, Boyer DR, Goldschmidt L, Rodriguez JA, Cascio D, Chong L, Gonen T, Eisenberg DS: **Atomic structures of low-complexity protein segments reveal kinked β sheets that assemble networks.** *Science* 2018, **359**:698–701.
38. Oligomer S, Laganowsky A, Liu C, Sawaya MR, Whitelegge JP, Park J, Zhao M, Pensalfini A, Soriaga AB, Landau M, et al.: **Atomic view of a toxic amyloid.** *Science* 2012, **191**:1228–1232.
39. Sangwan S, Zhao A, Adams KL, Jayson CK, Sawaya MR, Guenther EL, Eisenberg DS: **Atomic structure of a toxic , oligomeric segment of SOD1 linked to amyotrophic lateral sclerosis (ALS).** *Proc Natl Acad Sci USA* 2017, **114**:8770–8775.
40. Sangwan S, Sawaya MR, Murray KA, Hughes MP, Eisenberg DS: **Atomic structures of corkscrew-forming segments of SOD1 reveal varied oligomer conformations.** *Protein Sci* 2018, **27**:1231–1242.
41. Apostol MI, Perry K, Surewicz WK: **Crystal structure of a human prion protein fragment reveals a motif for oligomer formation.** *J Am Chem Soc* 2013, **135**:10202–10205.
42. Hoyer W, Grönwall C, Jonsson A, Ståhl S, Härd T: **Stabilization of a β -hairpin in monomeric Alzheimer's amyloid- β peptide inhibits amyloid formation.** *Proc Natl Acad Sci USA* 2008, **105**:5099–5104.
43. Mirecka EA, Shaykhalishahi H, Gauhar A, Akgül Ş, Lecher J, Willbold D, Stoldt M, Hoyer W: **Sequestration of a β -hairpin for control of α -synuclein aggregation.** *Angew Chemie - Int*

Ed 2014, **53**:4227–4230.

44. Mirecka EA, Feuerstein S, Gremer L, Schröder GF, Stoldt M, Willbold D, Hoyer W: **β -Hairpin of islet amyloid polypeptide bound to an aggregation inhibitor.** *Sci Rep* 2016, **6**:33474.
45. Sandberg A, Luheshi LM, Söllvander S, Pereira de Barros T, Macao B, Knowles TPJ, Biverstål H, Lendel C, Ekholm-Petterson F, Dubnovitsky A, et al.: **Stabilization of neurotoxic Alzheimer amyloid- β oligomers by protein engineering.** *Proc Natl Acad Sci USA* 2010, **107**:15595–15600.
46. Renaud JP, Chari A, Ciferri C, Liu WT, Rémigy HW, Stark H, Wiesmann C: **Cryo-EM in drug discovery: Achievements, limitations and prospects.** *Nat Rev Drug Discov* 2018, **17**:471–492.
47. Ragonis-Bachar P, Landau M: **Functional and pathological amyloid structures in the eyes of 2020 cryo-EM.** *Curr Opin Struct Biol* 2021, **68**:184–193.
48. Yu L, Edalji R, Harlan JE, Holzman TF, Lopez AP, Labkovsky B, Hillen H, Barghorn S, Ebert U, Richardson PL, et al.: **Structural characterization of a soluble amyloid β -peptide oligomer.** *Biochemistry* 2009, **48**:1870–1877.
49. Lendel C, Bjerring M, Dubnovitsky A, Kelly RT, Filippov A, Antzutkin ON, Nielsen NC, Härd T: **A hexameric peptide barrel as building block of amyloid- β protofibrils.** *Angew Chemie - Int Ed* 2014, **53**:12756–12760.
50. Kreutzer AG, Nowick JS: **Elucidating the structures of amyloid oligomers with macrocyclic β -hairpin peptides: Insights into Alzheimer's disease and other amyloid diseases.** *Acc Chem Res* 2018, **51**:706–718.

51. Spencer RK, Li H, Nowick JS: **X-ray crystallographic structures of trimers and higher-order oligomeric assemblies of a peptide derived from A β ₁₇₋₃₆**. *J Am Chem Soc* 2014, **136**:5595–5598.
52. Kreutzer AG, Hamza IL, Spencer RK, Nowick JS: **X-ray crystallographic structures of a trimer, dodecamer, and annular pore formed by an A β ₁₇₋₃₆ β -hairpin**. *J Am Chem Soc* 2016, **138**:4634–4642.
53. Kreutzer AG, Yoo S, Spencer RK, Nowick JS: **Stabilization, assembly, and toxicity of trimers derived from A β** . *J Am Chem Soc* 2017, **139**:966–975.
54. Spencer RK, Kreutzer AG, Salveson PJ, Li H, Nowick JS: **X-ray crystallographic structures of oligomers of peptides derived from β ₂-microglobulin**. *J Am Chem Soc* 2015, **137**:6304–6311.
55. Salveson PJ, Spencer RK, Nowick JS: **X-ray crystallographic structure of oligomers formed by a toxic β -hairpin derived from α -synuclein: trimers and higher-order oligomers**. *J Am Chem Soc* 2016, **138**:4458–4467.
56. Haerianardakani S, Kreutzer AG, Salveson PJ, Samdin TD, Guaglianone GE, Nowick JS: **Phenylalanine mutation to cyclohexylalanine facilitates triangular trimer formation by β -hairpins derived from A β** . *J Am Chem Soc* 2020, **142**:20708–20716.
57. Kreutzer AG, Spencer RK, McKnelly KJ, Yoo S, Hamza IL, Salveson PJ, Nowick JS: **A hexamer of a peptide derived from A β ₁₆₋₃₆**. *Biochemistry* 2017, **56**:6061–6071.
58. Salveson PJ, Spencer RK, Kreutzer AG, Nowick JS: **X-ray crystallographic structure of a compact dodecamer from a peptide derived from A β ₁₆₋₃₆**. *Org Lett* 2017, **19**:3462–3465.
59. Samdin TD, Wierzbicki M, Kreutzer AG, Howitz WJ, Valenzuela M, Smith A, Sahrai V,

Truex NL, Klun M, Nowick JS: **Effects of N-terminal residues on the assembly of constrained β -hairpin peptides derived from A β .** *J Am Chem Soc* 2020, **142**:11593–11601.

60. Kreutzer AG, Samdin TD, Guaglianone G, Spencer RK, Nowick JS: **X-ray crystallography reveals parallel and antiparallel β -sheet dimers of a β -hairpin derived from A β ₁₆₋₃₆ that assemble to form different tetramers.** *ACS Chem Neurosci* 2020, **11**:2340–2347.

61. Wetzel R: **Exploding the repeat length paradigm while exploring amyloid toxicity in Huntington's disease.** *Acc Chem Res* 2020, **53**:2347–2357.

62. Kaye R, Head E, Thompson JL, McIntire TM, Milton SC, Cotman CW, Glabe CG: **Common structure of soluble amyloid oligomers implies common mechanism of pathogenesis.** *Science* 2003, **300**:486–490.

63. Ghosh U, Thurber KR, Yau W-M, Tycko R: **Molecular structure of a prevalent amyloid- β fibril polymorph from Alzheimer's disease brain tissue.** *Proc Natl Acad Sci USA* 2021, **118**:e2023089118.

64. Kawai R, Chiba S, Okuwaki K, Kanada R, Doi H, Ono M, Mochizuki Y, Okuno Y: **Stabilization mechanism for a nonfibrillar amyloid β oligomer based on formation of a hydrophobic core determined by dissipative particle dynamics.** *ACS Chem Neurosci* 2020, **11**:385–394.

65. Piana S, Donchev AG, Robustelli P, Shaw DE: **Water dispersion interactions strongly influence simulated structural properties of disordered protein states.** *J Phys Chem B* 2015, **119**:5113–5123.

66. Man VH, Nguyen PH, Derreumaux P: **High-resolution structures of the amyloid- β 1-42 dimers from the comparison of four atomistic force fields.** *J Phys Chem B* 2017, **121**:5977–

5987.

67. Mehrazma B, Rauk A: **Exploring amyloid- β dimer structure using molecular dynamics simulations.** *J Phys Chem A* 2019, **123**:4658–4670.

68. Strodel B: **Amyloid aggregation simulations: challenges, advances and perspectives.** *Curr Opin Struct Biol* 2021, **67**:145–152.

69. Robustelli P, Piana S, Shaw DE: **Developing a molecular dynamics force field for both folded and disordered protein states.** *Proc Natl Acad Sci USA* 2018, **115**:E4758–E4766.

70. Ferrie JJ, Petersson EJ: **A unified de novo approach for predicting the structures of ordered and disordered proteins.** *J Phys Chem B* 2020, **124**:5538–5548.

71. Salvesson PJ, Haerianardakani S, Thuy-boun A, Yoo S, Kreutzer AG, Demeler B, Nowick JS: **Repurposing triphenylmethane dyes to bind to trimers derived from A β .** *J Am Chem Soc* 2018, **140**:11745–11754.

72. Lv G, Sun A, Wei P, Zhang N, Yi T: **A spiropyran-based fluorescent probe for the specific detection of β -amyloid peptide oligomers in Alzheimer's disease.** *Chem Sci* 2016, **52**:8865–8868.

73. Teoh CL, Su D, Sahu S, Yun S, Drummond E: **Chemical fluorescent probe for detection of A β oligomers.** *J Am Chem Soc* 2015, **137**:13503–13509.

74. Liu H, Qian C, Yang T, Wang Y, Luo J, Zhang C, Wang X, Wang X, Guo Z: **Small molecule-mediated co-assembly of amyloid- β oligomers reduces neurotoxicity through promoting non-fibrillar aggregation.** *Chem Sci* 2020, **11**:7158–7169.

75. Meric G, Robinson AS, Roberts CJ: **Driving forces for nonnative protein aggregation and approaches to predict aggregation-prone regions.** *Annu Rev Chem Biomol Eng* 2017,

8:139–159.

76. Ebo JS, Guthertz N, Radford SE, Brockwell DJ: **Using protein engineering to understand and modulate aggregation.** *Curr Opin Struct Biol* 2020, **60**:157–166.
77. Fernandez-Escamilla AM, Rousseau F, Schymkowitz J, Serrano L: **Prediction of sequence-dependent and mutational effects on the aggregation of peptides and proteins.** *Nat Biotechnol* 2004, **22**:1302–1306.
78. Louros N, Konstantoulea K, Vleeschouwer M De, Ramakers M, Schymkowitz J, Rousseau F: **WALTZ-DB 2.0: an updated database containing structural information of experimentally determined amyloid-forming peptides.** *Nucleic Acids Res* 2020, **48**:D389–D393.
79. Louros N, Orlando G, De Vleeschouwer M, Rousseau F, Schymkowitz J: **Structure-based machine-guided mapping of amyloid sequence space reveals uncharted sequence clusters with higher solubilities.** *Nat Commun* 2020, **11**:1–13.
80. Howitz WJ, Wierzbicki M, Cabanela RW, Saliba C, Motavalli A, Tran N, Nowick JS: **Interpenetrating cubes in the X-ray crystallographic structure of a peptide derived from medin_{19–36}.** *J Am Chem Soc* 2020, **142**:15870–15875.
81. Otzen D, Riek R: **Functional amyloids.** *Cold Spring Harb Perspect Biol* 2019, **11**:pii: a033860.

Chapter 2^b

Effects of *N*-Terminal Residues on the Assembly of Constrained β -Hairpin Peptides Derived from A β

INTRODUCTION

The first 16 residues of the β -amyloid peptide, A β , are thought to be important in the formation of fibrils and oligomers in Alzheimer's disease. These *N*-terminal residues are subject to many important mutations and post-translational modifications, and may interact with other proteins and metal cations.¹⁻⁷ These modifications and interactions have been observed to greatly affect A β fibril formation and oligomerization. Even without modification, these residues—₁DAEFRHDSGYEVHHQK₁₆—represent a significant number of amino acids capable of forming non-covalent interactions within and between monomers of A β , and should thus impact oligomerization.

Further supporting the ostensible importance of the *N*-terminus of A β are studies of the p3 peptide, an alternative cleavage product to full-length A β from the amyloid precursor protein.⁸ The p3 peptide, which lacks residues 1–16 has even been described as “non-amyloidogenic”, incapable of forming oligomers, devoid of any synaptotoxic effect, and

^b This chapter is adapted from Samdin, T.; Wierzbicki, M.; Kreutzer, A.G.; Howitz, W. J.; *et. al.*; Nowick, J. S. Effects of *N*-terminal Residues on the Assembly of Constrained β -Hairpin Peptides Derived from A β . *J. Am. Chem. Soc.* **2020**, *142* (26), 11593–11601.

even neuroprotective.^{9–13} However, a recent review from the Raskatov group has highlighted and summarized inconsistencies within the literature regarding the importance, biophysical, and biological properties of the p3 peptide.^{14–16} In a subsequent investigation, the Raskatov group demonstrated that the p3 peptide is capable of assembling to form amyloidogenic fibrils and toxic oligomers.¹⁷ These recent findings from Raskatov and others have shed some light on the importance of A β _{1–16}.

Elucidating the role of A β _{1–16} in the formation of A β oligomers offers the promise of furthering our understanding of the molecular basis of Alzheimer’s disease. Studying these oligomers is difficult, as these assemblies are heterogeneous—varying in structure, stability, and stoichiometry. Further compounding the challenge of studying A β , is its propensity to form insoluble fibrils, which are more stable than oligomers. A β oligomers are damaging to neurons and are thought to be present in the early stages of Alzheimer’s disease before the emergence of any pathohistological hallmarks or dementia symptoms.^{18–}

21

The assembly of A β oligomers has been tied to the ability of the A β peptide to fold and adopt a β -hairpin conformation.^{22,23} In 2008, Hard and Hoyer determined by NMR spectroscopy that A β _{1–40} adopts a β -hairpin structure when bound to an affibody. In this structure, residues 17–23 and 30–36 hydrogen bond to form an antiparallel β -sheet, with residues 24–29 as a loop, and the *N*- and *C*-terminal residues as unstructured segments. Our own investigations of peptides derived from the central and *C*-terminal regions of A β have revealed that adoption of a β -hairpin conformation primes the peptide to assemble.^{24–29}

In 2016, our laboratory reported peptide **1**, a β -hairpin mimic derived from A β _{16–36} that forms hexamers that can be observed by X-ray crystallography and SDS-PAGE.²⁸ The peptide is cytotoxic toward SH-SY5Y cells, and cytotoxicity correlates with oligomer formation in structure-

activity studies. Peptide **1** contains the heptapeptide fragments A β _{16–22} and A β _{30–36} in the “top” and “bottom” β -strands, that are constrained to an antiparallel β -sheet by two turn units of δ -linked ornithine, δ Orn (**Figure 2.1**).³⁰ The δ Orn that links Glu₂₂ to Ala₃₀ replaces a loop comprising residues 23–29, while the δ Orn that links Lys₁₆ to Val₃₆ helps constrain the peptide to a β -hairpin conformation. We incorporate an *N*-methyl group at the center of the top strand, on Phe₁₉, to prevent uncontrolled aggregation and fibril formation.

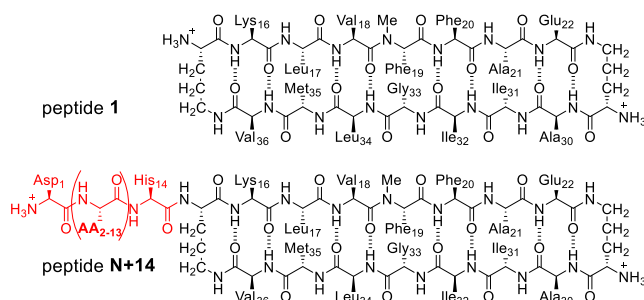


Figure 2.1. Extending the *N*-terminus of peptide **1** to include residues 1–14 as an *N*-terminal tail (red), giving peptide **N+14**. Residues in the tail comprise Asp₁, Ala₂, Glu₃, Phe₄, Arg₅, His₆, Asp₇, Ser₈, Gly₉, Tyr₁₀, Glu₁₁, Val₁₂, His₁₃, and His₁₄.

Although peptide **1** has provided insights into the structure, biophysical, and biological properties of hexamers formed by hydrophobic segments of A β , it lacks the important *N*-terminal region. In our initial report, REMD simulations of peptide **1** suggested that the hexamer could accommodate *N*- and *C*-terminal extensions without steric clashes.²⁸ In this investigation, we set out to test experimentally whether the hexamer could accommodate the *N*-terminus and to study the effects of the *N*-terminus on the structure, biophysical, and biological properties of the hexamer. Here we describe the synthesis of *N*-terminally extended homologues of peptide **1**. These *N*-terminally extended homologues bear “tails” of residues derived from A β _{1–14} and vary in length from 1 to 14 residues. Peptide **N+14**, which contains the entire *N*-terminus, is depicted in **Figure 2.1**. Peptides **1**, **N+14**, and other *N*-terminally extended homologues form hexamers in SDS-PAGE, and trimers and dimers in size exclusion chromatography (SEC). Peptide **N+1**, which contains a tail comprising

A β ₁₄, forms a hexamer composed of dimers and trimers in the X-ray crystallographic structure. These observations are significant because they may help bridge the gap in our knowledge of how A β oligomers assemble in the brain.

RESULTS AND DISCUSSION

Synthesis of Peptide N+14. We synthesized peptide **N+14** by Fmoc-based solid phase peptide synthesis, using Fmoc-Orn(Dde)-OH to incorporate an *N*-terminal tail of residues derived from A β ₁₋₁₄ (**Figure 2.2**). We began the synthesis by attaching Boc-Orn(Fmoc)-OH to 2-chlorotrityl resin. Residues 22 through 2 were then introduced by Fmoc-based SPPS using HCTU as the coupling reagent, with Fmoc-Orn(Dde)-OH replacing residue 15 in the natural sequence of A β . Residue 1 was coupled as Boc-Asp(*t*-Bu)-OH, capping the synthesis of the top strand. The Dde protecting group was then removed with 10% hydrazine in DMF, and residues 36 through 30 were coupled to residue 15 using Fmoc-based SPPS. We found microwave-assisted SPPS to be essential and used it for most of the coupling steps, other than attaching Boc-Orn(Fmoc)-OH to the resin and removing the Dde protecting group.³¹ The final Fmoc protecting group was removed from residue 30, and the acyclic branched peptide was cleaved from the resin with a solution of 20% HFIP in DCM. The peptide was cyclized with PyBop in solution, and deprotected with treatment by trifluoroacetic acid (TFA). Purification by reverse-phase HPLC typically afforded approximately 12 mg peptide **N+14** as the trifluoroacetate salt.^{32,33}

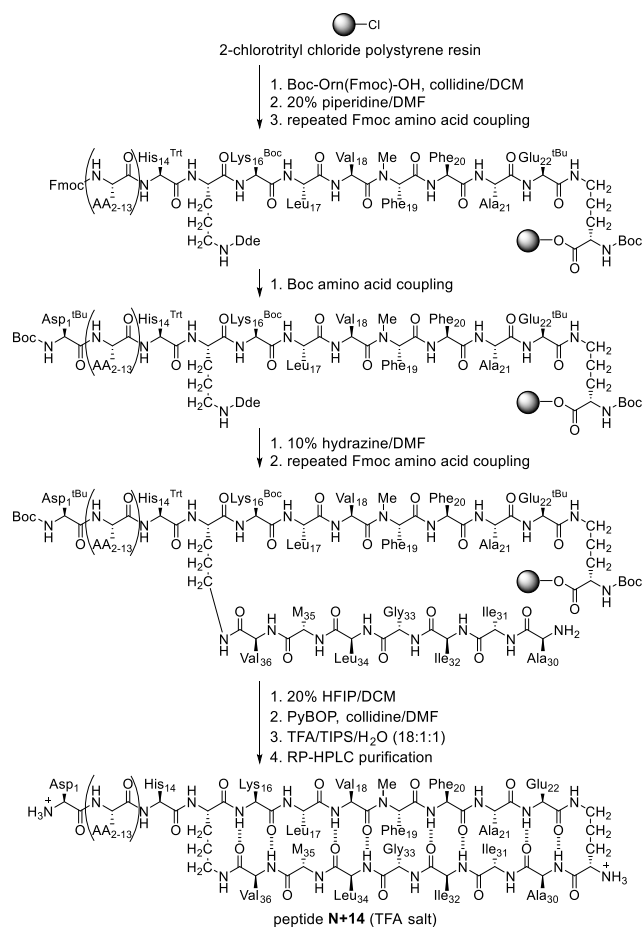


Figure 2.2. Synthesis of the *N*-terminally extended peptide, **N+14** derived from A β ₁₋₃₆.

Oligomerization and Folding of Peptides 1 and N+14. We studied the assembly and folding of peptide **1** and peptide **N+14** by SDS-PAGE, western blot, circular dichroism (CD) spectroscopy, and a cytotoxicity assay with SH-SY5Y cells. Like the A β peptide, peptide **1** and peptide **N+14** assemble to form oligomers in SDS-PAGE. We have previously reported peptide **1** (1.77 kDa) to run in SDS-PAGE with a molecular weight consistent with that of a hexamer (**Figure 2.3A**).²⁸ The band formed by peptide **1** is comet shaped and streaks downward from the 10 kDa ladder band, suggesting that the hexamer may be in rapid equilibrium with lower molecular weight species. An X-ray crystallographic structure of peptide **1** (PDB 5W4H) further corroborates the formation of a hexamer. In contrast to peptide **1**, the *N*-terminally extended homologue peptide **N+14** (3.45 kDa) forms two species by SDS-PAGE, which appear to be in slow equilibrium. One is an oligomer that migrates to just below the 17 kDa ladder band, which we interpret as a hexamer. The other migrates

just above the 4.6 kDa ladder band, which we interpret as a dimer. The hexamer band formed by peptide **N+14** in silver-stained SDS-PAGE is more intense than the putative dimer band, suggesting that this oligomer predominates at the 75 μ M concentration under which the gel was run. These SDS-PAGE studies show that the hexamer can accommodate residues 1–14, but that introduction of these residues appears to substantially reduce the rate of exchange between the hexamer and lower order species.

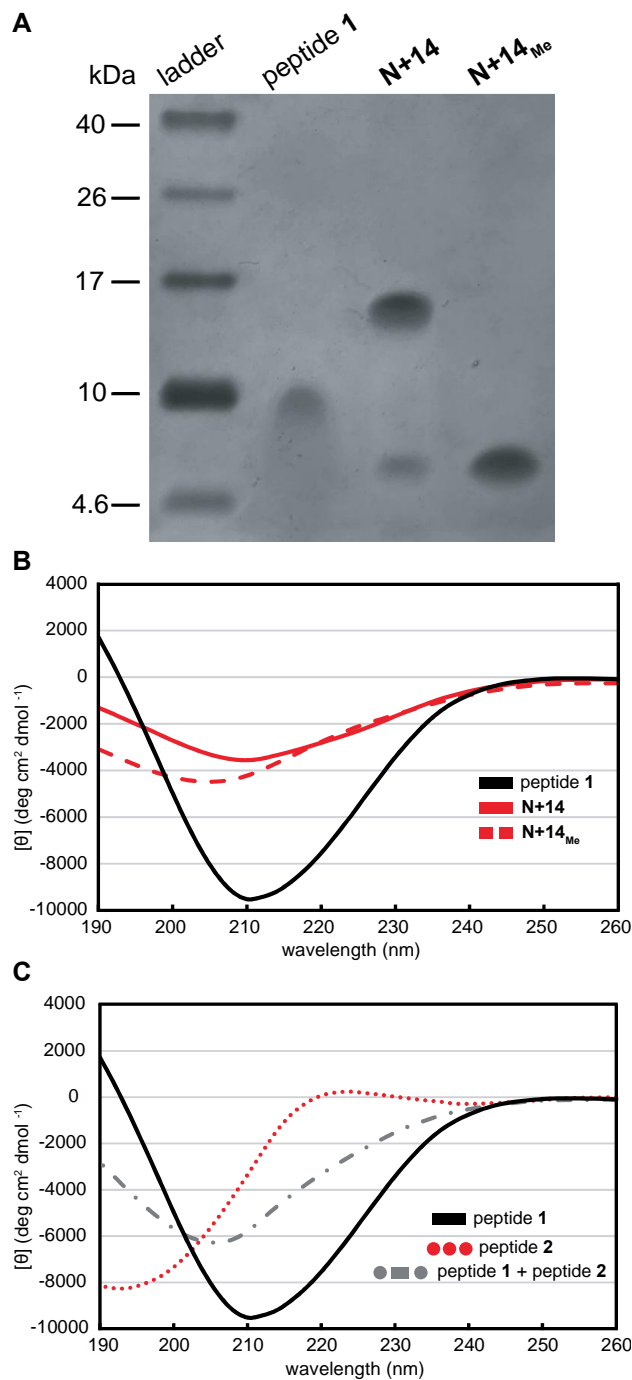


Figure 2.3. (A) Silver stained SDS-PAGE of peptides **1**, **N+14**, and **N+14_{Me}**. SDS-PAGE was performed in Tris buffer at pH 6.8 with 2% (w/v) SDS on a 16% polyacrylamide gel with 75 μ M solutions of peptide in each lane. (B) Circular dichroism (CD) spectra of peptides **1**, **2**, and an equimolar mixture of peptides **1** and **2**. CD spectra were acquired for each peptide at 50 μ M in 10 mM phosphate buffer at pH 7.4; the ellipticity was normalized for the number of residues in each peptide.

To compare the oligomerization of peptide **N+14** to full-length A β , we performed SDS-PAGE in a western blot against A β _{M1-42}, using the 6E10 antibody to visualize the

bands generated by each peptide (**Figure S2.1**).^{34–36} The 6E10 antibody recognizes the *N*-terminal epitope comprising residues Arg₅-His₆-Asp₇, which is shared by both peptide **N+14** and full-length A β .³⁷ A β _{M1–42} shows a strong band for the monomer, as well as weaker bands for oligomers. In contrast, the hexamer band for peptide **N+14** predominates. This difference in oligomerization may reflect the lack of stabilizing conformational constraints in the A β _{M1–42} peptide.²³ In peptide **N+14**, the δ Orn turn units help prime the peptide for assembly by stabilizing a β -hairpin conformation.

In the hexamer formed by peptide **1**, the bottom edges of the monomer subunits hydrogen bond to each other. To test whether peptide **N+14** assembles to form a similar hexamer, we prepared and studied peptide **N+14_{Me}**, a homologue of peptide **N+14** with an additional *N*-methyl group on Gly₃₃ (**Figure 2.4**). In the hexamer formed by peptide **1**, this additional *N*-methyl group has been shown to disrupt hydrogen bonding between Gly₃₃ of one monomer and Ile₃₁ of the adjacent monomer within the dimer subunit, thus interfering with assembly (**Figure S2.2**).^{28,38} If peptide **N+14** assembles to form a hexamer similar to peptide **1**, *N*-methylation of Gly₃₃ should also disrupt assembly of the hexamer. By SDS-PAGE, peptide **N+14_{Me}** migrates as a single band that runs parallel to the putative dimer band formed by peptide **N+14** (**Figure 2.3A**). In contrast to peptide **N+14**, peptide **N+14_{Me}** does not form a hexamer band. The migration of peptide **N+14_{Me}** confirms that *N*-methylation of Gly₃₃ in peptide **N+14** disrupts the assembly of higher order oligomers, and provides further evidence that peptide **N+14** assembles to form a hexamer similar in structure to peptide **1**.

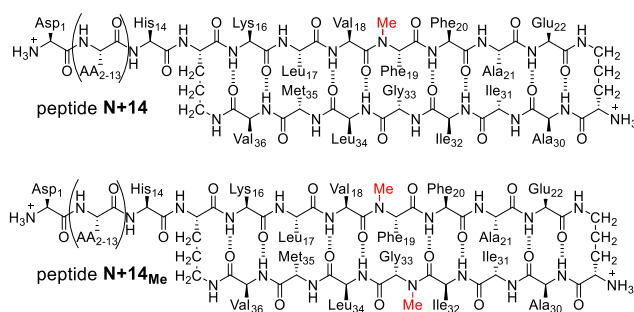


Figure 2. 4. Peptide **N+14_{Me}** is a homologue of peptide **N+14** with an additional *N*-methyl group on Gly₃₃ to block hexamer formation.

Peptide **1** adopts a β -hairpin conformation in the crystallographic hexamer.²⁸ In aqueous solution—where size exclusion chromatography (SEC) studies have shown peptide **1** to exist as a mixture of monomer, dimer, and trimer—circular dichroism (CD) studies suggest that peptide **1** also adopts a β -hairpin conformation (**Figure 2.3B**).²⁸ The CD spectrum of peptide **1** displays a negative band centered at *ca.* 210 nm, with increasing ellipticity at lower wavelengths and a positive ellipticity below 192 nm. To evaluate the ability of peptide **N+14** to adopt a β -hairpin, we compared the CD spectrum of peptide **N+14** to that of peptide **1** (**Figure 2.3B**). The CD spectrum of peptide **N+14** is substantially shallower than the CD spectrum of peptide **1**, with a weaker negative band centered at a slightly lower wavelength and no positive ellipticity above 190 nm. This spectrum appears to reflect an ensemble of β -hairpin and random coil conformations. The CD spectrum of peptide **N+14_{Me}** is similar to that of peptide **N+14**, suggesting that the additional *N*-methyl group on Gly₃₃ does not substantially alter the folding of peptide **N+14_{Me}**.

To better understand the CD spectrum of peptide **N+14**—in particular how residues 1–14 affect the β -hairpin formed by residues 16–22 and 30–36—we synthesized peptide **2**, the *C*-terminal amide of A β ₁₋₁₄ (H-DAEFRHDSGYEVHH-NH₂). The CD spectrum of peptide **2** shows a strong negative band at *ca.* 190 nm and a weak positive band centered at *ca.* 220 nm, reflecting a predominantly random coil conformation (**Figure 2.3C**). To test whether the spectrum of peptide **N+14** represents a linear combination of peptide **1** and

peptide **2**, we combined both peptides in equimolar concentrations and acquired the CD spectrum of the mixture. The CD spectrum of the mixture shows a negative band centered at *ca.* 208 nm with no positive band above 190 nm. Like the CD spectrum of peptide **N+14**, the spectrum of the mixture shows a diminished β -sheet-like conformation relative to peptide **1**.

To evaluate the cytotoxicity of peptide **N+14**, we compared it to peptide **1** in an LDH release assay against neuronally derived SH-SY5Y cells. We had previously reported that peptide **1** was toxic at concentrations of 50 μ M or higher.²⁸ Peptide **N+14** proved less cytotoxic than peptide **1**, even though it contains more residues from the sequence of full-length A β (**Figure S2.3**). The addition of residues 1–14 to peptide **1** does not enhance cytotoxicity, but rather diminishes the cytotoxicity. We envision that the cytotoxicity of peptide **1** is predominantly driven by the hydrophobic residues from the central region of A β , 16–22 and 30–36, and their interactions with cell membranes. These hydrophobic membrane interactions are likely offset by the hydrophilic tail in peptide **N+14**.

Oligomerization and Folding of Shorter N-Terminally Extended Homologues. To gain additional insights into the effects of *N*-terminal extension on the assembly of peptide **1**, we prepared seven additional *N*-terminally extended homologues of peptide **N+14** with shorter *N*-terminal tails: peptides **N+1**, **N+2**, **N+4**, **N+6**, **N+8**, **N+10**, and **N+12** (**Figure 2.5**). The CD spectra of these peptides all show minima between 210 and 220 nm (**Figure 2.6**). The minima are generally deeper for the peptides bearing shorter *N*-terminal extensions (**N+1** through **N+4**) (**Figure 2.6A**), and shallower for the peptides bearing longer *N*-terminal extensions (**N+6** through **N+12**) (**Figure 2.6B**). These differences reflect increased random coil character of the larger *N*-terminal extensions. The depth of the minimum of peptide **N+1** ($\Theta = -6190 \text{ deg cm}^2 \text{ dmol}^{-1}$) is substantially less than that of

peptide **1** ($\Theta = -9516 \text{ deg cm}^2 \text{ dmol}^{-1}$). This difference cannot be explained by a random coil conformation of the additional single residue, but rather suggests that *N*-acylation of the δ -linked ornithine turn unit diminishes the β -sheet folding of the macrocycle.^{39,40}

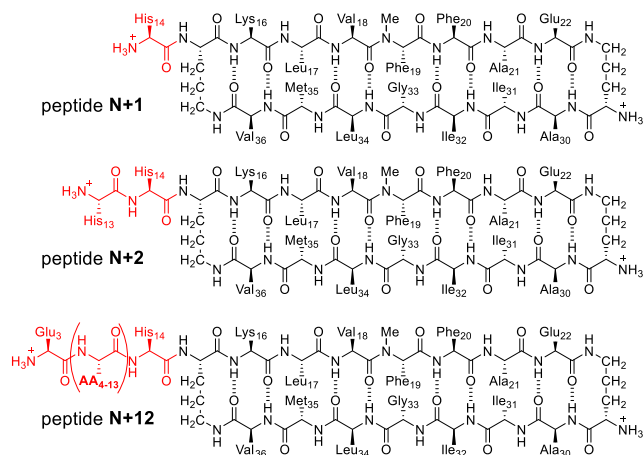


Figure 2.5. Peptides **N+1**, **N+2**, **N+4**, **N+6**, **N+8**, **N+10**, and **N+12** are homologues of peptide **N+14** with truncated tails.

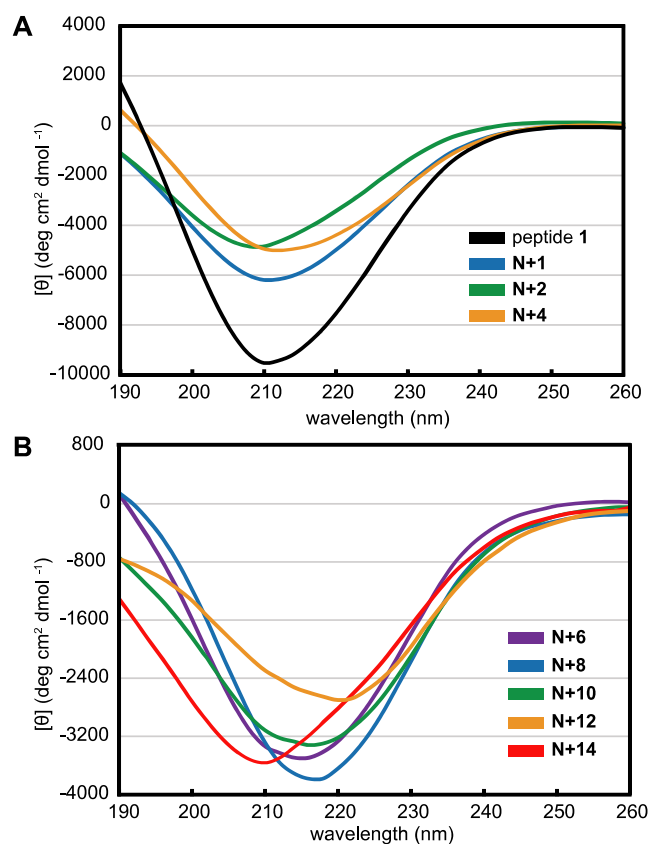


Figure 2.6. CD spectra of peptides **1** and **N+1** through **N+14**. CD spectra were acquired for each peptide at 50 μM in 10 mM phosphate buffer at pH 7.4; ellipticity was normalized for the number of residues in each peptide.

To determine the impact of these *N*-terminal extensions on the oligomerization of peptide **1**, we compared the assembly of peptide **1** and each *N*-terminally extended peptide using SDS-PAGE (**Figure 2.7**). We included trimers **1** and **2** as molecular-weight standards for comparison (**Figures S2.4 and S2.5**). Trimer **1** (5.3 kDa) and trimer **2** (5.3 kDa) are covalently stabilized trimers of β -hairpin peptides that we have previously reported to self-assemble and migrate respectively as 10.6 kDa hexamers and 21.2 kDa dodecamers.²⁶ SDS-PAGE reveals that each *N*-terminally extended peptide migrates as a hexamer. Peptide **1** migrates to approximately the same position as trimer **1**, and each of the longer *N*-terminally extended peptides migrates at a position between the hexamer formed by trimer **1** and the dodecamer formed by trimer **2**. The hexamer formed by peptide **N+1** (1.91 kDa) migrates to the top of the 10 kDa ladder band and streaks downward like peptide **1**.

Similarly, the hexamer formed by peptide **N+2** (2.05 kDa) migrates to just above the 10 kDa ladder band and also streaks downward. The streaking observed for peptides **N+1** and **N+2** suggests that the hexamers formed by each peptide are in equilibrium with smaller oligomers. The hexamer bands formed by peptides **N+4** (2.28 kDa), **N+6** (2.49 kDa), **N+8** (2.69 kDa), **N+10** (2.99 kDa), **N+12** (3.27 kDa), and **N+14** (3.45 kDa) are in comparable or higher positions than peptide **N+2** and migrate as tight bands between the 10 and 17 kDa ladder bands. The tightness of these bands may reflect an increase in hexamer stability that arises from stabilizing non-covalent interactions from the *N*-terminal tail. Peptides **N+2** through **N+14** also show bands at or above the 4.6 kDa ladder band which correspond to the putative dimer.

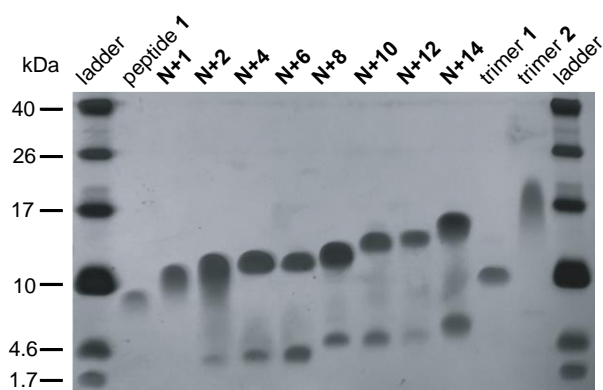


Figure 2.7. Silver stained SDS-PAGE and folding of peptide **1**, peptides **N+1** through **N+14**, and trimers **1** and **2**. SDS-PAGE was performed in Tris buffer at pH 6.8 with 2% (w/v) SDS on a 16% polyacrylamide gel with 75 μ M solutions of peptide in each lane.

To quantitatively assess the relationship between oligomer assembly and migration, we plotted the logarithm of oligomer molecular weights against the relative migration distance (R_f) of the hexamer bands (**Figure 2.8**). The ladder bands exhibit an excellent correlation between log MW and R_f ($R^2 = 0.999$, black), with the exception of the 1.7 kDa ladder band which was excluded from the analysis. The hexamers do not fall on this line, but rather are shifted 12–33% lower than their calculated molecular weights, thus appearing as pentamers or tetramers. The hexamer bands also exhibit a linear relationship between

log MW and R_f , albeit with a poorer fit to a straight line ($R^2 = 0.881$, red). For comparison we also plotted the log MW vs. R_f for the covalently stabilized trimers **1** and **2** (green), which run on the gel as hexamers and dodecamers. These oligomers fall slightly off the line for the ladder bands.

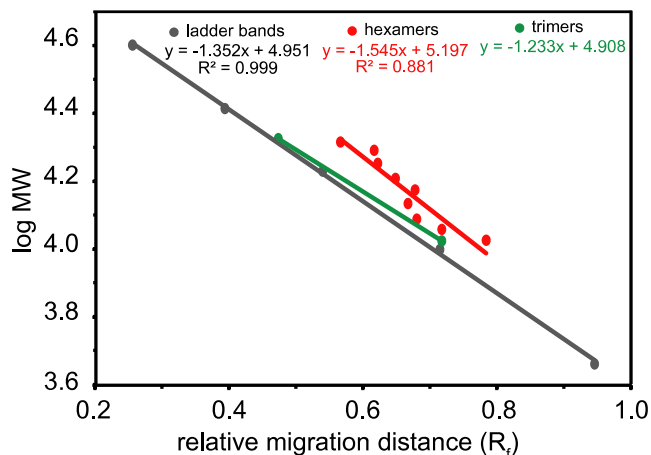


Figure 2.8. Oligomer molecular weights vs. relative migration distance (R_f) of peptide **1** and peptides **N+1** through **N+14** by SDS-PAGE (semi-log plot).

Membrane proteins often migrate by SDS-PAGE at an apparent molecular weight that does not correspond to the actual molecular weight of the protein.^{41–43} Often this “gel shifting” results in a lower apparent molecular weight. This behavior has been well characterized for full-length $A\beta$ and linear truncated variants of $A\beta$, where SDS binding correlates with hydrophobicity rather than the number of amino acids.⁴⁴ The low apparent molecular weights of the hexamer bands may thus reflect gel shifting, causing the hexamer bands to appear as smaller oligomers (pentamers or tetramers).

We used size exclusion chromatography (SEC) to better understand the solution-phase assembly of these *N*-terminally extended peptides. In SEC, peptide **1** does not assemble to form a hexamer (**Figure 2.9**). Peptide **1** elutes as a broad band comprising a large peak at 20.2 mL, a smaller peak at 19.1 mL, and a small peak at 17.9 mL.²⁸ These elution volumes fall at the low molecular weight range of the column, near the size

standards vitamin B12 (1.3 kDa, 19.7 mL) and aprotinin (6.5 kDa, 16.8 mL). Thus, the three peaks from peptide **1** appear to correspond to a monomer, a dimer, and a trimer (1.8 kDa, 3.6 kDa, and 5.3 kDa). Peptides **N+1** through **N+14** also run as broad bands that contain multiple features (**Figure 2.9**). The SEC traces of the *N*-terminally extended homologues exhibit main bands between peptide **1** and the aprotinin size standard and additional minor peaks that elute significantly after peptide **1**. The main bands are composed of several peaks which appear to correspond to monomer, dimer, and trimer. The *N*-terminally extended peptides also exhibit additional peaks that elute after vitamin B12, which may reflect adsorption of the peptides to the column.

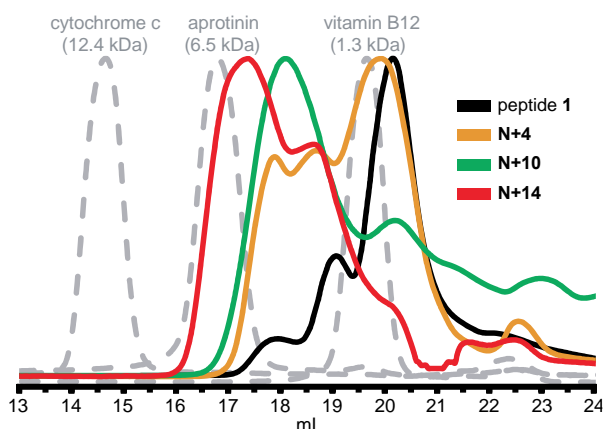


Figure 2.9. SEC traces of peptide **1** and select *N*-terminally extended peptides. SEC was performed on a 1.0 mg/mL solution of each peptide in 50 mM Tris buffer at pH 7.4 with 150 mM NaCl on a Superdex 75 Increase 10/300 column.

The broad band formed by peptide **N+14** shows a different distribution of monomer, dimer, and trimer peaks than peptide **1**. Peptide **N+14** elutes with a large peak at 17.4 mL, a smaller peak at 18.7 mL, and a small shoulder at 20.1 mL (**Figure 2.9**). We interpret these peaks to be the trimer (10.5 kDa), dimer (6.5 kDa), and monomer (3.5 kDa) of peptide **N+14**. The SEC trace of peptide **N+12** resembles the SEC trace of peptide **N+14** (**Figure S 2.6**). The SEC traces of peptides **N+1**, **N+2**, and **N+4** resemble the SEC trace of peptide **1** (**Figure S2.7**). The SEC traces of peptides **N+6**, **N+8**, and **N+10** differ from the SEC

traces of peptide **1** and peptide **N+14** (**Figure S2.8**). The SEC traces of peptides **N+6**, **N+8**, and **N+10** show two peaks, which correspond to a monomer peak and a dimer or trimer peak.

As controls we performed SEC on peptide **2** ($A\beta_{1-14}$, H-DAEFRHDSGYEVHH-NH₂) and peptide **N+14_{Me}**. Peptides **2** and **N+14_{Me}** elute between the vitamin B12 and aprotinin size standards (**Figure S2.9**). Peptide **2** elutes as a narrow band at 17.6 mL that corresponds to a monomer. Peptide **N+14_{Me}** elutes as a broader band at 18.9 mL that may correspond to monomer and/or dimer. Elution volumes for each peptide are summarized in supplementary Table 2.

To better assess the relationship between the assembly and elution volumes amongst the *N*-terminally extended homologues, we plotted the logarithm of the oligomer molecular weight against the elution volumes for peptide **1** and peptides **N+1** through **N+14** (**Figure 2.10**). The resulting graph revealed a linear relationship between the monomer, dimer, and trimer elution volumes, with increasing oligomer size correlating with decreased elution volumes. Collectively, the SEC studies show that at hundred micromolar concentrations, peptide **1** and peptides **N+1** through **N+14** form mixtures of monomers, dimers, and trimers that equilibrate slowly on the 40-minute time scale of the SEC experiment.⁴⁵

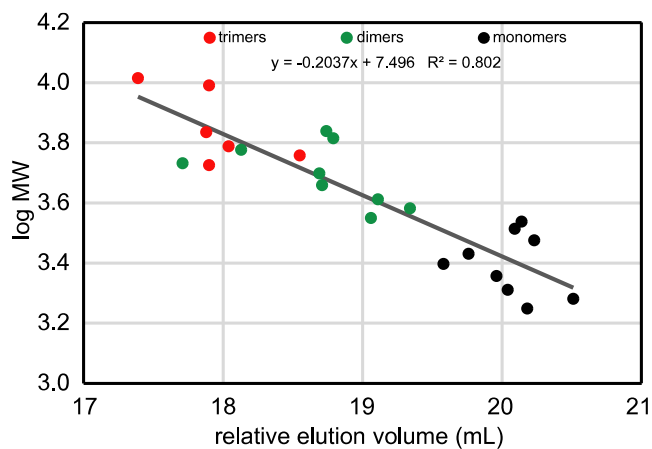


Figure 2.10. Oligomer molecular weights vs. elution volumes of peptide **1** and peptides **N+1** through **N+14** by SEC (semi-log plot). Elution values and oligomer molecular weight are summarized in Supplementary Table 2.

The SDS-PAGE and SEC studies reveal that *N*-terminally extended homologues of peptide **1** can assemble to form oligomers in aqueous environments in the presence or absence of sodium dodecyl sulfate. In SDS-PAGE, peptide **1** and each of the *N*-terminally extended homologues form hexamers. In SEC, peptide **1** and each of the of the *N*-terminally extended homologues do not form hexamers, but rather appear to elute as monomers, dimers, and trimers. The lipophilic environment produced by the SDS micelles in SDS-PAGE appears to drive the assembly of the hexamers.^{46–48}

X-ray crystallographic structure of peptide N+1. X-ray crystallography of peptide **N+1** (PDB 6VU4) corroborates the formation of the hexamers observed in SDS-PAGE (**Figure 2.11**). Peptide **N+1** afforded crystals suitable for X-ray diffraction from an aqueous solution containing 0.1 M HEPES buffer at pH 7.2, 0.2 M sodium citrate, and 25% isopropanol. X-ray diffraction data were collected at a resolution of 2.08 Å. The crystallographic phase determination was carried out through molecular replacement using the structure of peptide **1** (PDB 5W4H) as the search model. Supplementary Table 3 summarizes the crystallographic properties, crystallization conditions, data collection, and model refinement statistics for peptide **N+1**.

In the crystal structure, the asymmetric unit contains two molecules of peptide **N+1** that assemble edge-to-edge to form an out-of-register, antiparallel β -sheet dimer. Each monomer subunit folds to form a twisted β -hairpin stabilized by eight intramolecular hydrogen bonds between the top and bottom β -strands. The dimer itself is stabilized by four intermolecular hydrogen bonds between Ile₃₁ and Gly₃₃ in the bottom strands of both macrocycles (**Figures 2.11A and S2.10**). Three dimers further assemble to form a hexamer—a trimer of dimers—that is nearly identical to the hexamer formed by peptide **1** (**Figure S2.11**). The hexamer can also be interpreted as a dimer of trimers formed through face-to-face packing of two trimers (**Figure 2.11B and S2.10**). Each vertex of the trimer is stabilized by three hydrogen bonds: two between Ala₂₁ and δ Orn, and one between *N*-Me-

Phe₁₉ and Leu₁₇ (a total of nine hydrogen bonds per trimer). The hexamer is further stabilized by the packing of six sets of hydrophobic side chains from Leu₁₇, *N*-Me-Phe₁₉, Ala₂₁, Ile₃₁, and Met₃₅ (**Figure 2.S10**). In each of the two crystallographically independent monomers of peptide **N+1**, His₁₄ is clearly visible in the electron density map, further corroborating that the hexamer can accommodate the *N*-terminal A β residues (**Figure 2.11C**).

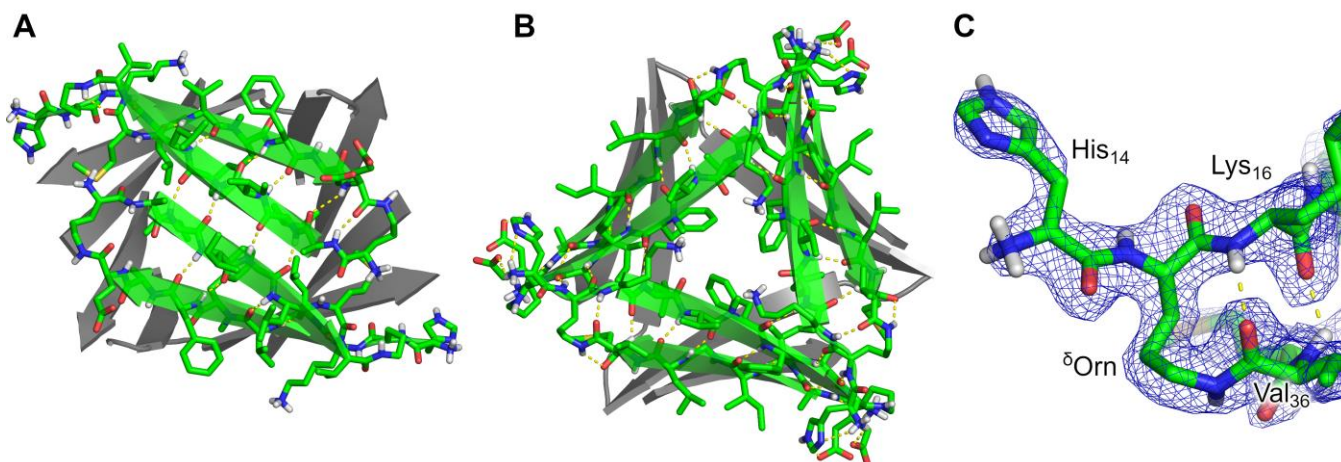


Figure 2.11. X-ray crystallographic structure of the hexamer formed by peptide **N+1** (PDB 6VU4). (A) The dimer subunit within the X-ray crystallographic structure of the hexamer formed by peptide **N+1**. (B) The trimer subunit. (C) 2Fo – Fc electron density map contoured at 1.3σ, showing His₁₄ in peptide **N+1**. R_{work} : 0.22, R_{free} : 0.26, PDB 6VU4.

SUMMARY AND CONCLUSION

To better mimic oligomers of full length Aβ, we have appended residues from Aβ_{1–14} as an *N*-terminal tail to macrocyclic β-hairpin peptide **1**, which comprises Aβ_{16–22} and Aβ_{30–36}. The synthesis of these tailed macrocycles was achieved through an orthogonal protecting group strategy using the amino acid protecting group Dde, in addition to Fmoc and Boc. Circular dichroism revealed that peptide **1** and the *N*-terminally extended homologues adopt β-sheet-like conformations, consistent with a model in which β-hairpins are key components of Aβ oligomers. In aqueous solution, peptide **1** and the *N*-terminally extended homologues form dimers and trimers in SEC, and hexamers in SDS-PAGE. The observations of dimers, trimers, and hexamers in solution are recapitulated in the X-ray crystallographic structure of peptide **N+1**. The consistent formation of hexamers by peptide **1** and the *N*-terminally extended homologues suggests that the *N*-terminus of Aβ does not substantially modify or impede the assembly of oligomers derived from Aβ_{1–36}. These findings are surprising in light of the purported importance of the *N*-terminus in the aggregation of Aβ in Alzheimer’s disease as they support a model in which the *N*-terminus is not critical for the assembly of Aβ oligomers.

ASSOCIATED CONTENT

Supporting Information

The Supporting Information is available free of charge on the ACS Publications website at <http://pubs.acs.org/>.

(1) Procedures for the synthesis of peptides **1**, **N+1** through **N+14**, **N+14_{Me}**, SDS-PAGE and silver staining, western blot analysis, circular dichroism studies, LDH-release assays, and size exclusion chromatography; (2) details of X-ray crystallographic data collection, processing, and refinement; (3) characterization data for peptide **N+1** (PDF). Crystallographic data for peptide **N+1** (cif file).

Crystallographic coordinates of peptide **N+1** were deposited into the Protein Data Bank (PDB) with code 6VU4.

AUTHOR INFORMATION

Corresponding Author

jsnowick@uci.edu

ORCID

Tuan D. Samdin: 0000-0003-3516-9175

Michał Wierzbicki: 0000-0002-9217-634X

Adam G. Kreutzer: 0000-0002-9724-6298

William J. Howitz: 0000-0001-6323-7126

Nicholas L. Truex: 0000-0002-7369-685X

James S. Nowick: 0000-0002-2273-1029

Notes

The authors declare no competing financial interest.

ACKNOWLEDGMENTS

We thank the National Institutes of Health (NIH) National Institute of General Medical Sciences (NIGMS) for funding (GRANT GM097562). We also thank the Laser Spectroscopy Labs at the University of California, Irvine for assistance with circular dichroism measurements. M.W. acknowledges the support from the Ministry of Science and Higher Education, Republic of Poland (Mobility Plus grant no. 1647/MOB/V/2017/0).

REFERENCES AND NOTES

- (1) Murray, B.; Sharma, B.; Belfort, G. N-Terminal Hypothesis for Alzheimer's Disease. *ACS Chem. Neurosci.* **2017**, *8* (3), 432–434. <https://doi.org/10.1021/acschemneuro.7b00037>.
- (2) Kepp, K. P. Bioinorganic Chemistry of Alzheimer's Disease. *Chem. Rev.* **2012**, *112* (10), 5193–5239. <https://doi.org/10.1021/cr300009x>.
- (3) Przygońska, K.; Pacewicz, M.; Sadowska, W.; Poznański, J.; Bal, W.; Dadlez, M. His6, His13, and His14 Residues in A β 1 – 40 Peptide Significantly and Specifically Affect Oligomeric Equilibria. **2019**, No. June, 1–13. <https://doi.org/10.1038/s41598-019-45988-1>.
- (4) Przygońska, K.; Poznański, J.; Mistarz, U. H.; Rand, K. D.; Dadlez, M. Side-Chain Moieties from the N-Terminal Region of A β Are Involved in an Oligomer-Stabilizing Network of Interactions. *PLoS One* **2018**, *13* (8), 1–25. <https://doi.org/10.1371/journal.pone.0201761>.
- (5) Sofola-Adesakin, O.; Khericha, M.; Snoeren, I.; Tsuda, L.; Partridge, L. PGLuA β Increases Accumulation of A β in Vivo and Exacerbates Its Toxicity. *Acta Neuropathol. Commun.* **2016**, *4* (1), 109. <https://doi.org/10.1186/s40478-016-0380-x>.
- (6) Jawhar, S.; Wirths, O.; Bayer, T. A. Pyroglutamate Amyloid- β (A β): A Hatchet Man in Alzheimer Disease. *J. Biol. Chem.* **2011**, *286* (45), 38825–38832. <https://doi.org/10.1074/jbc.R111.288308>.
- (7) Kummer, M. P.; Heneka, M. T. Truncated and Modified Amyloid-Beta Species. *Alzheimer's Res. Ther.* **2014**, *6* (3), 1–9. <https://doi.org/10.1186/alzrt258>.
- (8) Moghekar, A.; Rao, S.; Li, M.; Ruben, D.; Mammen, A.; Tang, X.; Brien, R. J. O. Large Quantities of A β Peptide Are Constitutively Released during Amyloid Precursor Protein Metabolism in Vivo and in Vitro. **2011**, *286* (18), 15989–15997. <https://doi.org/10.1074/jbc.M110.191262>.
- (9) Walsh, D. M.; Klyubin, I.; Fadeeva, J. V.; Cullen, W. K.; Anwyl, R.; Wolfe, M. S.; Rowan, M. J.; Selkoe, D. J. Naturally Secreted Oligomers of Amyloid Beta Protein Potently Inhibit Hippocampal Long-Term Potentiation in Vivo. *Nature* **2002**, *416* (6880), 535–539.
- (10) Dulin, F.; Léveillé, F.; Ortega, J. B.; Mornon, J. P.; Buisson, A.; Callebaut, I.; Colloc'h, N. P3 Peptide, a Truncated Form of A β Devoid of Synaptotoxic Effect, Does Not Assemble into Soluble Oligomers. *FEBS Lett.* **2008**, *582* (13), 1865–1870. <https://doi.org/10.1016/j.febslet.2008.05.002>.
- (11) Näslund, J.; Jensen, M.; Tjernberg, L. O.; Thyberg, J.; Terenius, L.; Nordstedt, C. The Metabolic Pathway Generating P3, an A β -Peptide Fragment, Is Probably Non-Amyloidogenic. *Biochemical and Biophysical Research Communications*. 1994, pp 780–787. <https://doi.org/10.1006/bbrc.1994.2527>.
- (12) Nhan, H. S.; Chiang, K.; Koo, E. H. The Multifaceted Nature of Amyloid Precursor Protein and Its Proteolytic Fragments: Friends and Foes. *Acta Neuropathol.* **2015**, *129* (1),

- 1–19. <https://doi.org/10.1007/s00401-014-1347-2>.
- (13) Han, W.; Ji, T.; Mei, B.; Su, J. Peptide P3 May Play a Neuroprotective Role in the Brain. *Med. Hypotheses* **2011**, *76* (4), 543–546. <https://doi.org/10.1016/j.mehy.2010.12.013>.
- (14) Kuhn, A. J.; Raskatov, J. Is the P3 (AB17-40, AB17-42) Peptide Relevant to the Pathology of Alzheimer’s Disease? *J. Alzheimer’s Dis.* **2020**, *74* (1).
- (15) Pike, C. J.; Overman, M. J.; Cotman, C. W. Amino-Terminal Deletions Enhance Aggregation of β -Amyloid Peptides in Vitro. *J. Biol. Chem.* **1995**, 23895–23898.
- (16) Lalowski, M.; Golabek, A.; Lemere, C. A.; Selkoe, D. J.; Wisniewski, H. M.; Beavis, R. C.; Frangione, B.; Wisniewski, T. The “Nonamyloidogenic” P3 Fragment (Amyloid B17-42) Is a Major Constituent of Down’s Syndrome Cerebellar Preamyloid. *J. Biol. Chem.* **1996**, *271* (52), 33623–33631. <https://doi.org/10.1074/jbc.271.52.33623>.
- (17) Kuhn, A. J.; Abrams, B. S.; Knowlton, S.; Raskatov, J. A. The Alzheimer’s Disease “Non-Amyloidogenic” P3 Peptide Revisited: A Case for Amyloid- α . *ACS Chem. Neurosci.* **2020**. <https://doi.org/10.1021/acchemneuro.0c00160>.
- (18) Cline, E. N.; Bicca, M. A.; Viola, K. L.; Klein, W. L. The Amyloid- β Oligomer Hypothesis: Beginning of the Third Decade. *J. Alzheimer’s Dis.* **2018**, *64* (s1), S567–S610. <https://doi.org/10.3233/JAD-179941>.
- (19) Ferreira, S. T.; Lourenco, M. V.; Oliveira, M. M.; De Felice, F. G. Soluble Amyloid-B Oligomers as Synaptotoxins Leading to Cognitive Impairment in Alzheimer’s Disease. *Front. Cell. Neurosci.* **2015**, *9* (May), 1–17. <https://doi.org/10.3389/fncel.2015.00191>.
- (20) Benilova, I.; Karran, E.; De Strooper, B. The Toxic A β Oligomer and Alzheimer’s Disease: An Emperor in Need of Clothes. *Nat. Neurosci.* **2012**, *15* (3), 349–357. <https://doi.org/10.1038/nn.3028>.
- (21) Selkoe, D. J.; Hardy, J. The Amyloid Hypothesis of Alzheimer’s Disease at 25 Years. *EMBO Mol. Med.* **2016**, *8* (6), 595–608. <https://doi.org/10.15252/emmm.201606210>.
- (22) Hoyer, W.; Gronwall, C.; Jonsson, A.; Stahl, S.; Hard, T. Stabilization of a β -Hairpin in Monomeric Alzheimer’s Amyloid- β Peptide Inhibits Amyloid Formation. *Proc. Natl. Acad. Sci.* **2008**, *105* (13), 5099–5104. <https://doi.org/10.1073/pnas.0711731105>.
- (23) Sandberg, A.; Luheshi, L. M.; Sollvander, S.; Pereira de Barros, T.; Macao, B.; Knowles, T. P. J.; Biverstal, H.; Lendel, C.; Ekholm-Petterson, F.; Dubnovitsky, A.; Lannfelt, L.; Dobson, C. M.; Hard, T. Stabilization of Neurotoxic Alzheimer Amyloid- β Oligomers by Protein Engineering. *Proc. Natl. Acad. Sci. U.S.A* **2010**, *107* (35), 15595–15600. <https://doi.org/10.1073/pnas.1001740107>.
- (24) Spencer, R. K.; Li, H.; Nowick, J. S. X-Ray Crystallographic Structures of Trimers and Higher-Order Oligomeric Assemblies of a Peptide Derived from A β 17-36. *J. Am. Chem. Soc.* **2014**, *136* (15), 5595–5598. <https://doi.org/10.1021/ja5017409>.
- (25) Kreutzer, A. G.; Hamza, I. L.; Spencer, R. K.; Nowick, J. S. X-Ray Crystallographic

- Structures of a Trimer, Dodecamer, and Annular Pore Formed by an A β 17-36 β -Hairpin. *J. Am. Chem. Soc.* **2016**, *138* (13), 4634–4642. <https://doi.org/10.1021/jacs.6b01332>.
- (26) Kreutzer, A. G.; Yoo, S.; Spencer, R. K.; Nowick, J. S. Stabilization, Assembly, and Toxicity of Trimers Derived from A β . *J. Am. Chem. Soc.* **2017**, *139* (2), 966–975. <https://doi.org/10.1021/jacs.6b11748>.
- (27) Salveson, P. J.; Spencer, R. K.; Kreutzer, A. G.; Nowick, J. S. X-Ray Crystallographic Structure of a Compact Dodecamer from a Peptide Derived from A β 16–36. *Org. Lett* **2017**, *19*, 3465. <https://doi.org/10.1021/acs.orglett.7b01445>.
- (28) Kreutzer, A. G.; Spencer, R. K.; McKnelly, K. J.; Yoo, S.; Hamza, I. L.; Salveson, P. J.; Nowick, J. S. A Hexamer of a Peptide Derived from A β 16-36. *Biochemistry* **2017**, *56* (45), 6061–6071. <https://doi.org/10.1021/acs.biochem.7b00831>.
- (29) Kreutzer, A. G.; Nowick, J. S. Elucidating the Structures of Amyloid Oligomers with Macrocyclic β -Hairpin Peptides: Insights into Alzheimer's Disease and Other Amyloid Diseases. *Acc. Chem. Res.* **2018**, *51* (3), 706–718. <https://doi.org/10.1021/acs.accounts.7b00554>.
- (30) Nowick, J. S.; Brower, J. O. A New Turn Structure for the Formation of ??-Hairpins in Peptides. *J. Am. Chem. Soc.* **2003**, *125* (4), 876–877. <https://doi.org/10.1021/ja028938a>.
- (31) Attempts to synthesize peptide **N+14** by manual coupling at room temperature resulted in poor resin swelling and complex mixtures of products containing only traces of peptide **N+14**.
- (32) The use of uronium coupling agents during macrolactamization results in the formation of a tetramethylguanidinylated adduct as an impurity that is difficult to separate from the desired peptide. The use of the phosphonium coupling agent PyBOP circumvents this problem.
- (33) Albericio, F.; Bofill, J. M.; El-Faham, A.; Kates, S. A. Use of Onium Salt-Based Coupling Reagents in Peptide Synthesis. *J. Org. Chem.* **1998**, *63* (26), 9678–9683. <https://doi.org/10.1021/jo980807y>.
- (34) A β _{M1-42} is an expressed homologue of A β ₁₋₄₂ that bears an additional methionine at the *N*-terminus and exhibits similar aggregation properties to A β ₁₋₄₂.
- (35) Yoo, S.; Zhang, S.; Kreutzer, A. G.; Nowick, J. S. An Efficient Method for the Expression and Purification of A β (M1-42). *Biochemistry* **2018**, *57* (26), 3861–3866. <https://doi.org/10.1021/acs.biochem.8b00393>.
- (36) Walsh, D. M.; Thulin, E.; Minogue, A. M.; Gustavsson, N.; Pang, E.; Teplow, D. B.; Linse, S. A Facile Method for Expression and Purification of the Alzheimer's Disease-Associated Amyloid β -Peptide. *FEBS J.* **2009**, *276* (5), 1266–1281. <https://doi.org/10.1111/j.1742-4658.2008.06862.x>.
- (37) Baghallab, I.; Reyes-Ruiz, J. M.; Abulnaja, K.; Huwait, E.; Glabe, C. Epitomic Characterization of the Specificity of the Anti-Amyloid A β Monoclonal Antibodies 6E10

- and 4G8. *J. Alzheimer's Dis.* **2018**, *66* (3), 1235–1244. <https://doi.org/10.3233/JAD-180582>.
- (38) Salvesson, P. J.; Haerianardakani, S.; Thuy-Boun, A.; Kreutzer, A. G.; Nowick, J. S. Controlling the Oligomerization State of A β -Derived Peptides with Light. *J. Am. Chem. Soc.* **2018**, *140* (17), 5842–5852. <https://doi.org/10.1021/jacs.8b02658>.
- (39) Woods, R. J.; Brower, J. O.; Castellanos, E.; Hashemzadeh, M.; Khakshoor, O.; Russu, W. A.; Nowick, J. S. Cyclic Modular β -Sheets. *J. Am. Chem. Soc.* **2007**, *129* (9), 2548–2558. <https://doi.org/10.1021/ja0667965>.
- (40) The minima of the *N*-terminally extended homologues are substantially shallower than that of peptide **1**. Out of concern that the weaker minima might reflect substantial differences in concentration across the samples, we measured the absorbance of each peptide at 214 nm (A_{214}) and normalized for number of residues (*n*). The A_{214}/n values of each peptide (peptides **N+1** through **N+14**) were all within $\pm 17\%$ of the A_{214}/n value of peptide **1**. These data are summarized in Table S1 in the Supporting Information.
- (41) Rath, A.; Glibowicka, M.; Nadeau, V. G.; Chen, G.; Deber, C. M. Detergent Binding Explains Anomalous SDS-PAGE Migration of Membrane Proteins. **2009**, *106* (6), 1760–1765.
- (42) Tulumello, D. V.; Deber, C. M. SDS Micelles as a Membrane-Mimetic Environment for Transmembrane Segments. **2009**, 12096–12103. <https://doi.org/10.1021/bi9013819>.
- (43) Shi, Y.; Mowery, R. A.; Ashley, J.; Hentz, M.; Ramirez, A. J.; Bilgicer, B.; Slunt-brown, H.; Borchelt, D. R.; Shaw, B. F. Abnormal SDS-PAGE Migration of Cytosolic Proteins Can Identify Domains and Mechanisms That Control Surfactant Binding. **2012**, *21*, 5–7. <https://doi.org/10.1002/pro.2107>.
- (44) Kawooya, J. K.; Emmons, T. L.; Gonzalez-dewhitt, P. A.; Camp, M. C.; Andrea, S. C. D. Electrophoretic Mobility of Alzheimers Amyloid- β Peptides in Urea – Sodium Dodecyl Sulfate – Polyacrylamide Gel Electrophoresis. **2003**, *323*, 103–113. <https://doi.org/10.1016/j.ab.2003.08.027>.
- (45) Solutions of peptide **1** and peptides **N+1** through **N+14** were prepared at 1.0 mg/mL (0.2 – 0.5 mM) in Tris buffer. Insoluble material was removed by centrifugation prior to injection onto the SEC column. The actual concentrations after centrifugation were estimated to be between 50 and 100 μ M on the basis of absorbance at 214 nm (Supplementary Table 2).
- (46) Nowick, J. S.; Chen, J. S. Molecular Recognition in Aqueous Micellar Solution: Adenine-Thymine Base-Pairing in SDS Micelles. *J. Am. Chem. Soc.* **1992**, *114* (3), 1107–1108. <https://doi.org/10.1021/ja00029a060>.
- (47) Nowick, J. S.; Chen, J. S.; Noronha, G. Molecular Recognition in Micelles: The Roles of Hydrogen Bonding and Hydrophobicity in Adenine-Thymine Base-Pairing in SDS Micelles. *J. Am. Chem. Soc.* **1993**, *115* (17), 7636–7644. <https://doi.org/10.1021/ja00070a007>.

- (48) Nowick, J. S.; Cao, T.; Noronha, G. Molecular Recognition between Uncharged Molecules in Aqueous Micelles. *J. Am. Chem. Soc.* **1994**, *116* (8), 3285–3289. <https://doi.org/10.1021/ja00087a014>.

Supporting information for:

**Effects of *N*-Terminal Residues on the Assembly of Constrained β -Hairpin Peptides
Derived from A β**

Contents

Supporting Figures and Tables	57
Figure S2.1	57
Figure S2.2	58
Figure S2.3	59
Supplementary Table 2.1	59
Figure S2.4	61
Figure S2.5	62
Figure S2.6	63
Figure S2.7	63
Figure S2.8	64
Figure S2.9	64
Supplementary Table 2.2	65
Figure S2.10	66
Figure S2.11	67
Supplementary Table 2.3	68
Materials and Methods ¹	69
<i>General information</i>	69
<i>Synthesis of peptide N+14</i>	70
<i>SDS-PAGE silver staining and western blot</i>	73
<i>Circular dichroism spectroscopy</i>	75
<i>Size exclusion chromatography</i>	75
<i>LDH release assays</i>	76
<i>Crystallization of peptide N+1</i>	77
<i>X-ray crystallographic data collection, data processing, and structure determination of N+1</i>	78
Characterization Data	80
<i>Characterization of peptide 1</i>	80
<i>Characterization of N+1</i>	82
<i>Characterization of N+4</i>	86
<i>Characterization of N+6</i>	88
<i>Characterization of N+8</i>	90

<i>Characterization of N+10</i>	92
<i>Characterization of N+12</i>	94
<i>Characterization of N+14</i>	96
<i>Characterization of N+14_{Me}</i>	98
<i>Characterization of peptide 2</i>	100

Supporting Figures and Tables

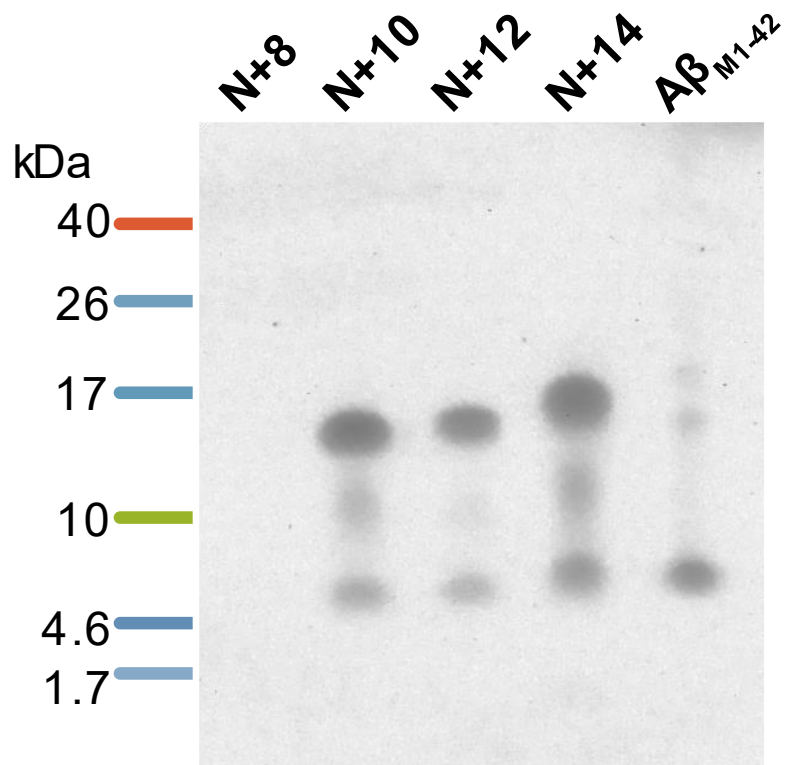


Figure S2.1. Western blot analysis of peptides N+8, N+10, N+12, N+14, and A β_{M1-42} using the 6E10 antibody.

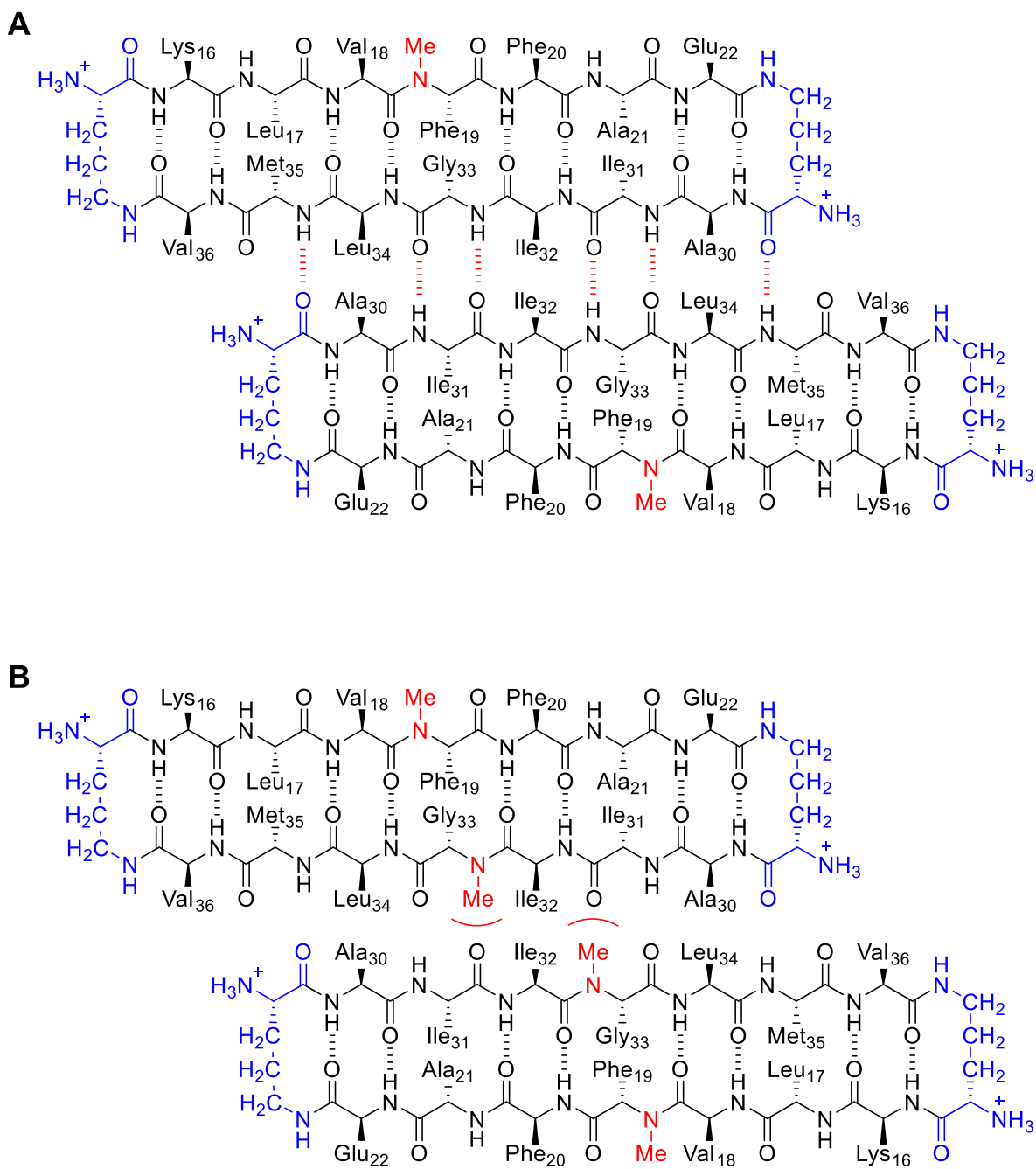


Figure S2.2. (A) The dimer subunit of the hexamer formed by peptide **1**. (B) *N*-Methylation of Gly₃₃ disrupts hydrogen bonding within the dimer subunit, and thus prevents assembly of the hexamer.

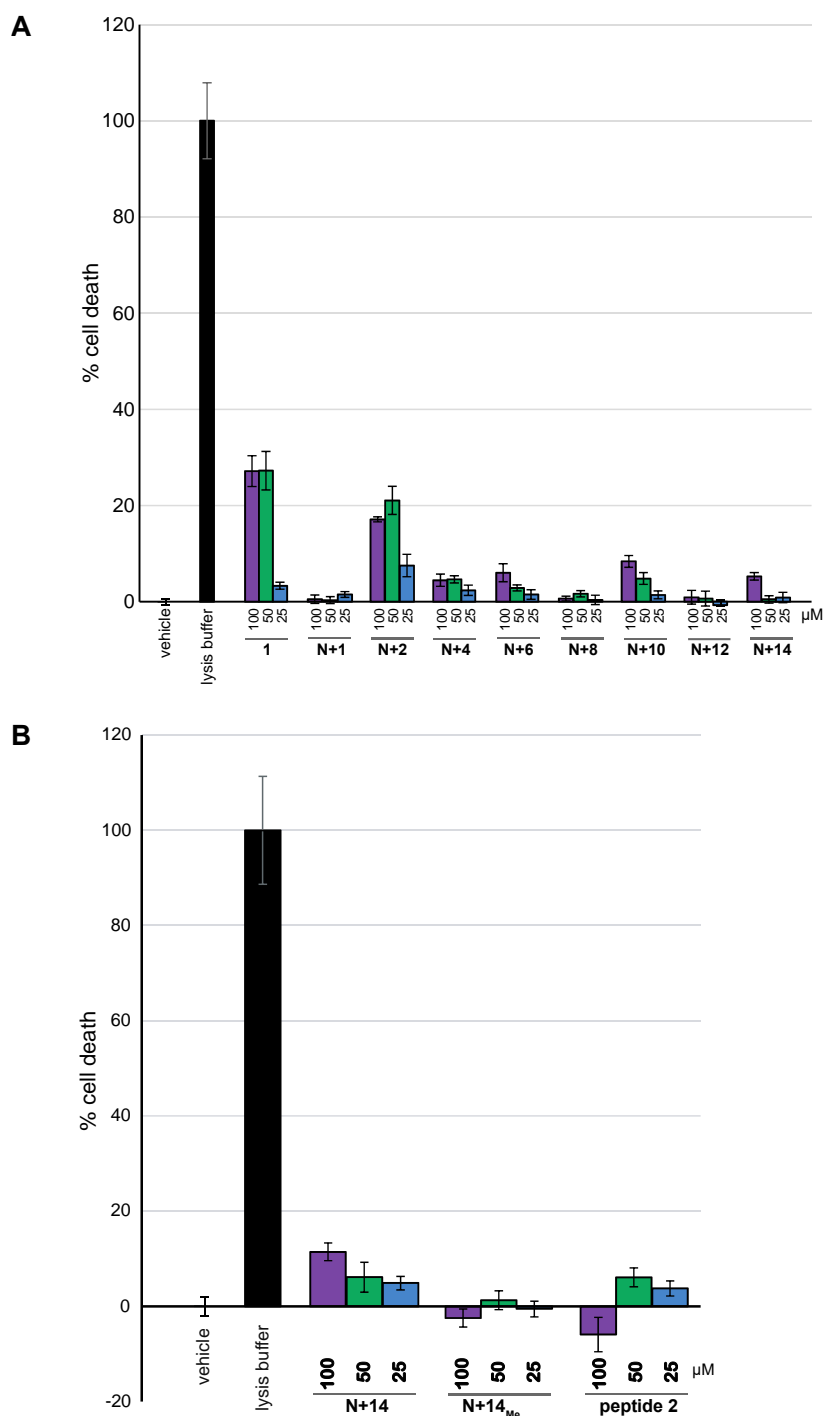


Figure S2.3. (A) Cytotoxicity of peptide 1 and the *N*-terminally extended homologues against SH-SY5Y cells, as assessed by an LDH release assay. Incorporation of the *N*-terminal residues of $A\beta$ did not increase toxicity. Data represent the mean of four replicate wells \pm the standard deviation. Deionized water (vehicle) was used as a negative control. (B) LDH release assay of peptides N+14, N+14_{Me}, and 2.

Supplementary Table 2.1. Normalized absorbance values and calculated percent differences of circular dichroism samples relative to peptide 1.

peptide	Abs _{214 nm}	Abs _{214 nm/n}	% diff.
1	0.186566263	0.011660391	0
2	0.390456799	0.013015227	11.61
3	0.140225015	0.010016073	-14.10
N+1	0.195346737	0.011490985	-1.45
N+2	0.221505983	0.012305888	5.53
N+4	0.267023077	0.013351154	14.50
N+6	0.243538737	0.011069943	-5.06
N+8	0.311190368	0.012966265	11.19
N+10	0.349382999	0.013437808	15.24
N+12	0.363346815	0.012976672	11.28
N+14	0.410958172	0.013698606	17.48

Out of concern that the differences observed between the circular dichroism (CD) spectra of peptide **1** and the *N*-terminally extended homologues might reflect differences in concentration across the samples, we corroborated the concentration of each sample by measuring the absorbance of each solution at 214 nm (A_{214}). A 10 mg/mL stock solution of each peptide was first prepared using deionized water. The stock solution was diluted with 10 mM sodium phosphate buffer at pH 7.4 to produce a 50 μ M solution of each peptide, and the absorbance at 214 nm was measured in a 1 mm quartz cuvette using Cary-60 spectrophotometer. The cuvette was immediately transferred to a Jasco J-810 circular dichroism spectropolarimeter, and the CD spectrum of the peptide was acquired, as described below. The A_{214} measurements were normalized for the number of residues (*n*) in each peptide. The A_{214}/n values of each peptide (peptides **N+1** through **N+14**) were all within $\pm 17\%$ of the A_{214}/n value of peptide **1**.

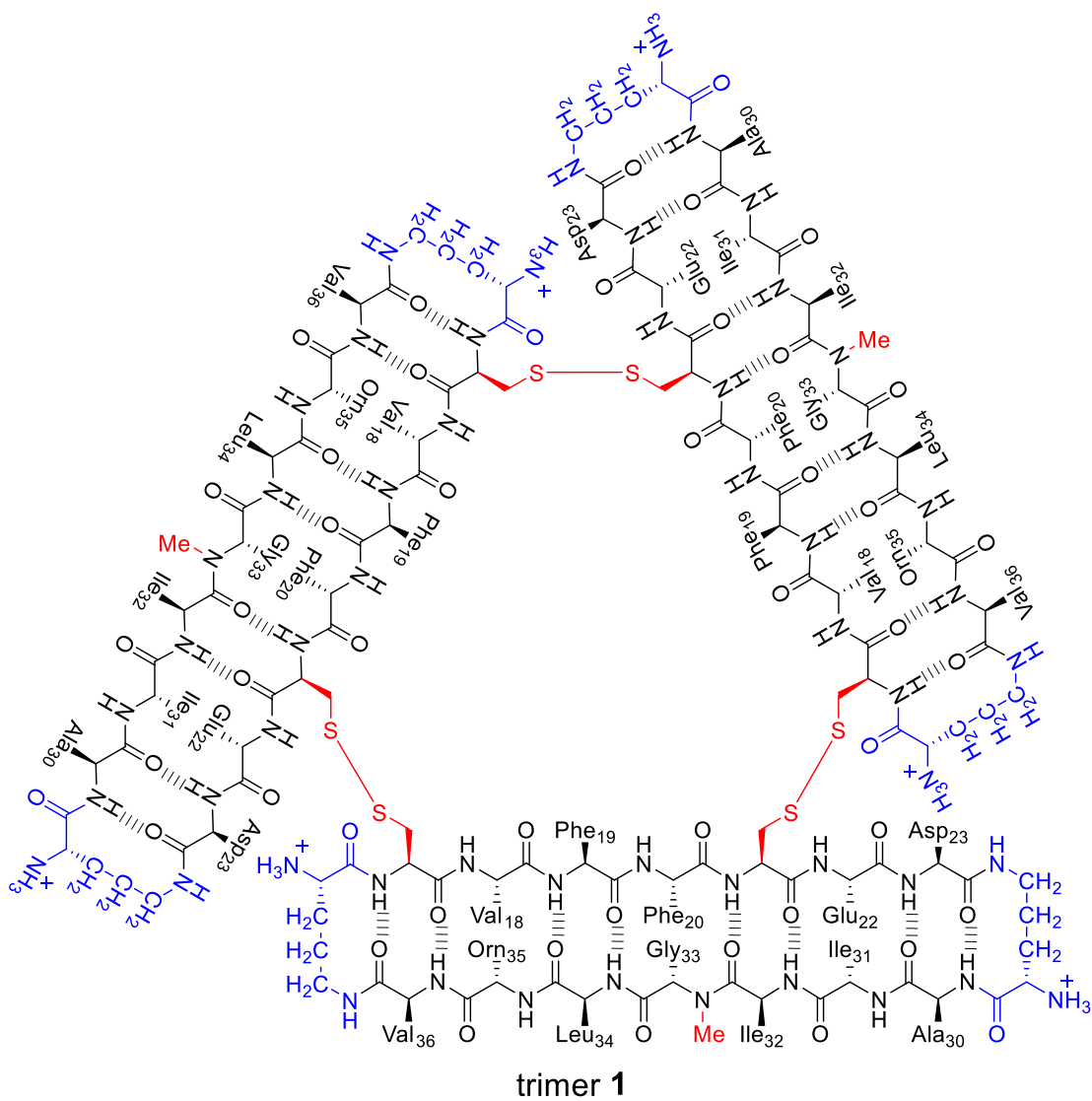


Figure S2.4. Covalently stabilized trimer 1. Trimer 1 assembles to form a hexamer in SDS-PAGE.

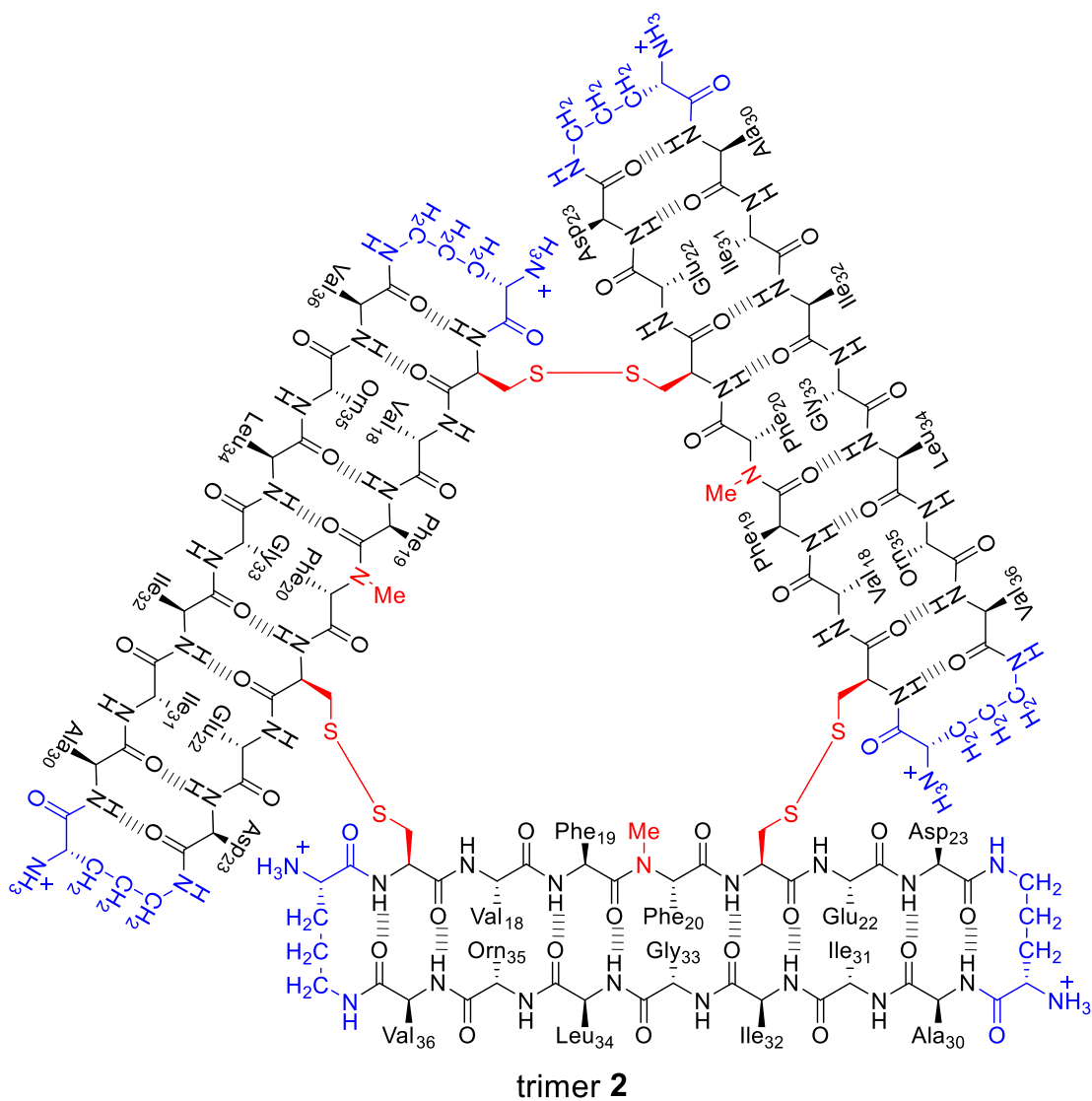


Figure S2.5. Covalently stabilized trimer 2. Trimer 2 assembles to form a dodecamer in SDS-PAGE.

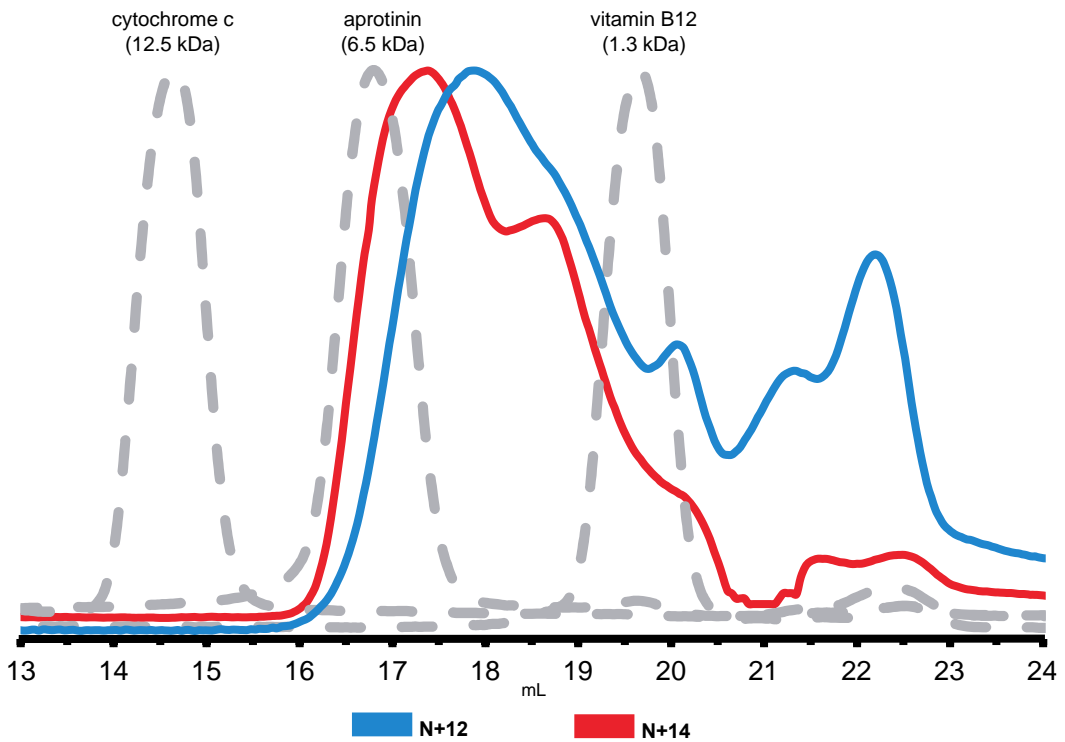


Figure S2.6. SEC traces of peptides N+12 and N+14. SEC was performed on a 1.0 mg/mL solution of each peptide in 50 mM Tris buffer at pH 7.4 with 150 mM NaCl on a Superdex 75 Increase 10/300 column.

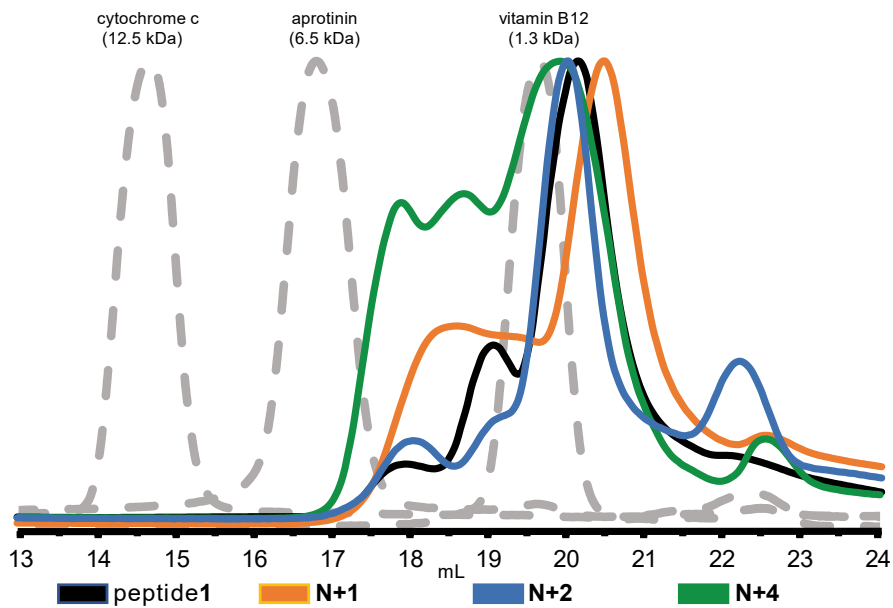


Figure S2.7. SEC traces of peptides 1, N+1, N+2, and N+4. SEC was performed on a 1.0 mg/mL solution of each peptide in 50 mM Tris buffer at pH 7.4 with 150 mM NaCl on a Superdex 75 Increase 10/300 column.

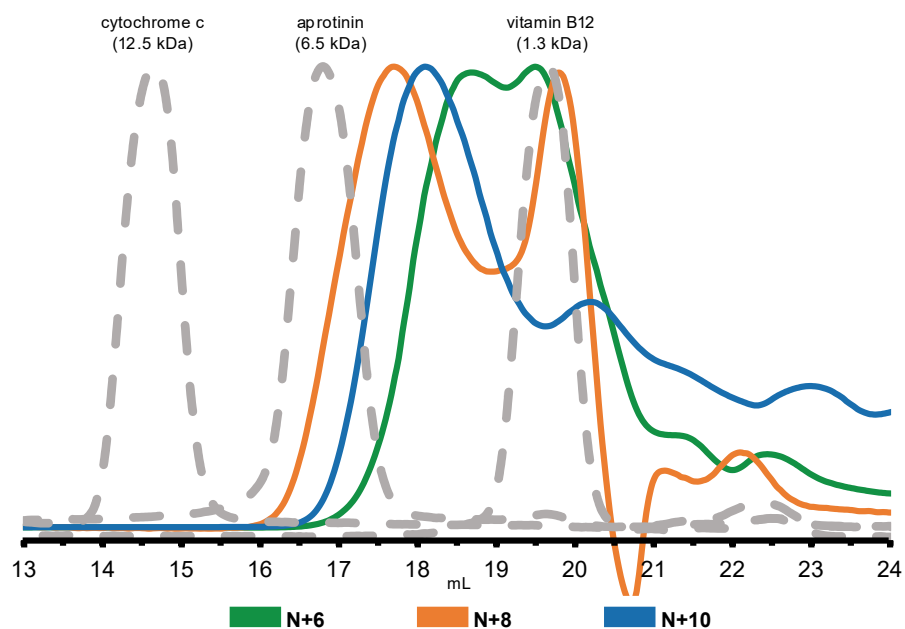


Figure S2.8. SEC traces of peptides N+6, N+8, and N+10. SEC was performed on a 1.0 mg/mL solution of each peptide in 50 mM Tris buffer at pH 7.4 with 150 mM NaCl on a Superdex 75 Increase 10/300 column.

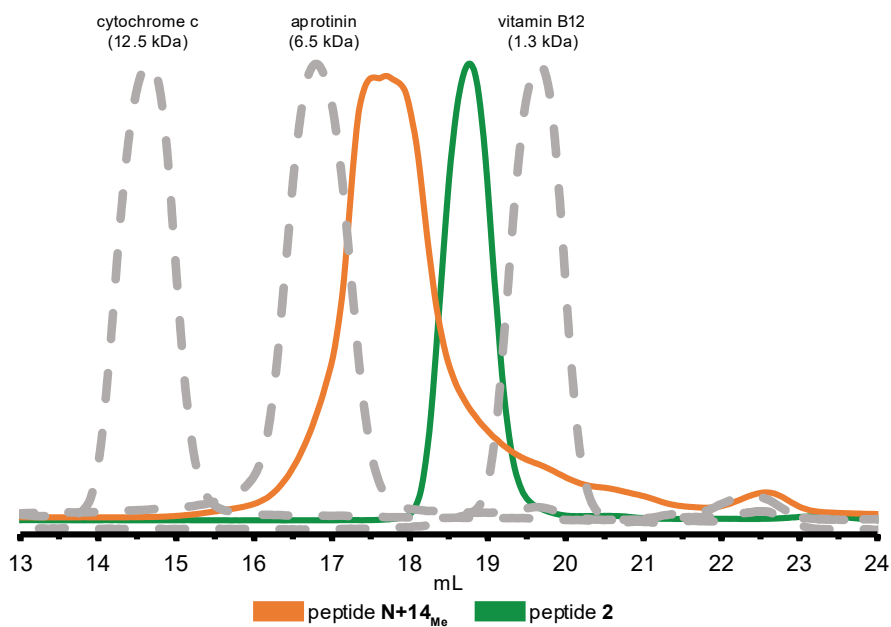


Figure S2.9. SEC traces of peptides 2 and N+14_{Me}. SEC was performed on a 1.0 mg/mL solution of each peptide in 50 mM Tris buffer at pH 7.4 with 150 mM NaCl on a Superdex 75 Increase 10/300 column.

Supplementary Table 2.2. Elution volumes of peptides **1, 2, N+1** through **N+14**, and **N+14_{Me}** by size exclusion chromatography. ^a

peptide	elution volume (mL)	putative oligomer size	molecular weight (kDa) ^b
peptide 1	20.18	monomer	1.77
	19.06	dimer	3.55
	17.90	trimer	5.32
N+1	20.51	monomer	1.91
	19.34	dimer	3.82
	18.55	trimer	5.73
N+2	20.04	monomer	2.05
	19.10	dimer	4.09
	18.04	trimer	6.14
N+4	20.0	monomer	2.28
	18.71	dimer	4.55
	17.88	trimer	6.83
	19.58	monomer	2.49
N+6	16.64	dimer or trimer	4.99 or 7.49
N+8	19.76	monomer	2.69
	17.76	dimer or trimer	5.39 or 8.09
N+10	20.23	monomer	2.99
	18.13	dimer or trimer	5.98 or 8.97
N+12	20.09	monomer	3.27
	18.79	dimer	6.54
	17.90	trimer	9.80
N+14	20.14	monomer	3.45
	18.74	dimer	6.54
	17.39	trimer	10.36
N+14 _{Me}	17.67	monomer or dimer	3.46 or 6.54
peptide 2	18.74	monomer	3.45

a. SEC was performed on a 1.0 mg/mL solution of each peptide in 50 mM Tris buffer at pH 7.4 with 150 mM NaCl on a Superdex 75 Increase 10/300 column.

b. Molecular weights of the monomers, dimers, and trimers are calculated from the structures of the molecules.

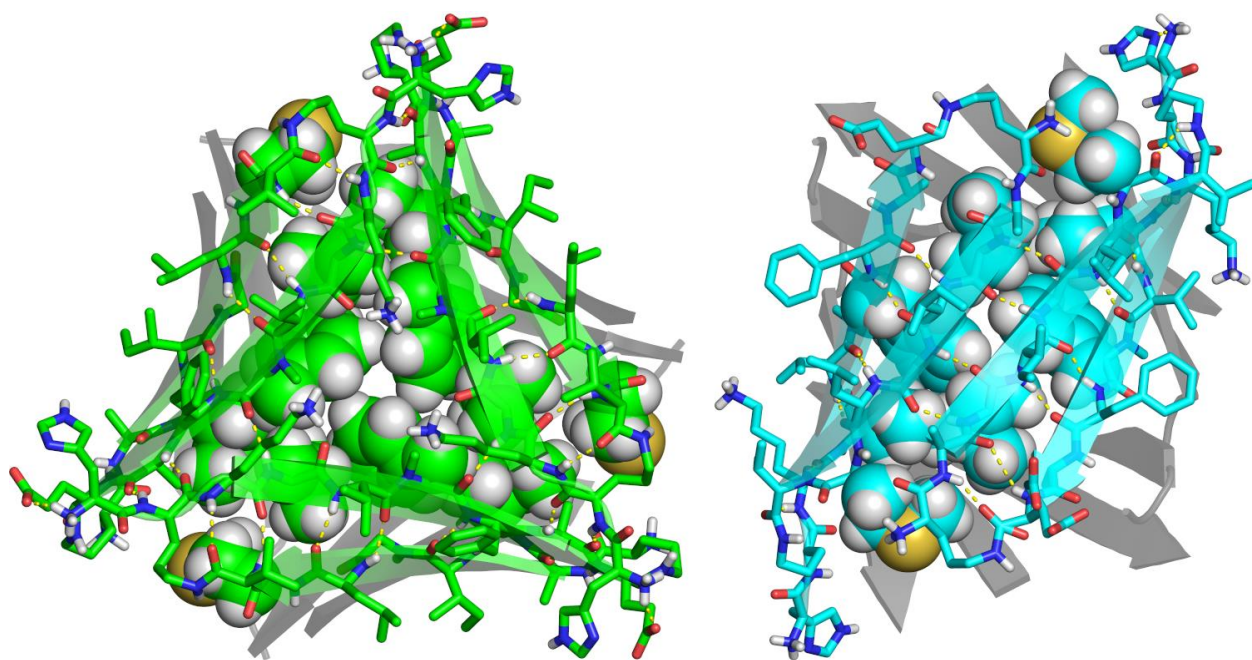


Figure S2.10. The trimer (left) and dimer (right) subunits within the X-ray crystallographic structure of the hexamer formed by peptide **N+1**. The trimer and dimer subunits are stabilized by backbone hydrogen bonding and the packing of hydrophobic side chain residues.

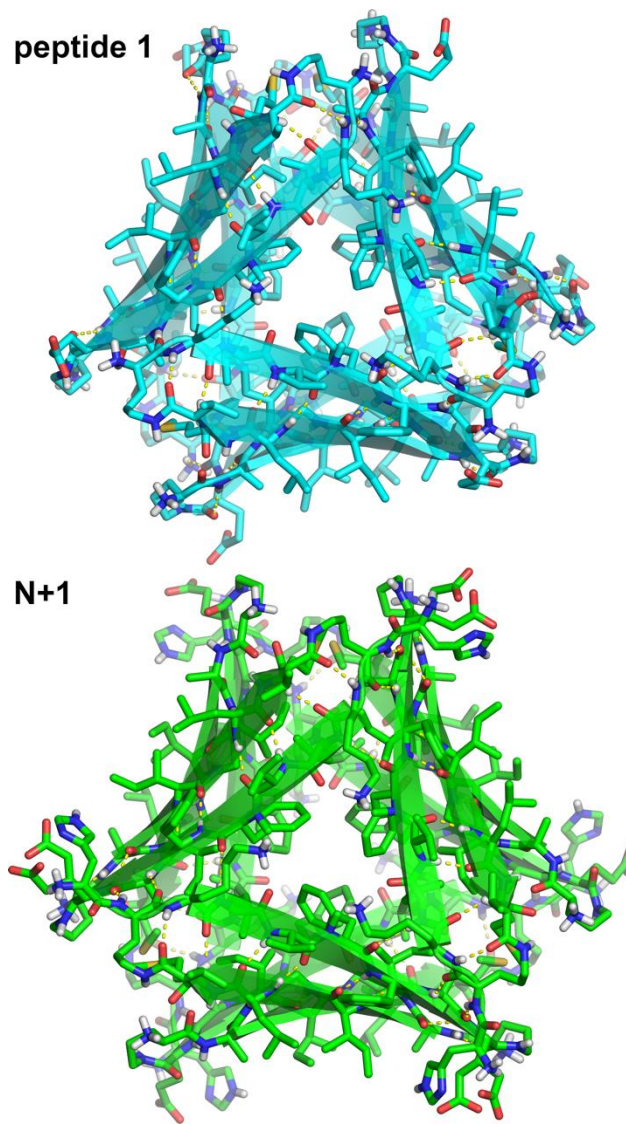


Figure S2.11. X-ray crystallographic structures of the hexamers formed by peptides **1** (PDB 5W4H), N+1 (PDB 6VU4).

Supplementary Table 2.3. Crystallographic properties, crystallization conditions, data collection, and model refinement statistics for peptide N+1.

peptide	N+1
PDB ID	6VU4
space group	F432
a, b, c (Å)	96.880, 96.880, 96.880
α, β, λ (°)	90, 90, 90
peptides per asymmetric unit	2
crystallization conditions	0.1 M HEPES buffer (pH 7.2), 0.2 M sodium citrate, 25% isopropyl alcohol ^a
wavelength (Å)	1.54
resolution range (Å)	24.22 - 2.08 (2.15 - 2.08)
total reflections	356508 (33112)
unique reflections	2632 (255)
multiplicity	135.5 (129.9)
completeness (%)	99.81 (100.00)
mean I/σ	174.29 (14.50)
Wilson B-factor	32.19
R_{merge}	0.7111 (1.321)
R_{measure}	0.7143 (1.326)
R_{pim}	0.06514 (0.1154)
CC1/2	0.937 (0.906)
CC*	0.984 (0.975)
R_{work}	0.2217 (0.2330)
R_{free}	0.2694 (0.4224)
number of non-hydrogen atoms	318
RMS(bonds)	0.003
RMS(angles)	0.77
Ramachandran favored (%)	92.86
Ramachandran allowed (%)	7.14
Ramachandran outliers (%)	0.00
Rotamer outliers (%)	0.00
clashscore	5.43
average B-factor	39.11

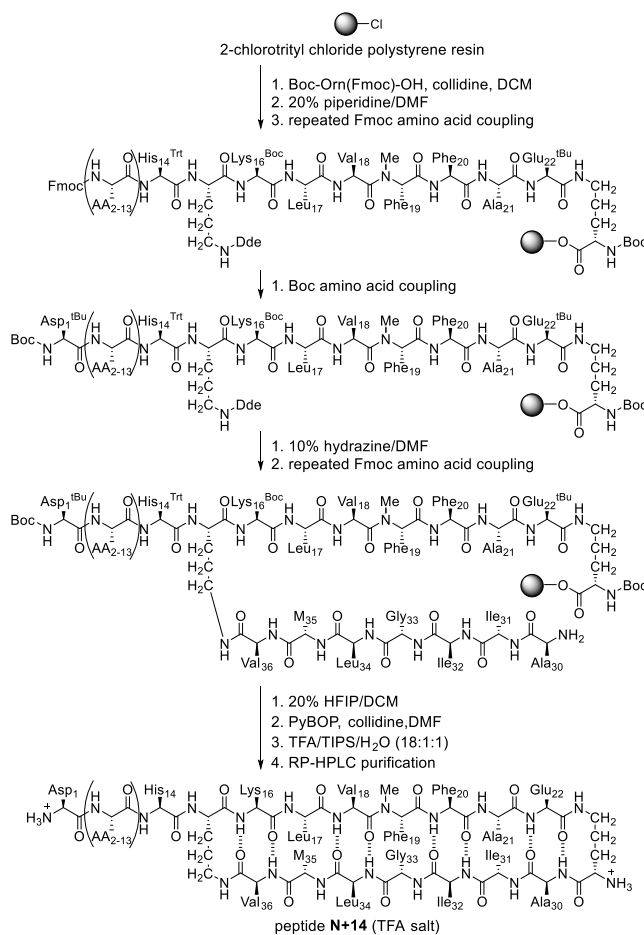
^aCrystals were soaked briefly in 1 M KI solution prior to data collection.

Materials and Methods¹

General information

All chemicals were used as received unless otherwise noted. Methylene chloride (CH_2Cl_2) was passed through alumina under nitrogen prior to use. Anhydrous, amine-free *N,N*-dimethylformamide (DMF) was purchased from Alfa Aesar. Deionized water (18 M Ω) was obtained from a Barnstead NANOpure Diamond water purification system. Analytical reverse-phase HPLC was performed on an Agilent 1260 Infinity II instrument equipped with a Phenomenex Aeris PEPTIDE 2.6 μ XB-C18 column. Preparative reverse-phase HPLC was performed on a Ranin instrument equipped with an Agilent Zorbax SB-C18 column. HPLC grade acetonitrile and deionized water, each containing 0.1% trifluoroacetic acid (TFA), were used for analytical and preparative reverse-phase HPLC. All peptides were prepared and used as the trifluoroacetate salts, and were assumed to have one trifluoroacetic acid molecule per amine group on each peptide.

Synthesis of peptide N+14



Scheme 2.1. Synthesis of the *N*-terminally extended peptide, **N+14** derived from *Aβ*₁₋₃₆.

a. Loading the resin. 2-Chlorotrityl chloride resin (300 mg, 1.4 mmol/g) was added to a Bio-RAD Poly-Prep chromatography column (10 mL). Dry CH₂Cl₂ (8 mL) was used to suspend and swell the resin for 30 min with gentle rocking. The solution was drained from the resin and a solution of Boc-Orn(Fmoc)-OH (0.78 equiv, 150 mg, 0.33 mmol) in 6% (v/v) 2,4,6-collidine in dry CH₂Cl₂ (8 mL) was added immediately and the suspension was gently rocked for 12 h. The solution was then drained and a mixture of CH₂Cl₂/MeOH/*N,N*-diisopropylethylamine (DIPEA) (17:2:1, 10 mL) was added immediately. The resin was gently rocked for 1 h, to cap the unreacted 2-chlorotrityl chloride resin sites. The resin was then washed twice with dry CH₂Cl₂ and dried by passing nitrogen through the vessel. This procedure typically yields 0.18 mmol of loaded resin (0.6 mmol/g loading).

b. Manual peptide coupling of residues 22 through 18. The resin loaded with Boc-Orn(Fmoc) was suspended in dry DMF and then transferred to a solid-phase peptide synthesis vessel. Residues 22 through 18 were manually coupled using Fmoc-protected amino acid building blocks. Each manual coupling cycle consisted of *i.* Fmoc-deprotection with of 20% (v/v) piperidine in DMF for 5 min at ambient temperature (5 mL), *ii.* washing with dry DMF (2x, 5 mL), *iii.* coupling of the amino acid (0.44 mmol, 4 equiv) with HCTU (174.0 mg, 0.44 mmol, 4 equiv) in 20% (v/v) 2,4,6-collidine in dry DMF (5 mL) for 30 min, and *iv.* washing the with dry DMF (2x, 5 mL). Residue 18, which follows N-Me-Phe19, was double coupled (4 equiv per coupling) using HATU (6 equiv) and HOAt (6 equiv) for 1 hr per coupling to ensure complete reaction. (We have found that coupling after N-methyl amino acids is difficult and requires rigorous coupling to minimize incomplete reaction.²)

c. Microwave-assisted coupling of residues 17 through 1 and 36 through 30. A CEM Liberty 1 Automated Microwave Peptide Synthesizer was used to couple residues 17 to 1 and 36 to 30. Fmoc-Orn(Dde)-OH replaces residue 15 in the natural sequence. Each coupling cycle consisted of *i.* Fmoc-deprotection with 20% (v/v) piperidine with 0.1 M Oxyma Pure in DMF for 2 min. at 50 °C, *ii.* washing with DMF (3x), *iii.* coupling of the amino acid (0.75 mmol, 5 equiv) in the presence of HCTU (0.675 mmol, 4.5 equiv) and 20% (v/v) *N*-methylmorpholine (NMM) in DMF for 10 min. at 50 °C, *iv.* washing with DMF (3x). For peptide **N+14**, residue 1 is coupled as Boc-Asp(*t*-Bu)-OH, to terminate the linear chain. For the shorter homologues (**N+12**, **N+10**, **N+8**, **N+6**, **N+4**, **N+2**, and **N+1**), the terminal residues (3, 5, 7, 9, 11, 13, and 14) were also coupled as the Boc protected amino acids (Boc-Glu(*t*-Bu)-OH, Boc-Arg(Pbf)-OH, Boc-Asp(*t*-Bu)-OH, Boc-Gly-OH, Boc-Glu(*t*-Bu)-OH, Boc-His(Trt)-OH, and Boc-His(Trt)-OH), to terminate the linear chain.

d. Hydrazine deprotection of Dde and microwave-assisted coupling of residues 36 through 30. The resin was transferred from the microwave synthesizer to a solid-phase peptide synthesis vessel and washed 3x using dry DMF. The Dde protecting group of residue 15 was then removed by treatment with a solution of 10% hydrazine in DMF for 20 minutes at ambient temperature. The resin was washed 8x with dry DMF and was then transferred back to the microwave synthesizer to couple residues 36 through 30. The final Fmoc group was removed with 20% (v/v) piperidine with 0.1 M Oxyma Pure in DMF (10 min 50 °C).

e. Cleavage of the peptide from resin. The resin was then transferred to a 10-mL Bio-Rad Poly-Prep chromatography column, and washed 3x with dry CH₂Cl₂. The acyclic branched peptide was cleaved from the resin by rocking the resin for 1 h with a solution of 1,1,1,3,3,3-hexafluoroisopropanol (HFIP) in CH₂Cl₂ (1:4, 8 mL). The suspension was filtered and the filtrate was collected in a 250-mL round-bottomed flask. The resin was washed with additional HFIP in CH₂Cl₂ (1:4, 8 mL). The combined filtrates were concentrated by rotary evaporation to give a white solid. The white solid was further dried by vacuum pump to afford the crude protected linear peptide, which was cyclized without further purification.

f. Cyclization of the acyclic peptide. The crude protected linear peptide was dissolved in dry DMF (150 mL). PyBOP (370 mg, 0.711 mmol, 6 equiv) and *N*-methylmorpholine (NMM) (0.33 mL, 1.8 mmol, 12 equiv) was added to the solution and the mixture was stirred under nitrogen for 48 h. The mixture was concentrated under reduced pressure to afford the crude protected cyclic peptide, a yellow film.

e. *Global deprotection of the cyclic branched peptide.* The protected cyclic peptide was dissolved in TFA/triisopropylsilane (TIPS)/H₂O (18:1:1, 10 mL) in a 250-mL round-bottomed flask equipped with a nitrogen-inlet adaptor. The solution was stirred for 1 h under nitrogen. The reaction mixture was then concentrated by rotary evaporation under reduced pressure to afford the crude cyclic peptide. The crude cyclic peptide was immediately subjected to purification by reverse-phase HPLC (RP-HPLC).

h. *Reverse-phase HPLC purification.* The peptide was dissolved in H₂O and acetonitrile (8:2, 10 mL), and the solution was filtered through a 0.2 µm syringe filter and purified by RP-HPLC. The solution of crude cyclic peptide was injected at 20% acetonitrile and eluted with a gradient of 20-60% CH₃CN over 90 min, with the column heated in a water bath at 70 °C. Each peptide eluted between 29-36% CH₃CN. The collected fractions were analyzed by analytical HPLC and MALDI-TOF, and the pure fractions were concentrated by rotary evaporation and lyophilized. Typical syntheses yielded between 12 and 44 mg of the peptide as the TFA salt.

SDS-PAGE silver staining and western blot

SDS-PAGE was performed on peptides **1**, **2**, **N+1** through **N+14**, **N+14_{Me}**, and trimers **1** and **2** using the reagents, recipes, and procedures for Tricine SDS-PAGE detailed in Schägger, H. *Nat. Protoc.* **2006**, *1*, 16–22. Each peptide was run on a 16% polyacrylamide gel with a 4% stacking polyacrylamide gel at 60 volts. A Spectra™ Multicolor Low Range Protein Ladder (ThermoFischer Scientific, catalog #: 26628) was loaded into the first lane of the gel. The remaining lanes were loaded with 5.0 µL aliquots of each peptide as 75 µM solutions in SDS-PAGE loading buffer, which were prepared as follows: A 10 mg/mL stock solution of each peptide was prepared with deionized water. Aliquots of the 10 mg/mL solutions were then diluted further

with deionized water and 6X SDS-PAGE loading buffer (G-Biosciences catalog #: 786-701) to create 75 μ M working solutions of each peptide.

Staining with silver nitrate was used to visualize peptide **1** and the *N*-terminally extended homologues in the SDS-PAGE gel. Reagents for silver staining were prepared according to procedures detailed in Simpson, R. J. *Cold Spring Harbor Protocol* **2007**. [We have found it important to prepare sodium thiosulfate, silver nitrate, and developing solutions fresh each time and to use high purity sodium carbonate to prepare the developing solution.] The gel was removed from the casting glass and rocked for 20 min in fixing solution (50% (v/v) methanol and 5% (v/v) acetic acid in deionized water). The fixing solution was then discarded and replaced with 50% (v/v) aqueous methanol for another 10 min of rocking. Next, the 50% methanol was discarded and replaced with deionized water for another 10 min of rocking. Next, the water was discarded and the gel was rocked in 0.02% (w/v) sodium thiosulfate in deionized water for 1 min. The sodium thiosulfate was discarded and the gel was rinsed twice with deionized water for 1 min. The gel was then submerged in pre-chilled 0.1% (w/v) silver nitrate in deionized water and rocked at 4 °C for 20 min. The silver nitrate solution was discarded and the gel was rinsed twice with deionized water. The gel was incubated in developing solution (2% (w/v) sodium carbonate, 0.04% (w/v) formaldehyde) until the solution began to brown. The developing solution was then immediately discarded and fresh silver nitrate solution was added to the gel until the desired intensity of staining was reached. When the desired intensity of staining was reached, the developing solution was discarded and the gel was submerged in 5% aqueous acetic acid.

Western blot analysis was performed on peptides **1**, **N+1** through **N+14**, and $A\beta_{M1-42}$ using the 6E10 antibody (BioLegend catalog #: 803004) to visualize the bands. After the SDS-PAGE described above, the bands were electroblotted from the gel to a nitrocellulose membrane in transfer buffer (25mM Tris, 192 mM glycine, pH 8.3, 20% v/v methanol) at 400 mA over 2 h. The

nitrocellulose membrane was then rocked for 1 h at ambient temperature in a blocking solution of 10% (w/v) non-fat powdered milk in low-Tween Tris-buffered saline (TBST: 20 mM Tris, 137 mM NaCl, 0.01% Tween 20, pH 7.6). The membrane was then incubated at 4 °C overnight in a solution of 6E10 antibody (2 µg/mL) in 5% (w/v) non-fat powdered milk in TBST. The membrane was then washed with TBST for 5 min (3X) while rocking, and then rocked for 15 min in 5% (w/v) non-fat powdered milk in TBST at ambient temperature. The membrane was then rocked for 1 hour in a solution of horseradish peroxidase conjugated anti-mouse antibody (100 µg/mL) (Jackson ImmunoResearch catalog #: 115-035-146) at ambient temperature. The membrane was then washed with TBST for 5 min (3X) while rocking. A 10-mL portion of chemiluminescence substrate (Thermo Scientific SuperSignal West Femto Maximum Sensitivity, product #34095) was prepared according to the manufacture's protocol. The membrane was allowed to incubate in the chemiluminescence substrate for 10 minutes before imaging. The blot was imaged using a standard digital SLR camera in dark room.

Circular dichroism spectroscopy

A 50 µM solution of each peptide was prepared by diluting the 10 mg/mL stock solution with 10 mM sodium phosphate buffer at pH 7.4. Each solution was transferred to a 1 mm quartz cuvette for data acquisition. Circular dichroism spectra were acquired on a Jasco J-810 circular dichroism spectropolarimeter at ambient temperature. Data were collected using 2.0 nm intervals from 260 nm to 190 nm and averaged over five accumulations with smoothing.

Size exclusion chromatography

Size exclusion chromatography was performed on peptides **1**, **2**, **N+1** through **N+14**, and **N+14_{Me}** using an AKTA Explorer 10 FPLC equipped with a GE Superdex Increase 75 10/300 GL column at ambient temperature. Each peptide was dissolved in deionized water to a concentration of 10 mg/ml. The peptide solutions were then diluted to 1.0 mg/mL by adding 75 µL of the 10-

mg/ml solutions to 675 μ L of TBS (50 mM Tris buffer pH 7.5 and 100 mM NaCl). The peptide solutions were centrifuged at 12,000 RPM for 2 minutes to precipitate insoluble material prior to injection, soluble material was then loaded onto the column at 0.5 ml/min over 1 min. After loading, the samples were run with TBS at 1.0 ml/min. Chromatograms were recorded at 214 nm and normalized to the highest absorbance value. Standards (cytochrome C, aprotinin, and vitamin B12) were run in the same fashion.

LDH release assays

The toxicity of peptides **1**, **2**, **N+1** through **N+14**, **N+14_{Me}** toward SH-SY5Y cells was assessed by LDH release assays. Cells were incubated in the presence or absence of equivalent concentrations of peptides **1**, **2**, **N+1** through **N+14**, **N+14_{Me}** for 72 h in 96-well plates. The LDH release assay was performed using the Pierce LDH Cytotoxicity Assay Kit from Thermo Scientific. Experiments were performed in replicates of four, and an additional 8 wells were used for controls. Cells were cultured in the inner 60 wells (rows B–G, columns 2–11) of the 96-well plate. DMEM:F12 media (100 μ L) was added to the outer wells (rows A and H and columns 1 and 12), in order to ensure the greatest reproducibility of data generated from the inner wells.

a. Preparation of stock solutions of peptides 1, 2, N+1 through N+14, N+14_{Me}. 10-mg/mL stock solutions of peptides **1**, **2**, **N+1** through **N+14**, **N+14_{Me}** were prepared gravimetrically by dissolving 1.0 mg of each compound in 100 μ L of 18 M Ω deionized water. The peptide stock solutions were used to create 10X working solutions of peptides **1**, **2**, **N+1** through **N+14**, **N+14_{Me}**.

b. Preparation of SH-SY5Y cells for LDH release assays. SH-SY5Y cells were plated in a 96-well plate at 30,000 cells per well. Cells were incubated in 100 μ L of a 1:1 mixture of DMEM:F12 media supplemented with 10% fetal bovine serum, 100 U/mL penicillin, and 100 μ g/mL

streptomycin at 37 °C in a 5% CO₂ atmosphere and allowed to adhere to the bottom of the plate for 24 hours.

c. Treatment of SH-SY5Y cells with peptides 1, 2, N+1 through N+14, N+14_{Me}. After 24 hours, the culture media was removed and replaced with 90 µL of serum-free DMEM:F12 media. 10-µL of the 10X working solutions of peptides **1**, **2**, **N+1** through **N+14**, **N+14_{Me}** were added to the wells on the 96-well plates. Experiments were run in replicates of four. Four wells were used as controls and received 10-µL aliquots of deionized water (vehicle). Another four wells were left untreated, to be subsequently used as controls with lysis buffer for the LDH release assay. Cells were incubated at 37 °C in a 5% CO₂ atmosphere for 72 hours.

Crystallization of peptide N+1

The hanging-drop vapor-diffusion method was used to determine initial crystallization conditions for peptides **N+1**. Peptide **2a** was screened in 96-well plate format using three crystallization kits (Crystal Screen, Index, and PEG/ION) from Hampton Research. A TTP LabTech Mosquito nanodisperse was used to make three 150 nL hanging drops for each well condition. The three hanging drops differed in the ratio of peptide to well solution for each condition in the 96-well plate. A 10 mg/mL solution of each peptide in deionized water was combined with a well solution in ratios of 1:1, 1:2, and 2:1 peptide:well solution at appropriate volumes to create the three 150 nL hanging drops. Crystals of peptide **N+1** grew in well conditions of 0.2 M sodium citrate, 0.1 M HEPES pH 7.5, and 20% (v/v) isopropyl alcohol.

Crystallization conditions for each peptide were optimized using a 4x6 matrix Hampton 24-well plate. For peptide **N+1** the 0.1 M HEPES buffer was varied in each row in increments of 0.1 pH units (6.9, 7.0, 7.1, and 7.2) and the percentage of isopropyl alcohol in each column in increments of 1% (v/v) (20%, 21%, 22%, 23%, 24%, 25%). Three hanging-drops were prepared

on borosilicate glass slides by combing a 10 mg/mL solution of peptide N+1 in deionized water with the well solution in the following amounts: 1 μ L:1 μ L, 2 μ L:1 μ L, and 1 μ L:2 μ L. Slides were inverted and pressed firmly against the silicone grease surrounding each well. Crystals were harvested with a nylon loop attached to a copper or steel pin, soaked briefly in 1 M KI solution, and flash frozen in liquid nitrogen prior to data collection. The optimized crystallization conditions for peptide N+1 is summarized Supplementary Table 3.

X-ray crystallographic data collection, data processing, and structure determination of N+1

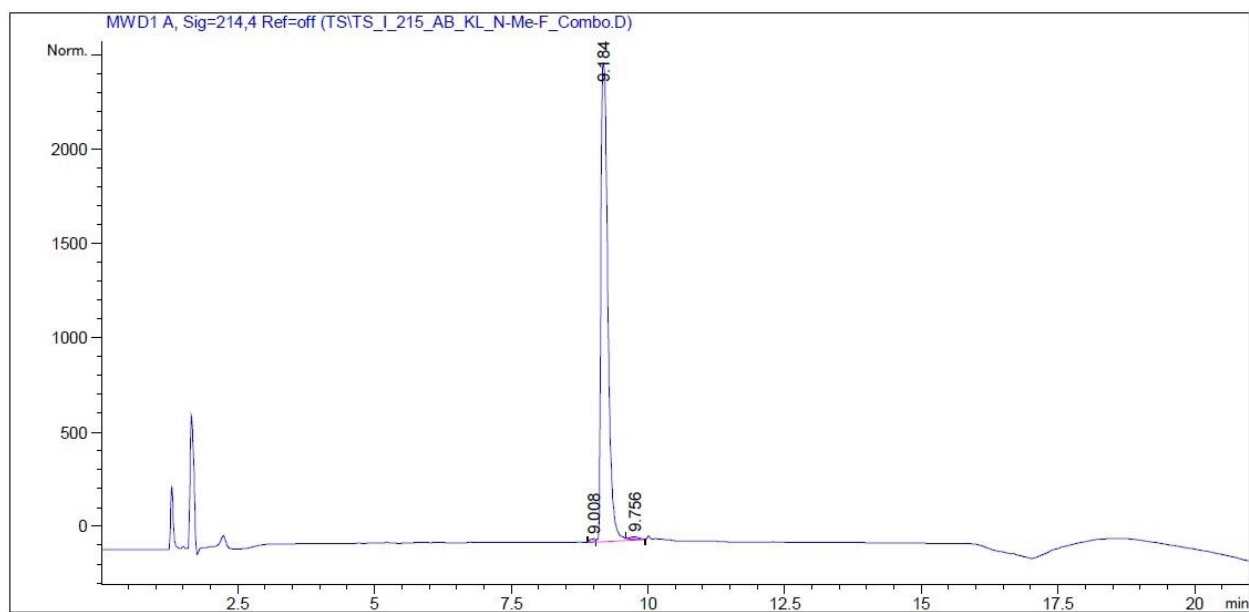
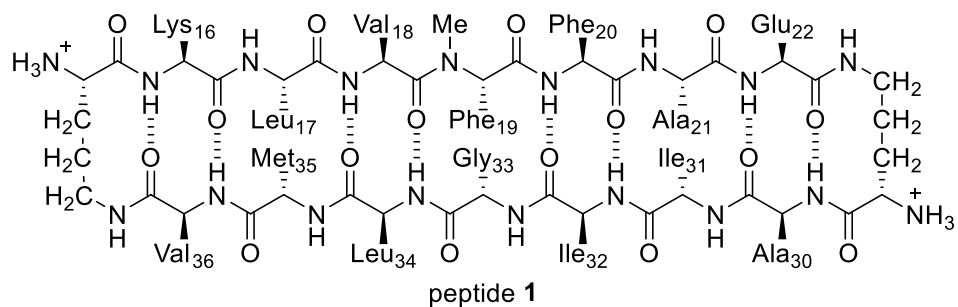
Diffraction data for N+1 were collected on a Rigaku Micromax-007HF X-ray diffractometer with a rotating copper anode using CrystalClear software. Datasets were indexed and integrated with XDS.³ Scaling and merging was done with pointless and aimless in CCP4.⁴ The structures were solved with molecular replacement in Phaser⁵ using a dimer formed by peptide 1 (PDB 5W4H) as the search model. The refinement was done with phenix.refine module of the Phenix suite, with manipulation of the model performed using Coot.⁶

References

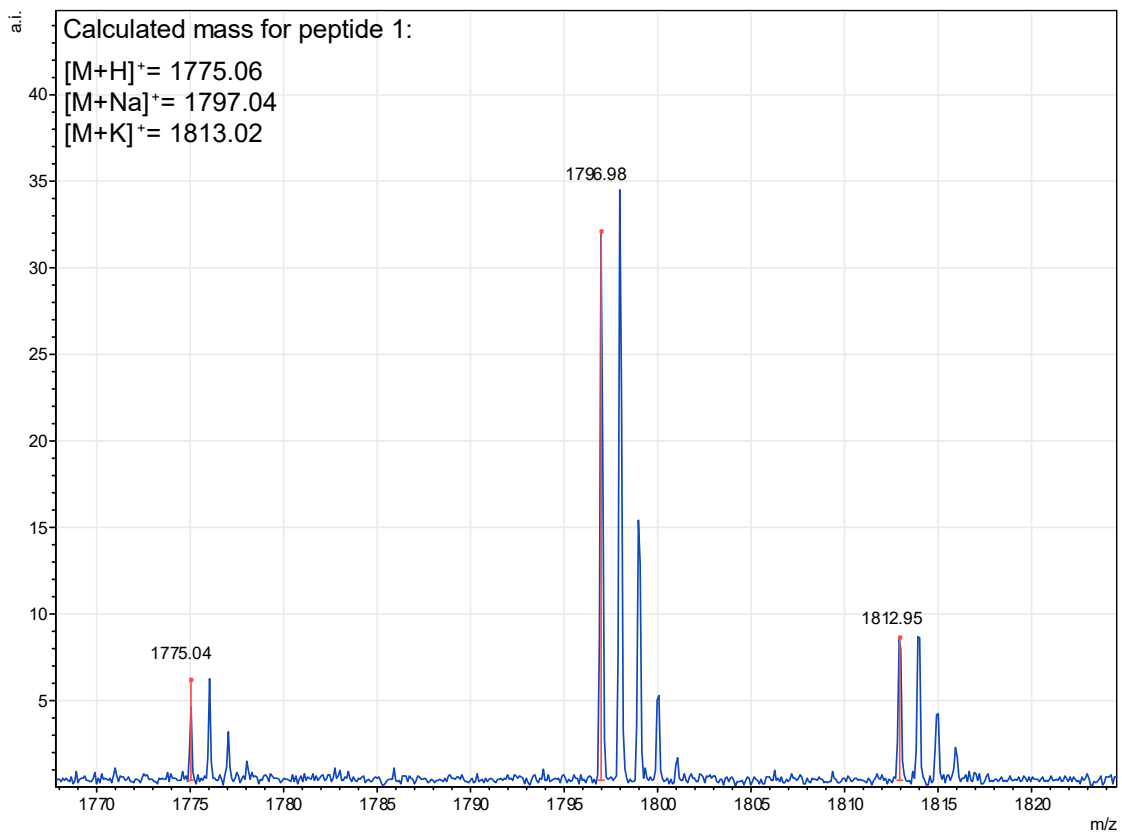
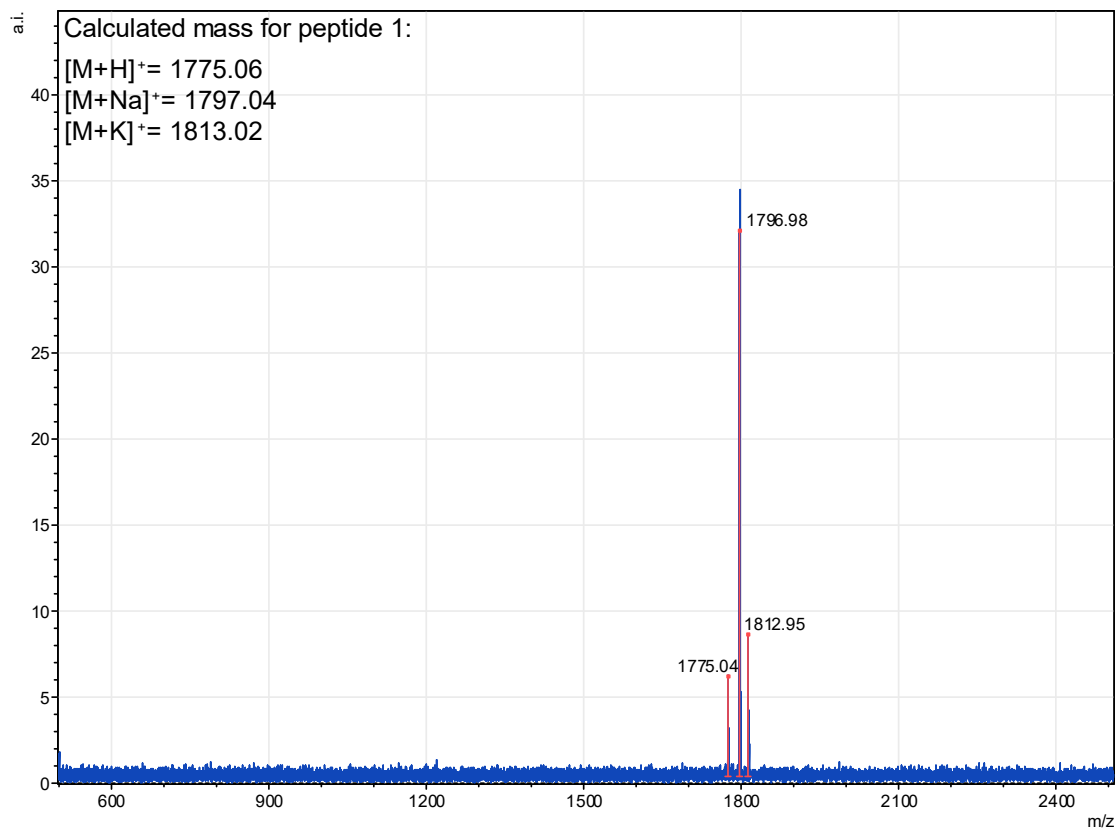
1. These procedures follow closely those that our laboratory has previously published. The procedures in this section are adapted from and in some cases taken verbatim from Kreutzer, A. G.; Hamza, I. L.; Spencer, R. K.; Nowick J. S. *J. Am. Chem. Soc.* **2016**, *138*, 4634–4642, Spencer, R. K.; Kreutzer, A. G.; Salveson, P. J.; Li, H.; Nowick, J. S. *J. Am. Chem. Soc.* **2015**, *137*, 6304–6311, Spencer, R. K.; Li. H.; Nowick, J. S. *J. Am. Chem. Soc.* **2014**, *136*, 5595– 5598, and Kreutzer, A. G.; Yoo, S.; Spencer, R. K.; Nowick, J. S. *J. Am. Chem, Soc.* **2017**, *139*, 966–975.
2. Humphrey, J. M.; Chamberlin, A. R. *Chem. Rev.* **1997**, *97*, 2243–2266.
3. Kabsch, W. *Acta Crystallogr., Sect. D: Biol. Crystallogr.* **2010**, *66*, 125–132.
4. Winn, M. D.; Ballard, C. C.; Cowtan, K. D.; Dodson, E. J.; Emsley, P.; Evans, P. R.; Keegan, R. M.; Krissinel, E. B.; Leslie, A. G. W.; McCoy, A.; McNicholas, S. J.; Murshudov, G. N.; Pannu, N. S.; Potterton, E. A.; Powell, H. R.; Read, R. J.; Vagin, A.; Wilson, K. S. *Acta Crystallogr., Sect. D: Biol Crystallogr.* **2011**, *67*, 235–242.
5. McCoy, A. J.; Grosse-Kunstleve, R. W.; Adams, P. D.; Winn, M. D.; Storoni, L. C.; Read, R. J. *J. Appl. Crystallogr.* **2007**, *40*, 658-674.
6. Adams, P. D.; Afonine, P. V.; Bunkoczi, G.; Chen, V. B.; Davis, I. W.; Echols, N.; Headd, J. J.; Hung, L. W.; Kapral, G. J.; Grosse-Kunstleve, R. W.; McCoy, A. J.; Moriarty, N. W.; Oeffner, R.; Read, R. J.; Richardson, D. C.; Richardson, J. S.; Terwilliger, T. C.; Zwart, P. H. *Acta Crystallogr., Sect. D: Biol. Crystallogr.* **2010**, *66*, 213–221
7. Emsley, P.; Lohkamp, B.; Scott, W. G.; Cowtan, K. *Acta Crystallogr., Sect. D: Biol. Crystallogr.* **2010**, *66*, 486–501

Characterization Data

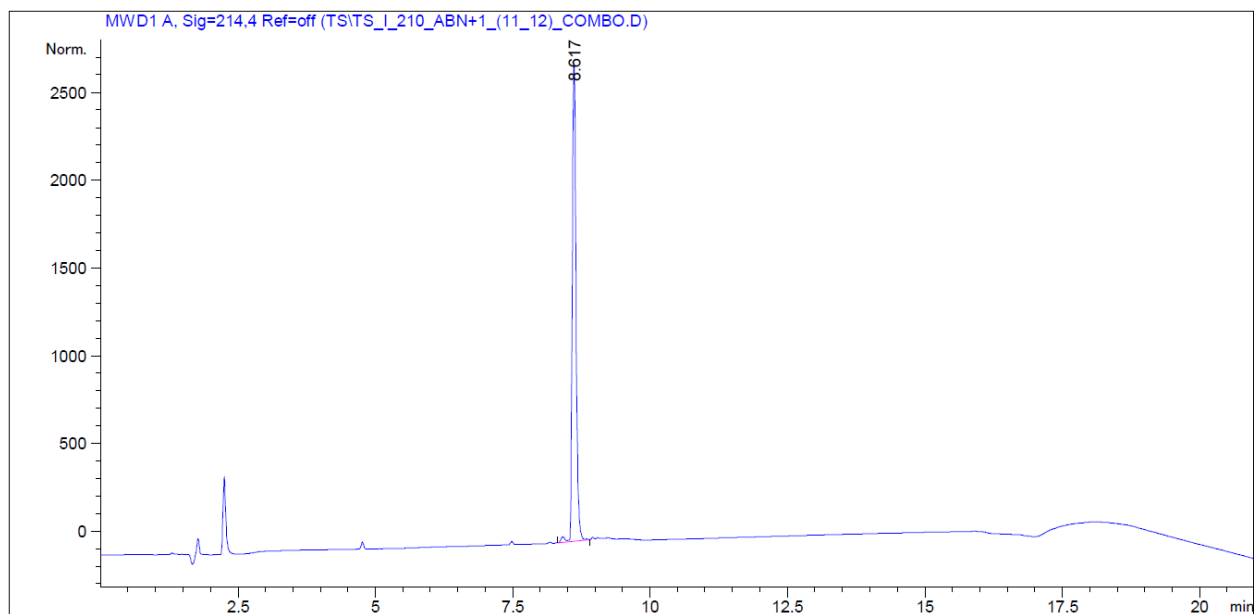
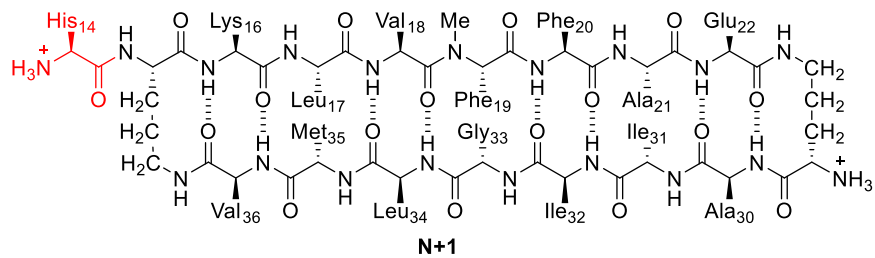
Characterization of peptide 1



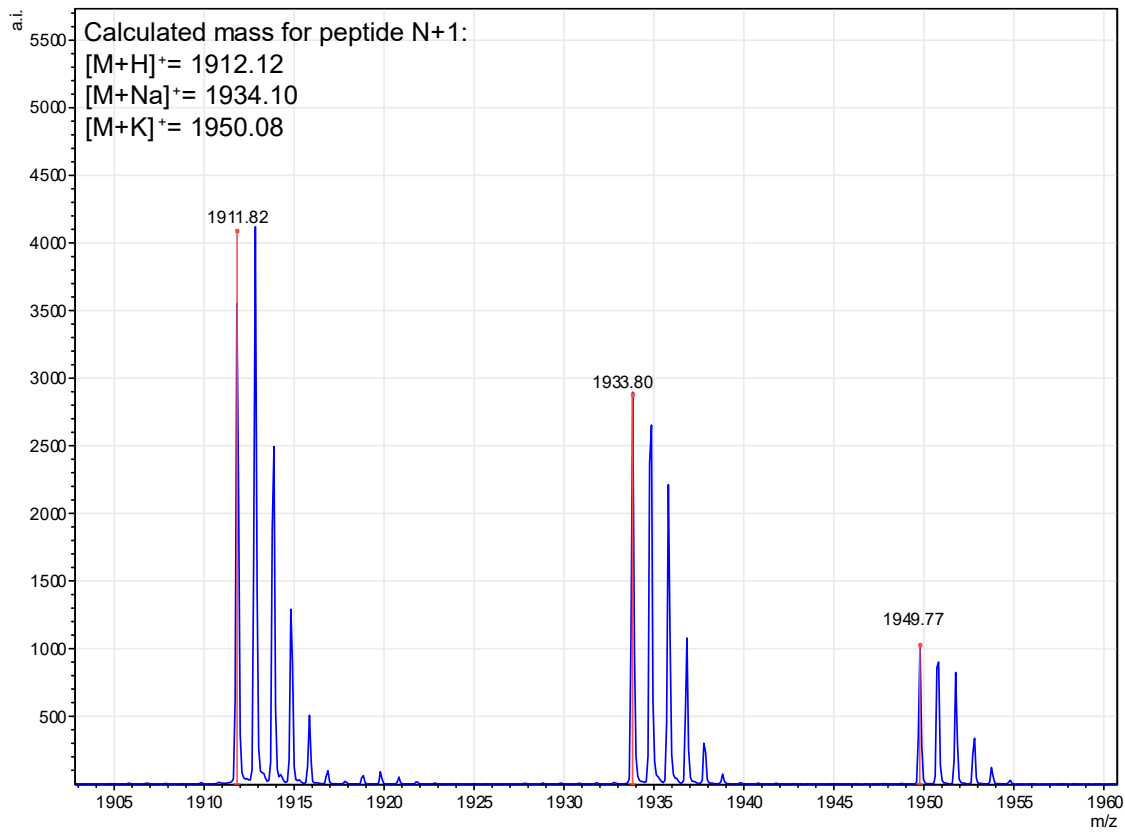
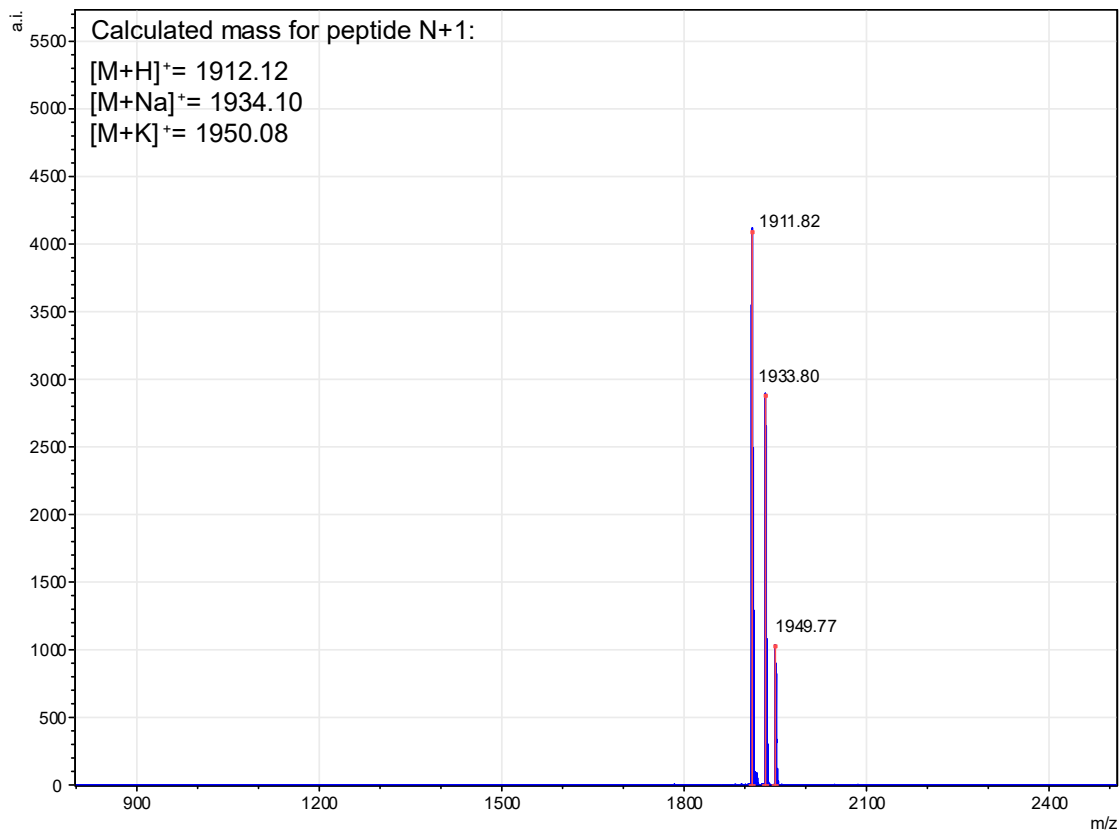
Peak #	RetTime [min]	Type	Width [min]	Area [mAU*s]	Height [mAU]	Area %
1	9.008	BV E	0.0814	78.69865	13.62904	0.3870
2	9.184	VV R	0.1387	2.01192e4	2285.21826	98.9293
3	9.756	VB E	0.1593	139.05769	12.54508	0.6838



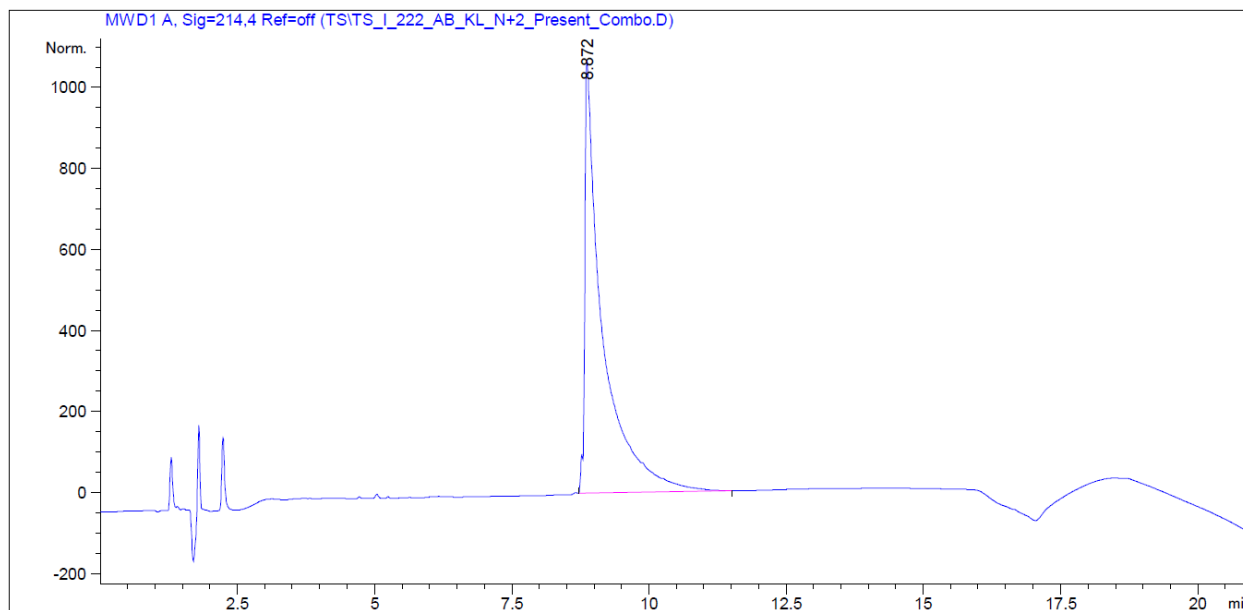
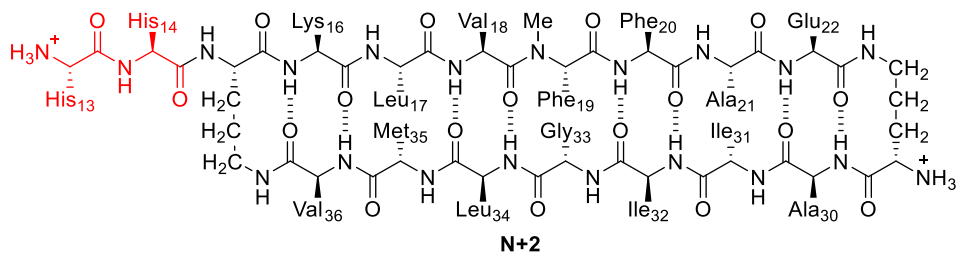
Characterization of **N+I**



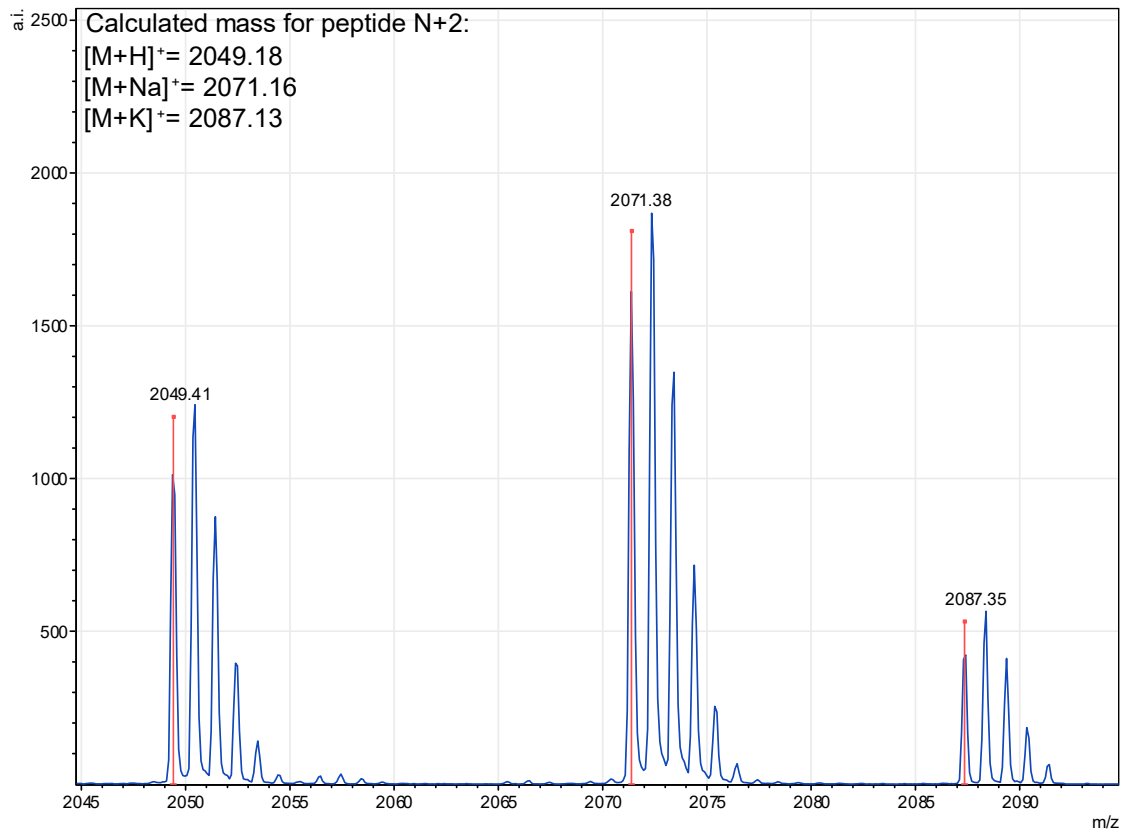
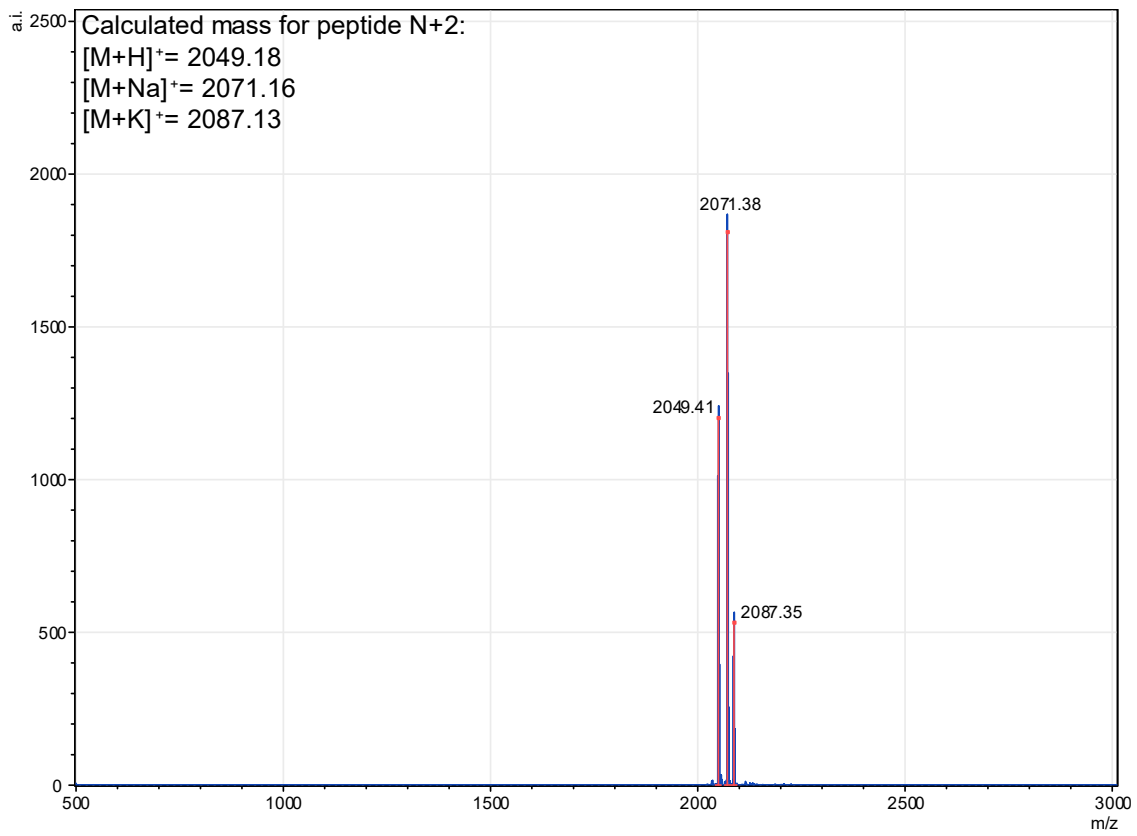
Peak #	RetTime [min]	Type	Width [min]	Area [mAU*s]	Height [mAU]	Area %
1	8.617	VV R	0.0756	1.18688e4	2466.48389	100.0000



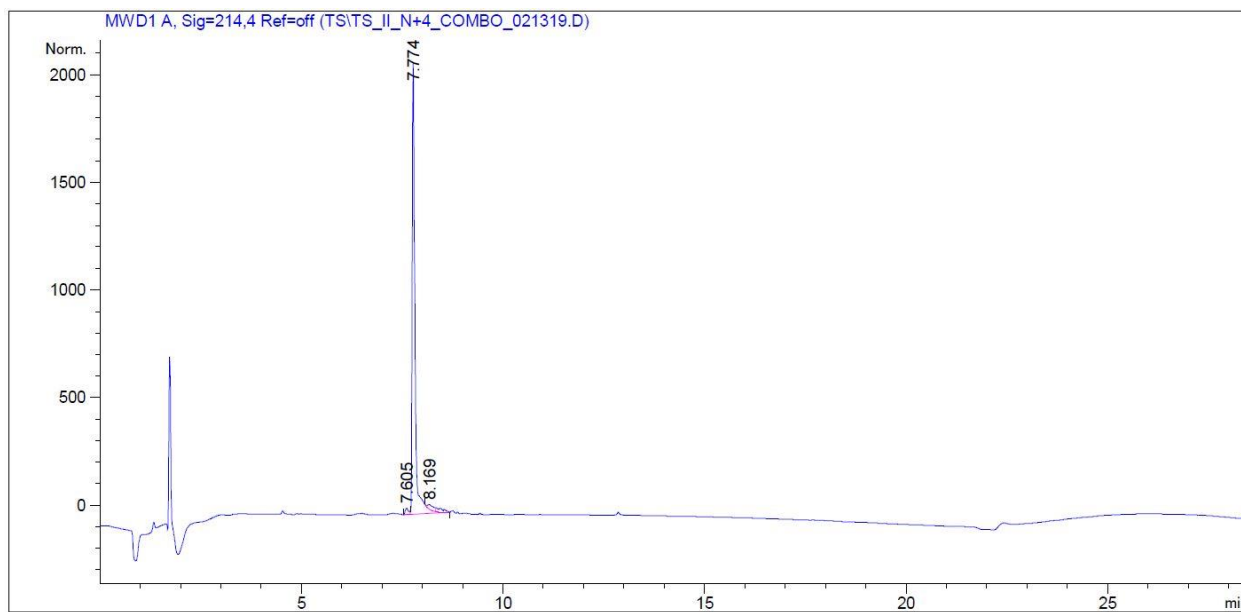
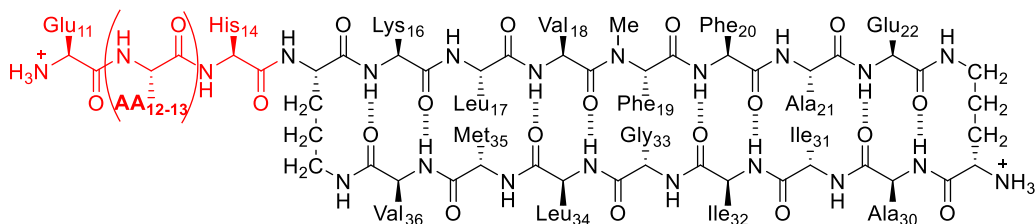
Characterization of N+2



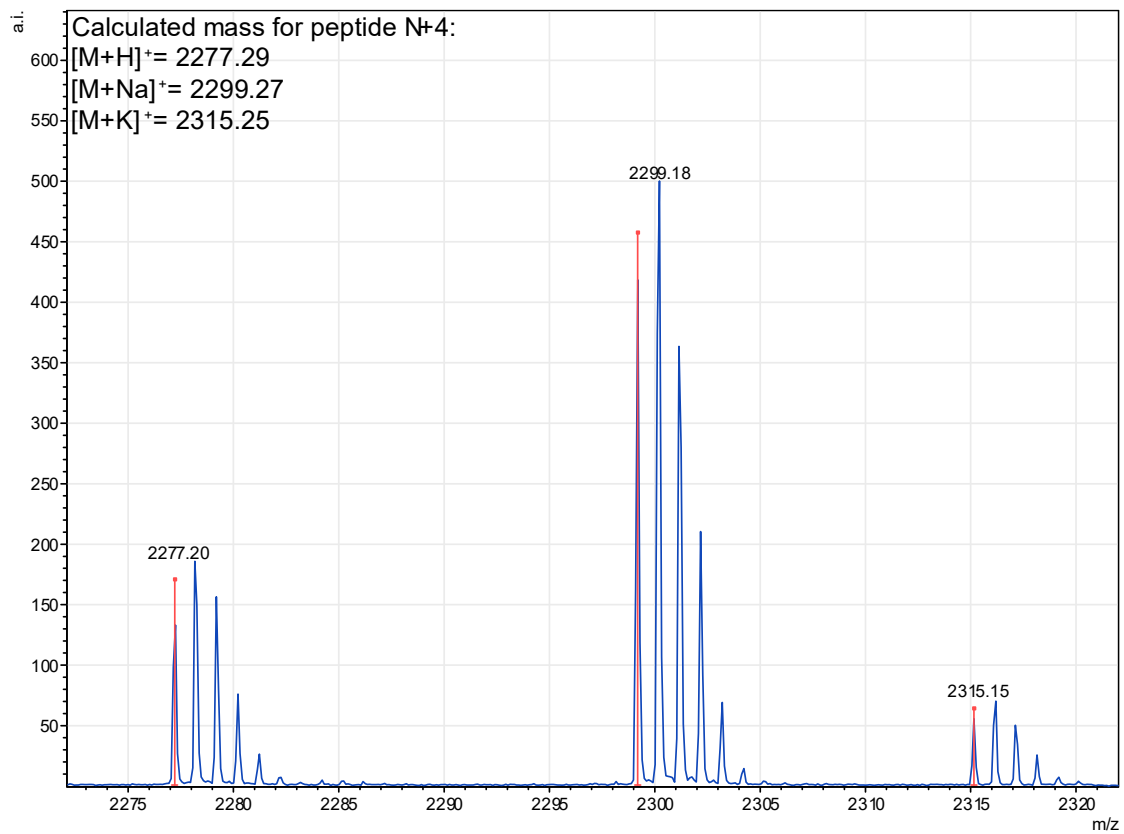
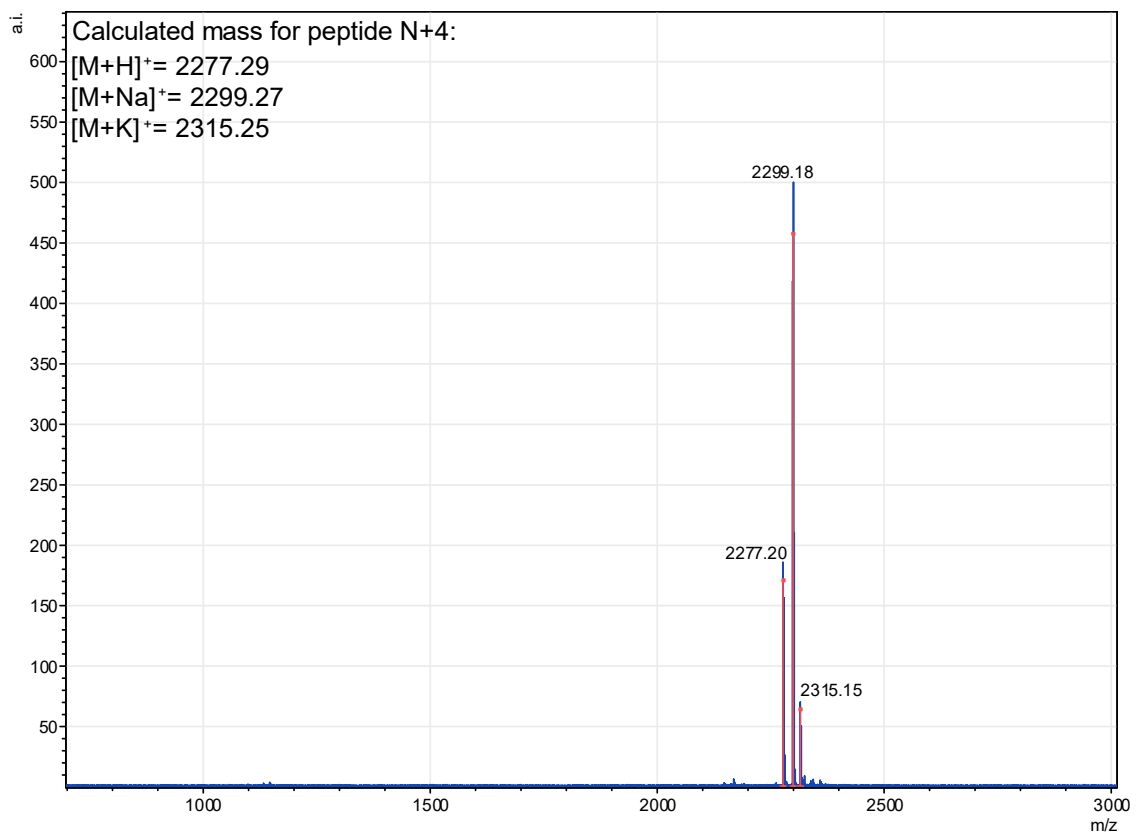
Peak #	RetTime [min]	Type	Width [min]	Area [mAU*s]	Height [mAU]	Area %
1	8.872	VV R	0.2878	2.15888e4	961.62427	100.0000



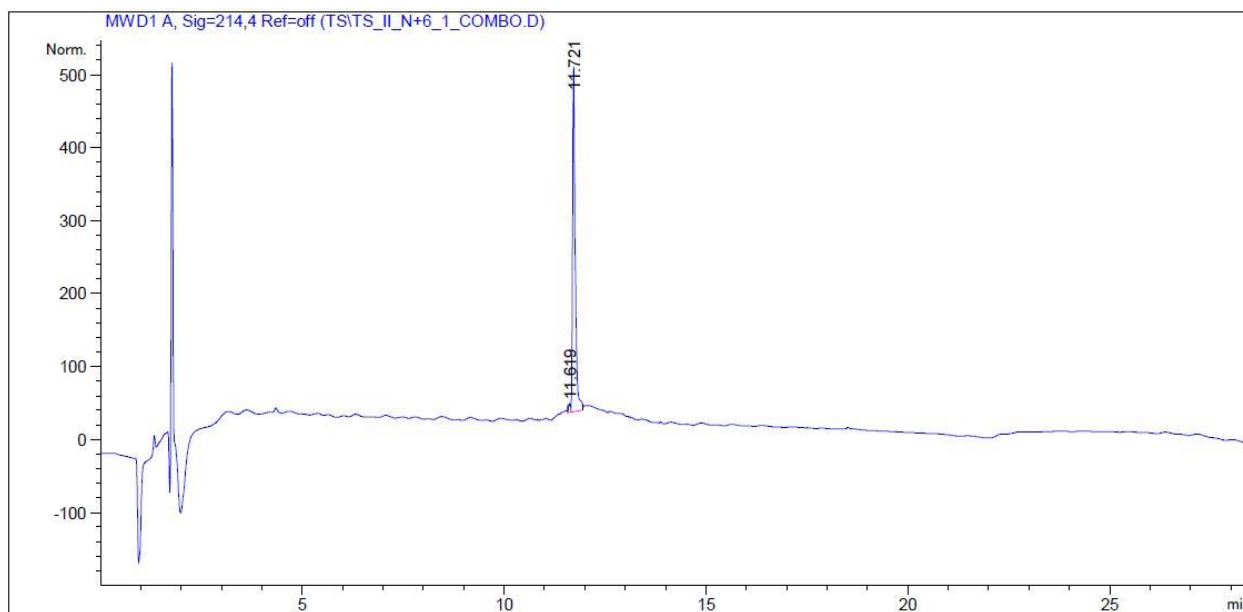
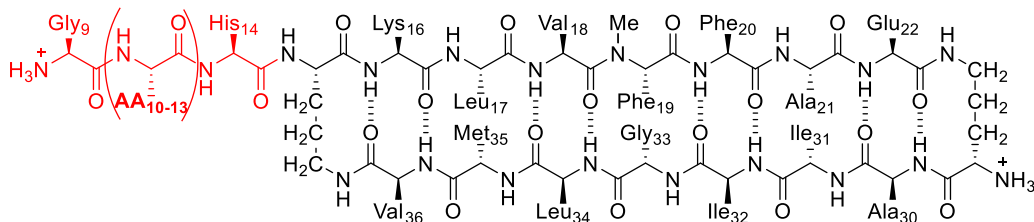
Characterization of N+4



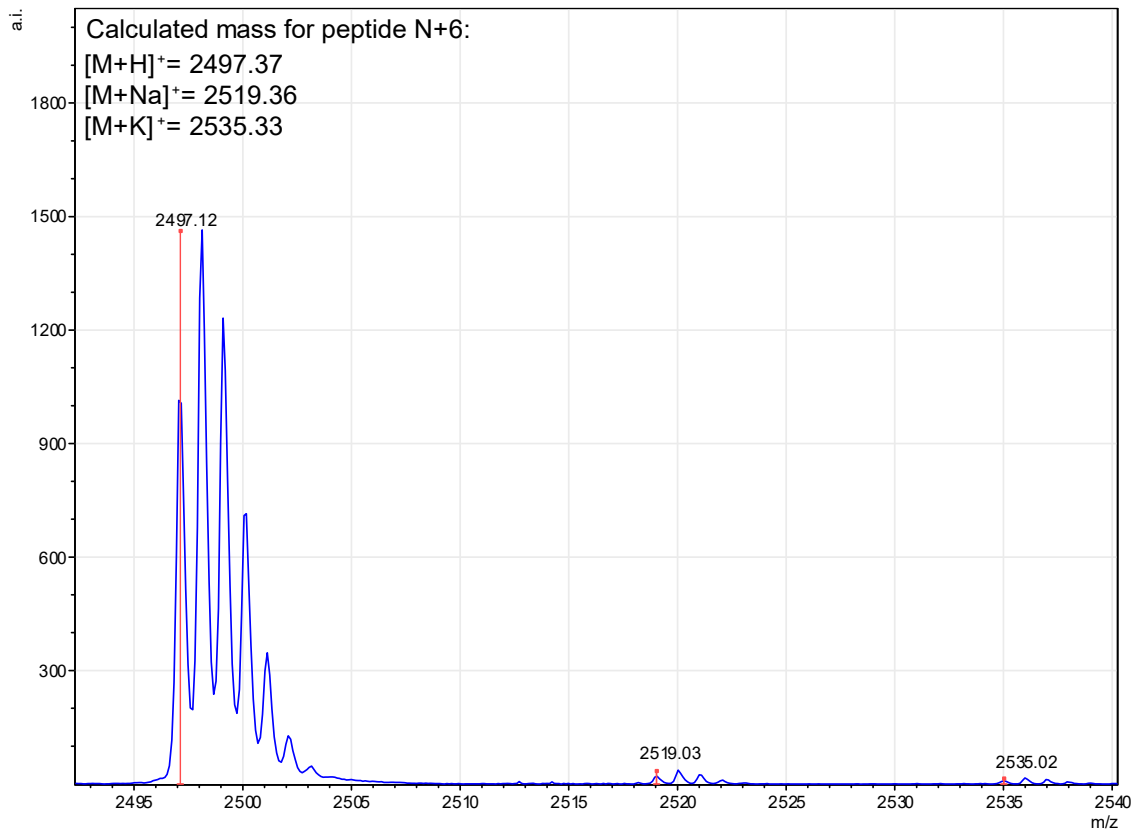
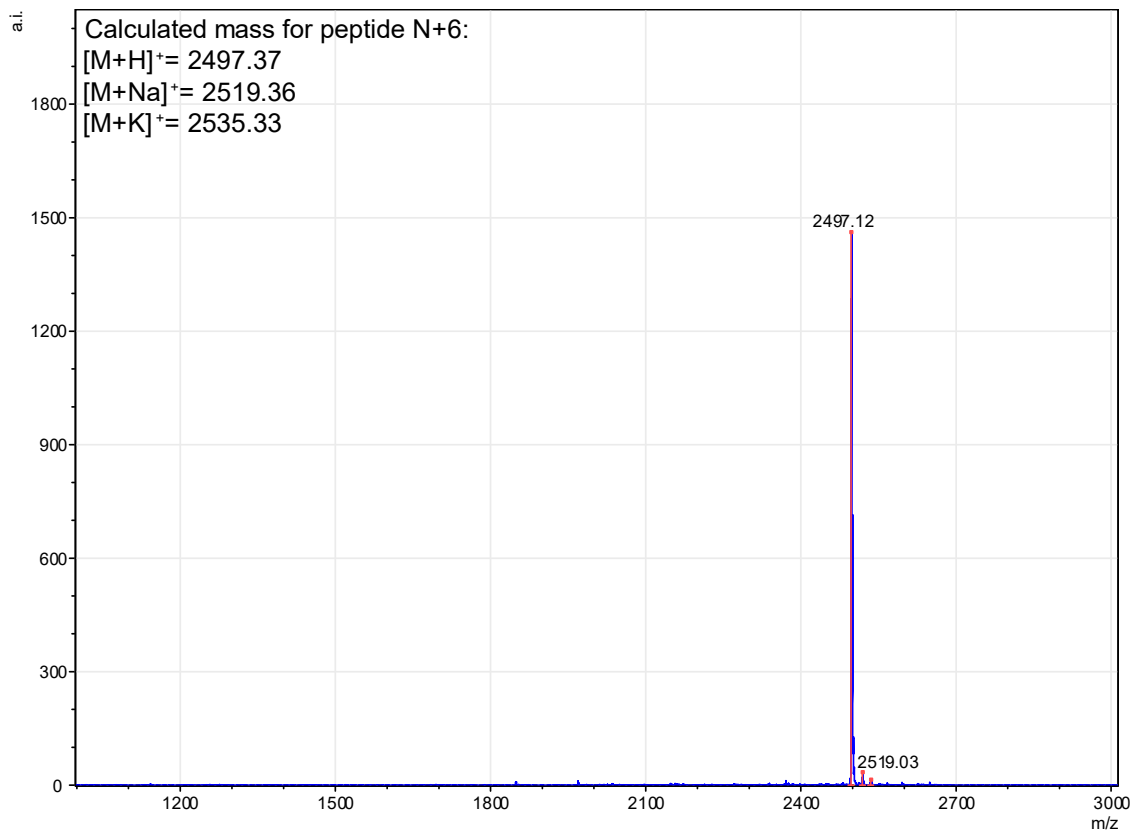
Peak #	RetTime [min]	Type	Width [min]	Area [mAU*s]	Height [mAU]	Area %
1	7.605	BV E	0.0805	151.97638	27.47144	1.5412
2	7.774	VV R	0.0701	9104.26660	1894.34375	96.1533
3	8.169	VV E	0.1663	227.32799	18.37850	2.3054



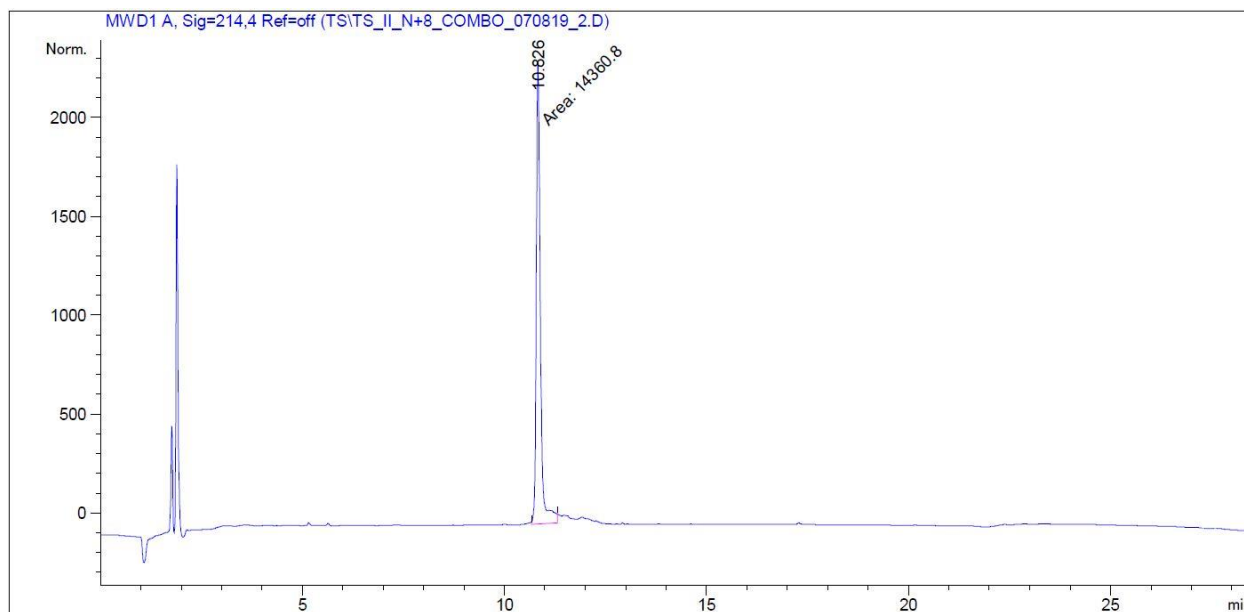
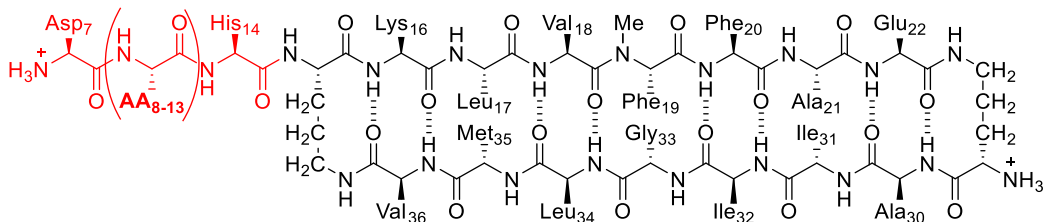
Characterization of N+6



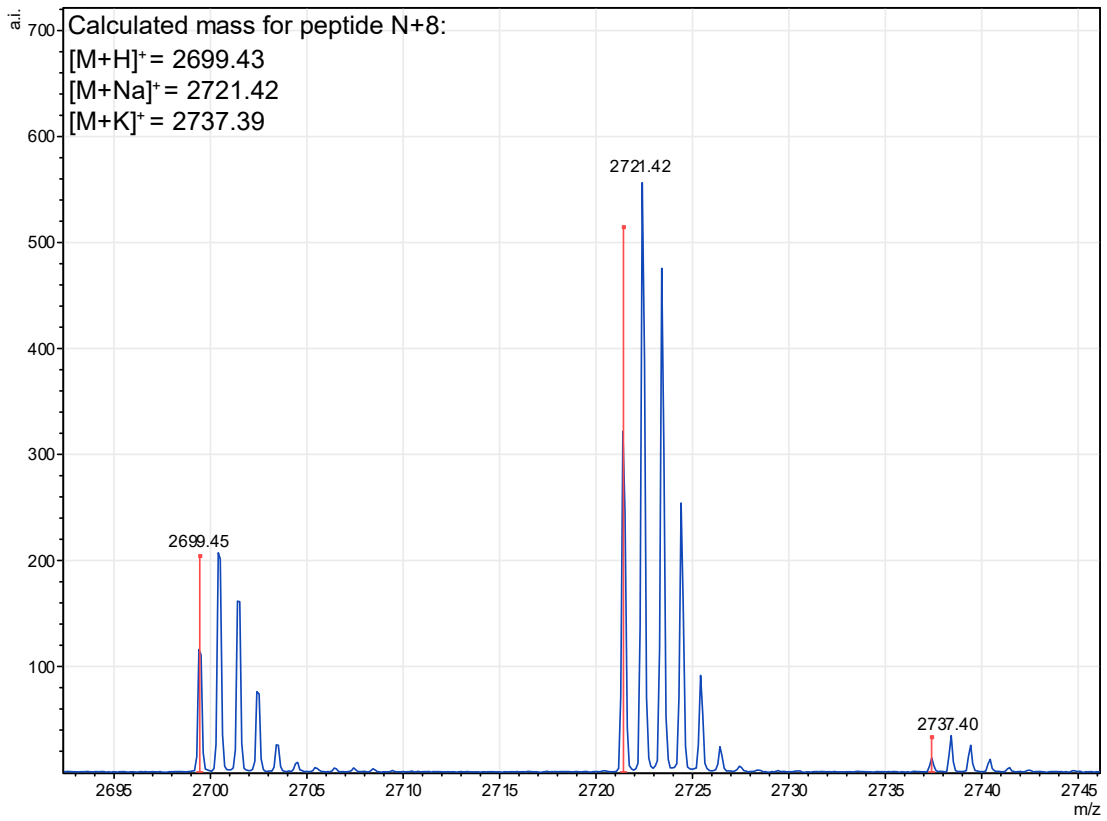
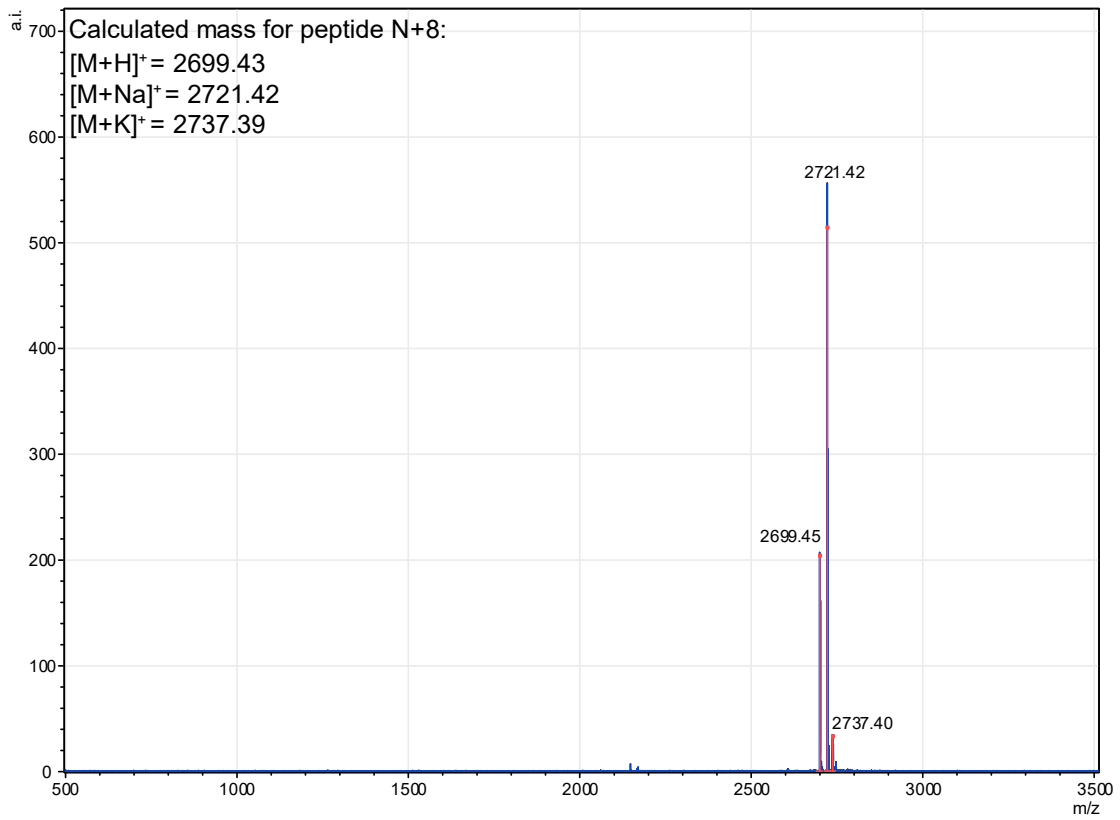
Peak #	RetTime [min]	Type	Width [min]	Area [mAU*s]	Height [mAU]	Area %
1	11.619	BV E	0.0462	21.64151	7.84065	1.6787
2	11.721	VV R	0.0664	1894.66553	421.83078	98.3213



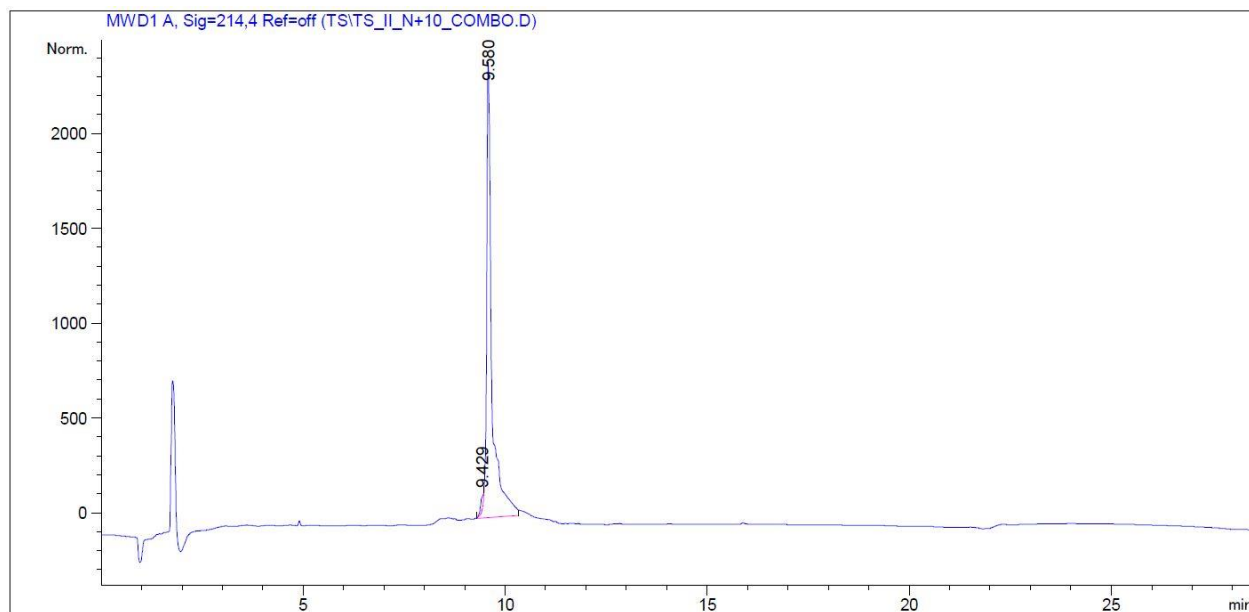
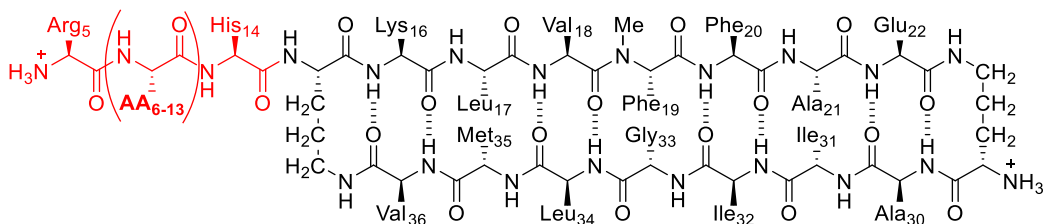
Characterization of N+8



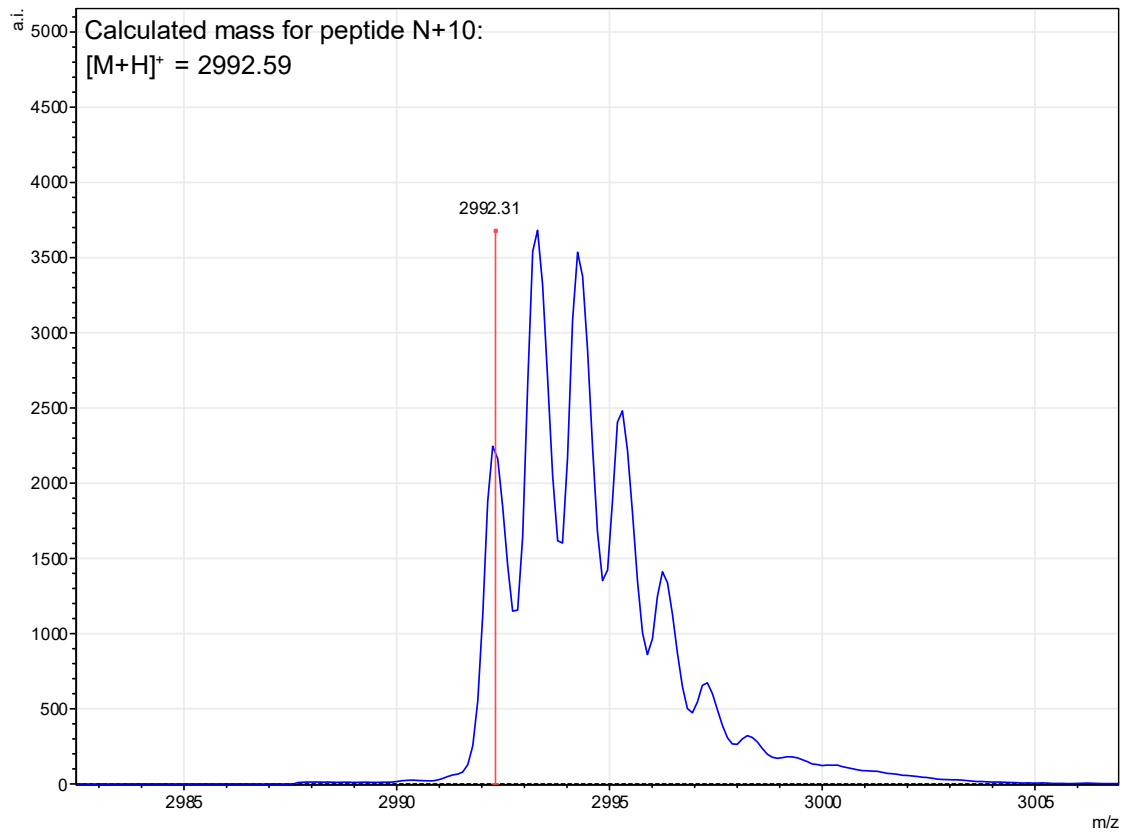
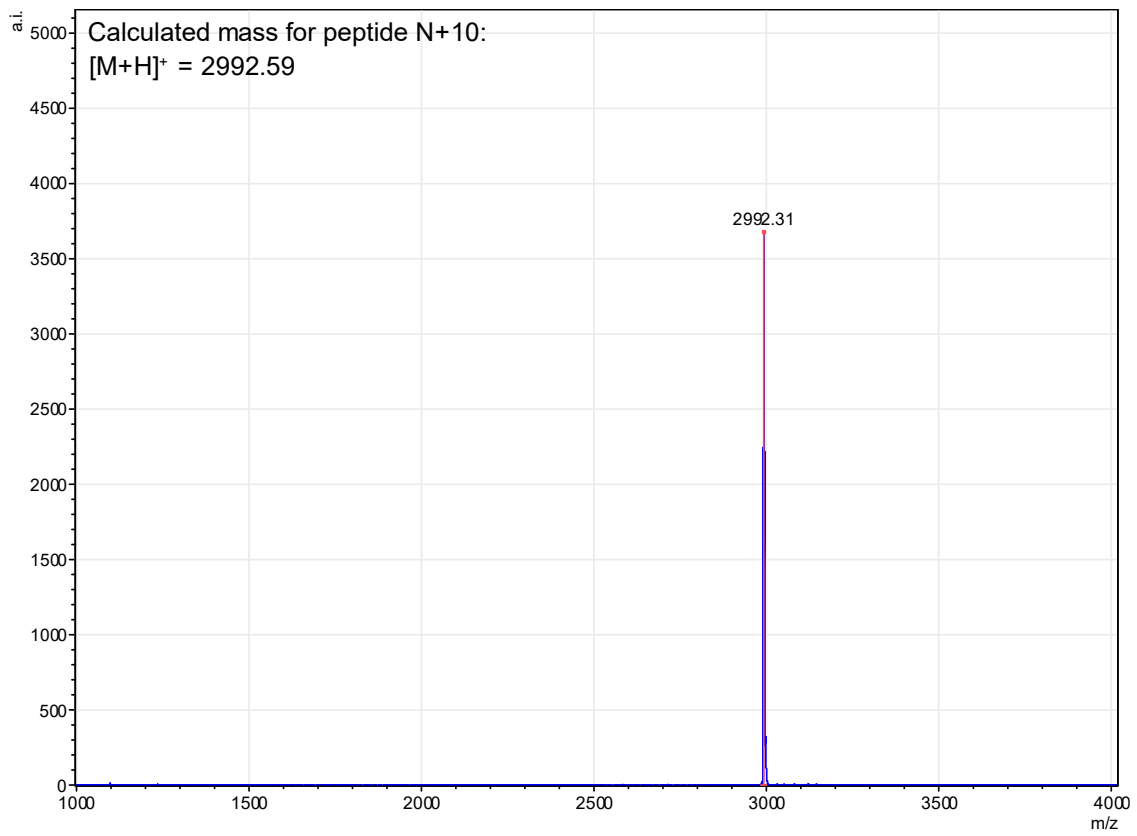
Peak #	RetTime [min]	Type	Width [min]	Area [mAU*s]	Height [mAU]	Area %
1	10.826	MM	0.3137	1.43608e4	2105.97363	100.0000



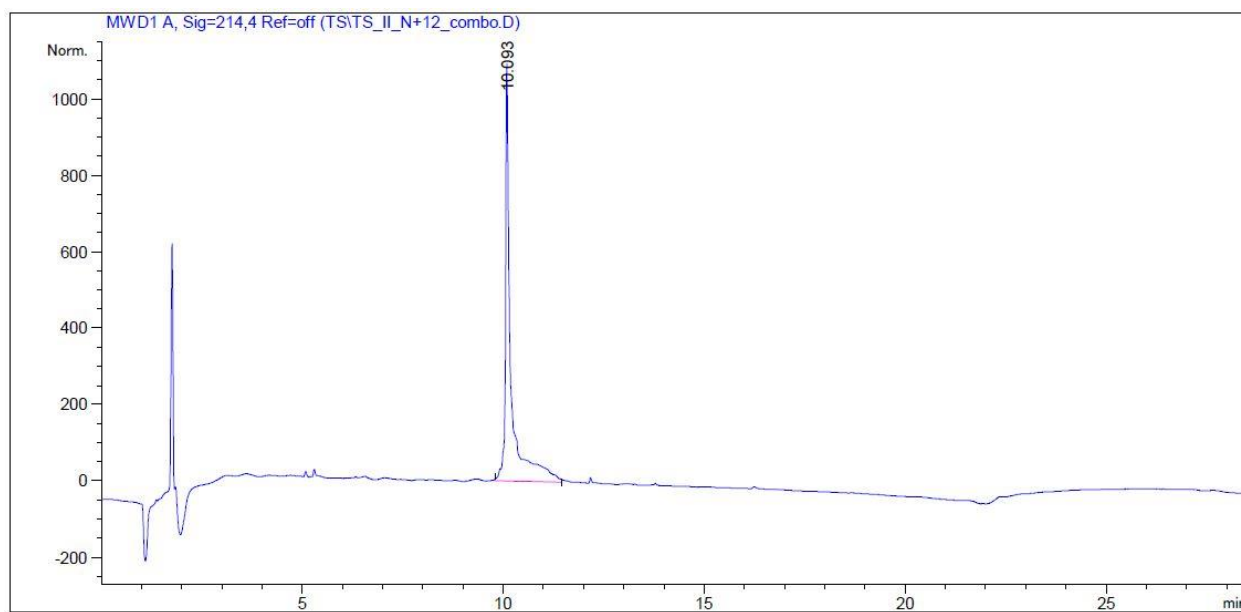
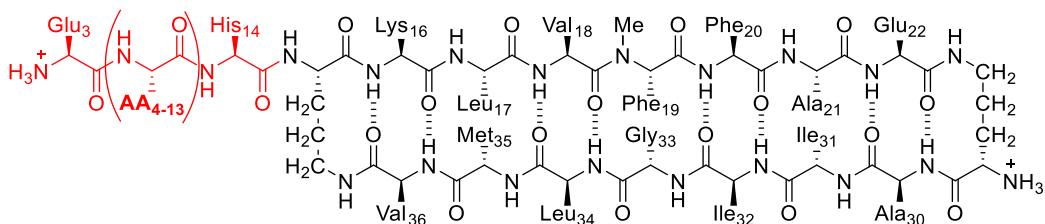
Characterization of N+10



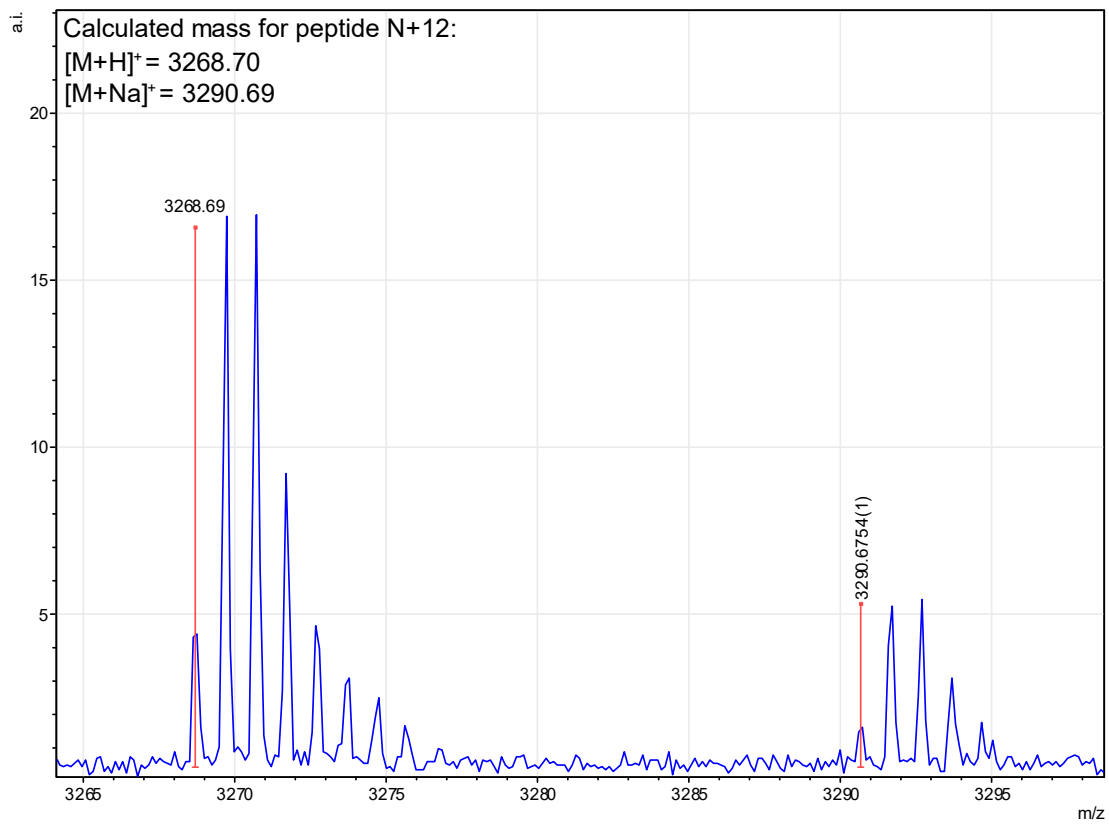
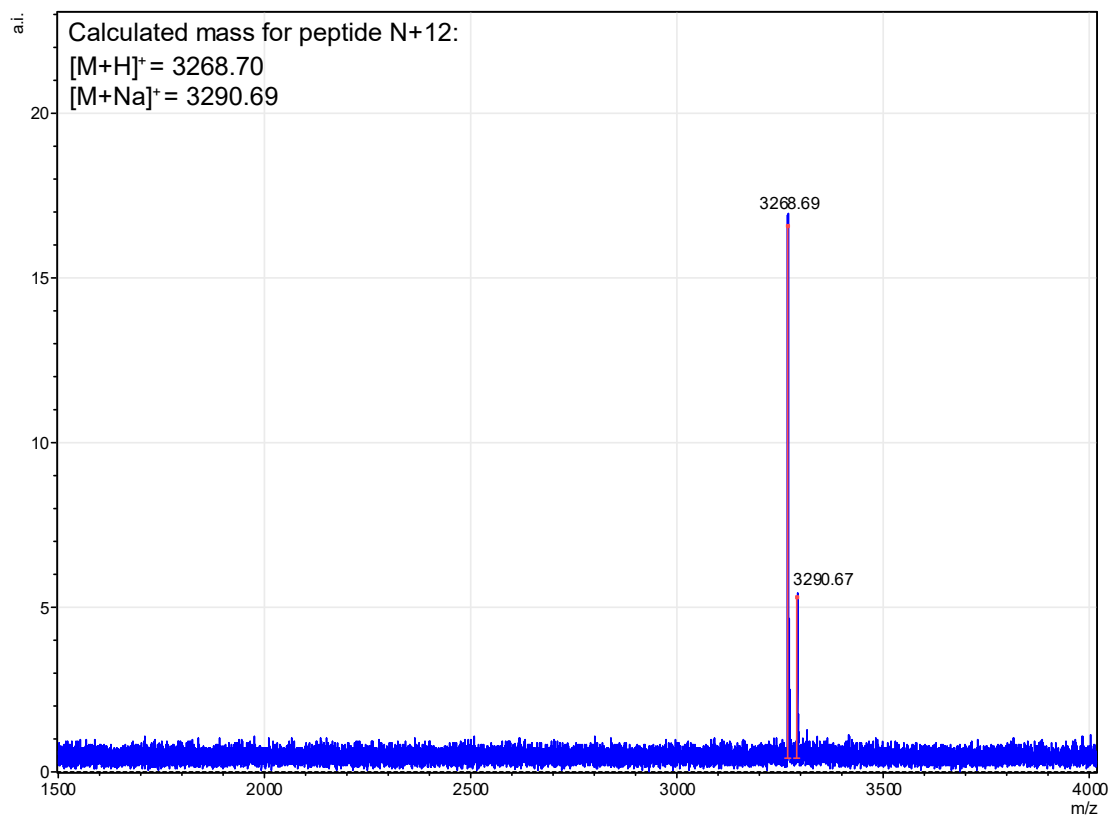
Peak #	RetTime [min]	Type	Width [min]	Area [mAU*s]	Height [mAU]	Area %
1	9.429	BV E	0.0606	346.39841	83.20280	2.8873
2	9.580	VV R	0.1160	1.64610e4	2132.79688	97.1127



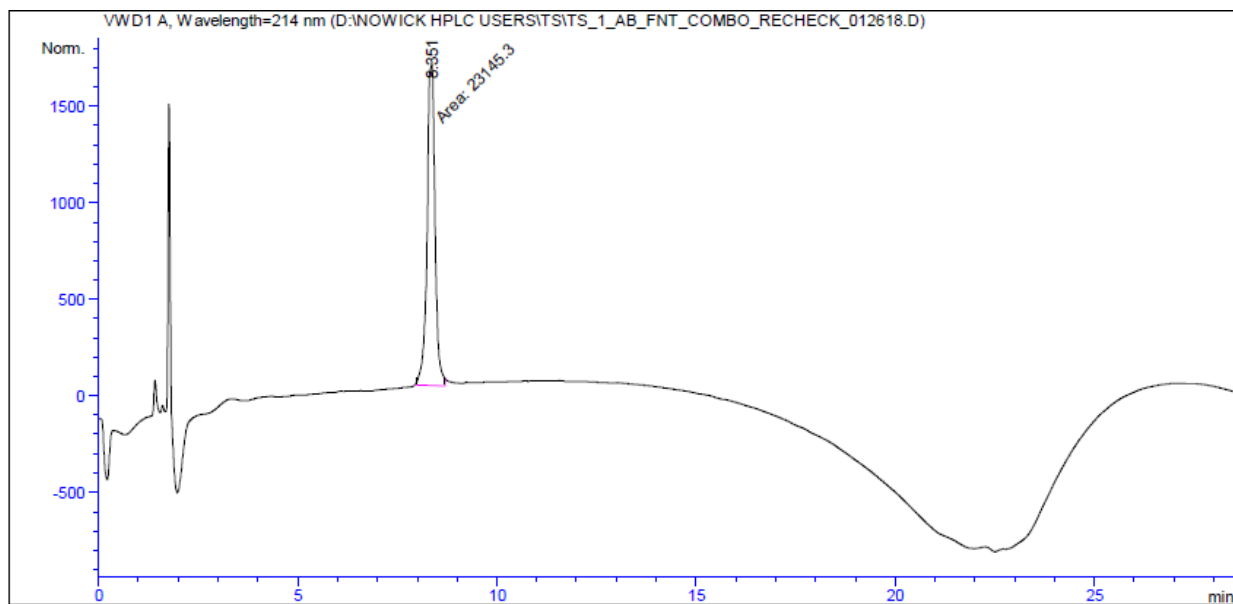
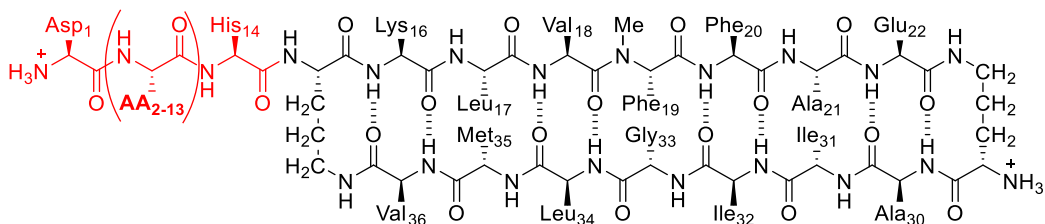
Characterization of N+12



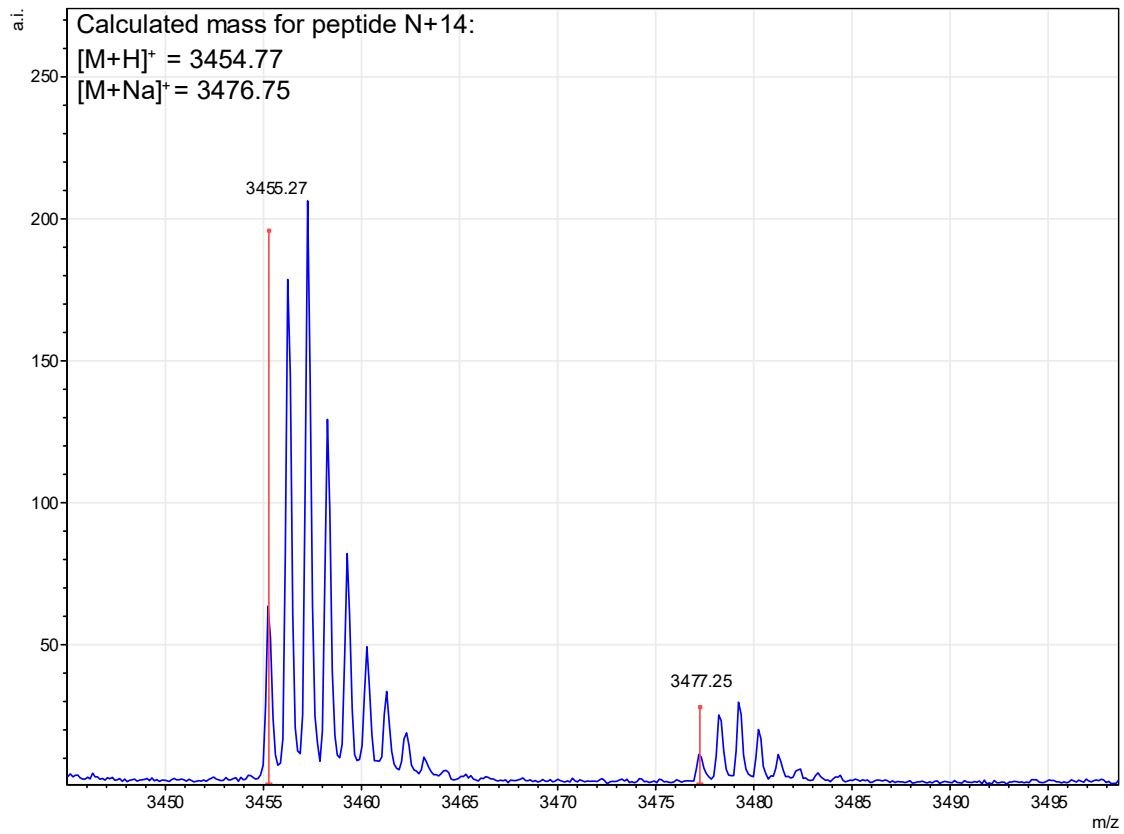
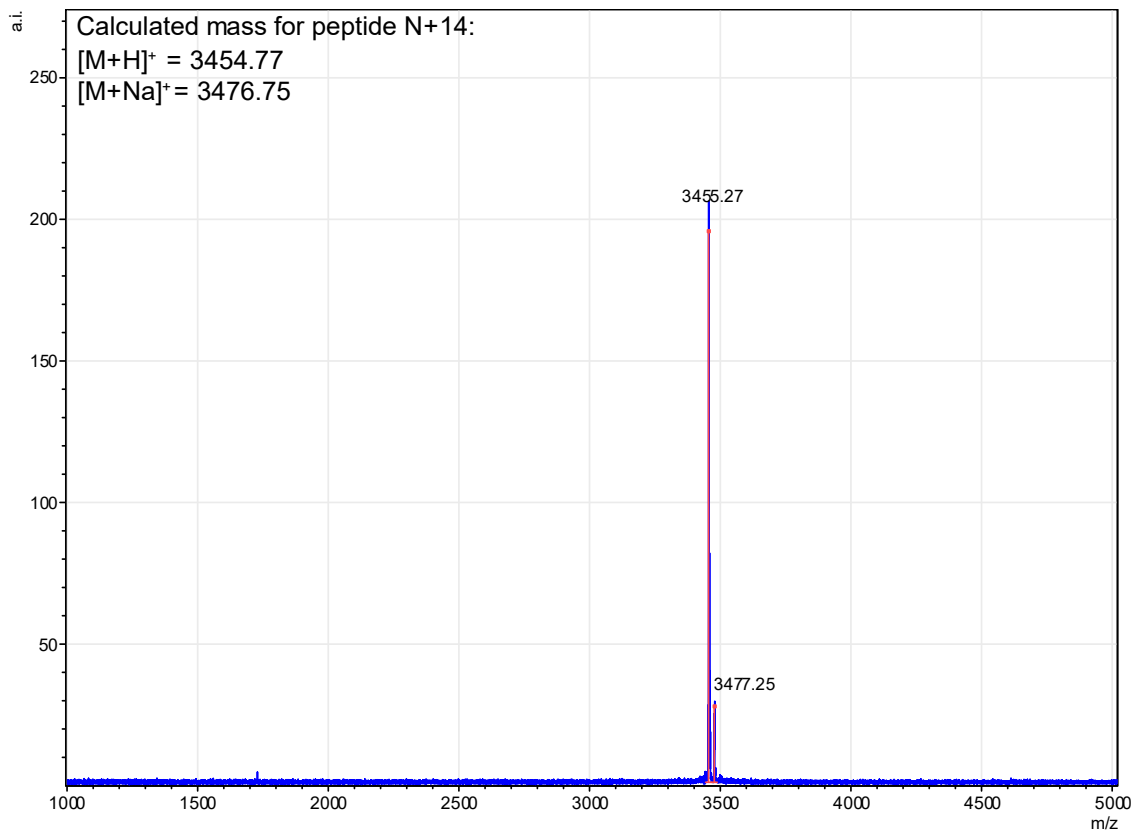
Peak #	RetTime [min]	Type	Width [min]	Area [mAU*s]	Height [mAU]	Area %
1	10.093	MF	0.6067	6318.32568	986.75244	100.0000



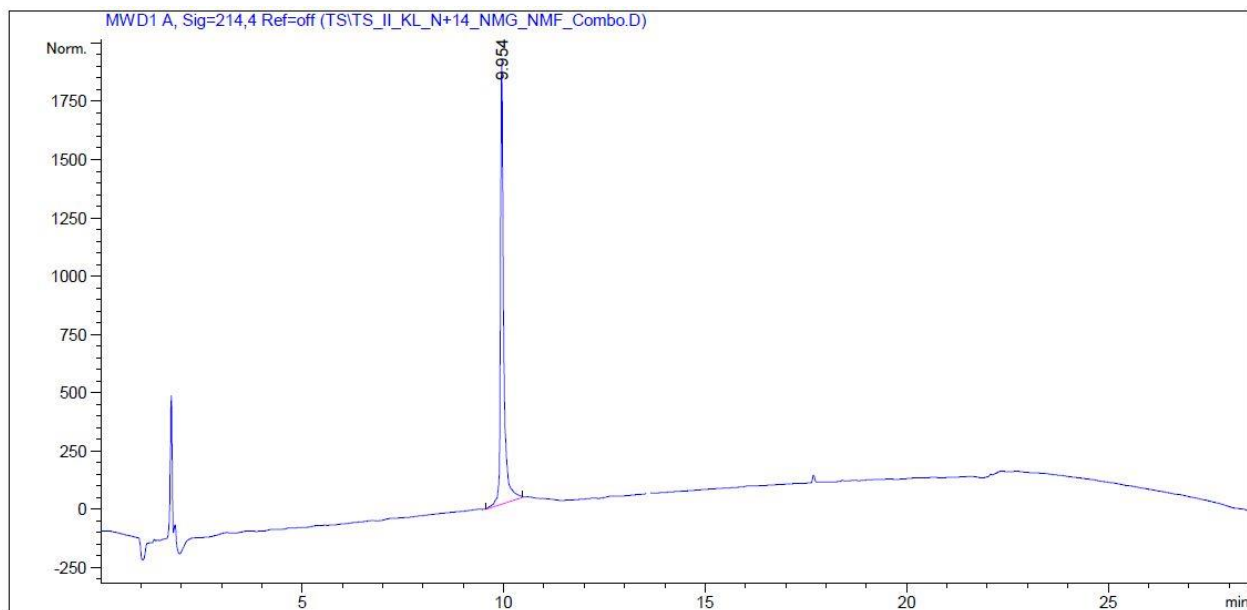
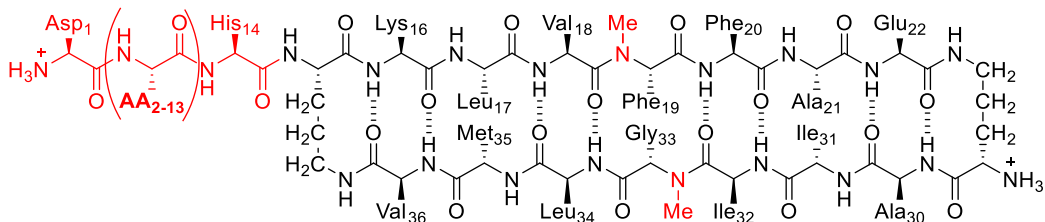
Characterization of N+14



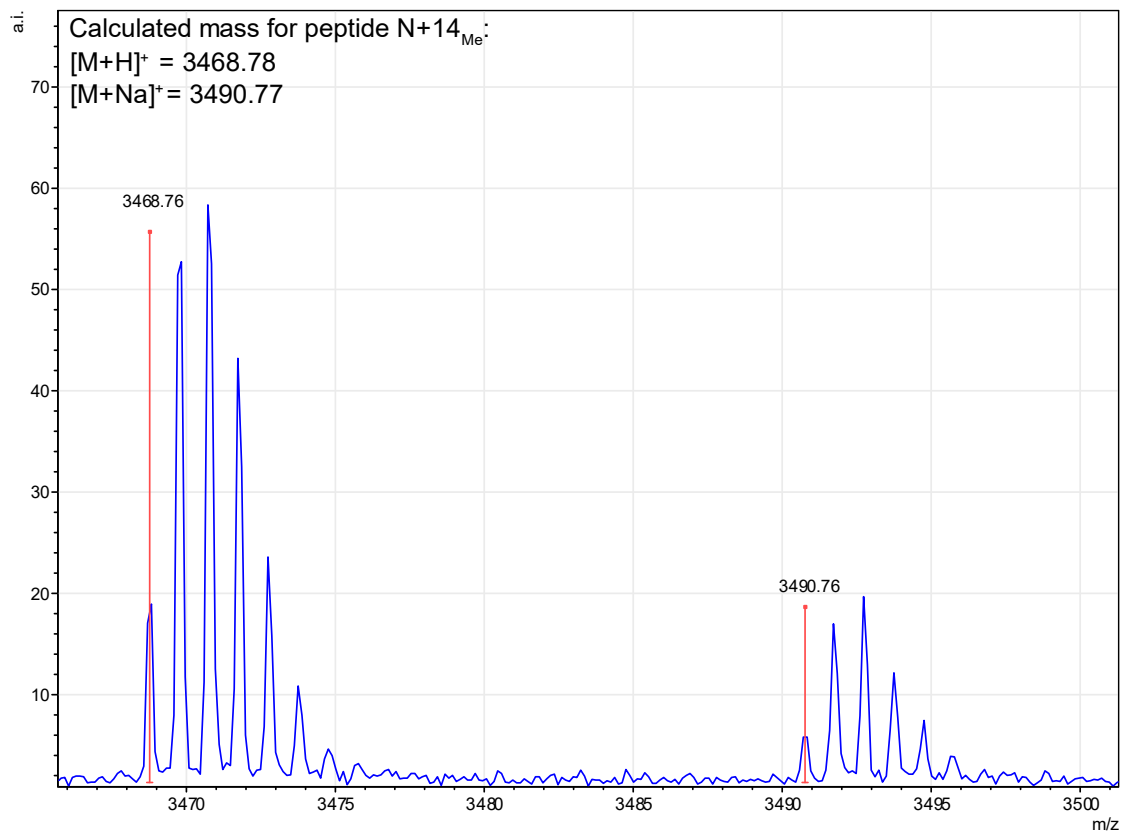
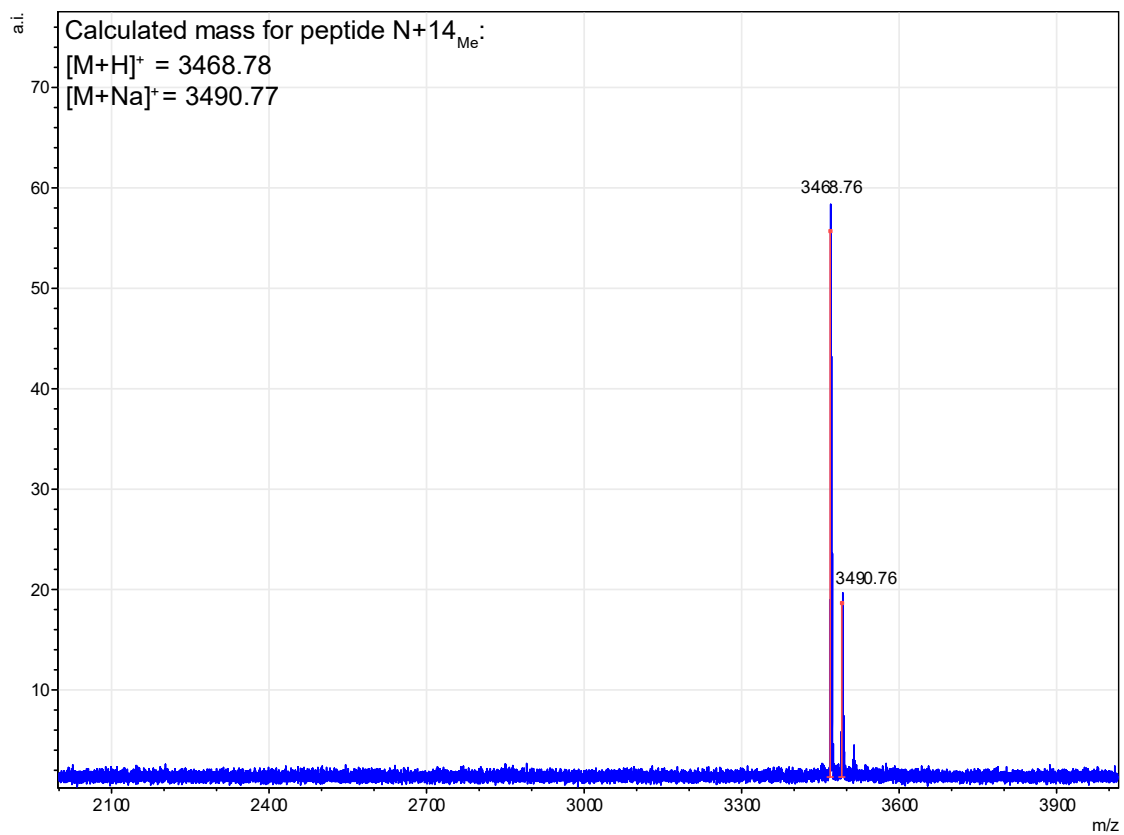
Peak #	RetTime [min]	Type	Width [min]	Area mAU *s	Height [mAU]	Area %
1	8.351	MM	0.2307	2.31453e4	1672.36609	100.0000



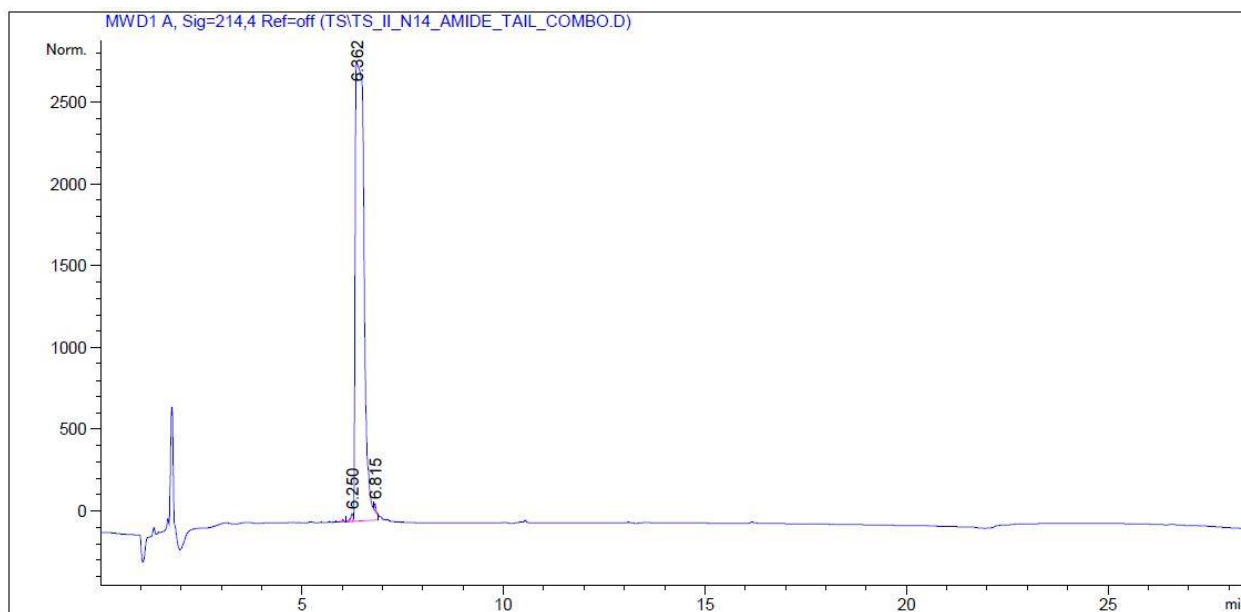
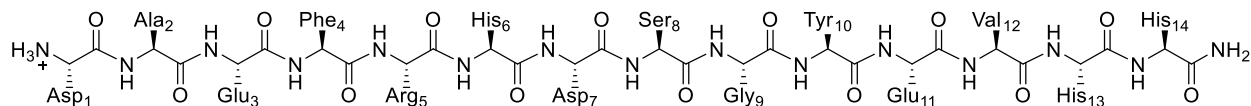
Characterization of *N+14Me*



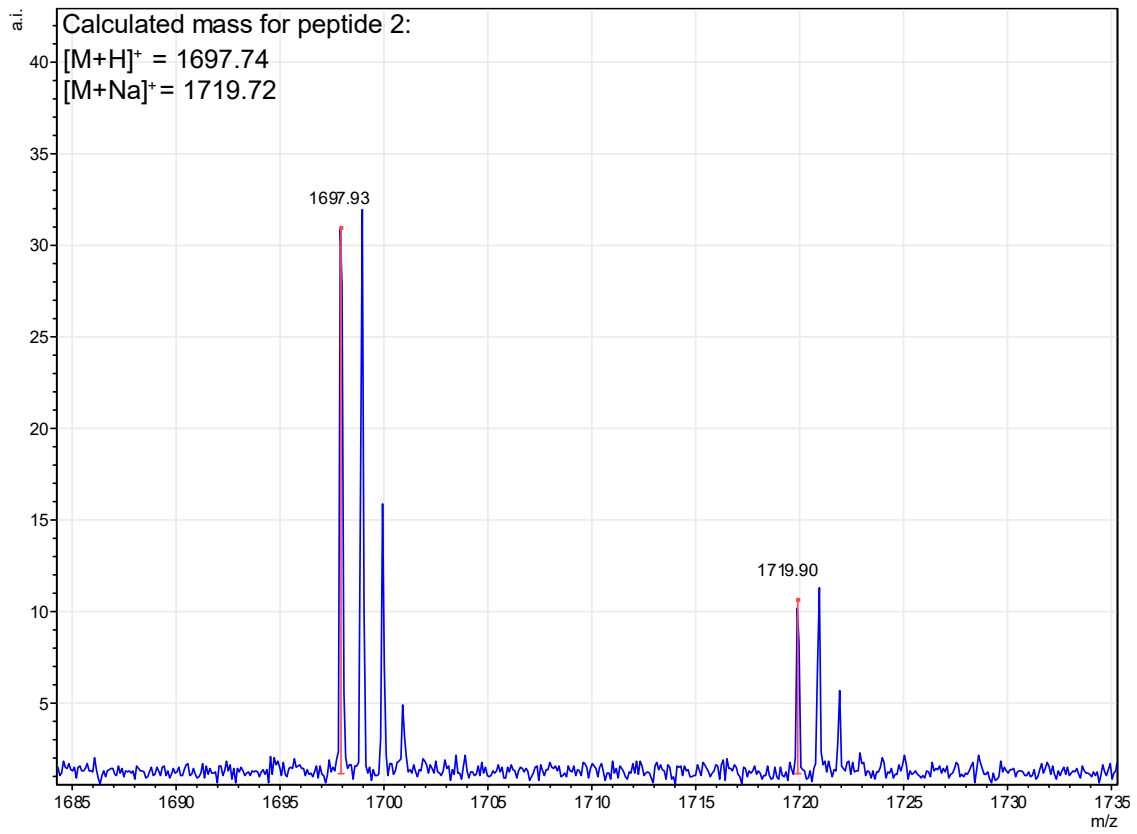
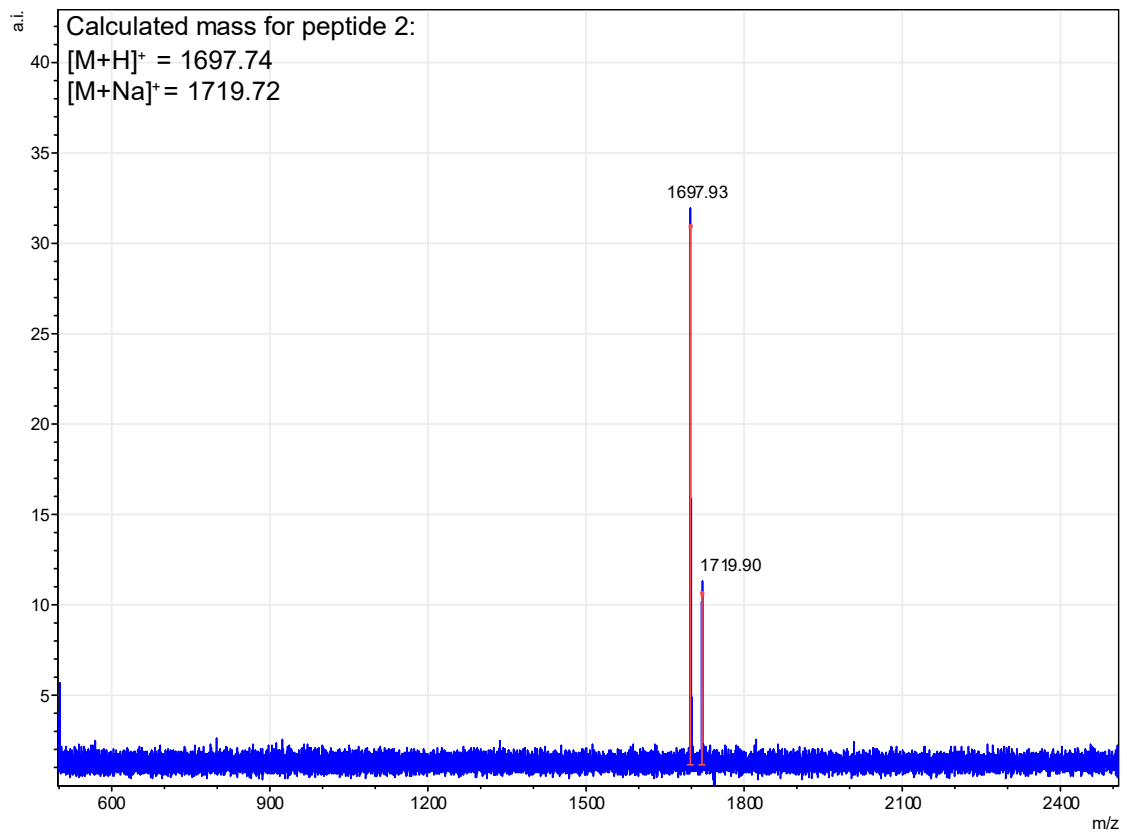
Peak #	RetTime [min]	Type	Width [min]	Area [mAU*s]	Height [mAU]	Area %
1	9.954	BV R	0.0673	9244.65234	1702.65344	100.0000



Characterization of peptide 2



Peak #	RetTime [min]	Type	Width [min]	Area [mAU*s]	Height [mAU]	Area %
1	6.250	BV E	0.0601	181.10962	42.13483	0.4690
2	6.362	VV R	0.1967	3.82930e4	2528.83789	99.1675
3	6.815	VV E	0.0421	101.44323	39.33643	0.3635



Chapter 3

A β -Barrel-Like Tetramer Formed by a Macrocyclic β -Hairpin Derived From A β

INTRODUCTION

The oligomers formed by the β -amyloid peptide A β are unstable and exhibit significant variation in their stoichiometry and structure.¹⁻⁵ This variation complicates efforts to understand how A β oligomers affect neurodegeneration associated with Alzheimer's disease.^{6,7} Establishing structure activity relationships between A β oligomers and their neurotoxicity will further our understanding of Alzheimer's disease and bolster efforts to develop diagnostics and drugs.⁸ Developing these connections requires expanding our library of high-resolution structures to better reflect the immense variation and heterogeneity in the structures of A β oligomers.

The NMR-based structure of a tetramer formed by full-length A β_{42} reported by Carulla et al. is the only atomic resolution structure of an A β oligomer that has been deposited in the Protein Data Bank, (PDB 6RHY).⁹ The tetramer comprises a six-stranded antiparallel β -sheet, with two β -hairpins of A β_{42} that bookend two antiparallel β -strands of A β_{42} (**Sup. Figure 3.1a**). Additional solution phase studies of this tetramer also provide evidence for the formation of an octamer. Using molecular dynamics (MD), Carulla et al. propose a model in which this tetramer, as well as the octamer, can act to disrupt a lipid membrane and facilitate water permeation. Collectively, these

studies have brought into sharp relief the importance of β -hairpins in the structures of A β oligomers.

Several other studies have also established the significance of the β -hairpin conformation in the formation of A β oligomers.^{10–15} In 2008, Härd and Hoyer reported the NMR structure of a monomer of A β ₄₀ adopting a β -hairpin conformation when sequestered and stabilized by an affibody.¹¹ Härd et al. subsequently stabilized this A β β -hairpin using an intermolecular disulfide-bridge and found that the stabilized β -hairpin formed oligomers that mimicked some of the properties of oligomers formed by unmodified A β .¹² NMR spectroscopic studies revealed that related disulfide stabilized β -hairpins derived from A β _{16–42} assembled to form a barrel-shaped hexamer stabilized by hydrophobic packing and edge-to-edge hydrogen bonding between β -hairpins (**Sup. Figure 3.1b**).¹⁴

β -Hairpins have also been reported as a key component in the structures of A β fibrils.¹⁶ Tycko et al. recently reported a unique A β ₄₀ fibril structure, where the typical core of parallel in-register β -sheets is coated by an outer layer of β -hairpins formed by A β (**Sup. Figure 3.1c**). A model of this β -hairpin created by Tycko et al., that fits the observed electron density and other data, shows residues 16–22 and 30–36 hydrogen bonding to form an antiparallel β -sheet, with the intervening residues 23–29 forming a loop (**Figure 3.1a**).

The β -hairpins reported by Carulla et al., Härd and Hoyer et al., and Tycko et al. all differ in the alignment of their β -strands (**Figure 3.1a**). In the tetramer reported by Carulla et al., β -strands comprising residues 9–21 and 28–40 hydrogen bond to form an antiparallel β -sheet, with residues 22–27 forming a loop. In the barrel-shaped hexamer reported Härd et al. β -strands comprising residues 17–22 and 30–36 hydrogen bond to form an antiparallel β -sheet, with residues 23–29 forming a loop. These differences in β -strand alignment alter the overall topology of β -hairpins by shifting residue pairings across β -strands, the hydrophobicity of β -hairpin surfaces,

and the size of loop segments between β -strands. In the β -hairpin reported by Carulla et al., Ile₃₂ is across from Phe₁₉; in the β -hairpin reported by Tycko et al., Gly₃₃ is across from Phe₁₉; and in the β -hairpin reported by Hård and Hoyer et al., Val₃₄ is across from Phe₁₉ (**Figure 3.1a**). These changes in alignment and topology may contribute to the immense variation and heterogeneity observed in the assembly and structures of A β fibrils and oligomers.

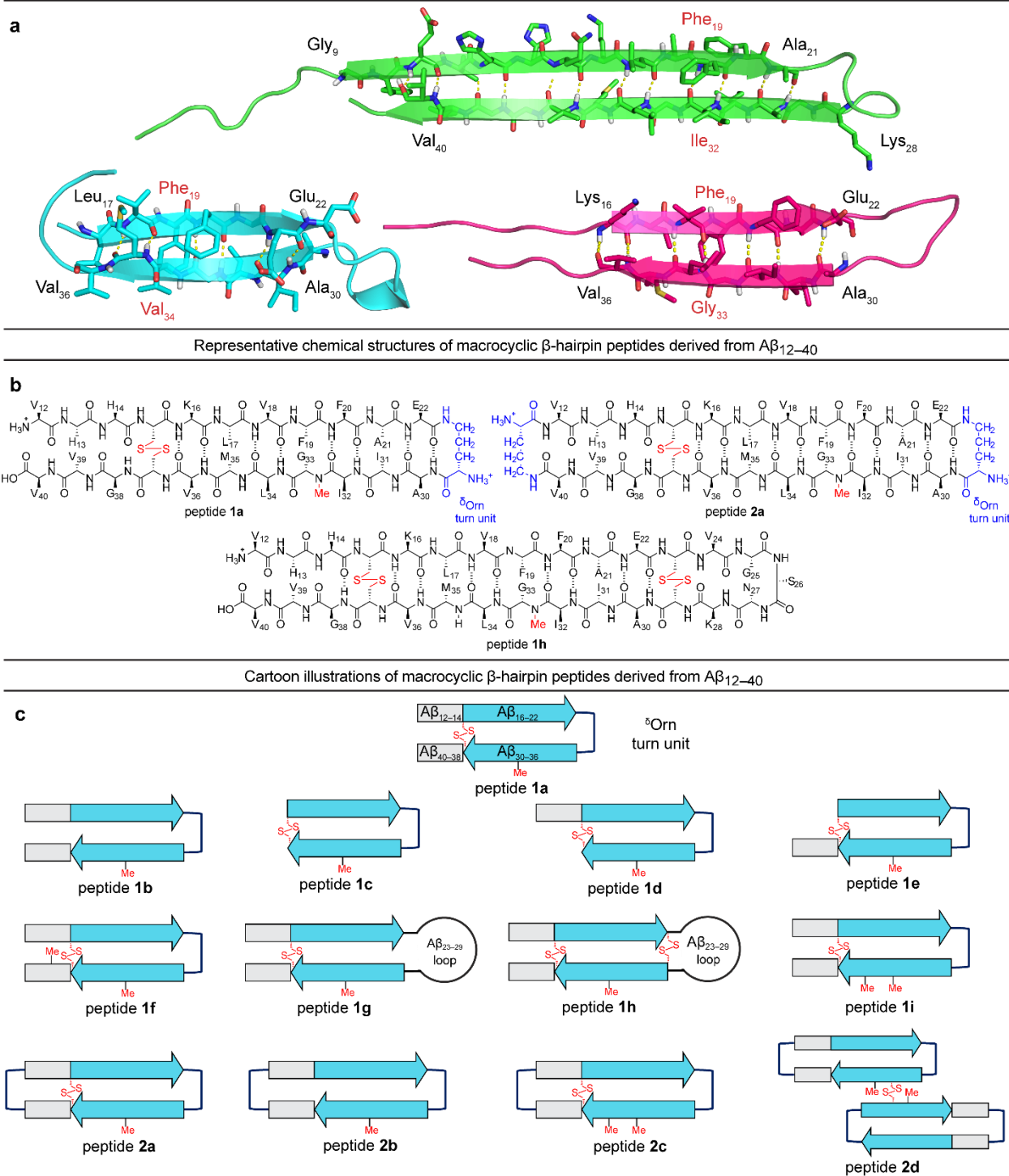


Figure 3.1. (a) Structures of A β β -hairpins reported by Carulla et al. (PDB 6RHY), Härd and Hoyer et al. (PDB 2OTK), and Tycko et al. (not deposited). (b and c) Chemical structures and cartoons of β -hairpin peptides derived from A β_{12-40} .

Here we report studies of β -hairpin peptides derived from A β and describe their assembly to form β -barrel-like tetramers and octamers. We began our investigation by preparing and

studying peptide **1a** and observed the assembly of an octamer by SDS-PAGE. To better understand the assembly of this octamer, we synthesized peptides **1b–i** and **2a–d** which are homologues of peptide **1a** also derived from A β (**Figure 3.1b and 3.1c**). Solution-phase studies of peptides **1b–i** and **2a–d** allowed us to identify key intramolecular and intermolecular interactions required for β -hairpin folding and octamer assembly. X-ray crystallographic studies of peptide **2a** reveal a hitherto unprecedented β -barrel-like tetramer assembled from β -hairpins derived from A β_{12-40} . Evidence for the assembly of a concatenated β -barrel-like octamer is also present within the crystal lattice of peptide **2a**, corresponding to solution-phase observations of oligomer assembly. These studies provide unique insights into the folding of A β and assembly of endogenous oligomers.

RESULTS

Design of peptides 1a–i and 2a–d.

We designed peptides **1a–i** and **2a–d** to mimic the folding of A β β -hairpins and probe their assembly into oligomers. In each of these peptides, we incorporated constraints to enforce folding and stabilize an alignment in which Val₁₂ is across from Val₄₀ — an alignment which matches that of the A β β -hairpin recently reported by Tycko et al (**Figure 3.1a and 3.1b**). Our laboratory routinely uses Fmoc-based solid phase peptide synthesis to constrain β -strand segments derived from amyloidogenic peptides and proteins to a β -hairpin conformation using δ Orn turn units and disulfide bridges.^{15,17–24} To prevent uncontrolled aggregation, we incorporate an *N*-methyl blocking group on one strand of the β -hairpin.

Peptide **1a** comprises two peptide β -strands of A β_{12-22} and A β_{30-40} linked by a δ Orn turn unit connecting residues 22 and 30, a cross-strand disulfide bridge replacing Gln₁₅ and Gly₃₇, and an *N*-methyl group on Gly₃₃ (**Figure 3.1b and 3.1c**). Peptide **1b** is a homologue of peptide **1a** that lacks the cross-strand disulfide bridge and contains the native Gln₁₅ and Gly₃₇ residues. Peptide **1c** restores this disulfide bridge but lacks the N- and C-terminal residues 12–14 and 38–40. Peptide

1d and **1e** are homologues of peptide **1a**, except that peptide **1d** lacks the C-terminal residues 38–40 and peptide **1e** lacks the N-terminal residues 12–14. Peptide **1f** is a homologue of peptide **1a** that bears an additional *N*-methyl group on Gly₃₈.

Peptide **1g**, is a homologue of peptide **1a** in which the δ Orn turn unit is replaced with a loop of residues comprising A β _{23–29}. Peptide **1h** is nearly identical to peptide **1g** except that it bears an additional cross-strand disulfide bridge replacing Asp₂₃ and Gly₂₉. Peptide **1i** is a homologue of peptide **1a** that bears an additional *N*-methyl group on Met₃₅. Peptide **2a** is a homologue of peptide **1a** that bears an additional δ Orn turn unit connecting residues 12 and 40. Peptide **2b** is a homologue of peptide **2a** that lacks the cross-strand disulfide bridge and restores Gln₁₅ and Gly₃₇. Peptide **2c** is a homologue of peptide **2a** that bears an additional *N*-methyl group on Met₃₅. Peptide **2d** is a dimer, comprising two monomers of peptide **2b** covalently linked by a disulfide bridge replacing Val₃₆ in each monomer.

Oligomerization of peptides 1a–h and 2a–d

Peptide **1a** (ca. 2.5 kDa) runs as an oligomer in SDS-PAGE, migrating at a molecular weight consistent with that of an octamer (ca. 20 kDa) (Figure 2a). The octamer band streaks downward from below the 26 kDa ladder band to the 4.6 kDa ladder band, suggesting that the octamer is in rapid equilibrium with lower molecular weight species. The formation of oligomers that can be observed in SDS-PAGE is a hallmark of A β . Unlike the oligomer formed by peptide **1a**, the oligomers formed by full-length, unmodified A β are heterogeneous in size and typically display a substantial band for the monomer (**Figure 3.2a**).^{25–27} The formation of a well-defined oligomer band by peptide **1a** suggests that this constrained A β β -hairpin peptide forms a well-defined supramolecular assembly in the membrane-like environment provided by the amphiphilic SDS molecules.

To better understand the assembly of the putative octamer, we prepared and studied structural homologues of peptide **1a**, peptides **1b–h** (**Figure 3.1c** and **Figure 3.2a**). Peptide **1b** (2.5 kDa) lacks a cross-strand disulfide bridge and does not assemble, migrating to just below the 4.6 kDa ladder band. Peptide **1c** (1.8 kDa) lacks the N- and C-terminal residues 12–14 and 38–40 and also does not assemble, migrating as a downward streaking band from the 4.6 kDa ladder band. In contrast to peptide **1c**, peptide **1d** (2.3 kDa) lacks just the C-terminal residues 38–40 and does assemble. Like peptide **1a**, peptide **1d** migrates as a downward streaking band from below the 26 kDa ladder band to the 4.6 kDa ladder band. The band formed by peptide **1d** is consistent with the molecular weight of an octamer that is in equilibrium with lower molecular weight species. Peptide **1e** (2.1 kDa) lacks just the N-terminal residues 12–14 but does not assemble. Instead, peptide **1e** migrates as an upward streaking band from the 4.6 kDa ladder band to the 17 kDa ladder band.

The non-assembly of peptide **1b** reveals that the cross-strand disulfide bridge near the N- and C-terminal residues is necessary for assembly of the putative octamer. The assembly of peptide **1d**, in contrast to peptides **1c** and **1e**, is surprising and suggests that residues 12–14 participate in intermolecular interactions crucial for assembly of the putative octamer.

To further examine the role of interactions between the N- and C-terminal residues of peptide **1a**, 12–14 and 38–40, in the assembly of the octamer, we prepared and studied peptide **1f**. In peptide **1f**, the *N*-methyl group on Gly₃₈ is positioned to disrupt hydrogen bonding interactions between residues 12–14 and 38–40. In contrast to peptide **1a**, peptide **1f** (2.5 kDa) does not assemble as an octamer, but instead migrates as a band between the 10 kDa and 4.6 kDa ladder bands that streaks downward. This result suggests that hydrogen bonding interactions between residues 12–14 and 38–40 are required for assembly of the putative octamer.

To examine whether the putative octamer formed by peptide **1a** can accommodate residues 23–29 as a loop, and to better mimic endogenous A β β -hairpins and A β oligomers we prepared and studied peptide **1g** (**Figure 3.1c**). In peptide **1g** a loop comprising residues 23–29 replaces the δ Orn turn unit. In contrast to peptide **1a**, peptide **1g** (3.0 kDa) does not assemble and instead migrates to just above the 4.6 kDa ladder band. This result would suggest that the putative octamer cannot accommodate residues 23–29 as a loop. We also considered an alternative premise, wherein the replacement of the δ Orn turn unit destabilizes the β -hairpin conformation of peptide **1g** thereby abrogating assembly. To test this hypothesis, we prepared and studied peptide **1h** (**Figure 3.1b and 3.1c**). Peptide **1h** incorporates an additional cross-strand disulfide bridge replacing Asp₂₃ and Gly₂₉, to fortify the β -hairpin conformation of the peptide. Peptide **1h** (3.0 kDa) migrates as two oligomers, a lower molecular weight oligomer consistent with a tetramer and a higher molecular weight oligomer consistent with an octamer. The tetramer band migrates to a position between the 10 and 17 kDa ladder bands and is much greater in intensity than the octamer band, which migrates to just below the 26 kDa ladder band. The difference in intensity between the tetramer and octamer bands suggest that peptide **1h** favors assembly of the tetramer.

Our laboratory routinely prepares and studies oligomers formed by macrocyclic β -hairpin peptides derived from A β .^{28,29} Two δ Orn turn units are used to stabilize these β -hairpin peptides to a macrocycle. Peptide **2a** is a macrocyclic homologue of peptide **1a**, that bears a second δ Orn turn unit connecting the N and C-terminal residues 12 and 40 (**Figure 3.1b and 3.1c**). Like peptide **1h**, peptide **2a** (2.6 kDa) migrates as two oligomers, a lower molecular weight oligomer consistent with a tetramer and a higher molecular weight oligomer consistent with an octamer. The tetramer band migrates to a position just above the 10 kDa ladder band, and the octamer band migrates to a position between the 17 and 26 kDa ladder bands. Both bands are equal in their intensity, with the octamer band streaking downward toward the tetramer band, suggesting that both species are in

equilibrium with each other. Peptide **2b** is a homologue of peptide **2a** that lacks the cross-strand disulfide bridge and does not assemble, instead migrating to just below the 4.6 kDa ladder band.

The assembly of a tetramer in addition to the octamer, by peptides **1h** and **2a**, was both surprising and unanticipated. In comparison to peptide **1a**, peptides **1h** and **2a** bear additional stabilizing constraints, a second disulfide bridge and a second δ Orn turn unit respectively. Rather than stabilize the assembly of the putative octamer formed by peptide **1a**, the introduction of these additional constraints appears to have had a destabilizing effect on octamer assembly. We speculate that these tetramers may be components of the putative octamer formed by peptide **1a**. The lack of assembly by peptide **2b**, despite the second δ Orn turn unit, suggests that the cross-strand disulfide bridge replacing Gln₁₅ and Gly₃₇ is essential for octamer assembly.

Folding of peptides 1a–h and 2a–d

CD spectroscopy reveals that peptide **1a** adopts a β -sheet conformation, suggesting that the peptide does fold into a conformation resembling a β -hairpin, as designed (**Figure 3.2b**). The spectrum of peptide **1a** displays a strong negative band centered at ca. 212 nm, with increasing ellipticity at lower wavelengths that reaches a maximum at ca. 198 nm before decreasing once again. In contrast to peptide **1a**, the CD spectrum of peptide **1b** reveals that the peptide does not fold and instead adopts a predominant random coil conformation. The CD spectrum of peptide **1b** displays a strong negative band centered at ca. 198 nm and a weak positive band at ca. 220 nm (**Figure 3.2b**). The CD spectra of peptides **1a**, **1c–f**, **1h**, and **2a** shows that each peptide folds to adopt a β -hairpin-like conformation. In contrast to peptides **1a**, **1c–f**, **1h**, and **2a**, peptides **1b**, **1g** and **2b** do not fold, and instead adopt random-coil-like conformations.

Differences in the CD spectra of peptides **1g** and **1h** reveal the impact of replacing the δ Orn turn unit with A β residues 23–29 (**Figure 3.2c**). The CD spectrum of peptide **1g** displays a broad and shallow negative band (ca. $\Theta = -5600 \text{ deg cm}^2 \text{ dmol}^{-1}$) centered at ca. 204 nm, suggestive of a

random-coil-like conformation. Differences between the CD spectra of peptides **1a** and **1g** likely reflect differences in the rigidity of each peptide due to the presence or absence of the δ Orn turn unit. In contrast to peptide **1g**, peptide **1h**, which bears an additional cross-strand disulfide bridge to restore rigidity, folds to adopt a β -hairpin-like conformation. Peptide **1h** displays a negative band (ca. $\Theta = -5000 \text{ deg cm}^2 \text{ dmol}^{-1}$) that is centered at ca. 212 nm with increasing ellipticity at lower wavelengths.

The CD spectra of peptides **2a** and **2b** suggests that the addition of a second δ Orn turn unit connecting residues 12 and 40 does not have a substantial effect on folding relative to peptides **1a** and **1b** (**Figure 3.2c**). The spectrum of peptide **2a** displays a strong negative band (ca. $\Theta = -7400 \text{ deg cm}^2 \text{ dmol}^{-1}$) centered at ca. 214 nm with increasing ellipticity at lower wavelengths, reflecting a β -hairpin-like conformation. Peptide **2b** displays a strong negative band centered at ca. 200 nm and a weak positive band at ca. 220 nm, indicative of a random coil conformation. Like the CD spectra of peptide **1b**, the loss of the cross-strand disulfide bridge that replaces Gln₁₅ Gln₃₇ ablates folding.

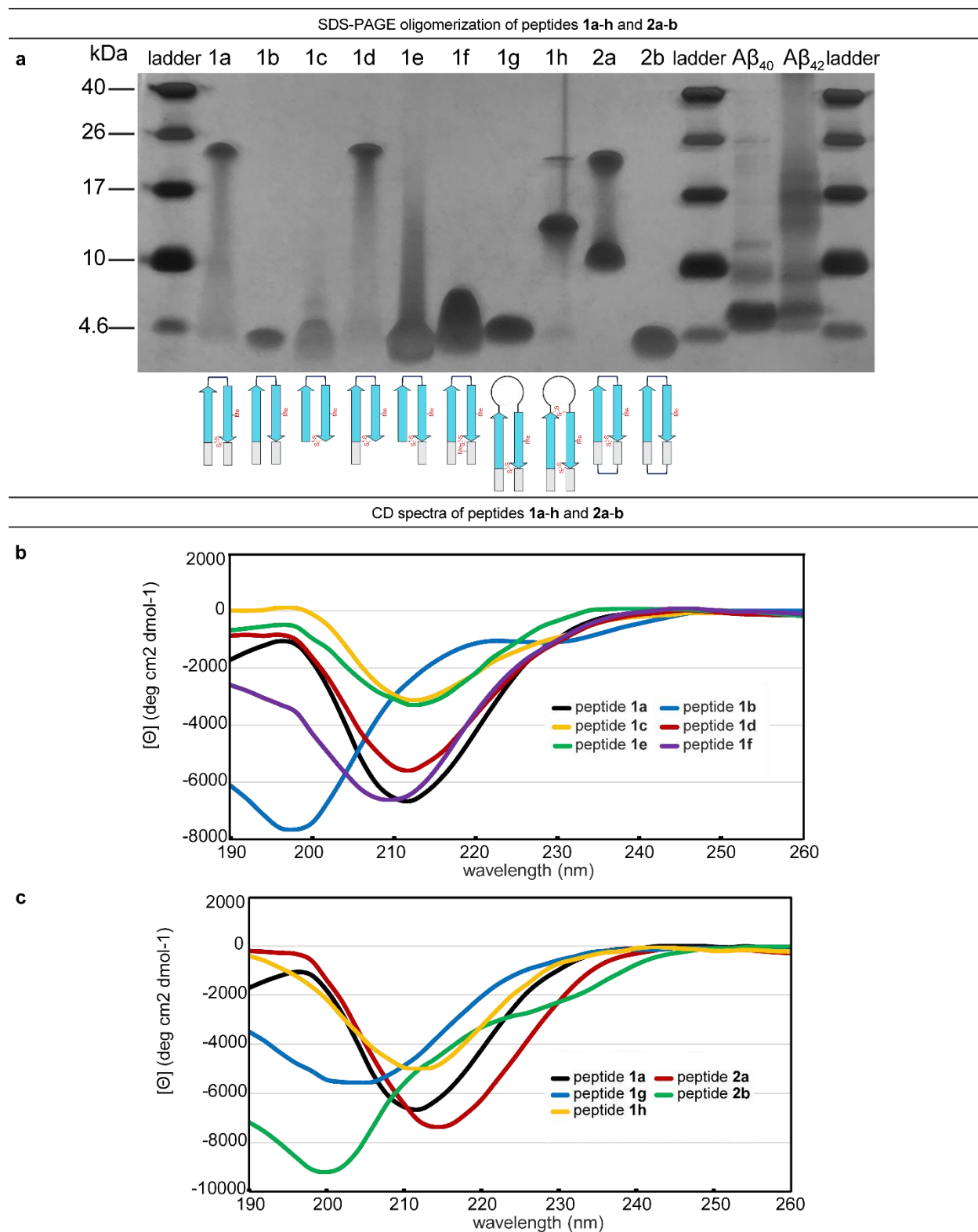


Figure 3.2. (a) Silver stained SDS-PAGE of peptides **1a-h**, **2a-b**, and $A\beta_{40}$ and $A\beta_{42}$. SDS-PAGE was performed in Tris buffer at pH 6.8 with 2% (w/v) SDS on a 16% polyacrylamide gel with 50 μ M solutions of peptide in each lane. (b and c) Circular dichroism (CD) spectra of peptides **1a-h** and **2a-b**. CD spectra were acquired for each peptide at 50 μ M in 10 mM phosphate buffer at pH 7.4; ellipticity was normalized for the number of residues in each peptide.

X-ray crystallographic and REMD studies of peptide 2a

X-ray crystallography reveals that twisted β -hairpin monomers of peptide **2a** assemble in the crystal lattice to form antiparallel dimers, that further assemble to form β -barrel-like tetramers and octamers. The β -barrel-like tetramers and octamers are stabilized by edge-to-edge hydrogen bonding and hydrophobic packing. Peptide **2a** afforded crystals suitable for X-ray diffraction from an aqueous solution of 0.1 M sodium cacodylate trihydrate buffer at pH 6.5, 0.2 M magnesium acetate tetrahydrate, and 30% v/v 2-methyl-2,4-pentanediol. Molecular replacement, using a search model derived from the crystallographic structure of a dimer formed by a macrocyclic β -hairpin peptide derived from A β_{16-36} (PDB 6WXM), was used to determine the X-ray crystallographic phases of peptide **2a**.³⁰ Supplementary table 3.1 summarizes the crystallographic properties, crystallization conditions, data collection, and model refinement statistics for peptide **2a**.

X-ray crystallography reveals that peptide **2a** folds to adopt a twisted β -hairpin conformation, corroborating the CD spectra of peptide **2a**. This β -hairpin is stabilized by eleven intramolecular hydrogen bonds formed between the β -strands comprising residues 12–22 and 30–40, and a disulfide bridge that replaces Gln₁₅ and Gly₃₇ (**Figure 3.3a**). Two monomers of peptide **2a** assemble to form a hydrogen-bonded antiparallel dimer (**Figure 3.3b**). This dimer is stabilized by two pairs of intermolecular hydrogen bonds formed between the backbone amides of Met₃₅ and Cys₃₇.

Two antiparallel dimers of peptide **2a** assemble further to form a β -barrel-like tetramer that is stabilized by edge-to-edge intermolecular hydrogen bonding and the packing of hydrophobic residues (**Figure 3.3c**). The tetramer is stabilized by four intermolecular hydrogen bonds between monomers of peptide **2a**. Two hydrogen bonds are formed between the backbone of His₁₃ in one monomer and the backbone of Ala₂₁ and Phe₁₉ in another monomer of peptide **2a**. The remaining

two hydrogen bonds are formed between the backbone of Phe₁₉ in one monomer and the backbone of His₁₃ and Cys₁₄ in another monomer of peptide **2a**. The interior of this β -barrel-like tetramer is lined with hydrophobic residues comprising Val, Phe, Leu, Ile, Met, and Cys that pack together and provide additional stability (**Figure 3.3d**).

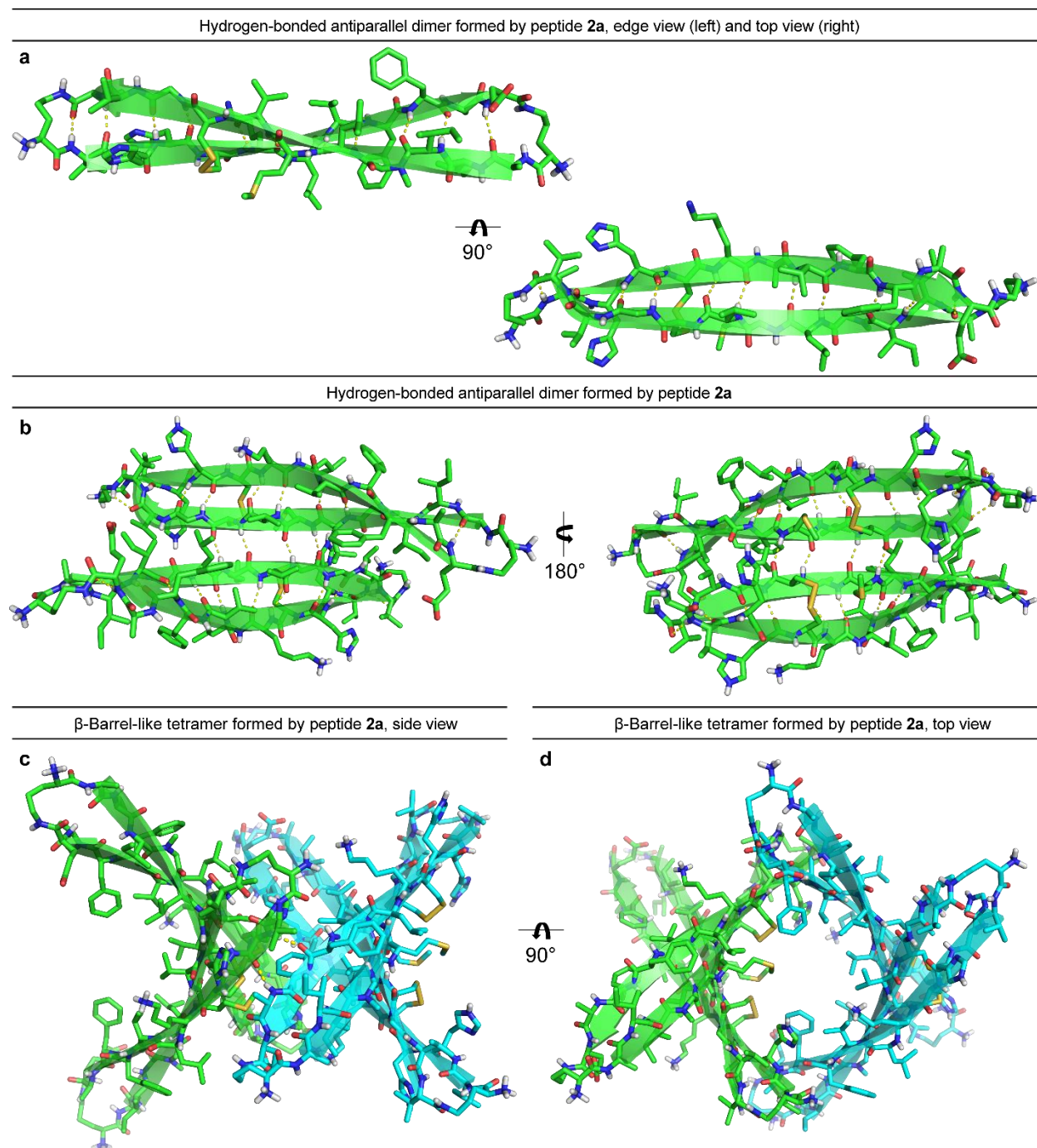


Figure 3.3. X-ray crystallographic structure of (a) twisted β -hairpin, (b) antiparallel dimer, and (c) side and (d) top views of the β -barrel-like tetramer formed by peptide **2a**.

The β -barrel-like tetramer formed by peptide **2a** is stabilized by parallel and antiparallel β -sheet interactions (**Figure 3.4a**). Intermolecular hydrogen bonds stabilize an antiparallel dimer comprising β -hairpins of peptide **2a**, green: green and blue: blue. Intermolecular hydrogen bonds also stabilize a parallel dimer comprising β -hairpins of peptide **2a**, green: blue and blue: green.

We envision that full-length A β can assemble in the same fashion as peptide **2a** to form a β -barrel-like tetramer. To understand what a tetramer containing residues 23–29 and additional N- and C-terminal residues might look like, we modeled A β_{9-42} into the crystallographic coordinates of each monomer in the tetramer formed by peptide **2a**. We built A β_{23-29} (DVGSNKG), A β_{9-11} (GYE), and A β_{41-42} (IA) into the crystallographic coordinates of the four peptide **2a** monomers that comprise the tetramer. The cross-strand disulfide bridge was replaced with the native residues Gln₁₅ and Gly₃₈, and the *N*-methyl group on Gly₃₈ was removed. We then performed REMD to generate realistic conformations of the loops and N- and C-terminal regions of the β -hairpins (**Figure 3.4b**). The REMD simulations show that A β_{9-42} could form a β -barrel-like tetramer without steric clashes.

Two β -barrel-like tetramers of peptide **2a** assemble further to form an octamer (**Figure 3.4c**). This octamer is stabilized by the same edge-to-edge hydrogen bonding and hydrophobic packing interactions that stabilize the tetramer. The octamer comprises two concatenated β -barrel-like tetramers of peptide **2a**, containing eight monomers of peptide **2a** in total. The openings of the two tetramers lie parallel to each other on the same axis. A third β -barrel-like tetramer is formed at the center of the octamer. The opening of this third tetramer lies on an axis perpendicular to the openings of the other two tetramers and is identical to the tetramer described in figures 3.4c and 3.4d. The assembly of the β -barrel-like tetramer and octamer corroborates the assembly of peptide **2a** in SDS-PAGE.

The crystal lattice of peptide **2a** comprises concatenated chains of antiparallel dimers that form β -barrel-like tetramers and octamers (**Figure 3.4c**). The arrangement and interaction of these dimers within the crystal lattice does not terminate in a manner that gives rise to discrete tetramer or octamer units. Instead, each edge and face of peptide **2a** is capable of participating in edge-to-edge hydrogen bonding and hydrophobic packing—enabling oligomerization. The crystallographic structure of the octamer formed by peptide **2a** provides insight toward understanding the structure of the octamer formed by peptide **1a**.

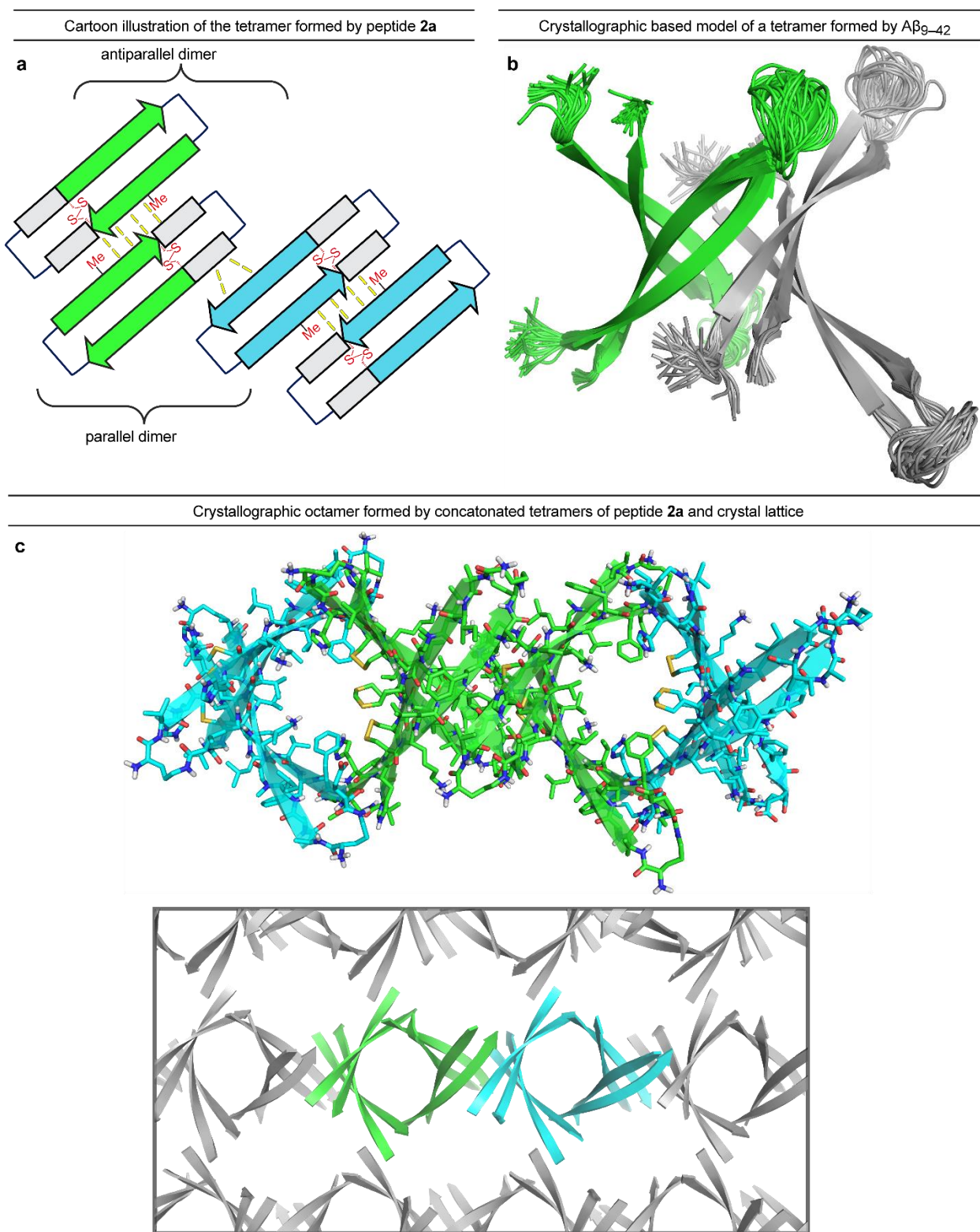


Figure 3.4. (a) Illustration of the parallel and antiparallel β -sheet interactions present in the β -barrel-like tetramer formed by peptide **2a**. (b) Crystallographic based model of an A β_{9-42} β -barrel-like tetramer. Superposition of 32 structures generated by REMD. (c) β -Barrel-like octamer and crystal lattice formed by peptide **2a**.

Reducing the disulfide bonds of peptides 1a and 2a, and oligomerization of peptides 1i and 2c-d

To better understand the importance of the cross-strand intramolecular disulfide bridge in the oligomerization of peptides **1a** and **2a**, we subjected each peptide to tris(2-carboxyethyl)phosphine (TCEP) and studied their migration by SDS-PAGE (**Figure 3.5a and 3.5b**). After TCEP reduction, peptide **1a** does not assemble as an octamer, and instead migrates as a downward streaking band between the 4.6 and 10 kDa ladder bands (**Figure 3.5a**). Similarly, peptide **2a** no longer migrates as an octamer following reduction by TCEP, but still migrates at a molecular weight consistent with that of a tetramer (**Figure 3.5b**). The persistence of a tetramer for peptide **2a** may reflect an incomplete reduction of the disulfide bond. Peptide **2a** migrates as a downward streaking band from the 4.6 to the 10 kDa ladder band. Neither peptide **1a** or **2a** migrates as an octamer following treatment with TCEP, highlighting the importance of the cross-strand disulfide bridge in the oligomerization of these A β derived peptides.

We studied the SDS-PAGE migration of peptides **1i** and **2c-d** to corroborate the crystallographic tetramer and octamer of peptide **2a** with the SDS-PAGE assembly of peptides **1a** and **2a** (**Figure 3.5a and 3.5b**). The crystallographic dimer formed by peptide **2a** is an integral component of the β -barrel-like tetramer and octamer and relies on a pair of intermolecular hydrogen bonds between Met₃₅ and Cys₃₇. If the crystallographic octamer formed by peptide **2a** is identical to the SDS-PAGE octamers of peptides **1a** and **2a**, disruption of this dimer should ablate the assembly of both peptides **1a** and **2a**. Peptide **1i** is a homologue of peptide **1a** that bears an additional *N*-methyl group on Met₃₅ (**Figure 3.1c**). Peptide **1i** does not assemble as an octamer and instead migrates to the 4.6 kDa ladder band (**Figure 3.5a**). Peptide **2c** is a homologue of peptide **2a** that bears an additional *N*-methyl group on Met₃₅ (**Figure 3.1c**). Peptide **1i** does not assemble as an octamer and instead migrates to the 4.6 kDa ladder band (**Figure 3.5b**). The lack of assembly

by peptides **1i** and **2c** corroborates the SDS-PAGE assembly of peptide **1a** and **2a** with the crystallographic β -barrel-like tetramer and octamer formed by peptide **2a**.

The SDS-PAGE migration of peptide **2d** provides further evidence that peptide **2a** forms the same oligomer by SDS-PAGE and in the crystal state. Peptide **2d** is a disulfide stabilized dimer of peptide **2b** (**Figure 3.1c**). Although peptide **2b** does not assemble by SDS-PAGE to form a tetramer or an octamer, monomers of peptide **2b** may be capable of assembly if they are covalently stabilized.¹⁹ In the antiparallel dimer formed by peptide **2a**, Val₃₆ in one monomer forms a non-hydrogen bonded pair with Val₃₆ in the other monomer. We speculated that a dimer of peptide **2b** could be stabilized by replacing this non-hydrogen bonded pair with a disulfide bond, enabling the SDS-PAGE assembly of peptide **2b**.

Peptide **2d** migrates at a molecular weight consistent with a tetramer (**Figure 3.5b**). The tetramer band formed by peptide **2d** streaks downward from a position between the 10 and 17 kDa ladder bands to between the 4 and 10 kDa ladder bands. Reduction of peptide **2d** by TCEP produces a band that migrates to just below the 4.6 kDa ladder band, in addition to the tetramer band. The migration of this lower molecular weight band parallels the position of the band formed by peptide **2b**, highlighting that assembly of peptide **2d** is dependent on the intermolecular disulfide bond.

Folding of peptides 1i and 2c–d

The presence of an additional *N*-methyl group on Met₃₅ appears to contribute to differences in the CD spectrum of peptide **1i** relative to peptide **1a** (**Figure 3.5c**). The CD spectrum of peptide **1i** is broader and shallower than peptide **1a**, displaying a negative band centered at ca. 210 nm that extends from ca. 196 nm to ca. 220 nm. In contrast to the differences between peptides **1a** and **1i**, the CD spectrum of peptide **2c** is closer in similarity to peptide **2a**. Peptide **2c** displays a strong negative band centered at ca. 214 nm with increasing ellipticity at lower wavelengths, reflecting a

β -hairpin-like conformation. The CD spectrum of peptide **2d** displays a strong negative band centered at ca. 212 nm and a strong positive band centered at ca. 196 nm, reflecting a β -hairpin-like conformation (**Figure 3.5c**). This result suggests that covalent stabilization of dimers of peptide **2d** not only enables assembly in SDS-PAGE, but β -hairpin-like folding as well.

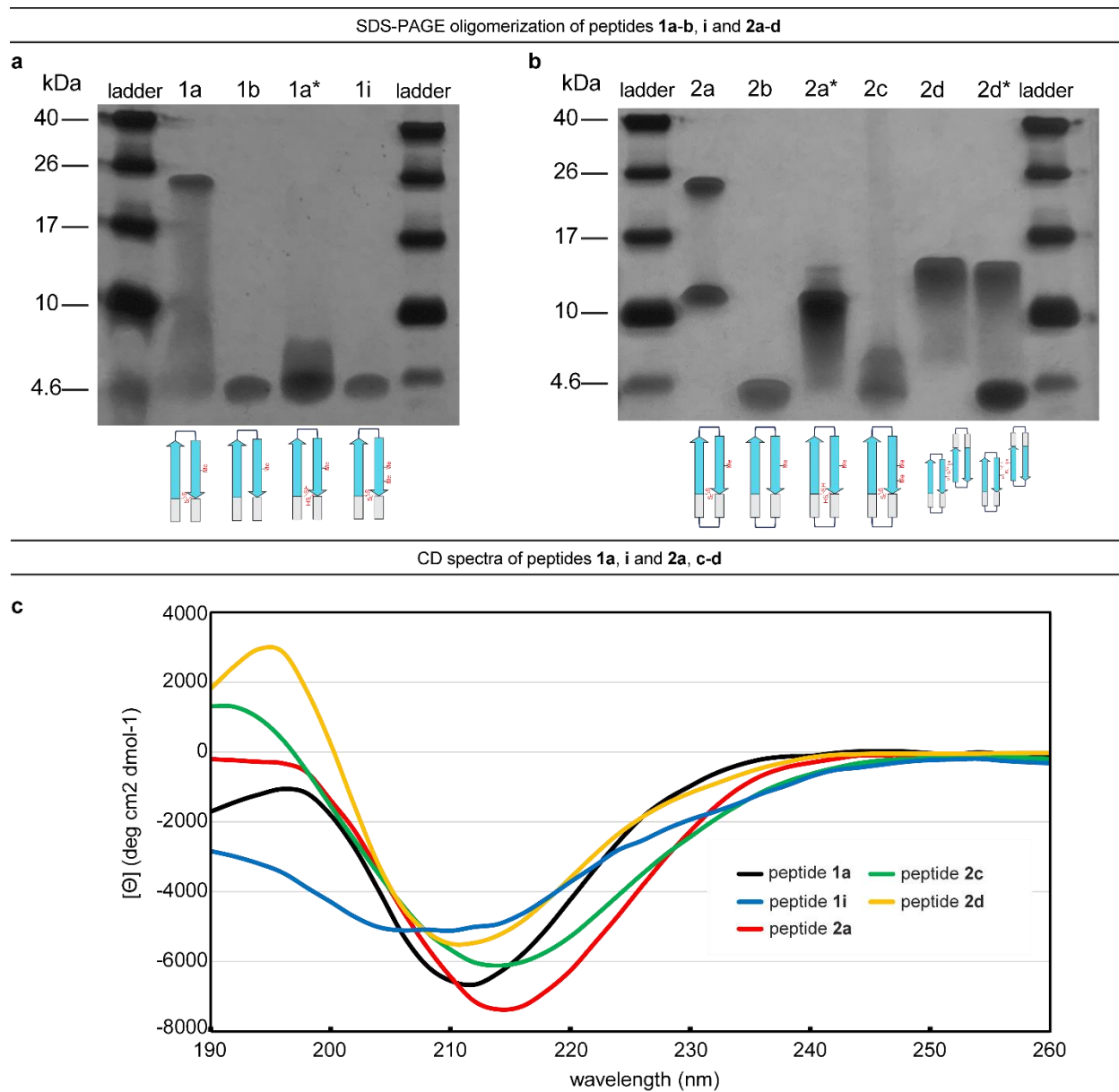


Figure 3.5. (a) Silver stained SDS-PAGE of peptides **1a–b, 1i**, and **2a–d**; lanes corresponding to peptides **1a***, **2a***, and **2d*** were treated with 10 mM TCEP. SDS-PAGE was performed in Tris buffer at pH 6.8 with 2% (w/v) SDS on a 16% polyacrylamide gel with 50 μ M solutions of peptide in each lane. (b and c) Circular dichroism (CD) spectra of peptides **1a, 1i, 2a**, and **2c–d**. CD spectra were acquired for each peptide at 50 μ M in 10 mM phosphate buffer at pH 7.4; ellipticity was normalized for the number of residues in each peptide.

Molecular dynamics simulations of a crystallographically derived tetramer in a lipid membrane

One mechanism by which A β oligomers are thought to exert toxicity is the disruption of cell membranes.^{9,31–33} We used molecular dynamics to simulate interactions between a β -barrel-like tetramer formed by A β_{9-42} and a lipid bilayer of 1-palmitoyl-2-oleoyl-sn-glycero-3-phosphocholine (POPC) molecules. We built the simulation using the CHARMM-GUI input generator and ran the simulation for 200 ns under the parameters of the CHARMM36m forcefield (**Figure 3.6**).^{34,35} Molecular graphics and simulation analyses were generated with VMD 1.9.3.³⁶

Over the course of 200 ns, the β -barrel-like tetramer formed by A β_{9-42} disrupts integrity of the POPC membrane, allowing water to cross the transmembrane space through the inner pore and along the outer face of the tetramer (**Figure 3.6a**). Although the inner pore of the tetramer is predominantly lined with hydrophobic residues (**Figure 3.3d**), water molecules are still able to enter and cross this space. Surprisingly, molecules of water were also able to enter the transmembrane space along the outer face of the tetramer, interacting with polar residues such as His, Gln, and Lys. As the simulation progress, each membrane leaflet experiences significant disruption, as seen by the position of the POPC headgroups (orange) (**Figure 3.6a**). We monitored changes in RMSD for residues 12–22 and 30–40, residues from the crystallographic β -strands of peptide **2a** and observed a plateau of ca 2.6Å after 100 ns (Figure S3.2). We were also able to measure the amount of water that crossed the transmembrane space through the pore of the tetramer (**Figure 3.6b-c**). After the simulation has reached its equilibrium point (ca. 100 ns), 10–40 molecules of water can be found within a cylindrical space defined by the pore, with an average density of 0.86 waters/ Å along the length of the pore.

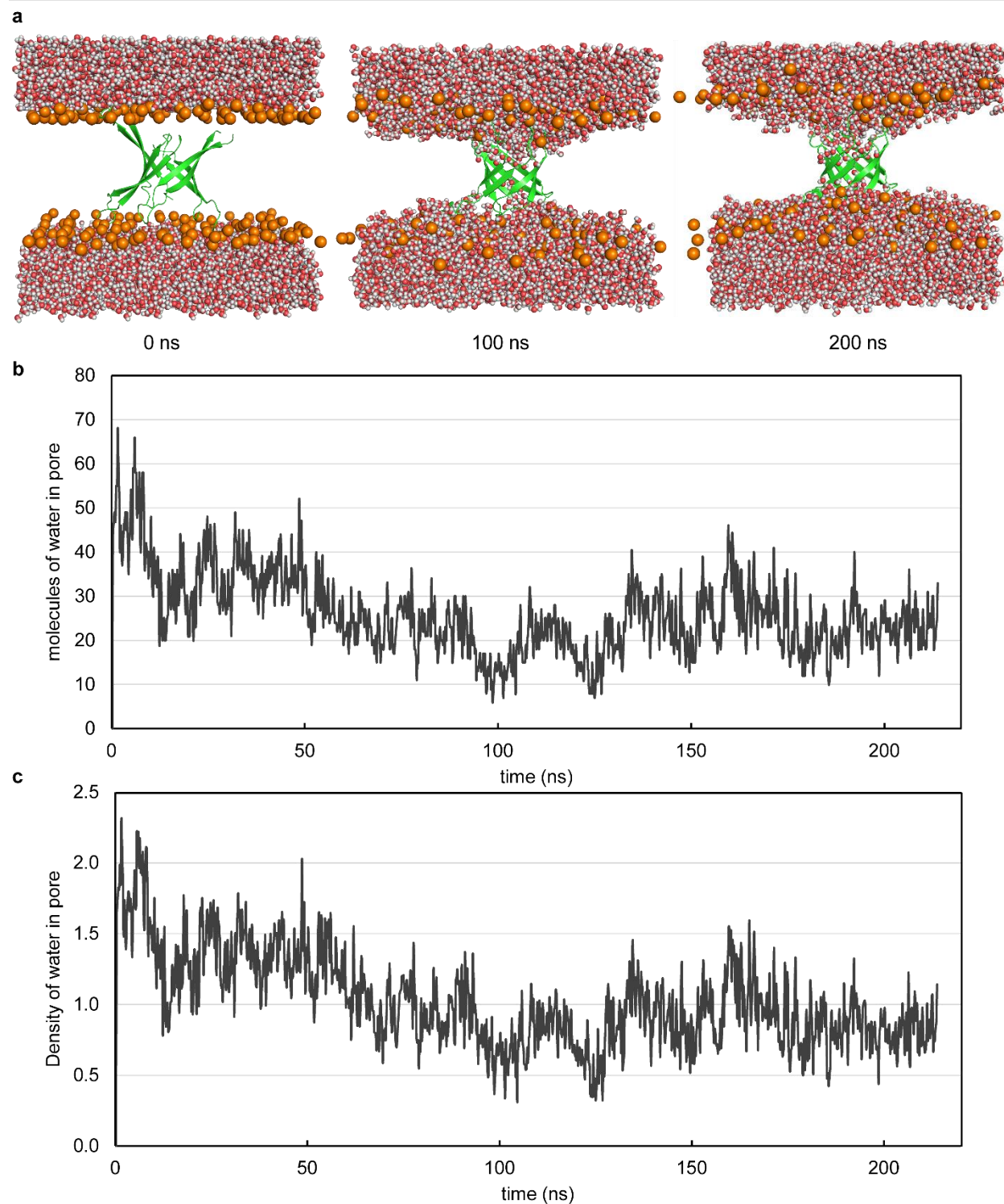


Figure 3.6. Molecular dynamics simulation of a β -barrel-like tetramer formed by $A\beta_{9-42}$ in a POPC lipid bilayer. (a) Simulation at 0, 100, and 200ns. (b) Total number of water molecules in the tetramer pore over the course of the simulation. (c) Density of water molecules per \AA , along the length of the pore.

DISCUSSION AND CONCLUSION

β -Hairpins are a key structural component of A β oligomers, with variations in β -hairpin alignment and topology likely contributing to some of the variation and heterogeneity observed in A β fibrils and oligomers. In this investigation, we stabilized several β -hairpin peptides derived from A β_{12-40} , using disulfide bridges and δ Orn turn units, to mimic endogenous A β oligomers and study the properties of the assemblies that formed. In SDS-PAGE, peptide **1a** assembles to form an oligomer that migrates at a molecular weight consistent with that of an octamer. Structural homologues of peptide **1a**, peptides **1b–h** and **2a–b**, reveal that the disulfide bridge and N-terminal residues 12–14 are required for peptide **1a** to assemble and form an octamer, and that this octamer can accommodate residues 23–29 as a loop. X-ray crystallographic studies reveal that peptide **2a** assembles to form a β -barrel-like tetramer and octamer, stabilized by edge-to-edge hydrogen bonding of antiparallel and parallel β -sheets, and hydrophobic packing. Molecular dynamics studies of a β -barrel-like tetramer assembled from a crystallographically derived model of A β_{9-42} reveal that the tetramer can disrupt lipid membrane and facilitate water permeation. These findings contribute to our understanding of how endogenous A β oligomers may assemble in the Alzheimer's brain, furthering our molecular understanding of Alzheimer's disease.

REFERENCES

1. Cline, E. N., Bicca, M. A., Viola, K. L. & Klein, W. L. The amyloid- β oligomer hypothesis: Beginning of the third decade. *J. Alzheimer's Dis.* **64**, S567–S610 (2018).
2. Benilova, I., Karran, E. & De Strooper, B. The toxic A β oligomer and Alzheimer's disease: an emperor in need of clothes. *Nat. Neurosci.* **15**, 349–357 (2012).
3. Selkoe, D. J. & Hardy, J. The amyloid hypothesis of Alzheimer's disease at 25 years. *EMBO Mol. Med.* **8**, 595–608 (2016).
4. Dobson, C. M., Knowles, T. P. J. & Vendruscolo, M. The amyloid phenomenon and its significance in biology and medicine. *Cold Spring Harb. Perspect. Biol.* **12**, pii: a033878 (2020).
5. Dear, A. J. *et al.* Kinetic diversity of amyloid oligomers. *Proc. Natl. Acad. Sci. U. S. A.* **117**, 28–31 (2020).
6. Kulenkampff, K., Perez, M. W., Sormanni, P., Habchi, J. & Vendruscolo, M. Quantifying misfolded protein oligomers as drug targets and biomarkers in Alzheimer and Parkinson diseases. *Nat. Rev. Chem.* (2021) doi:10.1038/s41570-021-00254-9.
7. De, S. *et al.* Soluble aggregates present in cerebrospinal fluid change in size and mechanism of toxicity during Alzheimer's disease progression. *Acta Neuropathol. Commun.* **7**, 120 (2019).
8. Glabe, C. G. Structural classification of toxic amyloid oligomers. *J. Biol. Chem.* **283**, 29639–29643 (2008).
9. Ciudad, S. *et al.* A β (1-42) tetramer and octamer structures reveal edge conductivity pores as a mechanism for membrane damage. *Nat. Commun.* **11**, 1–14 (2020).
10. Yu, L. *et al.* Structural characterization of a soluble amyloid β -peptide oligomer. *Biochemistry* **48**, 1870–1877 (2009).
11. Hoyer, W., Grönwall, C., Jonsson, A., Ståhl, S. & Härd, T. Stabilization of a β -hairpin in monomeric Alzheimer's amyloid- β peptide inhibits amyloid formation. *Proc. Natl. Acad. Sci. USA* **105**, 5099–5104 (2008).
12. Sandberg, A. *et al.* Stabilization of neurotoxic Alzheimer amyloid- β oligomers by protein engineering. *Proc. Natl. Acad. Sci. U.S.A* **107**, 15595–15600 (2010).
13. Aminov, R. I. A brief history of the antibiotic era: Lessons learned and challenges for the future. *Front. Microbiol.* **1**, 1–7 (2010).
14. Lendel, C. *et al.* A hexameric peptide barrel as building block of amyloid- β protofibrils. *Angew. Chemie - Int. Ed.* **53**, 12756–12760 (2014).
15. Kreutzer, A. G. & Nowick, J. S. Elucidating the structures of amyloid oligomers with macrocyclic β -hairpin peptides: Insights into Alzheimer's disease and other amyloid diseases. *Acc. Chem. Res.* **51**, 706–718 (2018).
16. Ghosh, U., Thurber, K. R., Yau, W.-M. & Tycko, R. Molecular structure of a prevalent

- amyloid- β fibril polymorph from Alzheimer's disease brain tissue. *Proc. Natl. Acad. Sci. U.S.A* **118**, e2023089118 (2021).
17. Spencer, R. K., Li, H. & Nowick, J. S. X-ray crystallographic structures of trimers and higher-order oligomeric assemblies of a peptide derived from A β ₁₇₋₃₆. *J. Am. Chem. Soc.* **136**, 5595–5598 (2014).
 18. Kreutzer, A. G., Hamza, I. L., Spencer, R. K. & Nowick, J. S. X-ray crystallographic structures of a trimer, dodecamer, and annular pore formed by an A β ₁₇₋₃₆ β -hairpin. *J. Am. Chem. Soc.* **138**, 4634–4642 (2016).
 19. Kreutzer, A. G., Yoo, S., Spencer, R. K. & Nowick, J. S. Stabilization, assembly, and toxicity of trimers derived from A β . *J. Am. Chem. Soc.* **139**, 966–975 (2017).
 20. Kreutzer, A. G. *et al.* A hexamer of a peptide derived from A β ₁₆₋₃₆. *Biochemistry* **56**, 6061–6071 (2017).
 21. Salveson, P. J., Spencer, R. K., Kreutzer, A. G. & Nowick, J. S. X-ray crystallographic structure of a compact dodecamer from a peptide derived from A β ₁₆₋₃₆. *Org. Lett.* **19**, 3462–3465 (2017).
 22. Samdin, T. D. *et al.* Effects of N-terminal residues on the assembly of constrained β -hairpin peptides derived from A β . *J. Am. Chem. Soc.* **142**, 11593–11601 (2020).
 23. Haerianardakani, S. *et al.* Phenylalanine mutation to cyclohexylalanine facilitates triangular trimer formation by β -hairpins derived from A β . *J. Am. Chem. Soc.* **142**, 20708–20716 (2020).
 24. Kreutzer, A. G., Samdin, T. D., Guaglianone, G., Spencer, R. K. & Nowick, J. S. X-Ray Crystallography Reveals Parallel and Antiparallel β -Sheet Dimers of a β -Hairpin Derived from A β ₁₆₋₃₆ that Assemble to Form Different Tetramers X-Ray Crystallography Reveals Parallel and Antiparallel β -Sheet Dimers of a β -Hairpin Derived from A β ₁₆₋₃₆. (2020) doi:10.1021/acscchemneuro.0c00290.
 25. Masters, C. L. *et al.* Amyloid plaque core protein in Alzheimer disease and Down syndrome. *Proc. Natl. Acad. Sci. U.S.A* **82**, 4245–4249 (1985).
 26. Podlisny, M. B. *et al.* Aggregation of secreted amyloid β -protein into sodium dodecyl sulfate-stable oligomers in cell culture. *Journal of Biological Chemistry* vol. 270 9564–9570 (1995).
 27. Marina, G. B. *et al.* Amyloid β -protein (A β) assembly: A β ₄₀ and A β ₄₂ oligomerize through distinct pathways. *Proc. Natl. Acad. Sci. U. S. A.* **100**, 330–335 (2003).
 28. Kreutzer, A. G. & Nowick, J. S. Elucidating the Structures of Amyloid Oligomers with Macrocyclic β -Hairpin Peptides: Insights into Alzheimer's Disease and Other Amyloid Diseases. *Acc. Chem. Res.* **51**, 706–718 (2018).
 29. Samdin, T. D., Kreutzer, A. G. & Nowick, J. S. Exploring amyloid oligomers with peptide model systems. *Curr. Opin. Chem. Biol.* **64**, 106–115 (2021).

30. Kreutzer, A. G., Samdin, T. D., Guaglianone, G., Spencer, R. K. & Nowick, J. S. X-ray crystallography reveals parallel and antiparallel β -sheet dimers of a β -hairpin derived from A β_{16-36} that assemble to form different tetramers. *ACS Chem. Neurosci.* **11**, 2340–2347 (2020).
31. Serra-Batiste, M. *et al.* A β_{42} assembles into specific β -barrel pore-forming oligomers in membrane-mimicking environments. *Proc. Natl. Acad. Sci. U. S. A.* **113**, 10866–10871 (2016).
32. Kandel, N., Zheng, T., Huo, Q. & Tatulian, S. A. Membrane Binding and Pore Formation by a Cytotoxic Fragment of Amyloid β Peptide. *J. Phys. Chem. B* **121**, 10293–10305 (2017).
33. Sun, Y. *et al.* Spontaneous formation of β -sheet nano-barrels during the early aggregation of Alzheimer's amyloid beta. *Nano Today* **38**, 101125 (2021).
34. Jo, S., Kim, T., Iyer, V. G. & Im, W. CHARMM-GUI: A Web-Based Graphical User Interface for CHARMM. *J. Comput. Chem.* **29**, 1859–1865 (2008).
35. Huang, J. *et al.* CHARMM36m: An improved force field for folded and intrinsically disordered proteins. *Nat. Methods* **14**, 71–73 (2016).
36. Humphrey, W., Dalke, A. & Schulten, K. VMD: Visual Molecular Dynamics. *J. Mol. Graph.* **14**, 33–38 (1996).

Supporting information for:

A β -Barrel-Like Tetramer Formed by a Macrocyclic β -Hairpin Derived From A β

Table of Contents

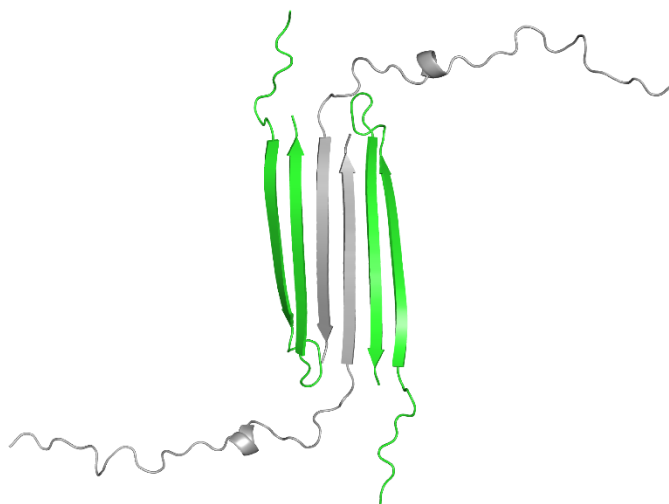
Supporting Figures and Tables	129
Figure S3.1	129
Table S3.1	130
Figure S3.2	132
Materials and Methods	133
General information	133
Synthesis of peptides 1a–i	134
Synthesis of peptides 2a–d	136
SDS-PAGE, TCEP reduction, and silver staining	140
Circular dichroism spectroscopy	141
Crystallization of peptide 2a	141
X-ray crystallographic data collection, data processing, and structure determination of peptide 2a	142
Replica Exchange Molecular Dynamics Simulation of an A β_{9-42} β -barrel-like tetramer	142
Molecular Dynamics Simulation of an A β_{9-42} β -barrel-like tetramer in a lipid membrane	143
Characterization Data	145
Characterization of peptide 1a	145
Characterization of peptide 1b	147
Characterization of peptide 1c	149
Characterization of peptide 1d	151
Characterization of peptide 1e	153
Characterization of peptide 1f	155
Characterization of peptide 1g	157
Characterization of peptide 1h	159
Characterization of peptide 1i	161

Characterization of peptide 2a	163
Characterization of peptide 2b	165
Characterization of peptide 2c	167
Characterization of peptide 2d	170

Supporting Figures and Tables

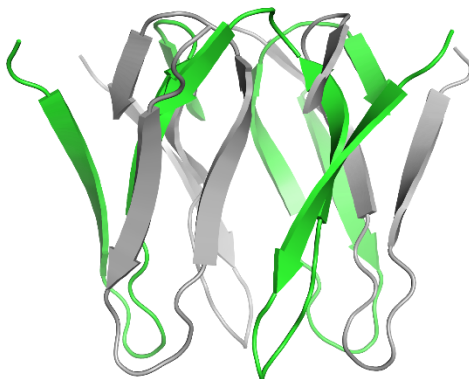
Tetramer of A β_{1-42} , formed by the A β β -hairpin reported by Carulla et al. (PDB 6RHY), *Nat. Commun.*, **11**, 1–14 (2020)

a



Barrel-like-hexamer of A β_{16-42} , formed by the A β β -hairpin reported by Härd et al., *Angew. Chemie - Int. Ed.*, **53**, 12756–12760 (2014)

b



A β_{40} Fibrils with A β β -hairpins proposed by Tycko et al., *Proc. Natl. Acad. Sci.*, **118**, e2023089118 (2021)

c

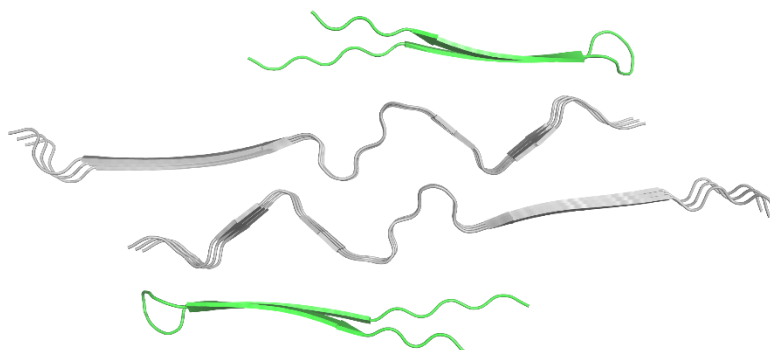


Figure S3.1. (a) NMR structure of the tetramer formed by the β -hairpin, reported by Carulla et al. (b) NMR structure of the barrel-like hexamer formed by an A β derived β -hairpin, reported by Härd et al. (c) A β_{40} fibril structure with proposed A β_{40} β -hairpins, reported by Tycko et al.

Supplementary Table 3.1. Crystallographic properties, crystallization conditions, data collection, and model refinement statistics for peptide **2a**.

peptide	2a
Wavelength (Å)	1.0
Resolution range	36.52 - 2.1 (2.175 - 2.1)
Space group	P 41 21 2
Unit cell	44.3265, 44.3265, 64.4265 90, 90, 90
Total reflections	198405 (19442)
Unique reflections	4086 (393)
Multiplicity	48.6 (49.5)
Completeness (%)	99.83 (100.00)
Mean I/sigma(I)	21.83 (2.00)
Wilson B-factor	43.80
R-merge	0.3661 (1.108)
R-meas	0.37 (1.118)
R-pim	0.05249 (0.1504)
CC1/2	0.998 (0.795)
CC*	1 (0.941)
Reflections used in refinement	4079 (393)
Reflections used for R-free	406 (39)
R-work	0.2639 (0.3241)
R-free	0.2941 (0.3099)
CC(work)	0.911 (0.810)
CC(free)	0.879 (0.730)
Number of non-hydrogen atoms	376
RMS(bonds)	0.016
RMS(angles)	0.89
Ramachandran favored (%)	100.00
Ramachandran allowed (%)	0.00
Ramachandran outliers (%)	0.00
Rotamer outliers (%)	0.00

Clashscore	5.59
Average B-factor	54.16
crystallization conditions	0.2 M Mg acetate tetrahydrate, 0.1M Na cacodylate trihydrate (pH 7.0), 30% v/v 2-methyl-2,4-pentenediol

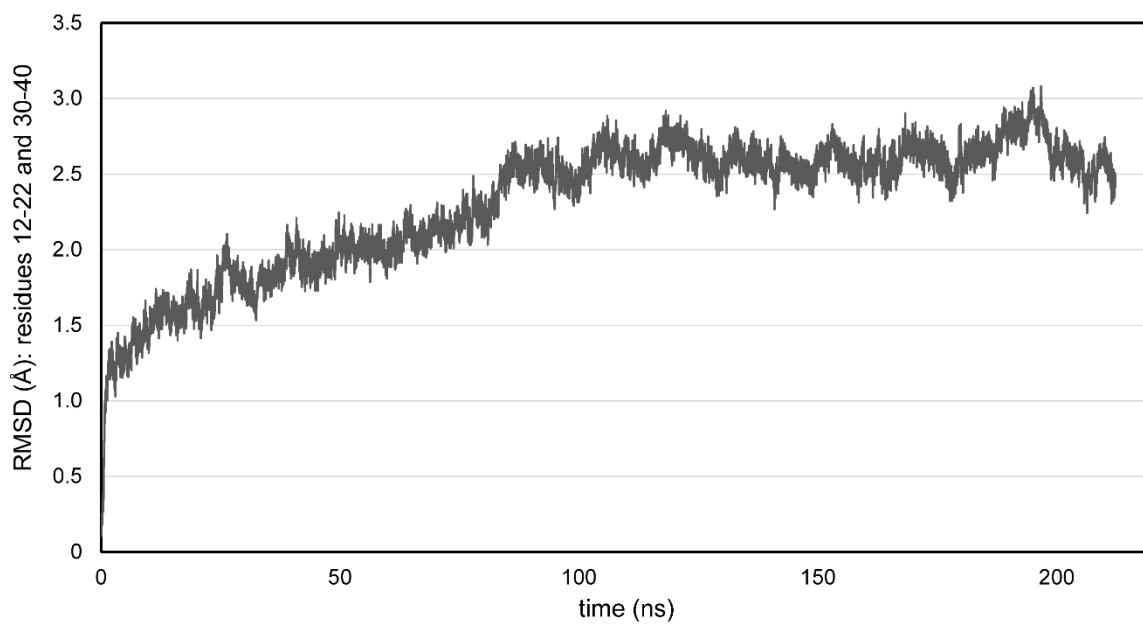


Figure S2.3. Time (ns) vs. RMSD (Å). RMSD was measured for residues 12–22 and 30–40, which were derived from the crystal structure of the β -barrel-like tetramer formed by peptide **2a**.

Materials and Methods¹

General information

All chemicals were used as received unless otherwise noted. Methylene chloride (CH_2Cl_2) was passed through alumina under nitrogen prior to use. Anhydrous, amine-free *N,N*-dimethylformamide (DMF) was purchased from Alfa Aesar. Deionized water (18 M Ω) was obtained from a Barnstead NANOpure Diamond water purification system. Analytical reverse-phase HPLC was performed on an Agilent 1260 Infinity II instrument equipped with a Phenomenex Aeris PEPTIDE 2.6u XB-C18 column. Preparative reverse-phase HPLC was performed on a Ranin instrument equipped with an Agilent Zorbax SB-C18 column. HPLC grade acetonitrile and deionized water, each containing 0.1% trifluoroacetic acid (TFA), were used for analytical and preparative reverse-phase HPLC. All peptides were prepared and used as the trifluoroacetate salts and were assumed to have one trifluoroacetic acid molecule per amine group on each peptide.

Synthesis of peptides 1a–i

a. Loading the resin. For peptides **1a–b** and **1e–h**, 2-chlorotriyl chloride resin (300 mg, 1.4 mmol/g) was added to a Bio-RAD Poly-Prep chromatography column (10 mL). Dry CH₂Cl₂ (8 mL) was used to suspend and swell the resin for 30 min with gentle rocking. The solution was drained from the resin and a solution of Fmoc-Val-OH (0.78 equiv, 50 mg, 0.33 mmol) in 6% (v/v) 2,4,6-collidine in dry CH₂Cl₂ (8 mL) was added immediately and the suspension was gently rocked for 12 h. The solution was then drained and a mixture of CH₂Cl₂/MeOH/*N,N*-diisopropylethylamine (DIPEA) (17:2:1, 10 mL) was added immediately. The resin was gently rocked for 1 h, to cap the unreacted 2-chlorotriyl chloride resin sites. The resin was then washed twice with dry CH₂Cl₂ and dried by passing nitrogen through the vessel. This procedure typically yields 0.18 mmol of loaded resin (0.6 mmol/g loading).

For peptides **1c–d**, rink amide AM resin (300 mg, 0.68 mmol/g) was added to a Bio-RAD Poly-Prep chromatography column (10 mL). Dry DMF (8 mL) was used to suspend and swell the resin for 30 min with gentle rocking. The solution was drained from the resin and a solution of 20% (v/v) piperidine in DMF was added immediately and the suspension was gently rocked for 1 h. The 20% (v/v) piperidine in DMF was drained from the resin, and the resin was then washed twice with dry DMF. A solution of Fmoc-Cys-Trt (0.78 equiv, 50 mg, 0.33 mmol), HATU (4.5 equiv), HOAt (4.5 equiv), in 20% (v/v) 2,4,6-collidine in dry CH₂Cl₂ (8 mL) was added immediately and the suspension was gently rocked for 12 h. The solution was then drained and a mixture of acetic anhydride/pyridine (3:2, 8 mL) was added immediately. The resin was gently rocked for 0.5 h, to cap the unreacted rink amide resin sites. The resin was then washed twice with dry CH₂Cl₂ and dried by passing nitrogen through the vessel. This procedure typically yields 0.18 mmol of loaded resin (0.6 mmol/g loading).

b. Manual peptide coupling. The resin loaded with Boc-Orn(Fmoc) was suspended in dry DMF and then transferred to a solid-phase peptide synthesis vessel. For peptides **1a–b** and **1e–h**, residues 40 through 32 were manually coupled using Fmoc-protected amino acid building blocks. For peptides **1c–d**, residues 37 through 32 were manually coupled using Fmoc-protected amino acid building blocks. Each manual coupling cycle consisted of *i.* Fmoc-deprotection with of 20% (v/v) piperidine in DMF for 5 min at ambient temperature (5 mL), *ii.* washing with dry DMF (2x, 5 mL), *iii.* coupling of the amino acid (0.44 mmol, 4 equiv) with HCTU (174.0 mg, 0.44 mmol, 4 equiv) in 20% (v/v) 2,4,6-collidine in dry DMF (5 mL) for 30 min, and *iv.* washing the with dry DMF (2x, 5 mL). Residue 32, which follows N-Me-Gly₃₃, was double coupled (4 equiv per coupling) using HATU (6 equiv) and HOAt (6 equiv) for 1 hr per coupling to ensure complete reaction. (We have found that coupling after N-methyl amino acids is difficult and requires rigorous coupling to minimize incomplete reaction.²)

c. Microwave-assisted coupling of residues 31 through 12. For peptides **1a–i**, a CEM Liberty Blue Automated Microwave Peptide Synthesizer was used to couple residues 31 to 12. For peptides **1a–f** and **1i**, Fmoc-Orn(Dde)-OH replaces residues 23–29 in the natural sequence. Each coupling cycle consisted of *i.* Fmoc-deprotection with 20% (v/v) piperidine with 0.1 M Oxyma Pure in DMF for 2 min. at 50 °C, *ii.* washing with DMF (3x), *iii.* coupling of the amino acid (0.75 mmol, 5 equiv) in the presence of HCTU (0.675 mmol, 4.5 equiv) and 20% (v/v) *N*-methylmorpholine (NMM) in DMF for 10 min. at 50 °C, *iv.* washing with DMF (3x).

d. Cleavage and global deprotection of the peptide from resin. The resin was then transferred to a 10-mL Bio-Rad Poly-Prep chromatography column, and washed 3x with dry CH₂Cl₂. The linear peptide was cleaved from the resin by rocking the resin for 1 h with a solution of trifluoroacetic acid (TFA) (TIPS)/H₂O (18:1:1, 10 mL). During the 1 h deprotection, two 50-mL conical tubes

containing 40-mL of dry ether were chilled on dry ice. The solution was drained and split between the two conical tubes of ether. The tubes were then centrifuged at 800 x g for 25 mins. The ether supernatant was poured off and the pelleted peptide was dried overnight under vacuum.

e. Oxidation of the disulfide bridge. The crude, pelleted peptide was resuspended in a solution of 20% v/v dimethyl sulfoxide (DMSO), 50 mL in each tube. The suspension was gently rocked at room temperature for 48 h. The reaction mixture was concentrated under reduced pressure until only DMSO remained.

For ACM containing peptides a solution of 0.1 M iodine in glacial acetic acid (15 mL), 50% aq. acetic acid (250 mL), and 1 M HCl (25 mL) was used to remove the ACM protecting group and oxidize the peptide.

g. Reverse-phase HPLC purification. The peptide: DMSO mixture was dissolved in H₂O and acetonitrile (8:2, 5 mL), and the solution was filtered through a 0.2 µm syringe filter and purified by RP-HPLC. The solution of crude peptide was injected at 20% acetonitrile and eluted with a gradient of 20-60% CH₃CN over 90 min. Each peptide eluted between 29-36% CH₃CN. The collected fractions were analyzed by analytical HPLC and MALDI-TOF, and the pure fractions were concentrated by rotary evaporation and lyophilized. Typical syntheses yielded between 5 and 62 mg of the peptide as the TFA salt.

Synthesis of peptides 2a–d

The synthesis of peptides **2a–d** generally followed the same procedures as for peptides **1a–i**, except for the following:

a. Loading the resin. For peptides **2a–d**, 2-chlorotriptyl chloride resin (300 mg, 1.4 mmol/g) was added to a Bio-RAD Poly-Prep chromatography column (10 mL). Dry CH₂Cl₂ (8 mL) was used

to suspend and swell the resin for 30 min with gentle rocking. The solution was drained from the resin and a solution of Boc-Orn-Fmoc-OH (0.78 equiv, 150 mg, 0.33 mmol) in 6% (v/v) 2,4,6-collidine in dry CH₂Cl₂ (8 mL) was added immediately and the suspension was gently rocked for 12 h. The solution was then drained and a mixture of CH₂Cl₂/MeOH/*N,N*-diisopropylethylamine (DIPEA) (17:2:1, 10 mL) was added immediately. The resin was gently rocked for 1 h, to cap the unreacted 2-chlorotriyl chloride resin sites. The resin was then washed twice with dry CH₂Cl₂ and dried by passing nitrogen through the vessel. This procedure typically yields 0.18 mmol of loaded resin (0.6 mmol/g loading).

b. Manual peptide coupling. The resin loaded with Boc-Orn(Fmoc) was suspended in dry DMF and then transferred to a solid-phase peptide synthesis vessel. Residues 40 through 32 were manually coupled using Fmoc-protected amino acid building blocks. Each manual coupling cycle consisted of *i.* Fmoc-deprotection with 20% (v/v) piperidine in DMF for 5 min at ambient temperature (5 mL), *ii.* washing with dry DMF (2x, 5 mL), *iii.* coupling of the amino acid (0.44 mmol, 4 equiv) with HCTU (174.0 mg, 0.44 mmol, 4 equiv) in 20% (v/v) 2,4,6-collidine in dry DMF (5 mL) for 30 min, and *iv.* washing the with dry DMF (2x, 5 mL). Residue 32, which follows N-Me-Gly₃₃, was double coupled (4 equiv per coupling) using HATU (6 equiv) and HOAt (6 equiv) for 1 hr per coupling to ensure complete reaction. (We have found that coupling after N-methyl amino acids is difficult and requires rigorous coupling to minimize incomplete reaction.²)

c. Microwave-assisted coupling of residues 31 through 12. A CEM Liberty Blue Automated Microwave Peptide Synthesizer was used to couple residues 31 to 12. Fmoc-Orn(Dde)-OH replaces residues 23–29 in the natural sequence. Each coupling cycle consisted of *i.* Fmoc-deprotection with 20% (v/v) piperidine with 0.1 M Oxyma Pure in DMF for 2 min. at 50 °C, *ii.* washing with DMF (3x), *iii.* coupling of the amino acid (0.75 mmol, 5 equiv) in the presence of

HCTU (0.675 mmol, 4.5 equiv) and 20% (v/v) *N*-methylmorpholine (NMM) in DMF for 10 min. at 50 °C, iv. washing with DMF (3x).

e. Cleavage of the peptide from resin. The resin was then transferred to a 10-mL Bio-Rad Poly-Prep chromatography column, and washed 3x with dry CH₂Cl₂. The acyclic peptide was cleaved from the resin by rocking the resin for 1 h with a solution of 1,1,1,3,3,3-hexafluoroisopropanol (HFIP) in CH₂Cl₂ (1:4, 8 mL). The suspension was filtered and the filtrate was collected in a 250-mL round-bottomed flask. The resin was washed with additional HFIP in CH₂Cl₂ (1:4, 8 mL). The combined filtrates were concentrated by rotary evaporation to give a white solid. The white solid was further dried by vacuum pump to afford the crude protected linear peptide, which was cyclized without further purification.

f. Cyclization of the acyclic peptide. The crude protected linear peptide was dissolved in dry DMF (150 mL). PyBOP (370 mg, 0.711 mmol, 6 equiv) and *N*-methylmorpholine (NMM) (0.33 mL, 1.8 mmol, 12 equiv) was added to the solution and the mixture was stirred under nitrogen for 48 h. The mixture was concentrated under reduced pressure to afford the crude protected cyclic peptide, a yellow film.

e. Global deprotection of the cyclic peptide. The protected cyclic peptide was dissolved in TFA/triisopropylsilane (TIPS)/H₂O (18:1:1, 10 mL) in a 250-mL round-bottomed flask equipped with a nitrogen-inlet adaptor. The solution was stirred for 1 h under nitrogen. The reaction mixture was then concentrated by rotary evaporation under reduced pressure to afford the crude cyclic peptide. During the 1 h deprotection, two 50-mL conical tubes containing 40-mL of dry ether were chilled on dry ice. The solution was drained and split between the two conical tubes of ether. The tubes were then centrifuged at 800 x g for 25 mins. The ether supernatant was poured off and the pelleted peptide was dried overnight under vacuum.

e. Oxidation of the disulfide bridge. The crude, pelleted peptide was resuspended in a solution of 20% v/v dimethyl sulfoxide (DMSO), 50 mL in each tube. The suspension was gently rocked at room temperature for 48 h. The reaction mixture was concentrated under reduced pressure until only DMSO remained.

g. Reverse-phase HPLC purification. The peptide: DMSO mixture was dissolved in H₂O and acetonitrile (8:2, 5 mL), and the solution was filtered through a 0.2 μm syringe filter and purified by RP-HPLC. The solution of crude peptide was injected at 20% acetonitrile and eluted with a gradient of 20-60% CH₃CN over 90 min. Each peptide eluted between 29-36% CH₃CN. The collected fractions were analyzed by analytical HPLC and MALDI-TOF, and the pure fractions were concentrated by rotary evaporation and lyophilized. Typical syntheses yielded between 8 and 38 mg of the peptide as the TFA salt.

SDS-PAGE, TCEP reduction, and silver staining

SDS-PAGE was performed on peptides **1a–i** and **2a–d** using the reagents, recipes, and procedures for Tricine SDS-PAGE detailed in Schagger, H. *Nat. Protoc.* **2006**, *1*, 16–22. Each peptide was run on a 16% polyacrylamide gel with a 4% stacking polyacrylamide gel at 60 volts. A Spectra™ Multicolor Low Range Protein Ladder (ThermoFischer Scientific, catalog #: 26628) was loaded into the first lane of the gel. The remaining lanes were loaded with 8.0 μ L aliquots of each peptide as 50 μ M solutions in SDS-PAGE loading buffer, which were prepared as follows: A 10 mg/mL stock solution of each peptide was prepared with deionized water. Aliquots of the 10 mg/mL solutions were then diluted further with deionized water and 6X SDS-PAGE loading buffer (G-Biosciences catalog #: 786-701) to create 100 μ M working solutions of each peptide.

To reduce the disulfide bonds present in peptides **1a**, **2a**, and **2b** 50 μ M solutions of each peptide were sonicated for 1h in 10mM TCEP prior to gel loading. After 1h had elapsed the solution was diluted further with 6X SDS-PAGE loading buffer (G-Biosciences catalog #: 786-701) to create 100 μ M working solutions of each peptide.

Staining with silver nitrate was used to visualize peptides **1a–i** and **2a–d** in the SDS-PAGE gel. Reagents for silver staining were prepared according to procedures detailed in Simpson, R. J. *Cold Spring Harbor Protocol* **2007**. [We have found it important to prepare sodium thiosulfate, silver nitrate, and developing solutions fresh each time and to use high purity sodium carbonate to prepare the developing solution.] The gel was removed from the casting glass and rocked for 20 min in fixing solution (50% (v/v) methanol and 5% (v/v) acetic acid in deionized water). The fixing solution was then discarded and replaced with 50% (v/v) aqueous methanol for another 10 min of rocking. Next, the 50% methanol was discarded and replaced with deionized water for another 10 min of rocking. Next, the water was discarded and the gel was rocked in 0.02% (w/v) sodium thiosulfate in deionized water for 1 min. The sodium thiosulfate was discarded and the gel was rinsed twice with deionized water for 0.5 min. The gel was then submerged in pre-chilled 0.1%

(w/v) silver nitrate in deionized water and rocked at 4 °C for 20 min. The silver nitrate solution was discarded and the gel was rinsed twice with deionized water. The gel was incubated in developing solution (2% (w/v) sodium carbonate, 0.04% (w/v) formaldehyde) until the solution began to brown. The developing solution was then immediately discarded and fresh silver nitrate solution was added to the gel until the desired intensity of staining was reached. When the desired intensity of staining was reached, the developing solution was discarded and the gel was submerged in 5% aqueous acetic acid.

Circular dichroism spectroscopy

A 50 μ M solution of each peptide was prepared by diluting the 10 mg/mL stock solution with 10 mM sodium phosphate buffer at pH 7.4. Each solution was transferred to a 1 mm quartz cuvette for data acquisition. Circular dichroism spectra were acquired on a Jasco J-810 circular dichroism spectropolarimeter at ambient temperature. Data were collected using 2.0 nm intervals from 260 nm to 190 nm and averaged over five accumulations with smoothing.

Crystallization of peptide 2a

The hanging-drop vapor-diffusion method was used to determine initial crystallization conditions for peptide **2a**. Peptide **2a** was screened in 96-well plate format using three crystallization kits (Crystal Screen, Index, and PEG/ION) from Hampton Research. A TTP LabTech Mosquito nanodisperse was used to make three 150 nL hanging drops for each well condition. The three hanging drops differed in the ratio of peptide to well solution for each condition in the 96-well plate. A 10 mg/mL solution of each peptide in deionized water was combined with a well solution in ratios of 1:1, 1:2, and 2:1 peptide:well solution at appropriate volumes to create the three 150 nL hanging drops. Crystals of peptide **2a** grew in well conditions of 0.2 M magnesium acetate tetrahydrate, 0.1 M sodium cacodylate trihydrate pH 6.5, and 30% (v/v) 2-methyl-2,4-pentanediol.

Crystallization conditions for each peptide were optimized using a 4x6 matrix Hampton 24-well plate. For peptide **2a** the 0.1 M sodium cacodylate trihydrate buffer was varied in each row in increments of 0.5 pH units (6.0, 6.5, 7.0, and 7.5) and the percentage of 2-methyl-2,4-pentanediol in each column in increments of 2% (v/v) (26%, 28%, 30%, 32%, 34%, 36%). Three hanging-drops were prepared on borosilicate glass slides by combing a 10 mg/mL solution of peptide **2a** in deionized water with the well solution in the following amounts: 1 μ L:1 μ L, 2 μ L:1 μ L, and 1 μ L:2 μ L. Slides were inverted and pressed firmly against the silicone grease surrounding each well. Crystals were harvested with a nylon loop attached to a copper or steel pin, soaked briefly in MPD, and flash frozen in liquid nitrogen prior to data collection. The optimized crystallization conditions for peptide **2a** is summarized Supplementary Table 3.1.

X-ray crystallographic data collection, data processing, and structure determination of peptide 2a

Diffraction data for **2a** were collected at the Stanford Synchrotron Radiation Light source, beamline 12.2, at 1.00 Å wavelength. Datasets were indexed and integrated with XDS. Scaling and merging was done with pointless and aimless in CCP4. The structures were solved with molecular replacement in Phaser using a dimer formed by macrocyclic β -hairpin peptide derived from A β ₁₆₋₃₆ (PDB 6WXM) as the search model. The refinement was done with phenix.refine module of the Phenix suite, with manipulation of the model performed using Coot.

Replica Exchange Molecular Dynamics Simulation of an A β ₉₋₄₂ β -barrel-like tetramer

A model of an A β ₉₋₄₂ β -barrel-like tetramer was generated by replica-exchange molecular dynamics as follows: Starting coordinates for A β ₉₋₄₂ was generated from the crystallographic coordinates of peptide **2a**. Symmetry mates of peptide **2a** were displayed in PyMOL. Each respective tetramer was selected and saved to a new PDB file. The delta-linked ornithine residues were deleted from each macrocycle. Three alanine residues were added to the N-terminus of the β -hairpin, and two alanine residues were added to the C-terminus. Seven alanine residues were

added to connect Glu₂₂ and Ala₃₀. These added residues were minimized in PyMOL using the clean function, ensuring that the crystallographic coordinates of A β ₁₂₋₂₂ and A β ₃₀₋₄₀ were not perturbed. After this minimization, each added alanine was mutated to its corresponding wild-type residue from A β . The mutated residues were again minimized in PyMOL using the clean function. Each N-Me-Gly₃₃ was replaced with the wild-type Gly. Each Cys₁₅ and Cys₃₇ was replaced with the wild-type Gln and Gly.

The autopsf plugin in VMD was used to prepare the required files for simulation. The coordinates for A β ₁₂₋₂₂ and A β ₃₀₋₄₀ were fixed throughout the simulation. REMD simulations were run in NAMD with the CHARMM22 force field and generalized Born implicit solvent (GBIS) on 32 replicas. The temperatures for these replicas varied between 300 and 800K. The simulation was performed for 10 ns. Representative coordinates were selected uniformly from the last 9 ns of the simulation

Molecular Dynamics Simulation of an A β ₉₋₄₂ β -barrel-like tetramer in a lipid membrane

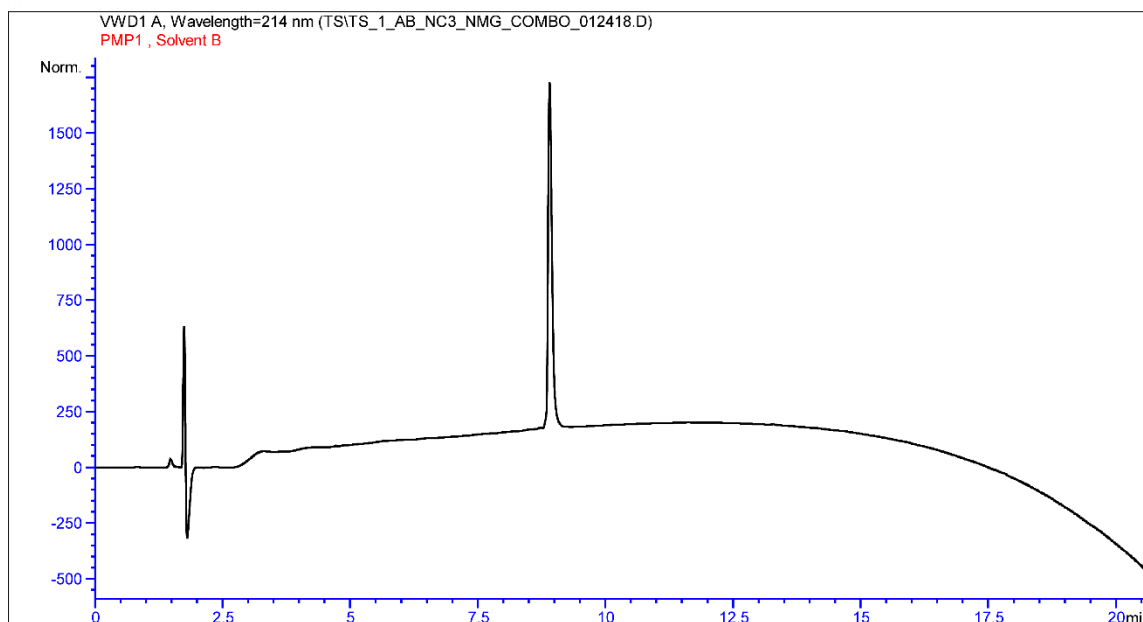
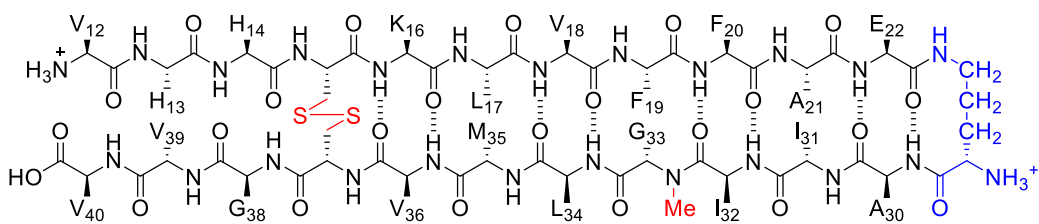
The CHARMM-GUI input generator was used to insert a β -barrel like tetramer formed by A β ₉₋₄₂ into a 87Åx87Å planar POPC bilayer. The tetramer was embedded in the membrane with the pore-like opening aligned to the principal Z-axis of the membrane bilayer. The protonation state of titratable amino acids were chosen for a corresponding system pH of 7.4, with the histidine sidechains left neutral. The CHARMM36m forcefield was used to parametrize the system. Molecular graphics and simulation analyses were generated with VMD 1.9.3

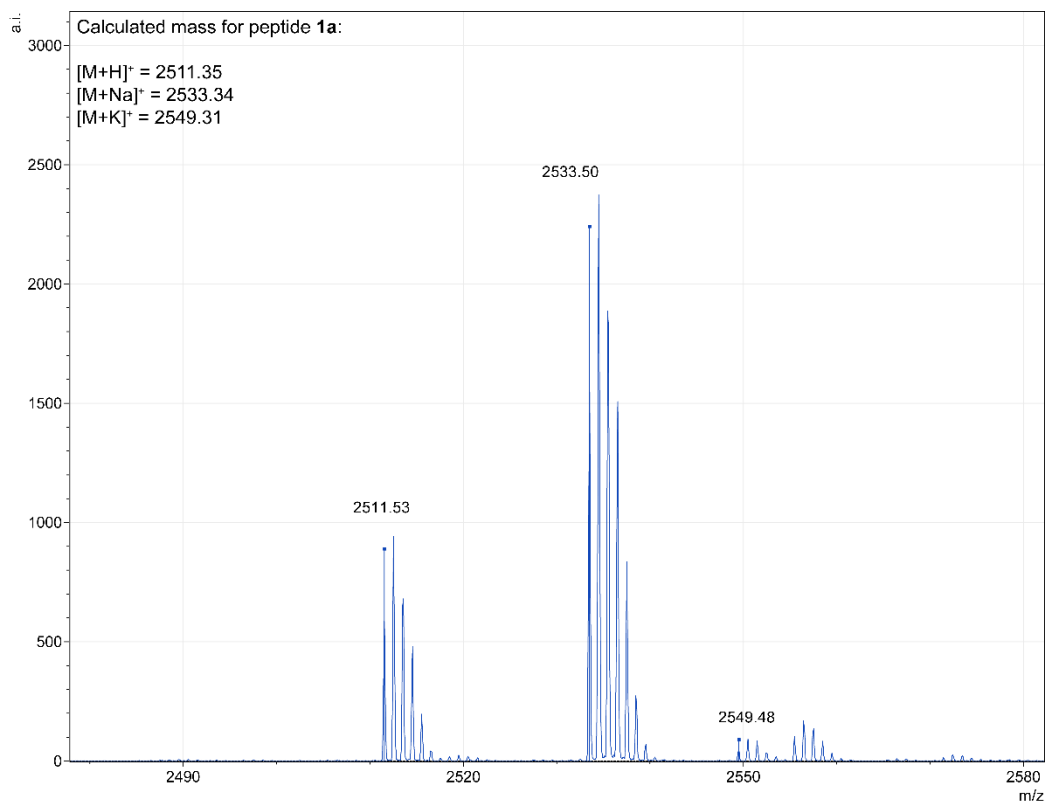
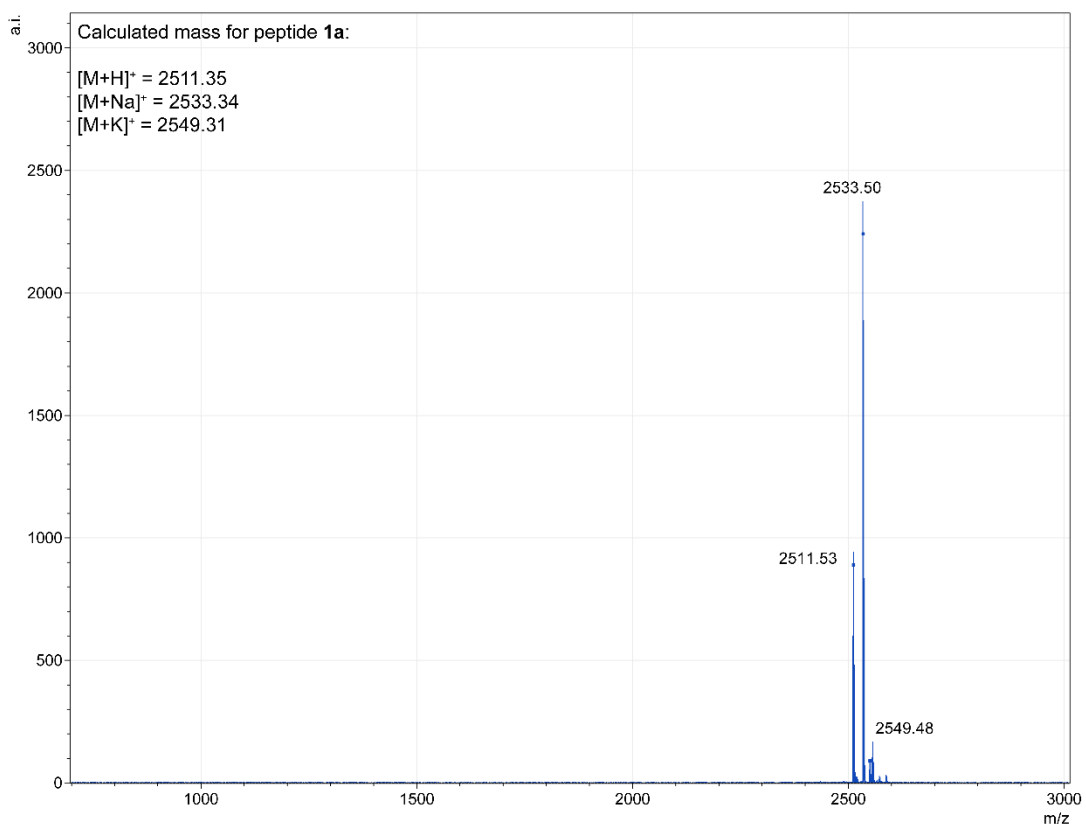
References

1. These procedures follow closely those that our laboratory has previously published. The procedures in this section are adapted from and in some cases taken verbatim from Kreutzer, A. G.; Hamza, I. L.; Spencer, R. K.; Nowick J. S. *J. Am. Chem. Soc.* **2016**, *138*, 4634–4642, Spencer, R. K.; Kreutzer, A. G.; Salveson, P. J.; Li, H.; Nowick, J. S. *J. Am. Chem. Soc.* **2015**, *137*, 6304–6311, Spencer, R. K.; Li. H.; Nowick, J. S. *J. Am. Chem. Soc.* **2014**, *136*, 5595– 5598, and Kreutzer, A. G.; Yoo, S.; Spencer, R. K.; Nowick, J. S. *J. Am. Chem, Soc.* **2017**, *139*, 966–975, Samdin, T. D.; Wierzbicki, M.; Kreutzer, A. G.; Howitz, W. J.; Valenzuela, M.; Smith, A.; Sahrai, V.; Truex, N. L.; Klun, M.; Nowick, J. S. *J. Am. Chem. Soc.* **2020**, *142*, 11593–11601.

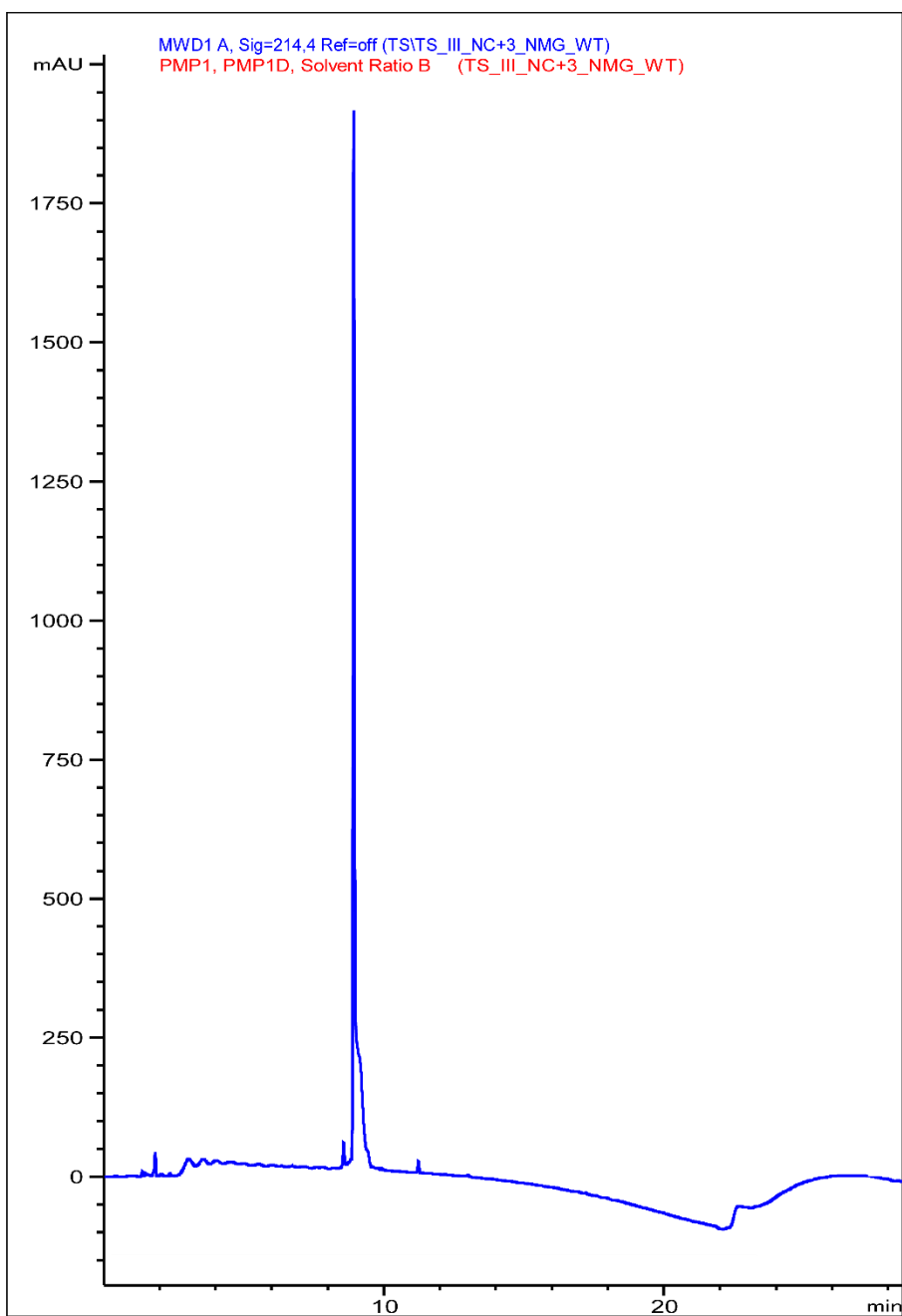
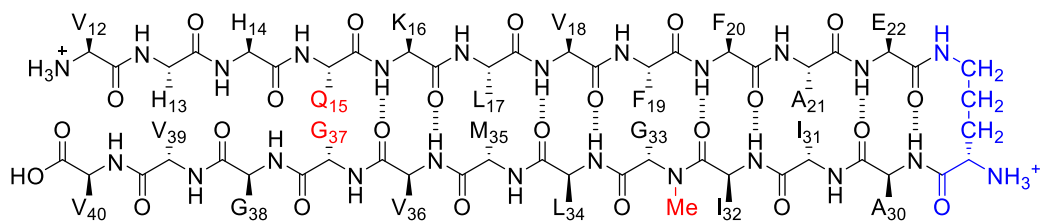
Characterization Data

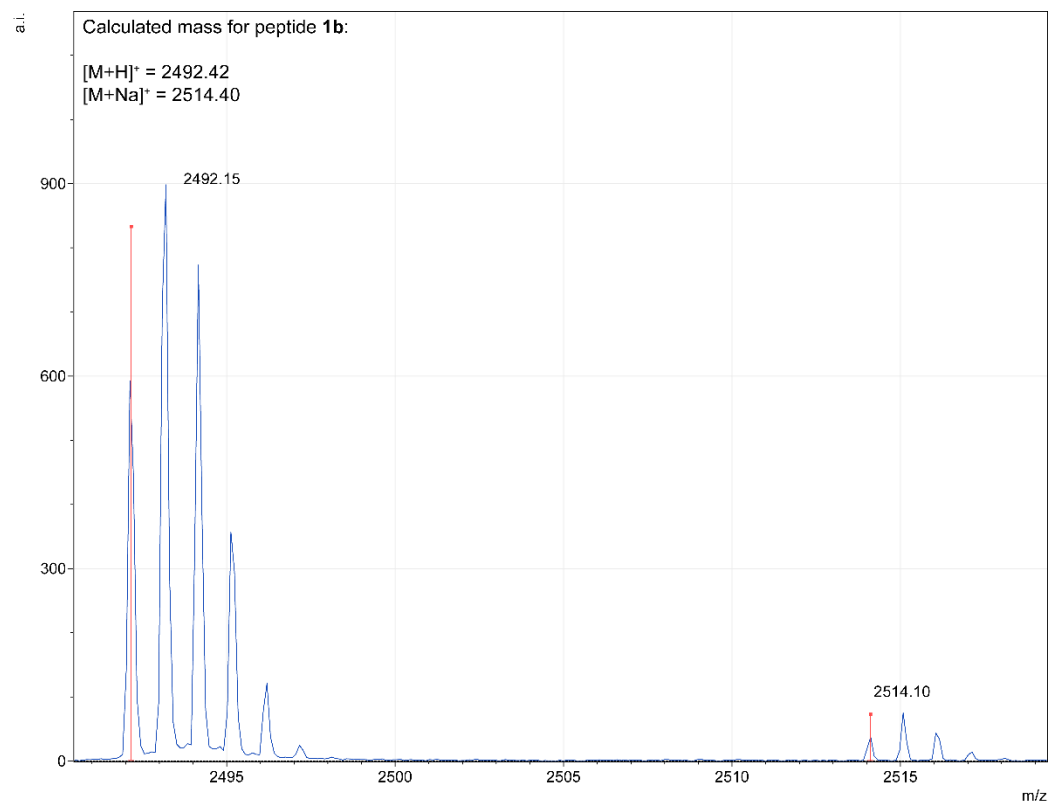
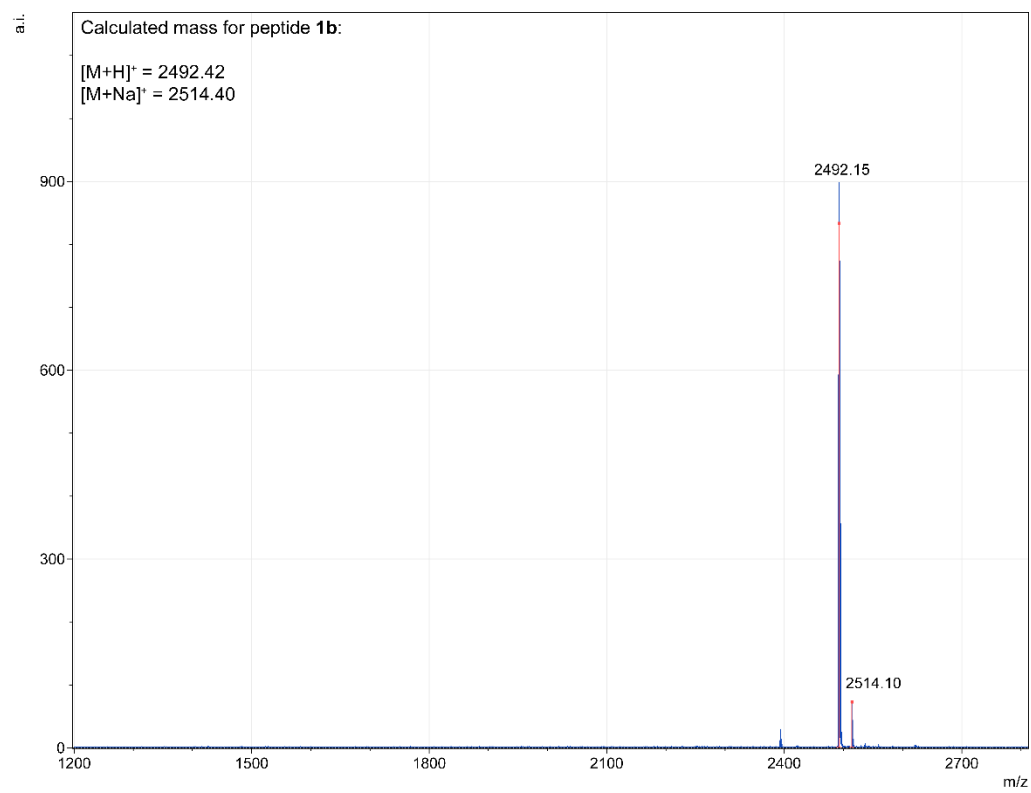
Characterization of peptide *1a*



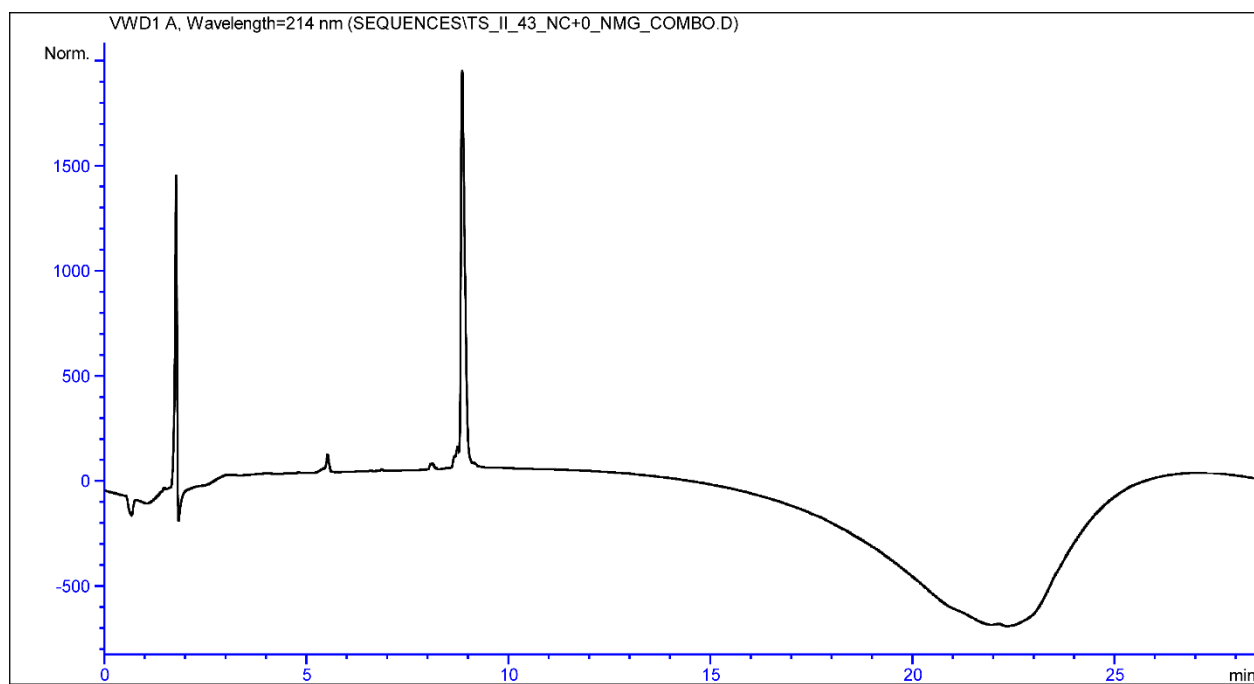
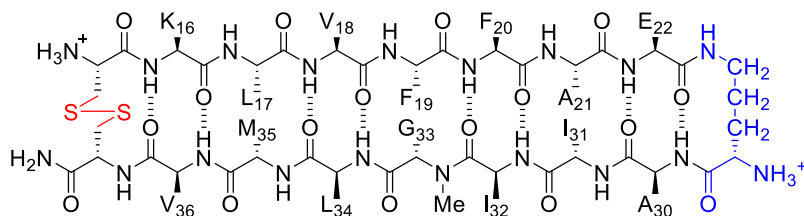


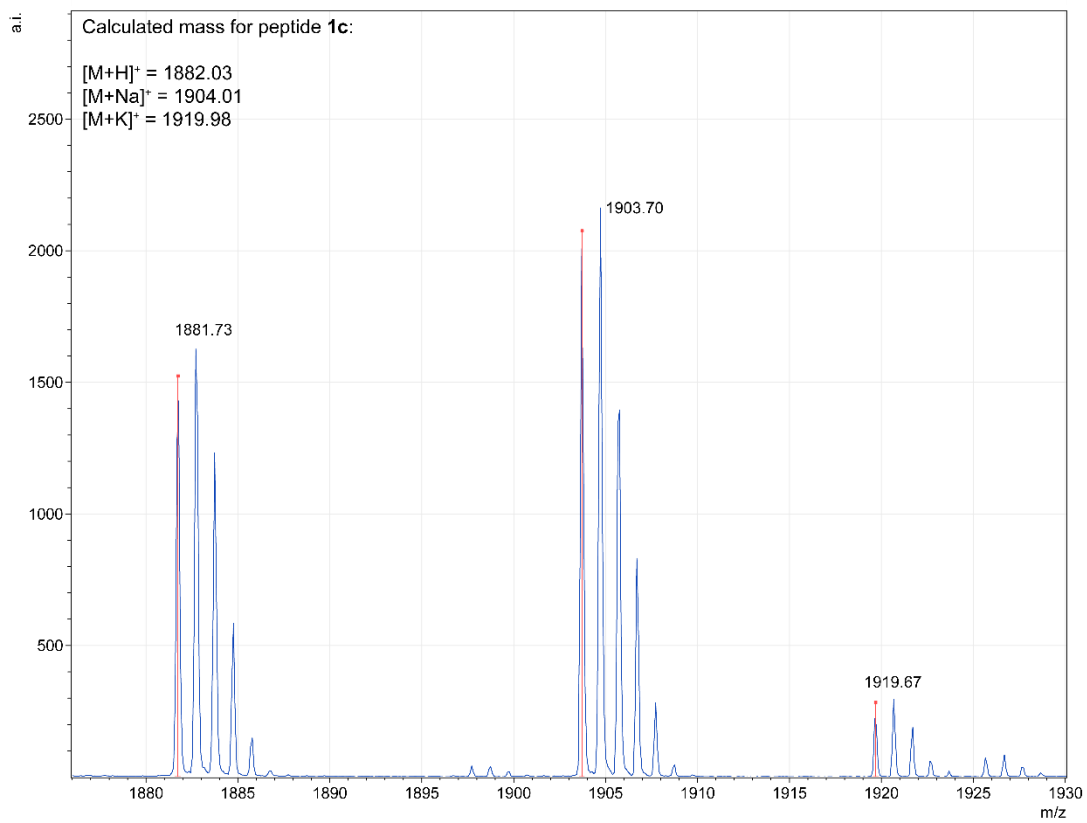
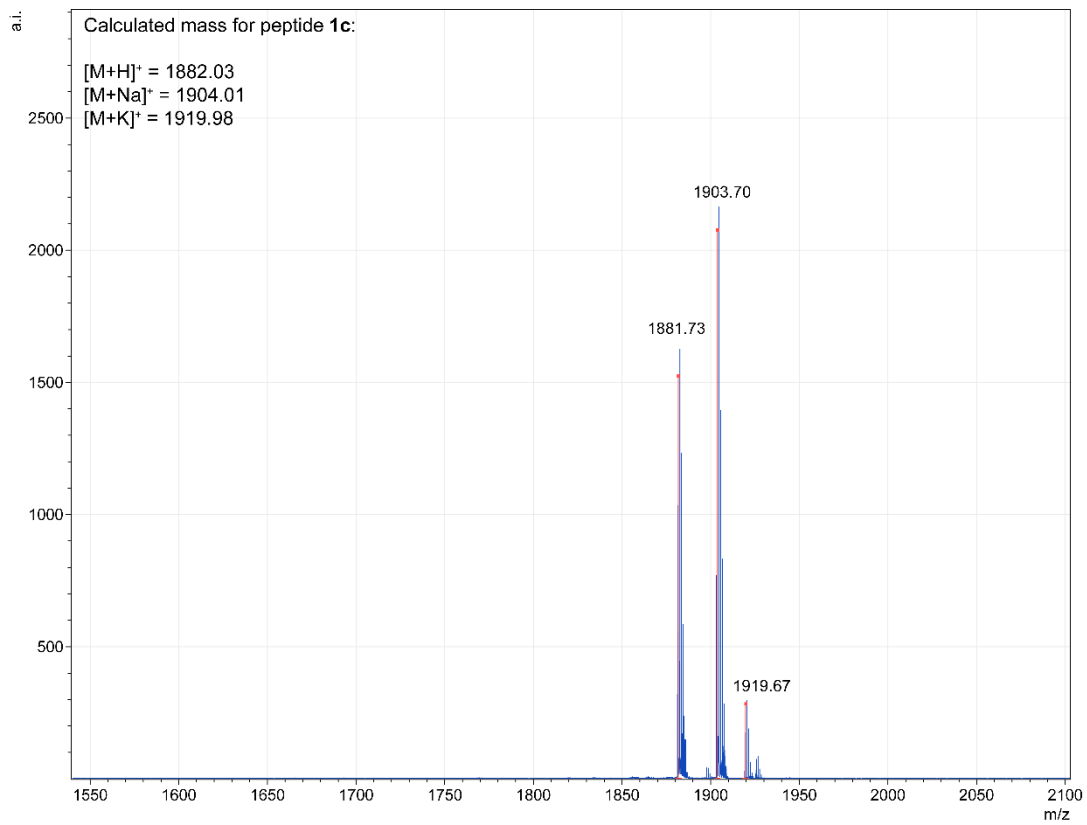
Characterization of peptide **1b**



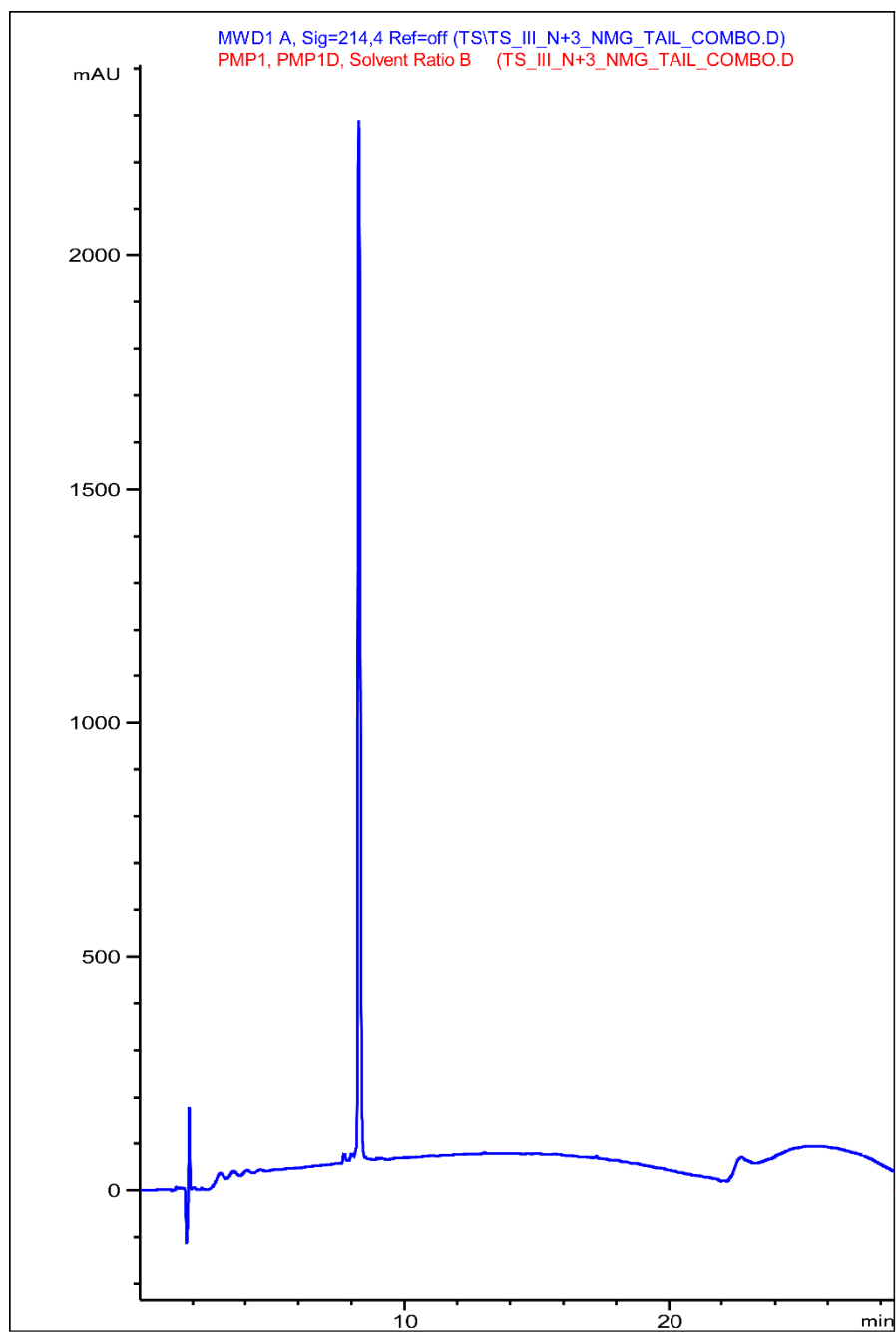
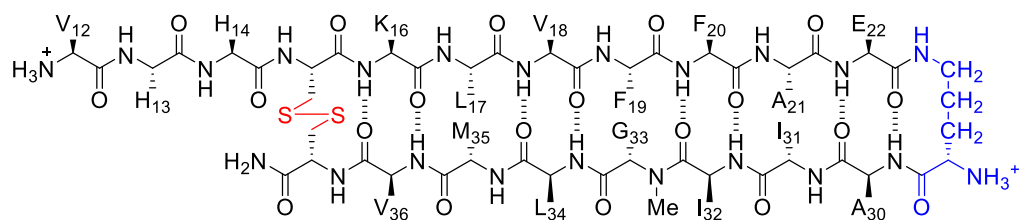


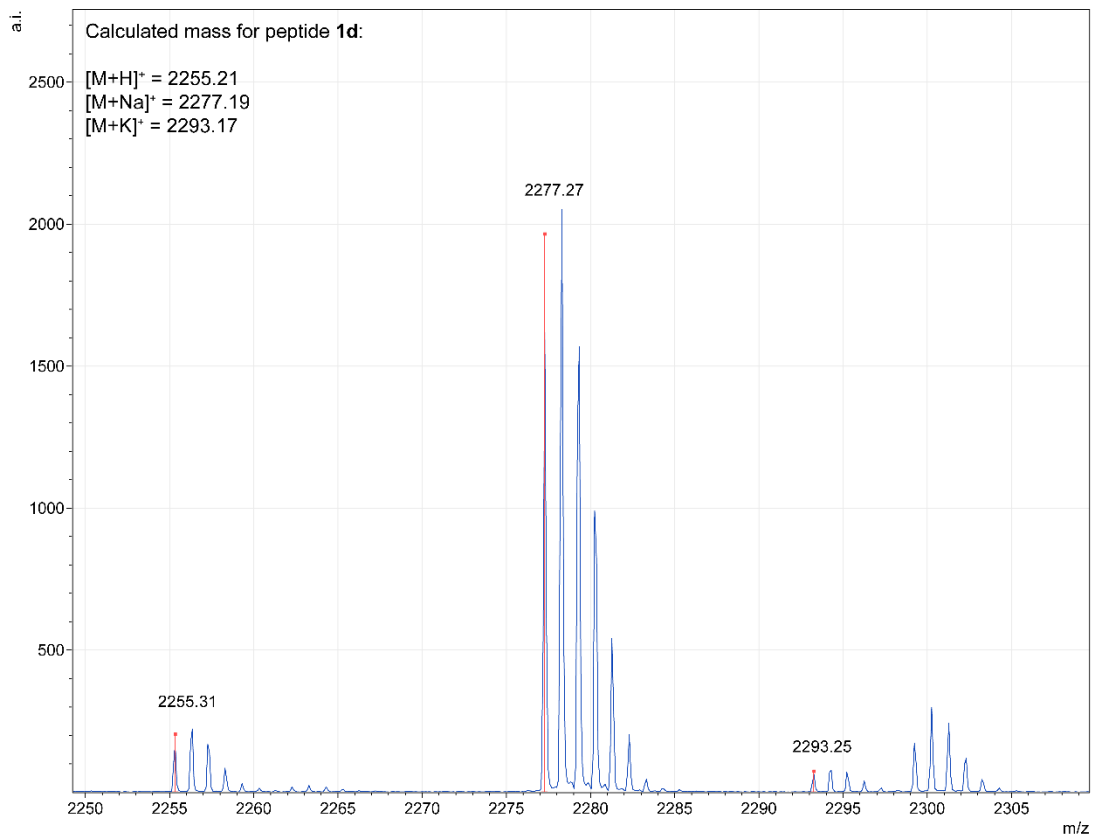
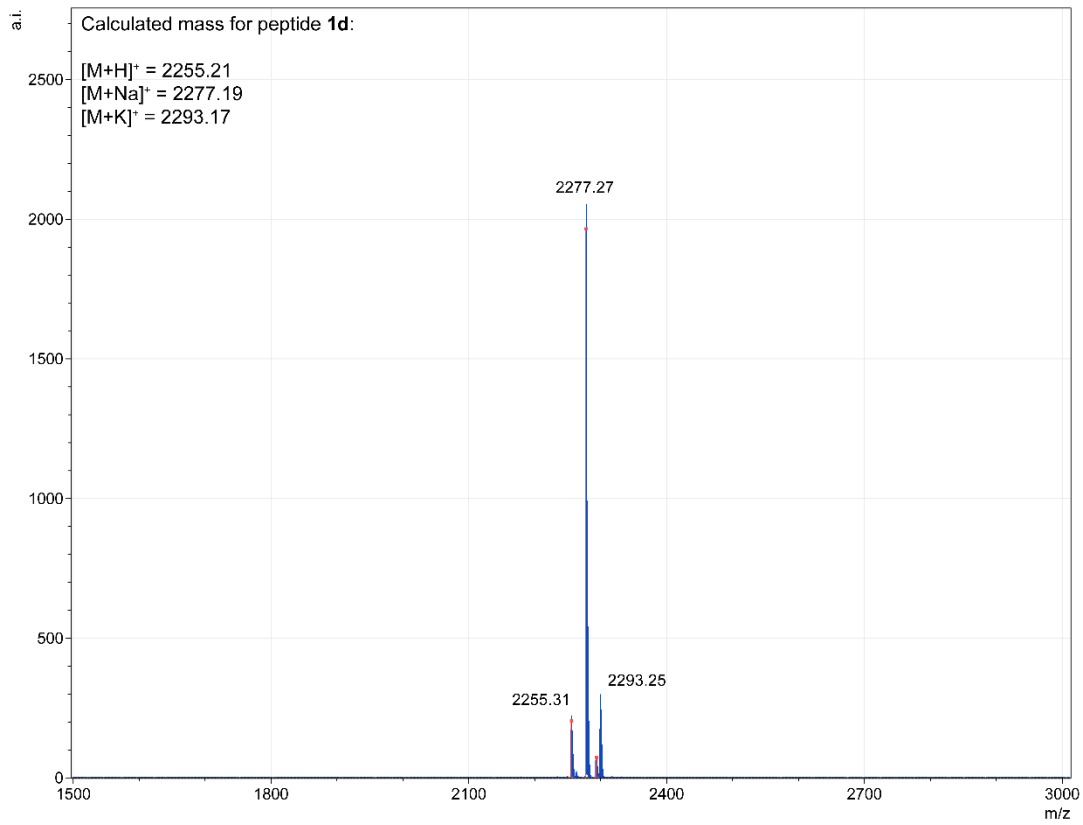
Characterization of peptide **1c**



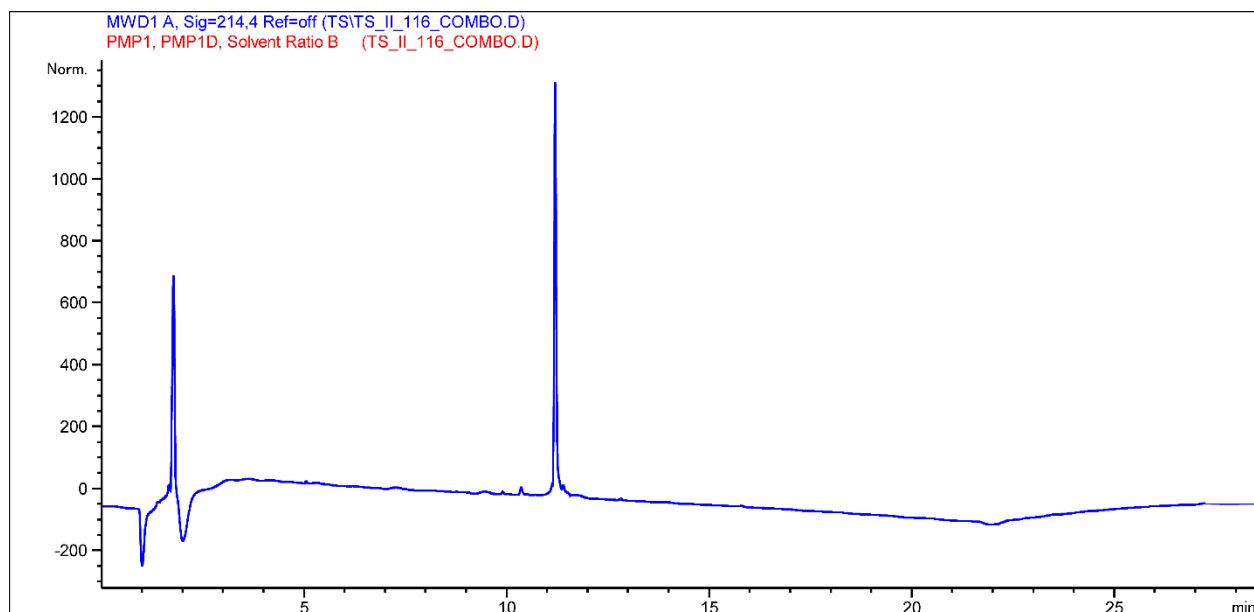
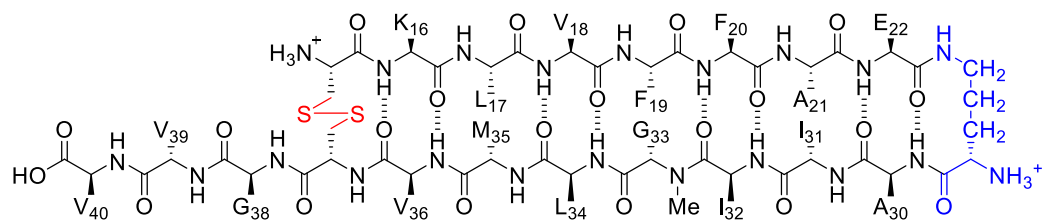


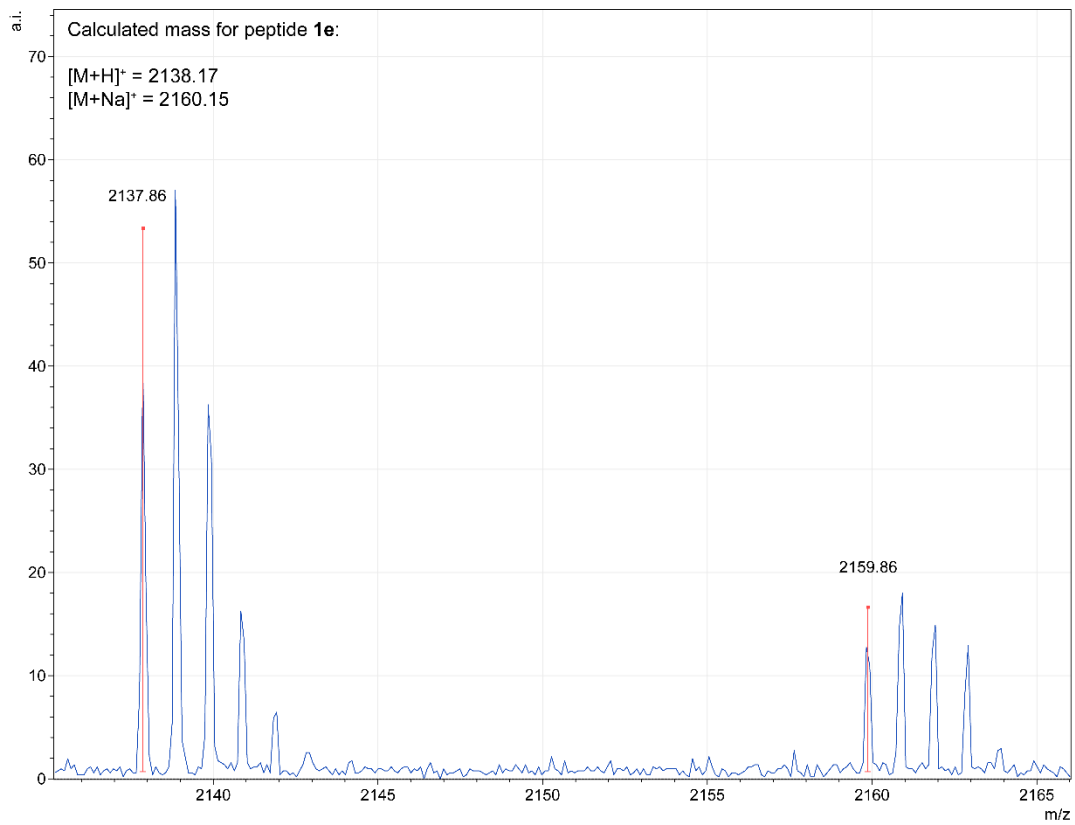
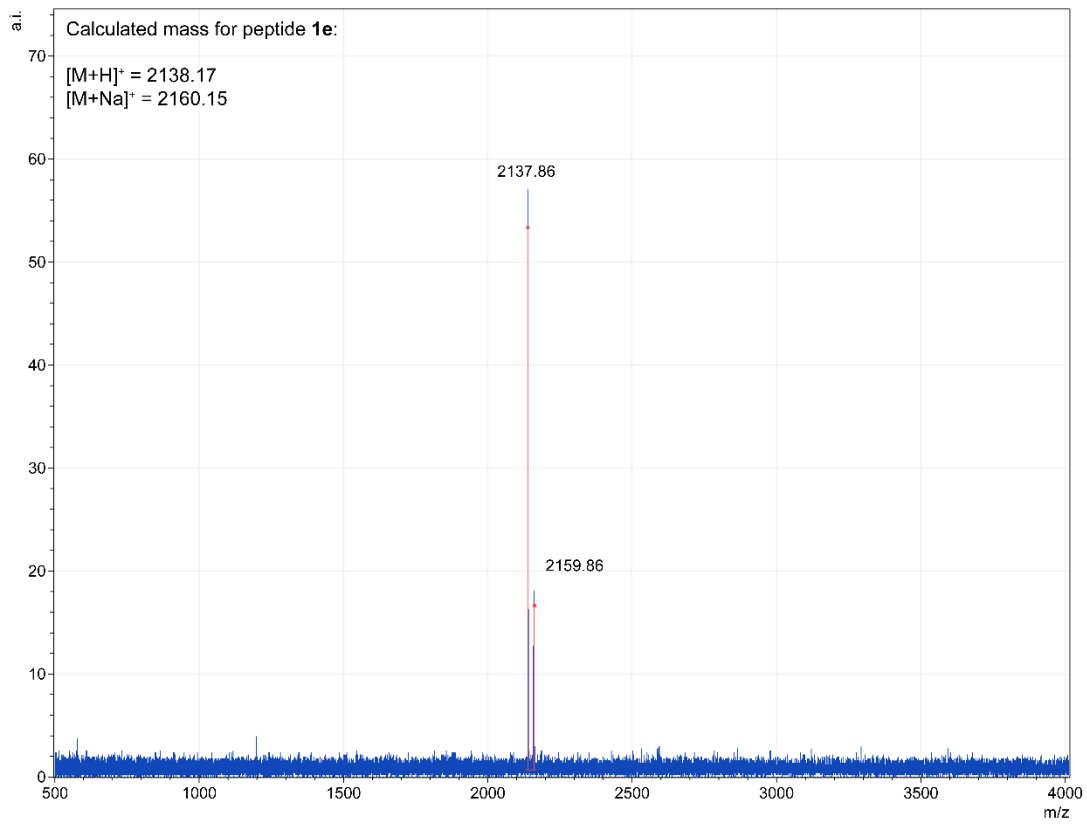
Characterization of peptide **1d**



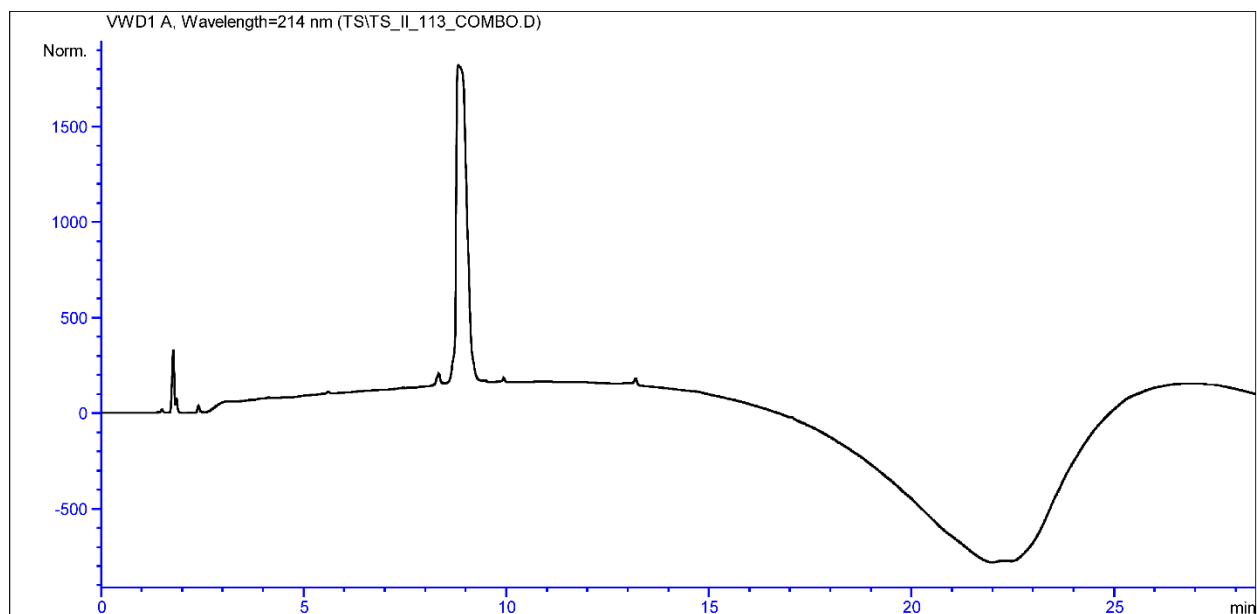
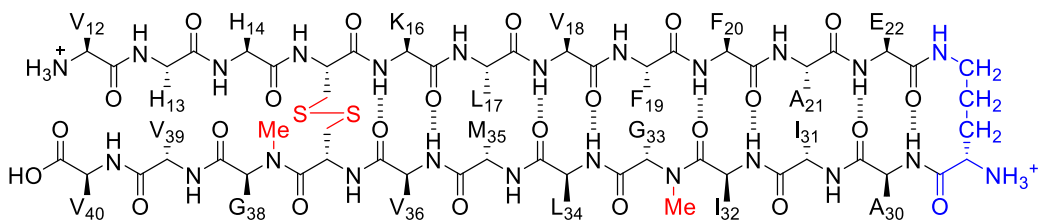


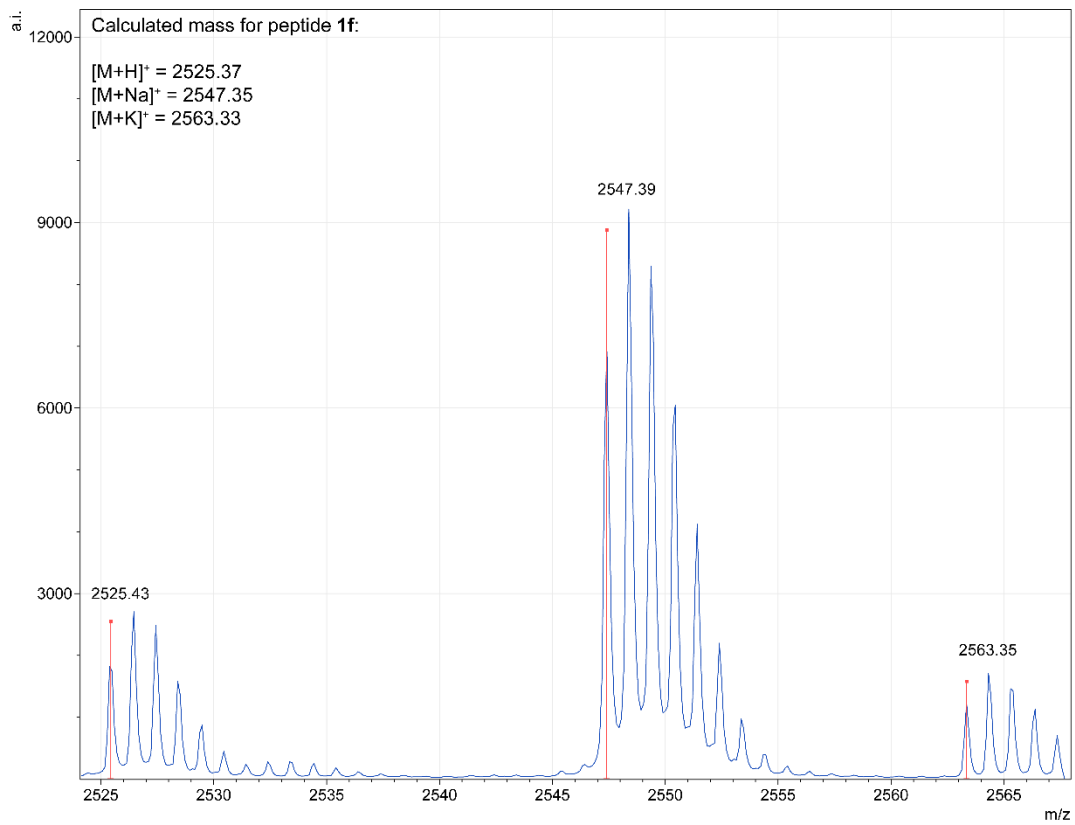
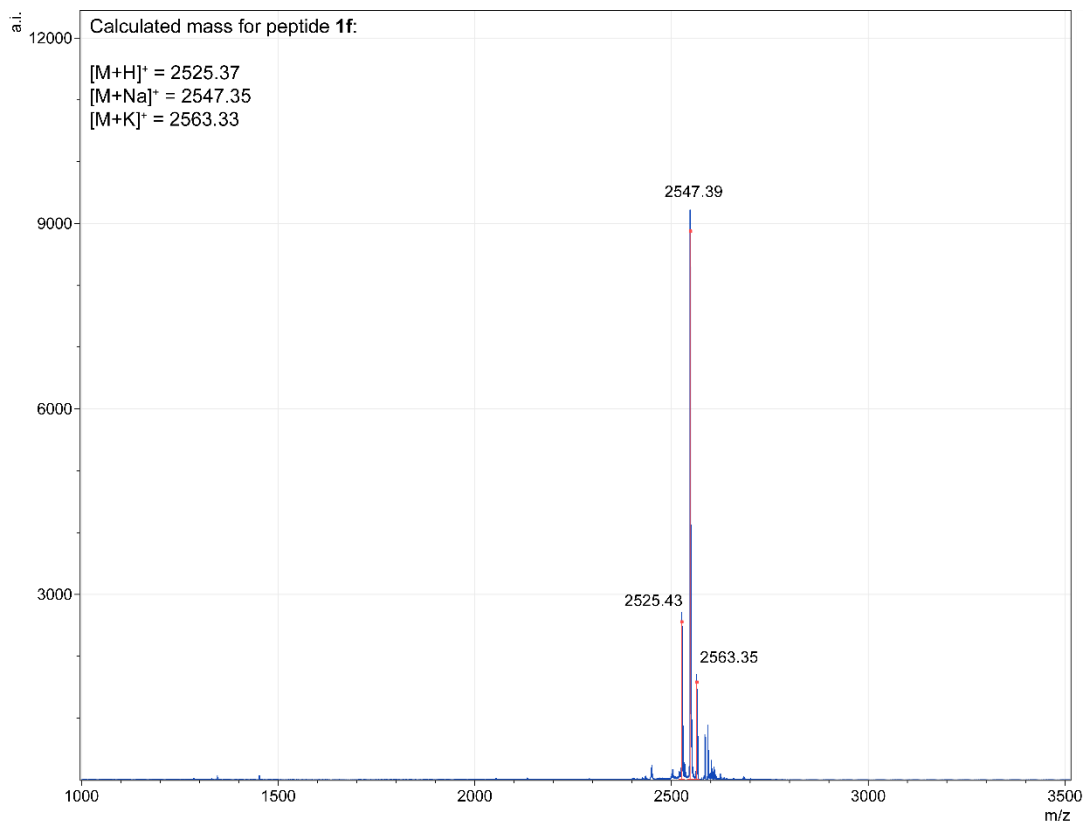
Characterization of peptide **1e**



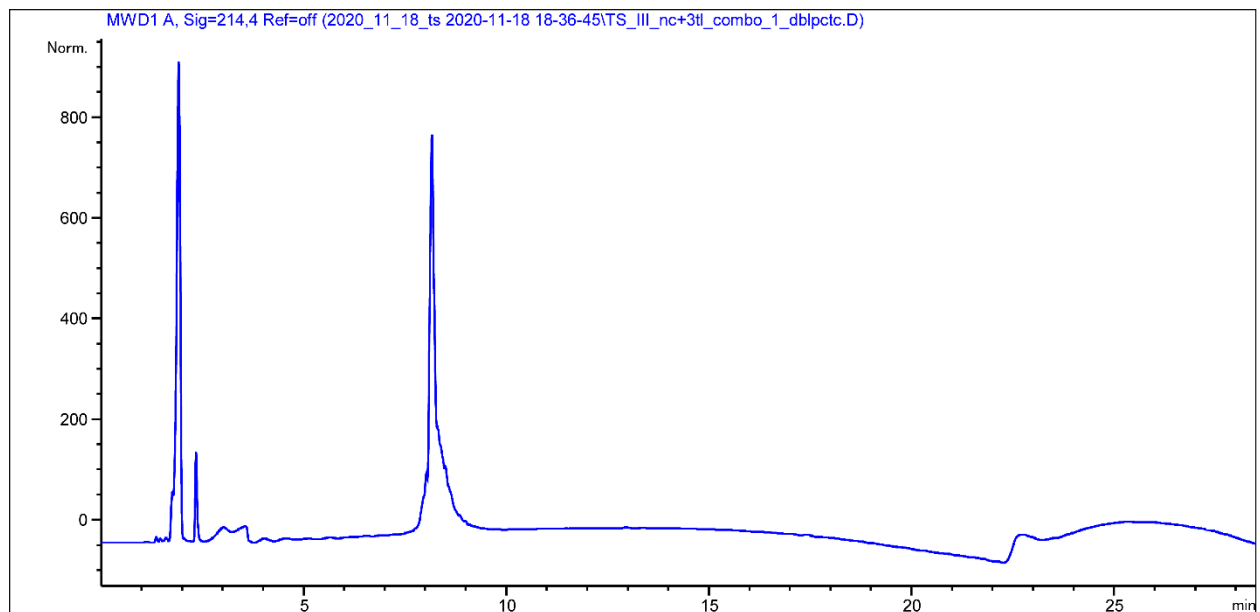
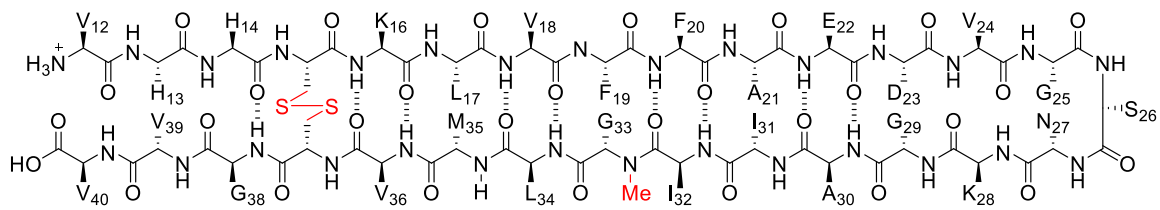


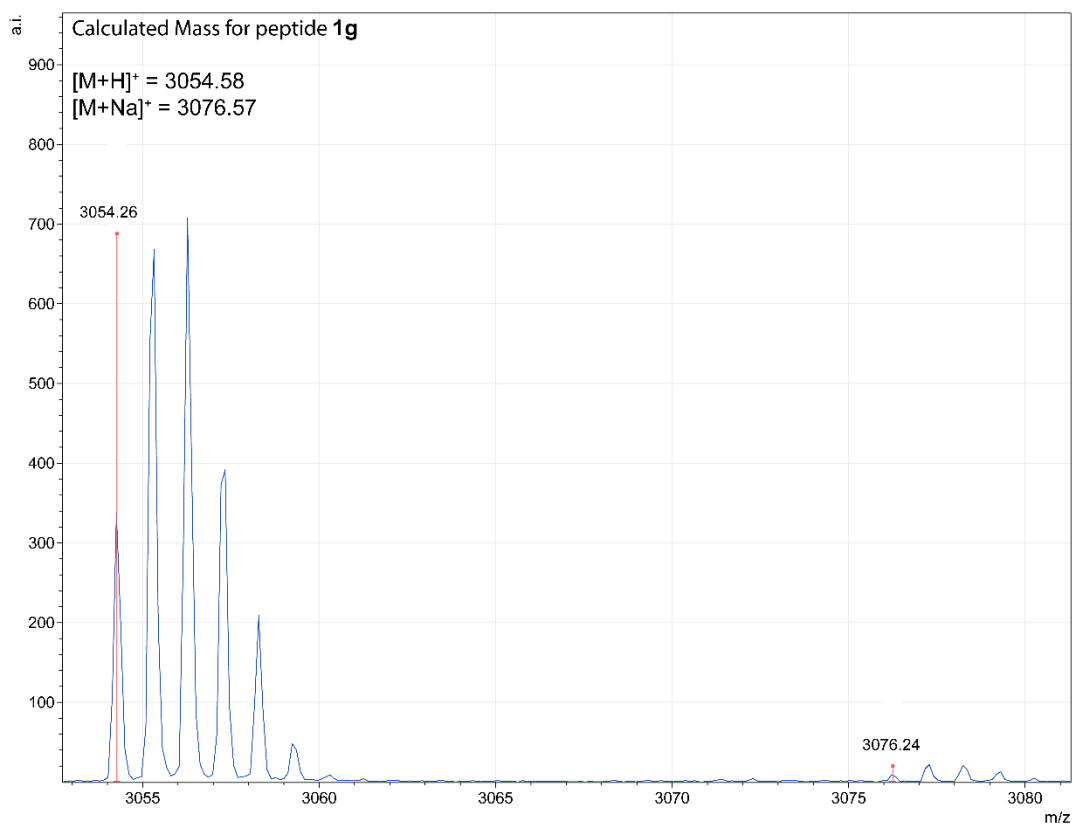
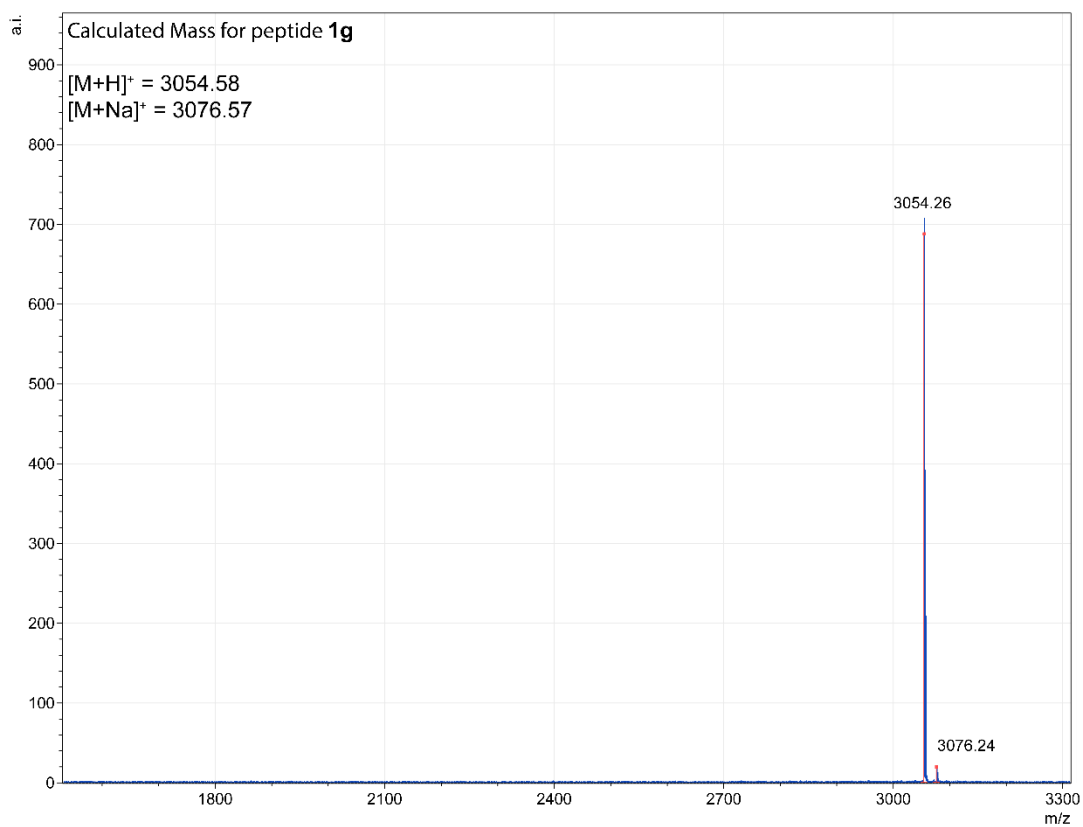
Characterization of peptide **1f**



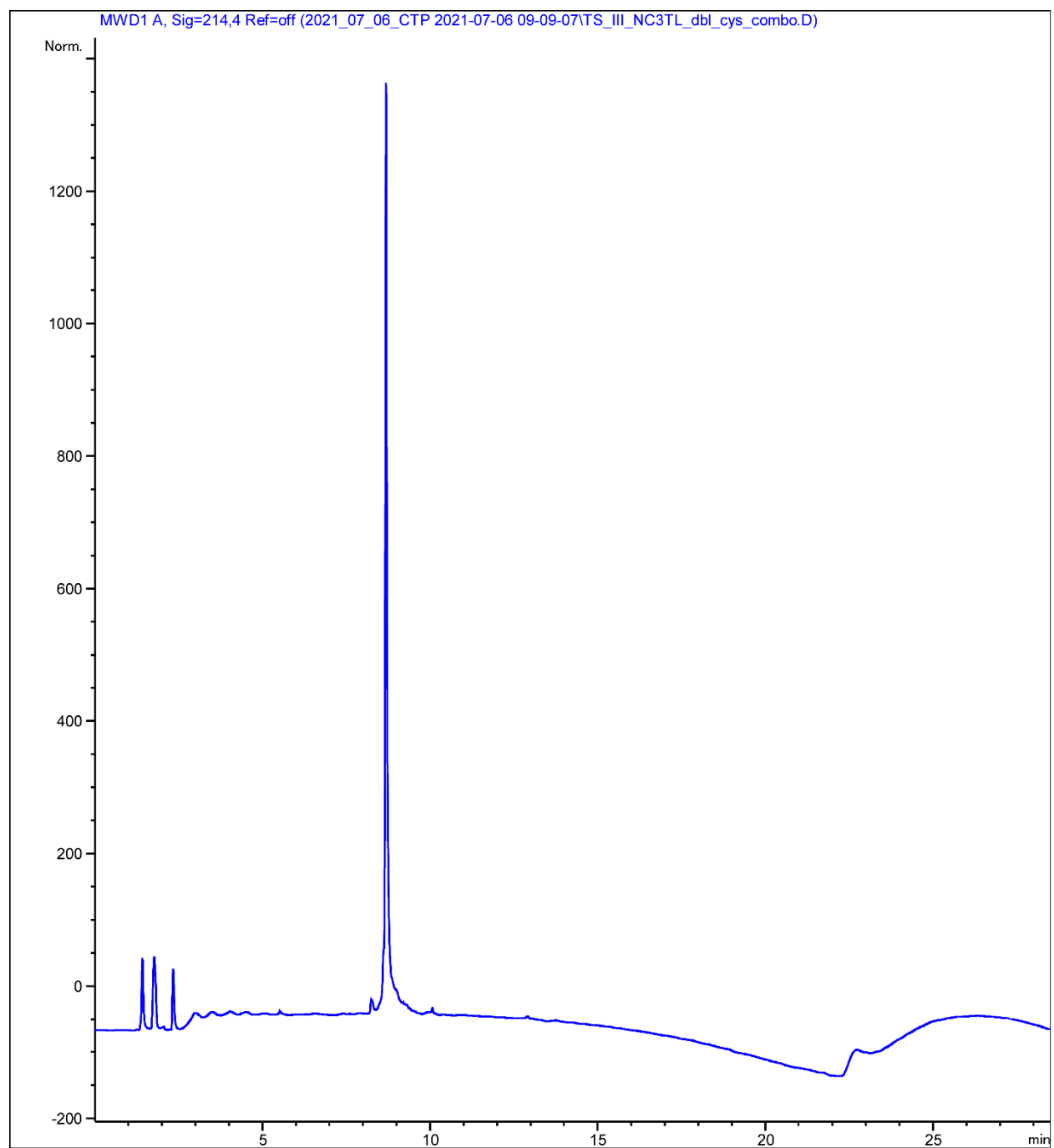
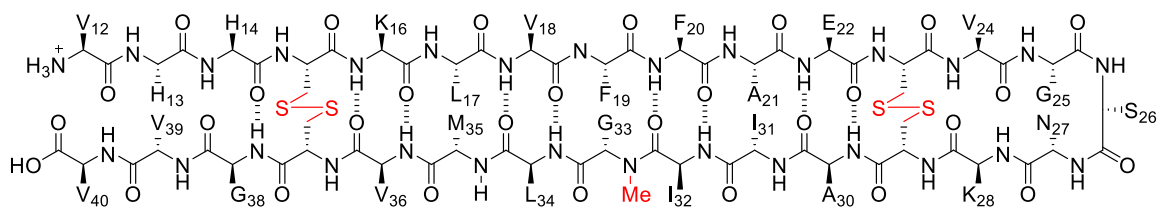


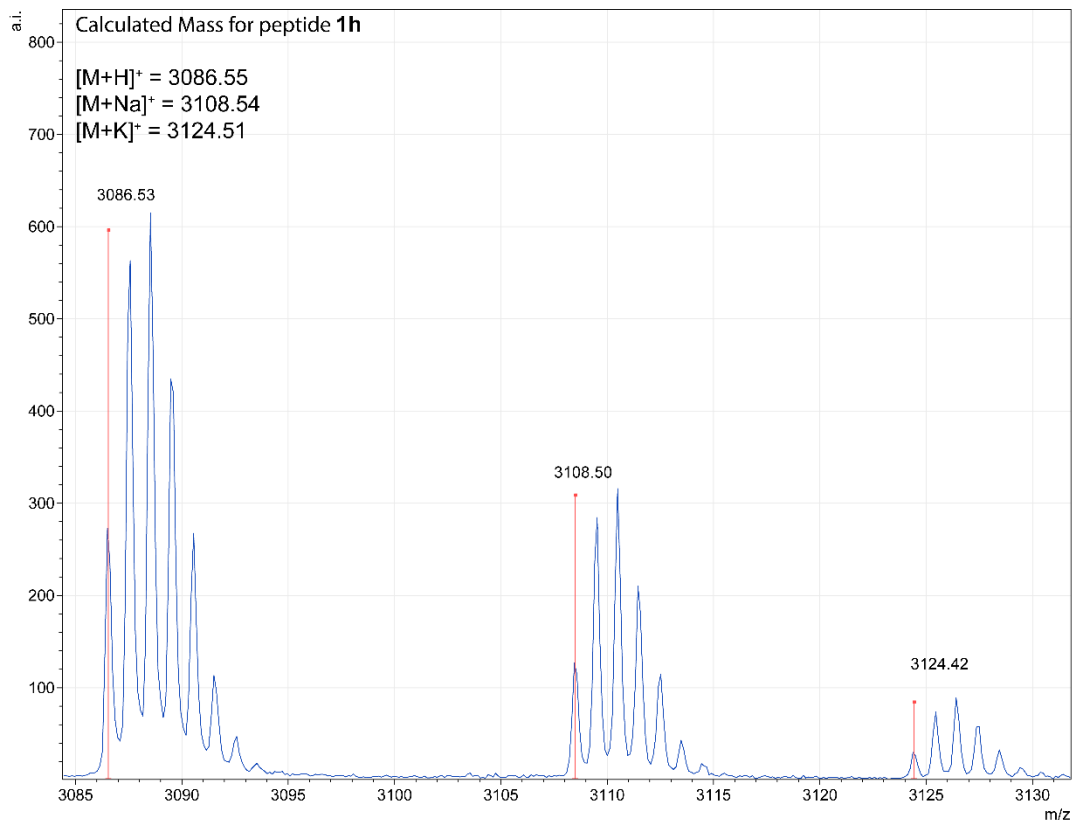
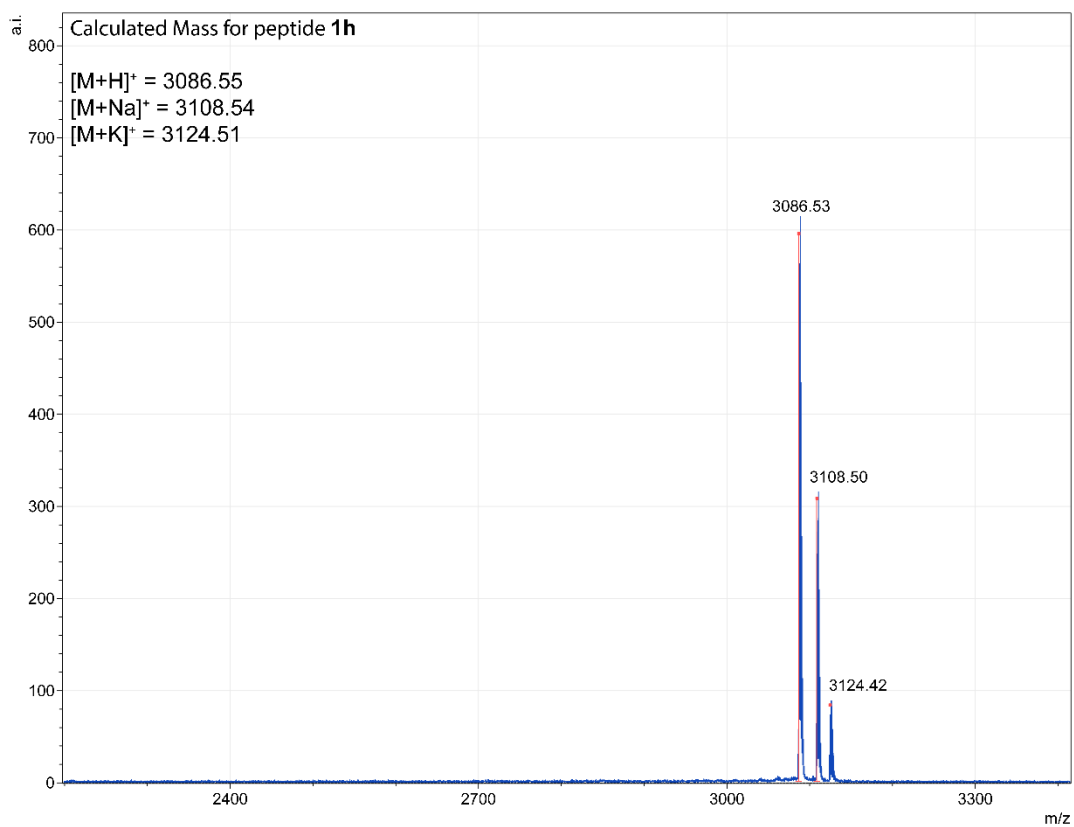
Characterization of peptide **1g**



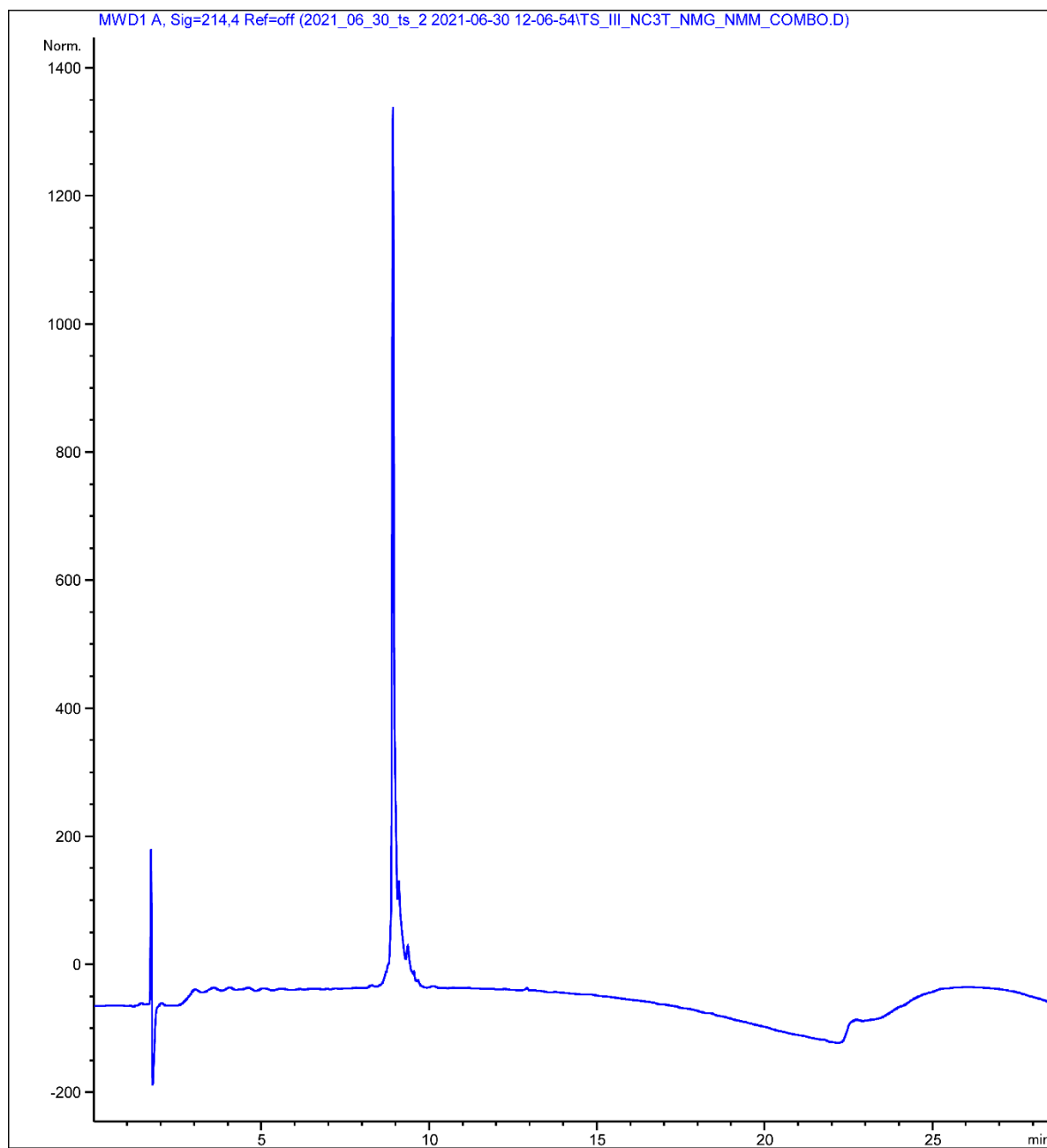
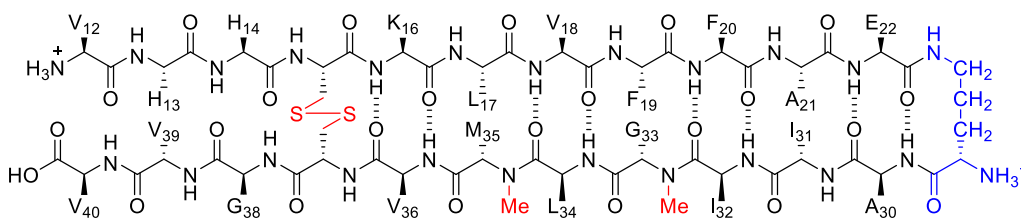


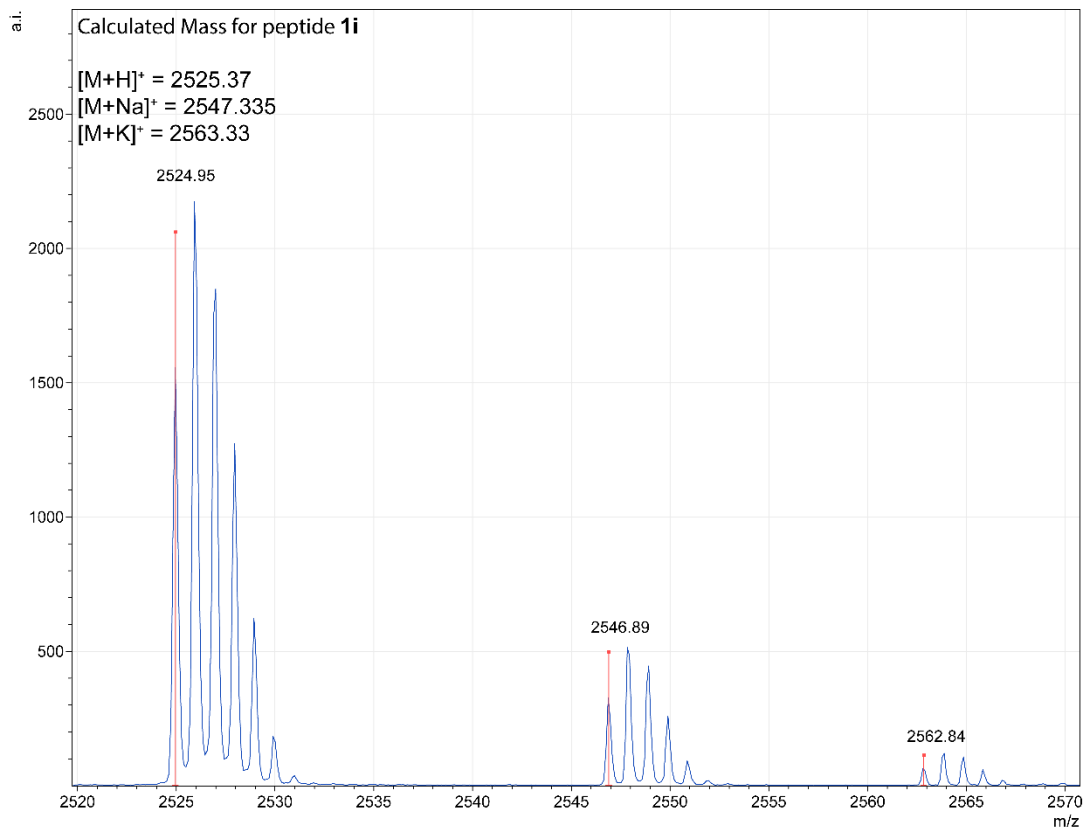
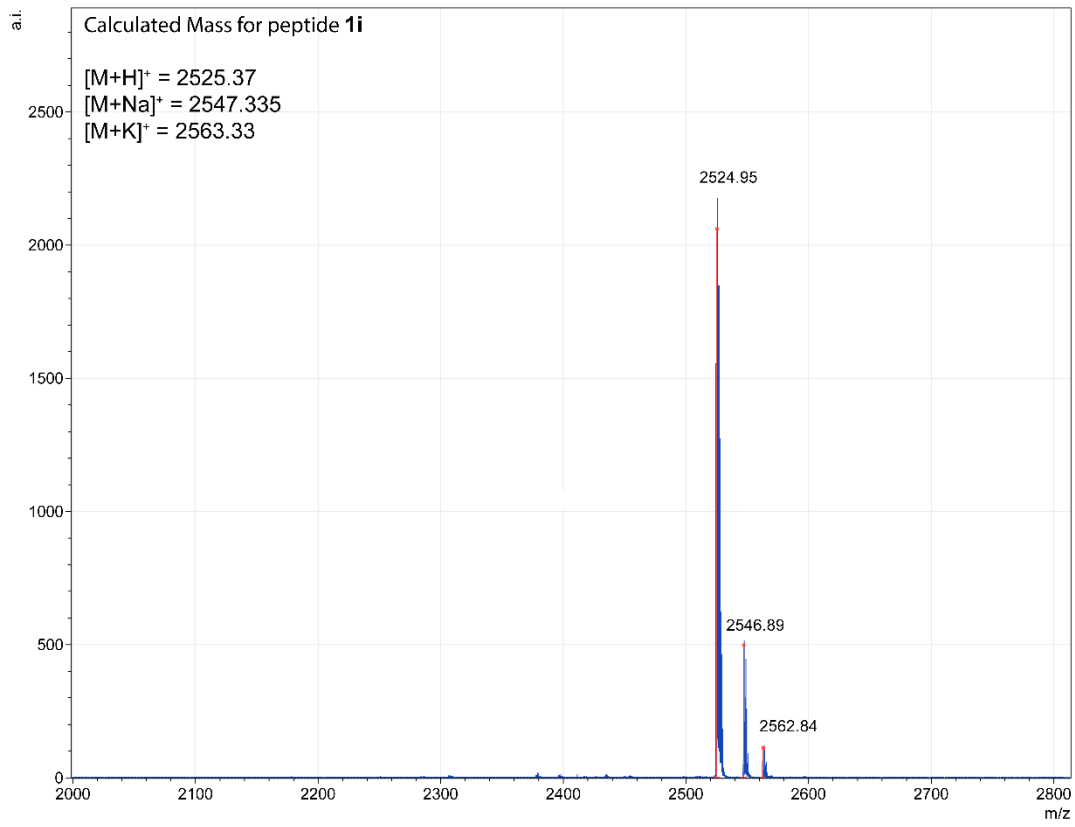
Characterization of peptide **1h**



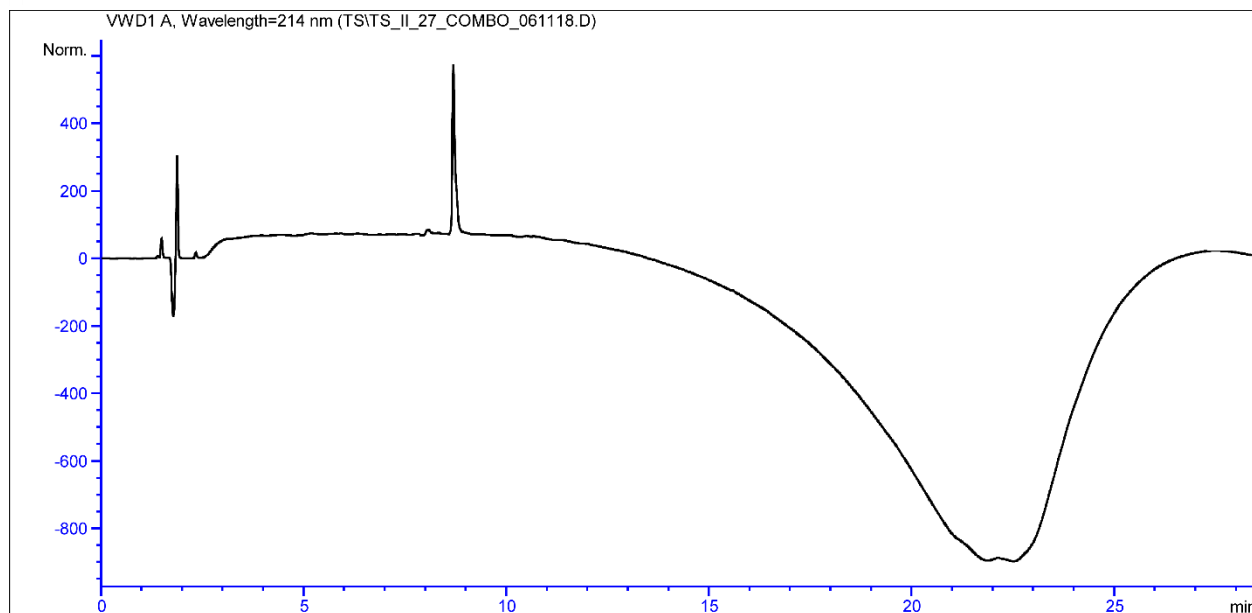
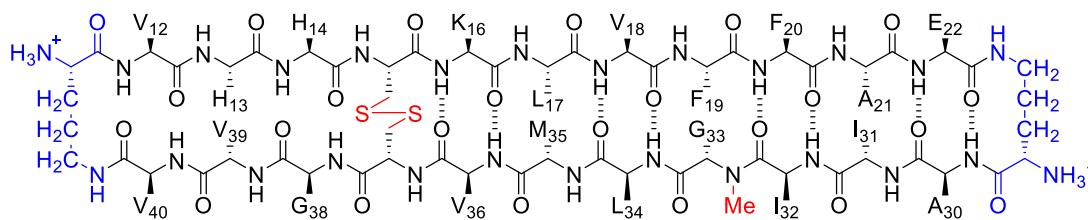


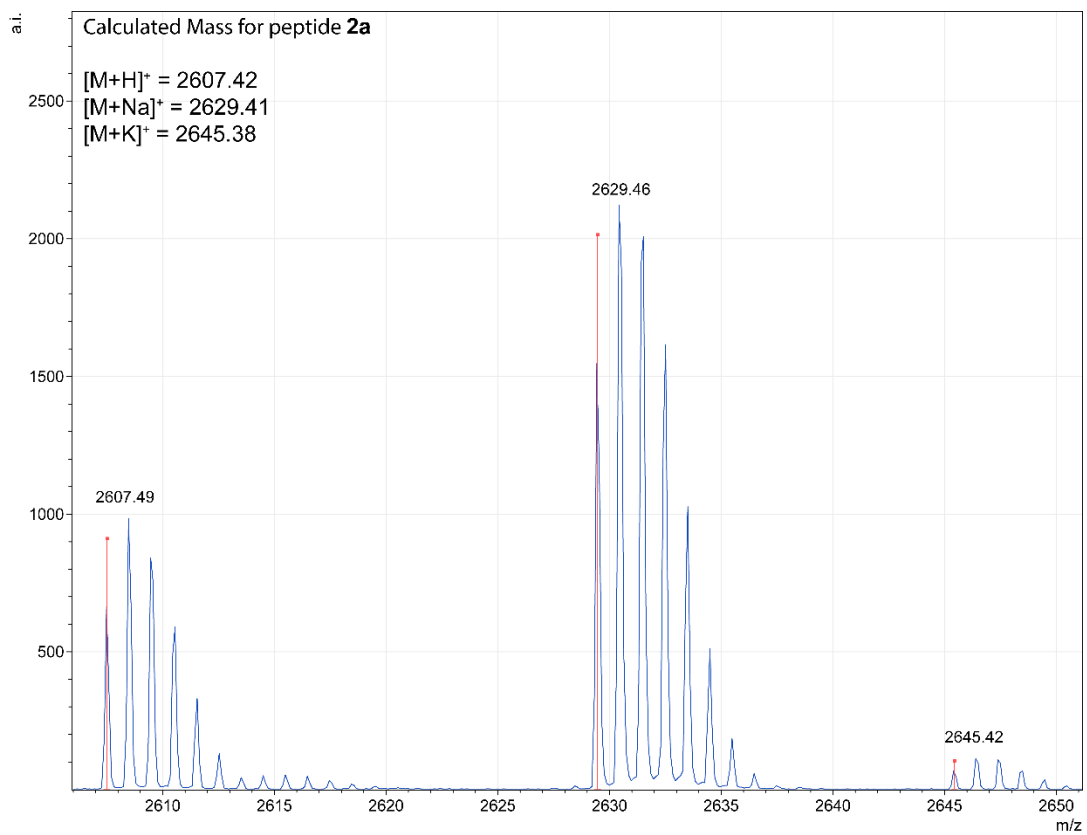
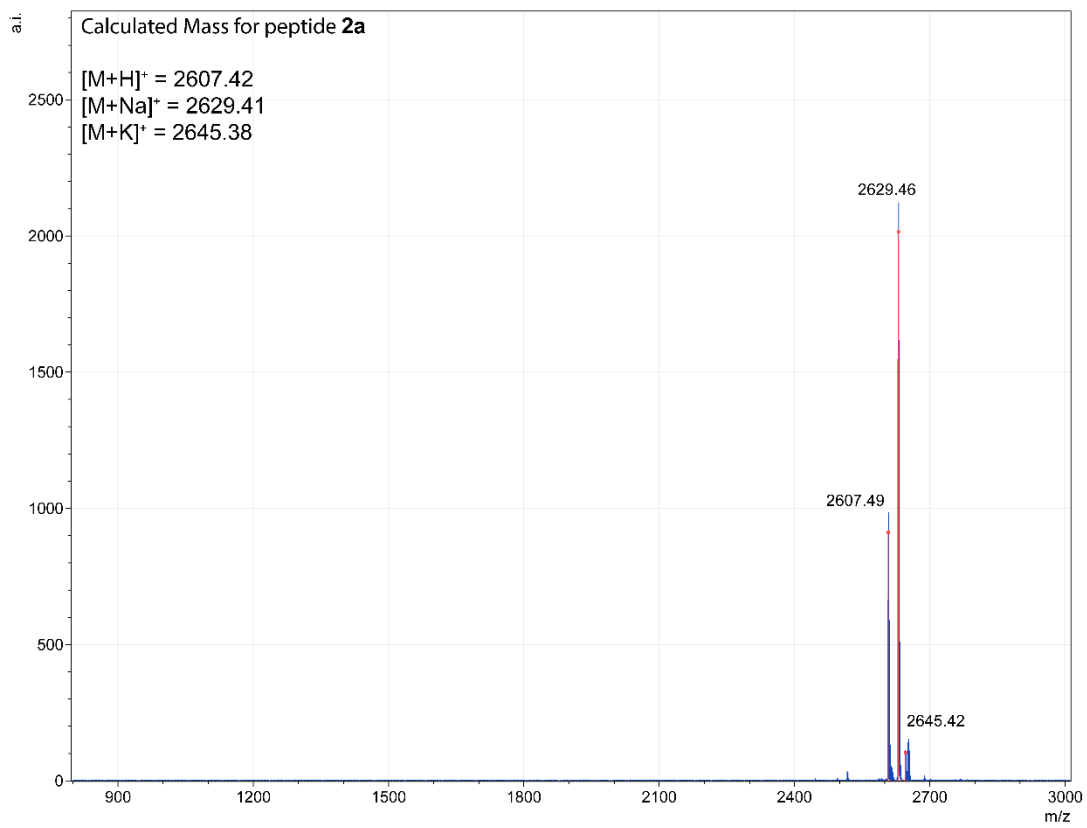
Characterization of peptide **1i**



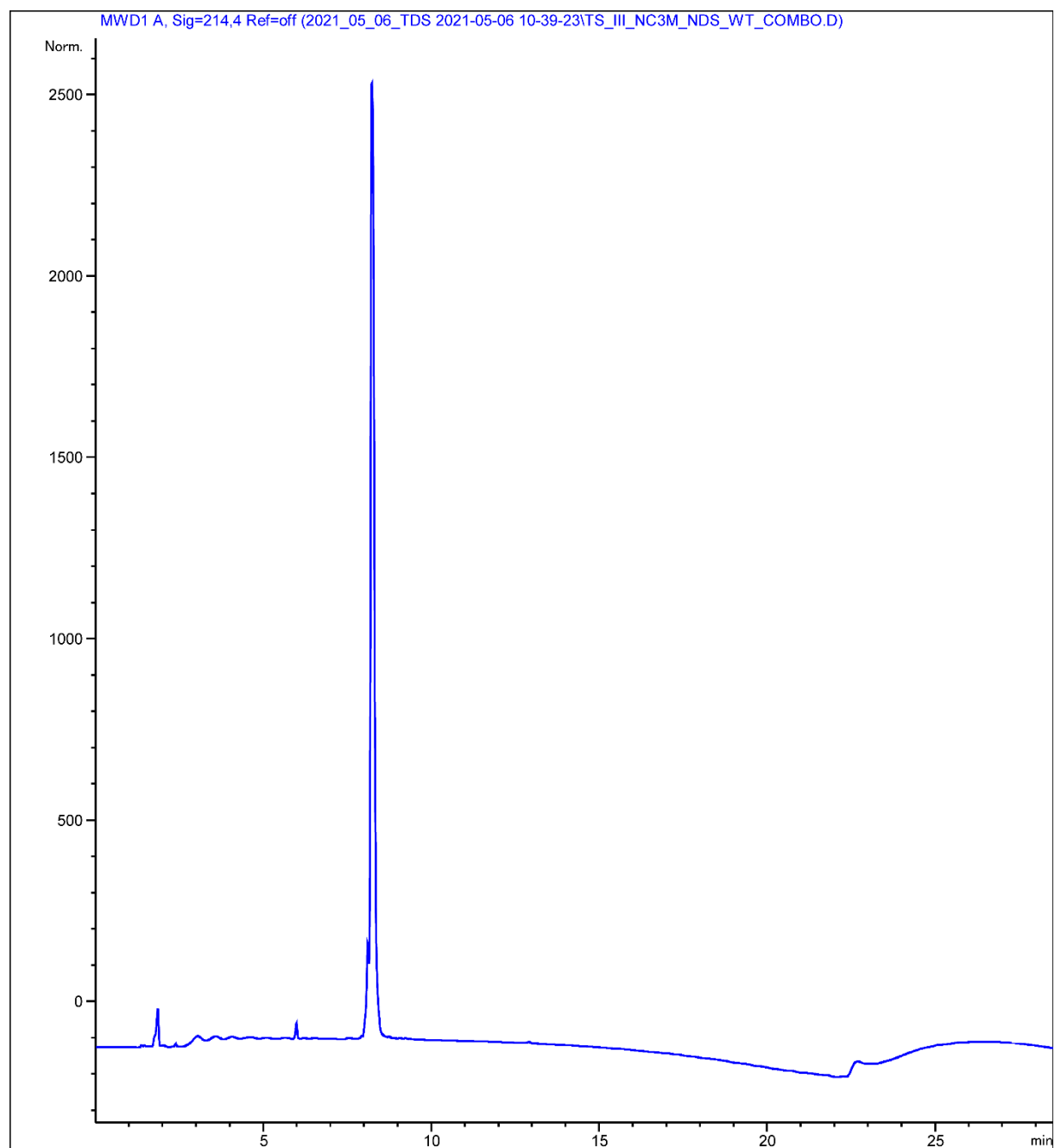
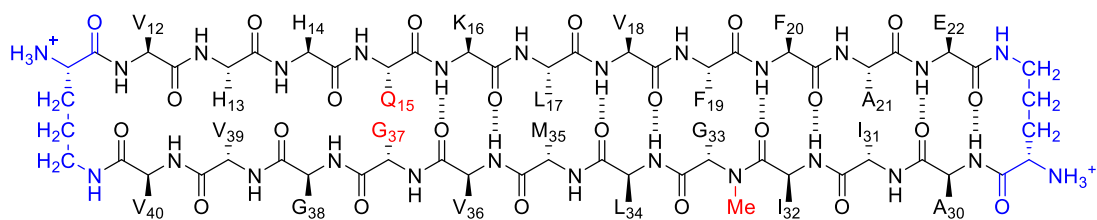


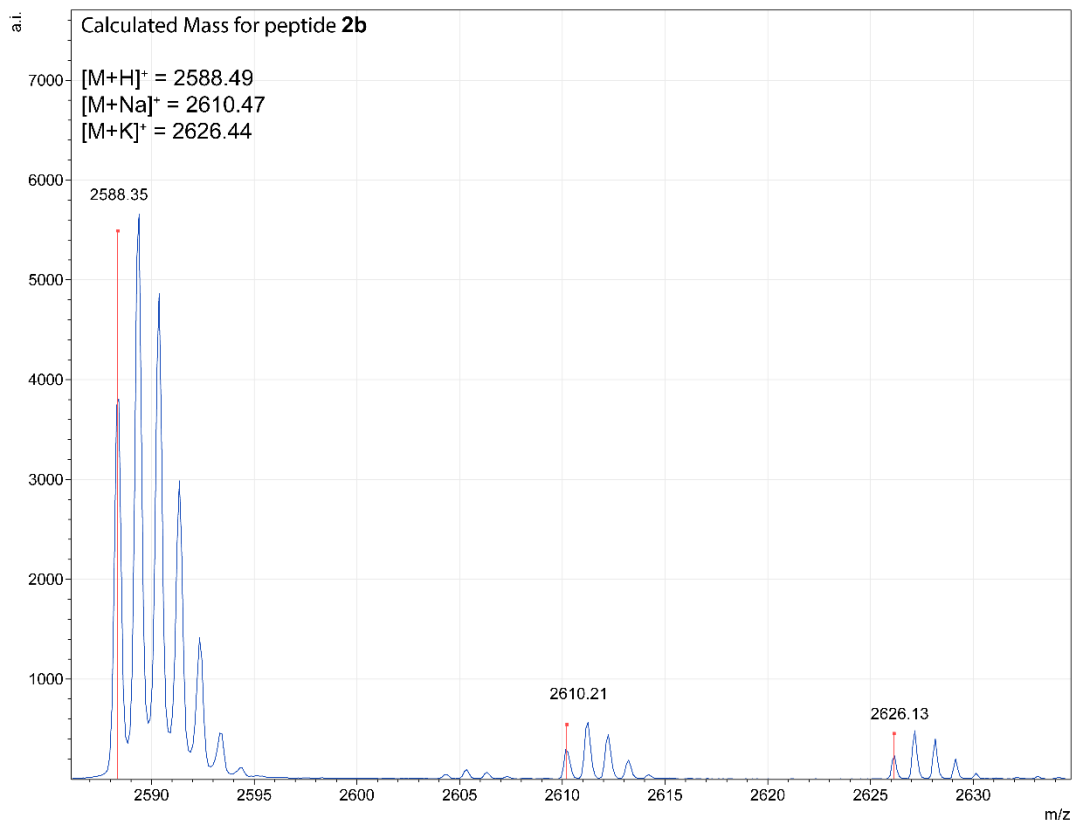
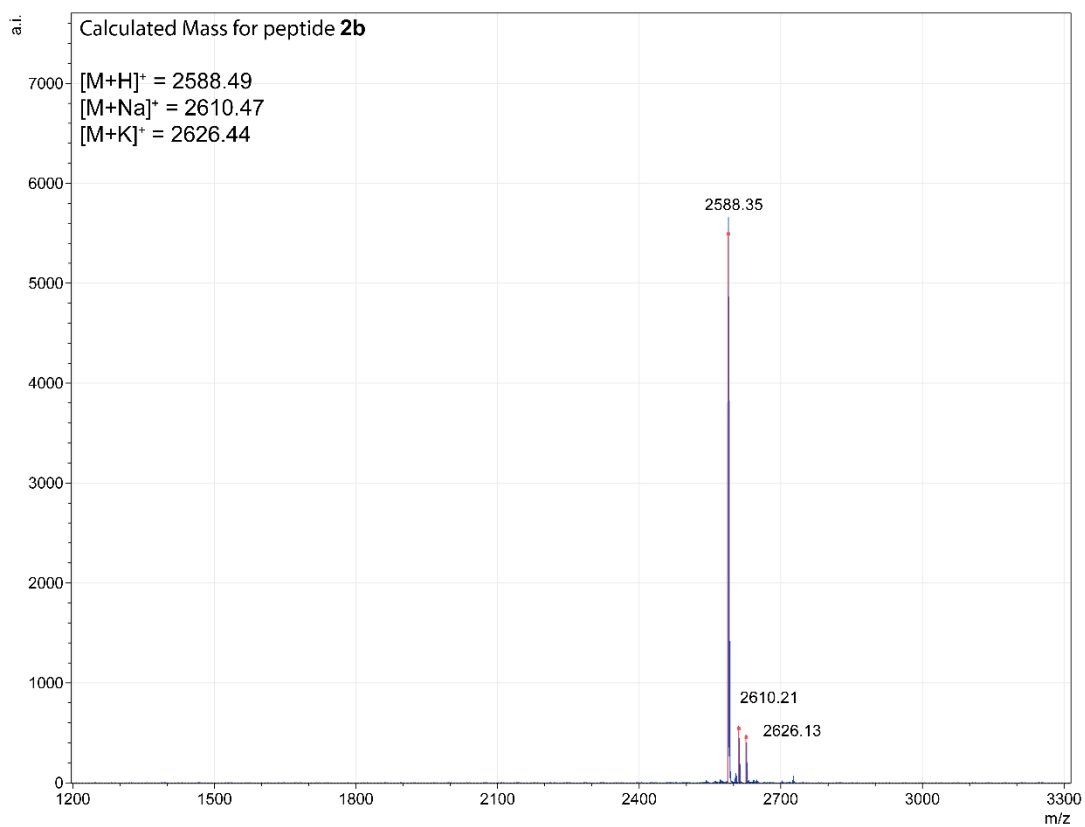
Characterization of peptide 2a



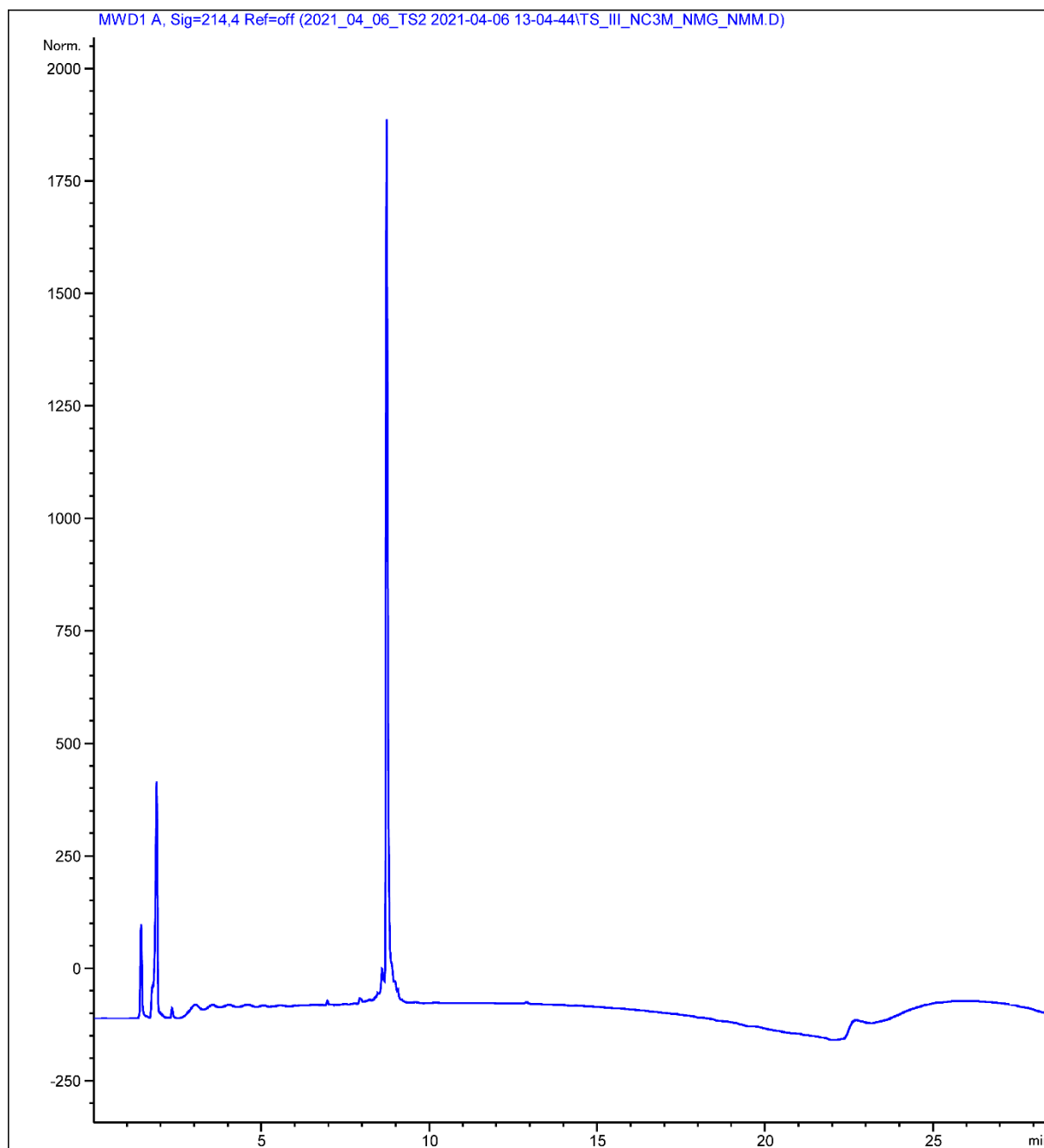
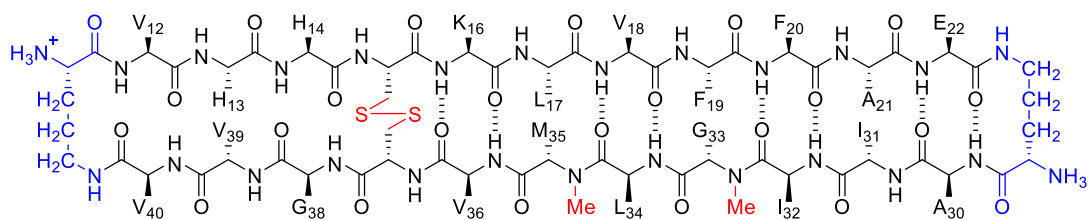


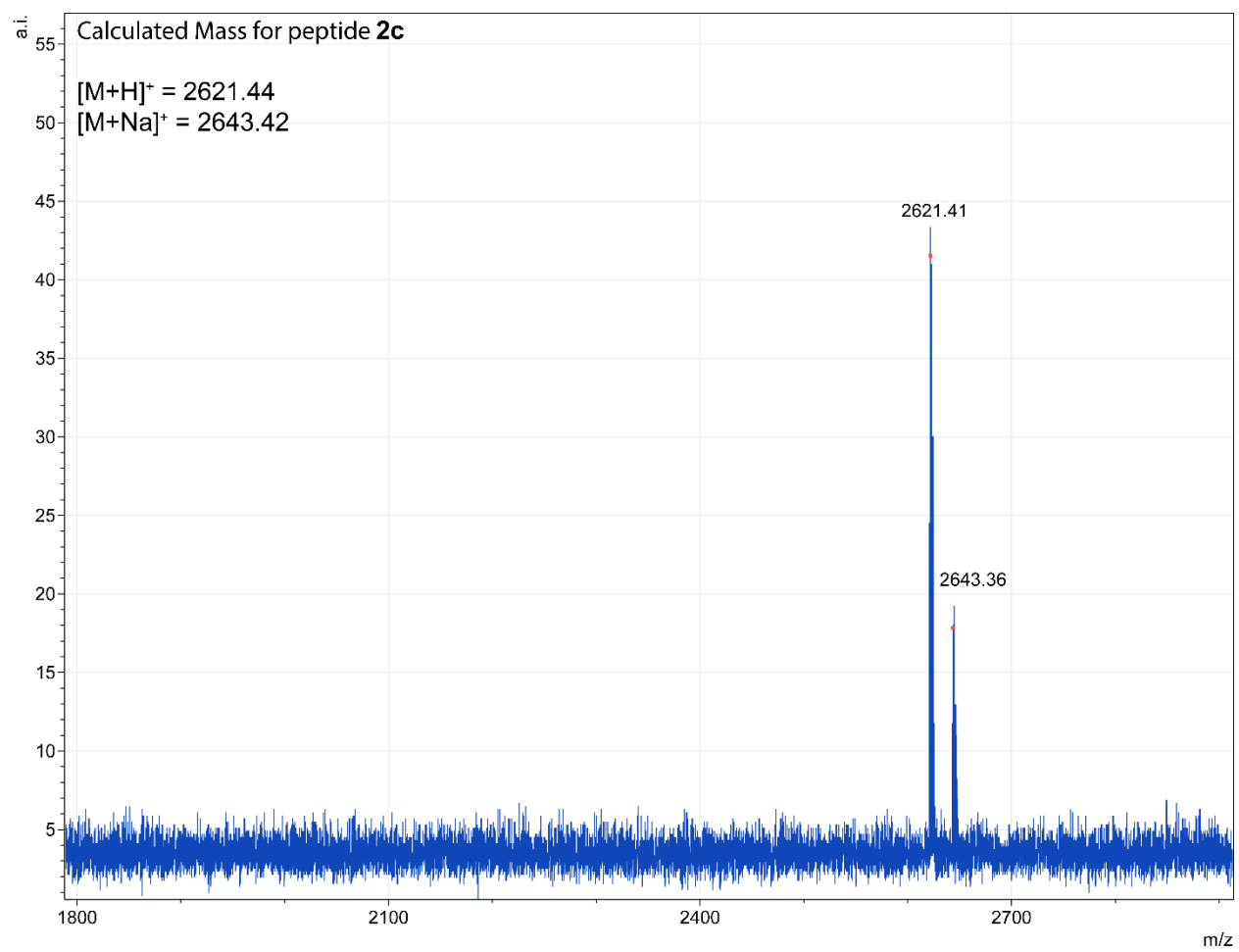
Characterization of peptide **2b**

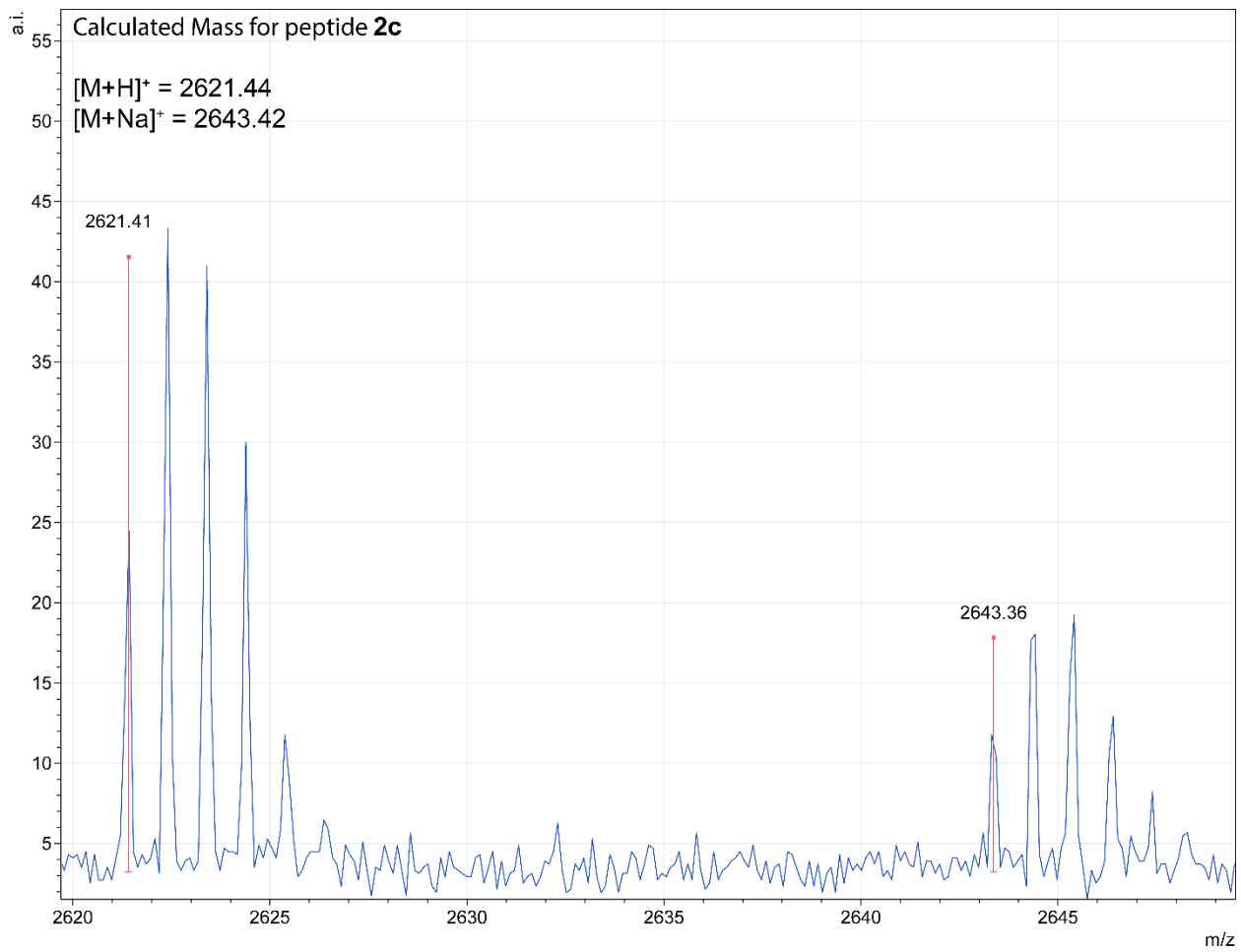




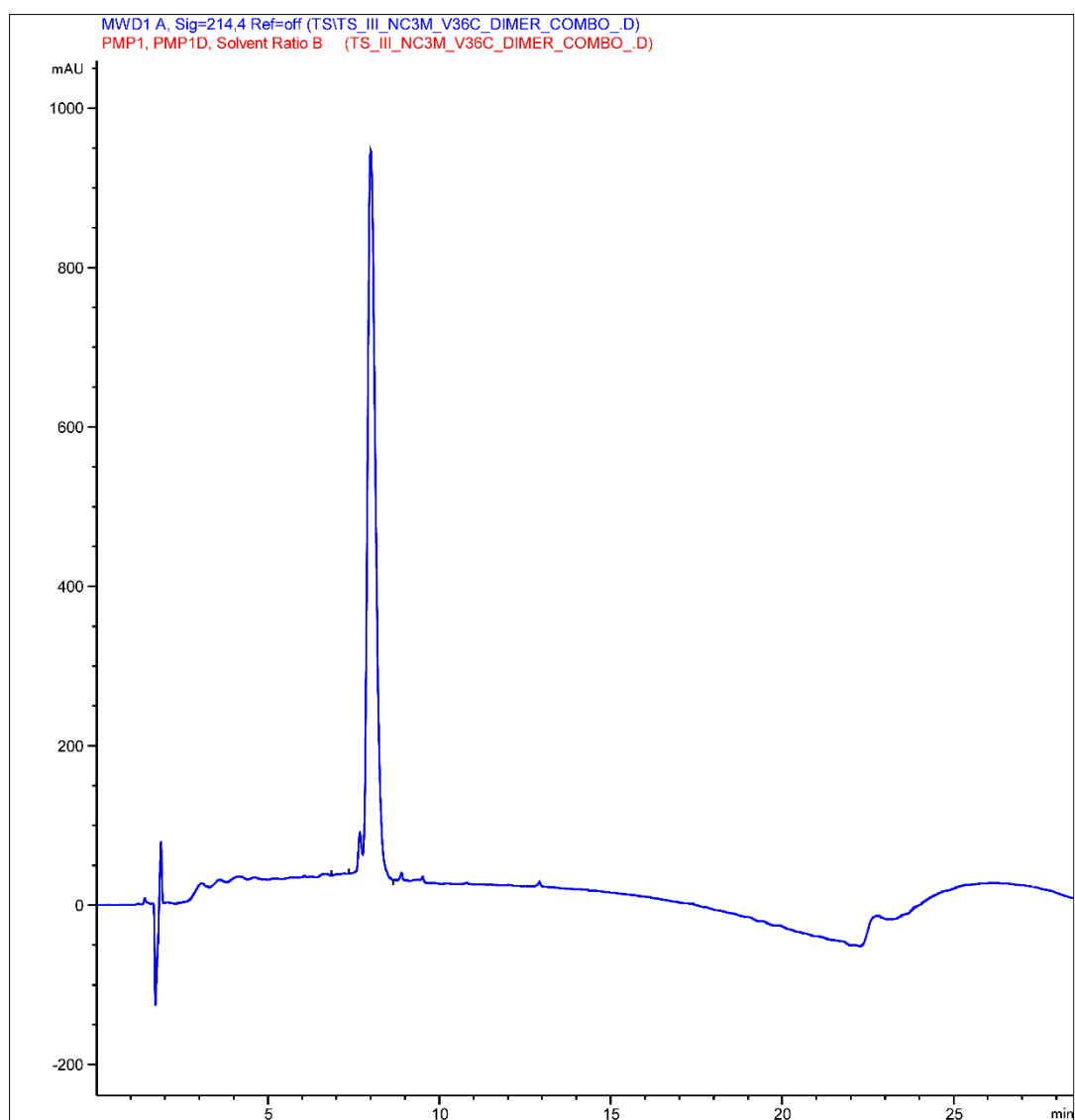
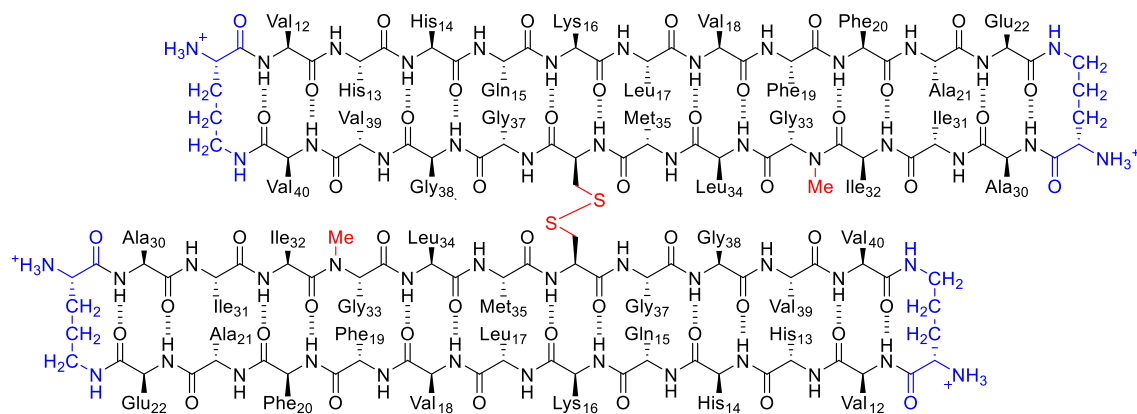
Characterization of peptide 2c

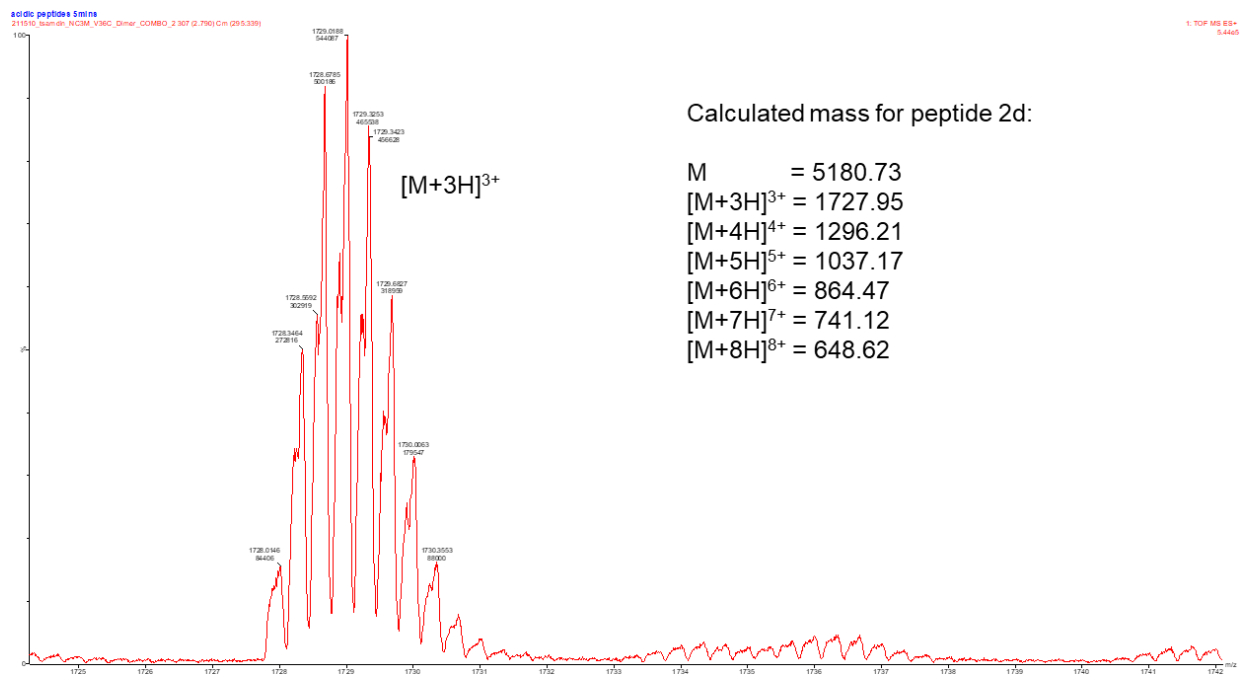
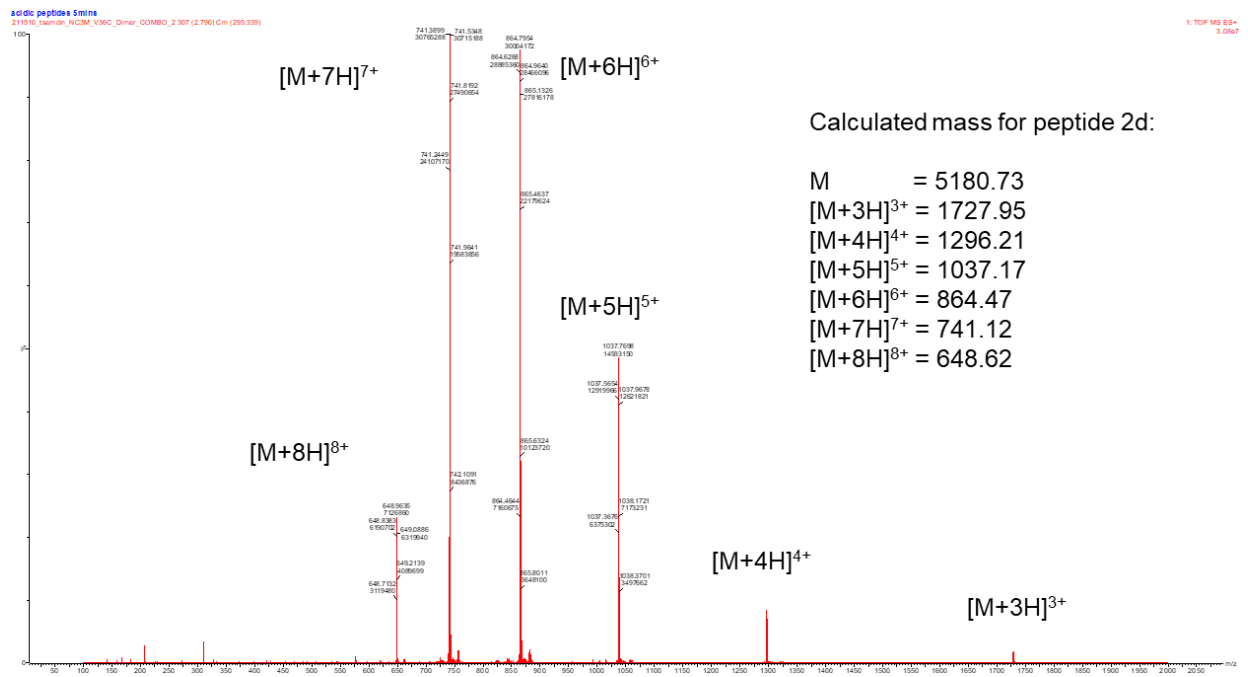


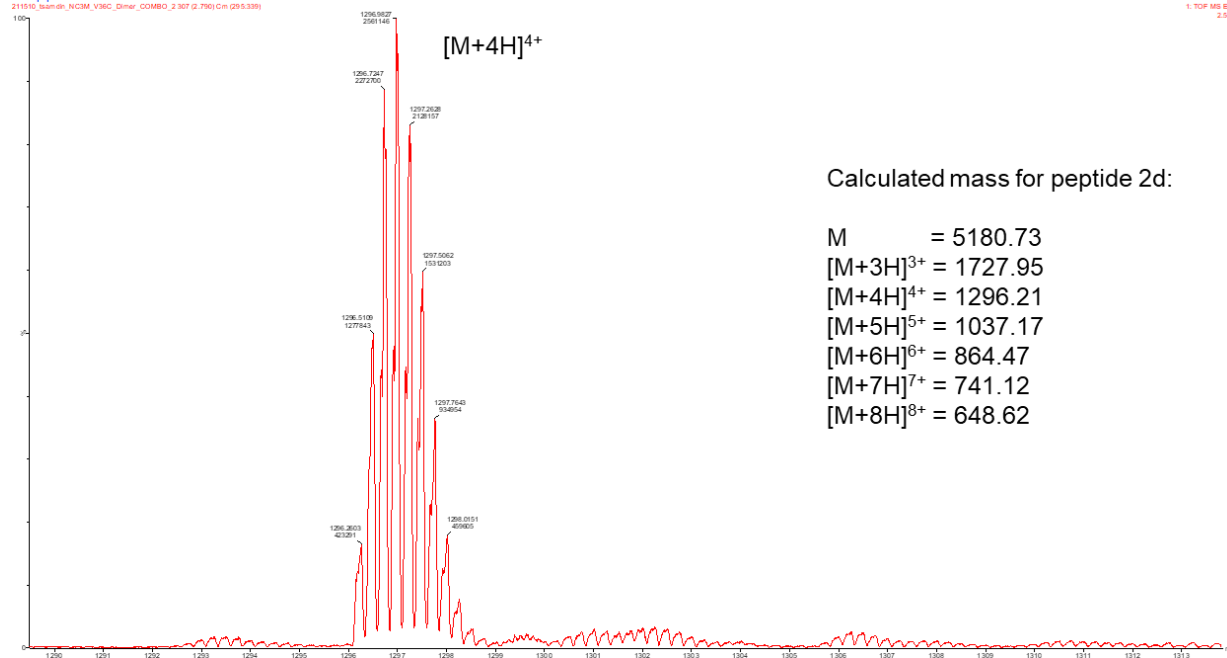




Characterization of peptide 2d

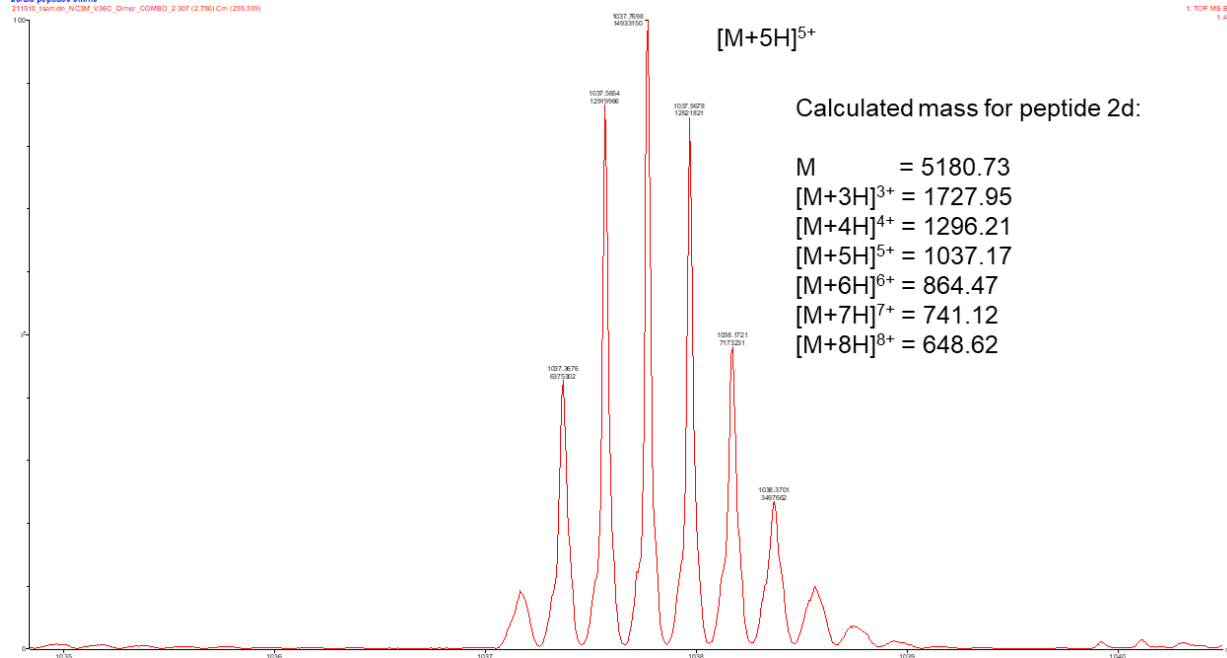






Calculated mass for peptide 2d:

- M = 5180.73
- [M+3H]³⁺ = 1727.95
- [M+4H]⁴⁺ = 1296.21
- [M+5H]⁵⁺ = 1037.17
- [M+6H]⁶⁺ = 864.47
- [M+7H]⁷⁺ = 741.12
- [M+8H]⁸⁺ = 648.62



Calculated mass for peptide 2d:

- M = 5180.73
- [M+3H]³⁺ = 1727.95
- [M+4H]⁴⁺ = 1296.21
- [M+5H]⁵⁺ = 1037.17
- [M+6H]⁶⁺ = 864.47
- [M+7H]⁷⁺ = 741.12
- [M+8H]⁸⁺ = 648.62

Chapter 4

Application of an α -Methyl Amino Acid in Crystallographic Studies of a β -Hairpin Derived from A β

INTRODUCTION

The propensity of the β -amyloid peptide, A β , to aggregate into fibrils poses a challenge for investigations seeking to understand the structures and properties of A β oligomers.¹ Further complicating studies of A β oligomers, is the significant variation they display in their stoichiometry and stability—presenting as a heterogenous mixture of monomer and oligomers in biophysical sizing assays. Various protocols have emerged within the literature detailing methods and procedures for the preparation of A β oligomers, however, even these methods cannot overcome poor quality control in the A β starting material.^{2–4} Alternatively, chemical crosslinking of prepared A β oligomers has emerged as an accessible approach to reduce some heterogeneity and enable studies of stable A β oligomers.^{5–9} However, non-specificity in chemical cross-linking sites or variation in the secondary structure of A β monomers can affect the properties of stabilized oligomers.

The covalent stabilization of A β β -hairpins has emerged as a strategy to increase the homogeneity and stability of A β oligomers.^{10–13} β -hairpins are as a key structural element of A β oligomers.^{10–12,14,15} Hård, Hoyer, and co-workers elucidated the NMR structure of an A β β -hairpin where residues 17–23 and 30–36 hydrogen bond to form an antiparallel β -sheet, with residues 24–

29 forming a loop, and the remaining N- and C-terminal residues left as unstructured segments.¹⁰ In subsequent studies, Härd, and co-workers reported that a disulfide stabilized homologue of the A β β -hairpin that they had previously reported, mimicked properties of endogenous A β oligomers.¹¹ They further reported that this covalently stabilized β -hairpin assembled to form a β -barrel like hexamer, stabilized by edge-to-edge hydrogen bonding and hydrophobic packing.¹²

More recently, Carulla and co-workers recently reported the NMR structure of an A β ₄₂ tetramer, comprising a six-stranded antiparallel β -sheet formed by two β -hairpins of A β ₄₂ surrounding two antiparallel β -strands of A β ₄₂.¹⁵ In this tetramer structure, the β -hairpins are formed by residues 9–21 and 28–40 hydrogen bonding to form an antiparallel β -sheet, with residues 22–27 forming a loop, and the remaining N- and C-terminal residues left as unstructured segments. To study the stoichiometry and properties of this tetramer in other biophysical assays, Carulla and co-workers subjected them to chemical crosslinking across the acid side-chains of Asp and Glu.¹⁶

To reduce heterogeneity and facilitate studies of oligomers formed by A β derived peptides, the Nowick laboratory has developed macrocyclic β -hairpin peptides as synthetic tools to mimic endogenous oligomers (**Figure 4.1**).^{17,18} These peptides typically comprise two heptapeptide β -strand segments derived from A β that are covalently linked by two δ Orn turn units that constrain the peptide to a macrocycle. To prevent uncontrolled aggregation, we incorporate an *N*-methyl amino acid on one strand of the macrocycle. These model systems limit structural heterogeneity and provide a measure of preorganization that primes the peptide to assemble and form oligomers that can be studied using X-ray crystallography.^{19–26}

In 2014, we reported the X-ray crystallographic structure of triangular trimers and ball-shaped dodecamers formed by peptide **1** (**Figure 4.1**). Peptide **1** comprises two β -strands comprising A β residues 17–23 and 30–36, two δ Orn turn units that constrain the peptide to a

macrocycle, and an *N*-methyl group on Phe₂₀. To improve solubility, Met₃₅ is replaced by an α -linked Orn. Using X-ray crystallography, we observed three monomers of peptide **1** assembling to form a triangular trimer that is stabilized by edge-to-edge hydrogen bonding between monomers (**Figure 4.2**). Within the crystal lattice we also observed the assembly of a ball-shaped dodecamer, stabilized by the hydrophobic packing of four triangular trimers.

In the crystallographic structure of the triangular trimer formed by peptide **1**, three *N*-methyl groups on Phe₂₀ project inwards, towards the center of the trimer (magenta) (**Figure 4.2**). The methyl groups prevent the formation of three additional intermolecular hydrogen bonding interactions between three pairs of backbone amides and carbonyl oxygens that would be present with the native Phe₂₀ residue. In the same investigation, we also studied the crystallographic assembly of a structural homologue of peptide **1** that bore an *N*-methyl group on Gly₃₃ instead of Phe₂₀. Even with the methyl group on the other strand of the macrocycle, this homologue still assembled to form triangular trimers that were nearly identical to those formed by peptide **1**. Further, this homologue was further stabilized by three additional hydrogen bonds with coordinating waters at the center of the trimer, that were absent in the structure of peptide **1**.

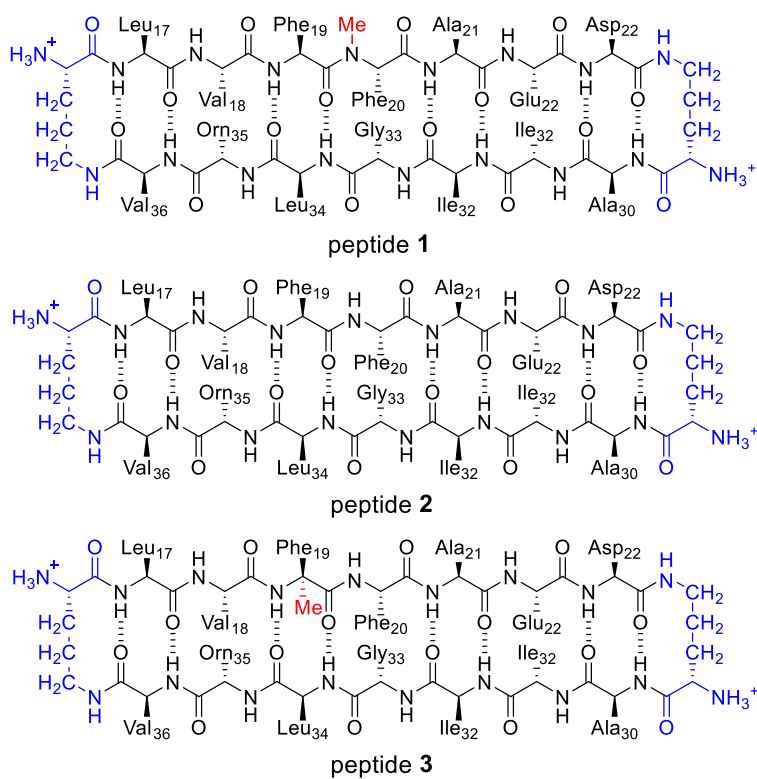


Figure 4.1. Chemical structures of macrocyclic β -hairpin peptides derived from $A\beta_{17-23}$ and $A\beta_{30-36}$ with δ Orn turn units (blue) and methyl groups (red). Peptide 1 contains an *N*-methyl group on Phe₂₀. Peptide 2 does not contain a methyl group. Peptide 3 contains an α -methyl group on Phe₁₉.

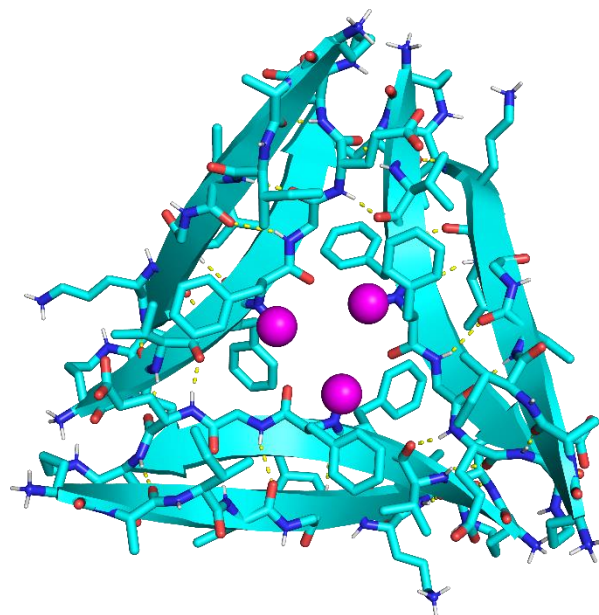


Figure 4.2. X-ray crystallographic structure of a triangular trimer formed by peptide 1, (PDB 4NW9).

Although the location of the *N*-methyl group does not affect the crystallographic assembly of a macrocyclic β -hairpin peptide that comprises A β residues 17–23 and 30–36, the presence of the *N*-methyl group does alter the hydrogen bonding edge of the macrocycle. Interactions at the hydrogen bonding edges of β -hairpins are an important facet of A β oligomerization. Restoring the hydrogen bonding interactions lost due to the incorporation of an *N*-methyl group on Phe₂₀ may alter the assembly of peptide **1**, and better mimic endogenous A β oligomers.

In this project, we set out to restore three intermolecular hydrogen bonds absent in the crystal structure of in peptide **1** and develop a model system that more closely mimics endogenous A β oligomers. (**Figure 4.1**). We initially attempted to remove the methyl group entirely, furnishing peptide **2**. However, while peptide **2** does show evidence of oligomerization, it does not crystallize. We then turned toward incorporating an α -methyl group in the top strand of peptide **1**, in place of an *N*-methyl group, furnishing peptide **3**. We were gratified to discover that like peptide **1**, peptide **3** crystallizes, assembling to form the same triangular trimers and ball-shaped dodecamers as peptide **1**.

RESULTS AND DISCUSSION

Oligomerization of peptides 1–3

Peptides **1** and **3** do not self-assemble by SDS-PAGE, migrating as single bands to just below the 4.6 kDa ladder band (**Figure 4.3**). Peptide **2b** does self-assemble, migrating as a heterogeneous mixture of oligomers with molecular weights that correspond to trimer, tetramer, and pentamer. The difference in self-assembly between peptides **1** and **3**, and peptide **2** is likely due to the presence of the methyl blocking groups. This result shows that the α -methyl group on Phe₁₉ in peptide **3** can still block assembly, while allowing peptide **3** the opportunity to form the intermolecular hydrogen bonds absent in the crystal structure of peptide **1**.

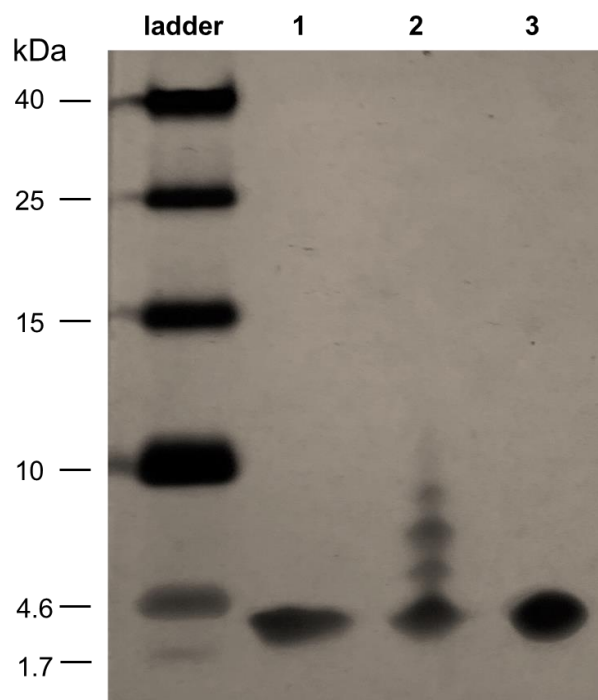


Figure 4.3. Silver stained SDS-PAGE of peptides **1–3**. SDS-PAGE was performed in Tris buffer at pH 6.8 with 2% (w/v) SDS on a 16% polyacrylamide gel with 50 μ M solutions of peptide in each lane.

X-ray crystallographic studies of peptide 3

X-ray crystallography reveals that peptide **3** folds to adopt a twisted β -hairpin, stabilized by the same intramolecular hydrogen bonds that stabilize the residues 17–22 and 30–36 in peptide **1** (**Figure 4.4**). The methyl groups (violet) extend away from the β -hairpins formed by peptides **1** and **3**. An overlay of peptides **1** and **3** reveals that the monomers do not differ significantly in their structure. Molecular replacement, using a search model derived from the crystallographic structure of the trimer formed by peptide **1** (PDB 5SUR), was used to determine the X-ray crystallographic phases of peptide **3**. Supplementary table 4.1 summarizes the crystallographic properties, crystallization conditions, data collection, and model refinement statistics for peptide **3**.

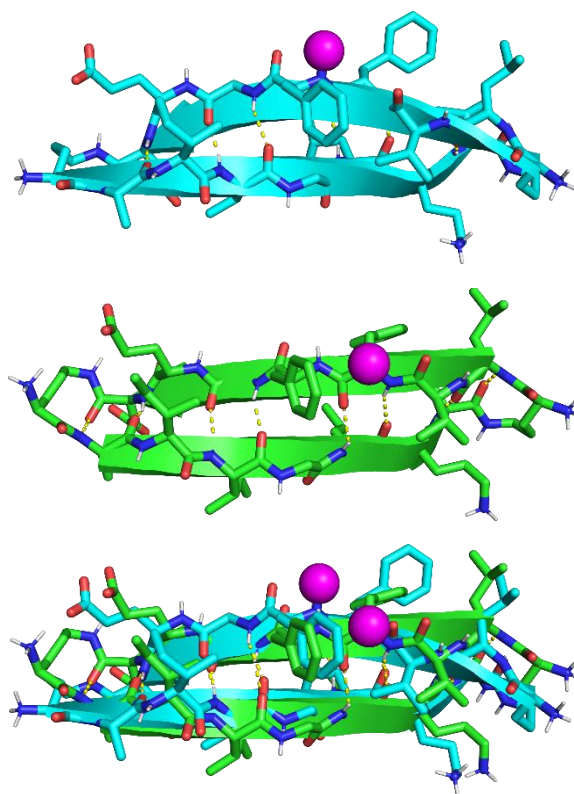


Figure 4.4. X-ray crystallographic structure of monomer formed by peptides **1** (blue) and **3** (green) and overlay.

Like peptide **1**, peptide **3** assembles further in the crystal lattice, forming triangular trimers and ball shaped dodecamers (**Figure 4.5** and **4.6**). The triangular trimers formed by peptide **3**

assemble through edge-to-edge hydrogen bonding interactions and the packing of hydrophobic residues at one face of the trimer. The α -methyl groups on Phe₁₉ are accommodated at the center of the trimer. Unlike peptide **1b**, the backbone amide and carbonyl oxygens of Phe₂₀ in peptide **3** can form hydrogen bonds. Three additional hydrogen bonds are observed to form at the center of the triangular trimer formed by peptide **3**. Further, the triangular trimer formed by peptide **3** is similar but not identical to the trimer formed by peptide **1** (Figure 4.5). We speculate that the presence of these three additional hydrogen bonds causes a shift in the edge-to-edge registration of monomers in the trimer. Like peptide **1**, the triangular trimers formed by peptide **3** can assemble to form a ball-shaped dodecamer (Figure 4.6).

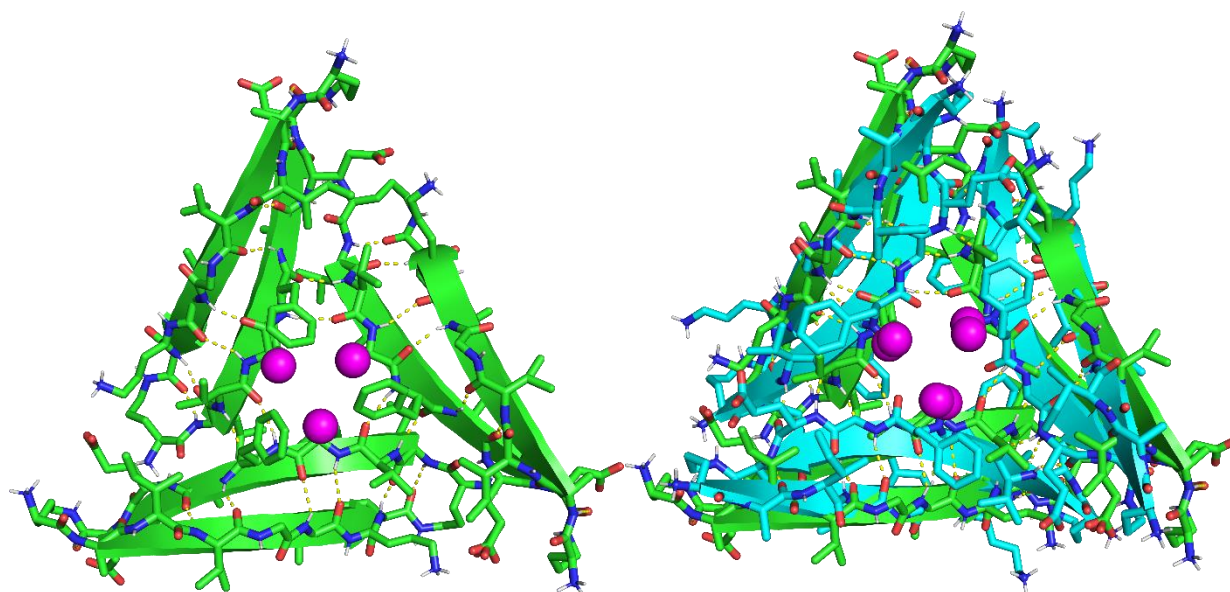


Figure 4.5. X-ray crystallographic structure of a triangular trimer formed by peptide **3** (green) and overlay with trimer formed by peptide **1** (blue: PDB 4NW9).

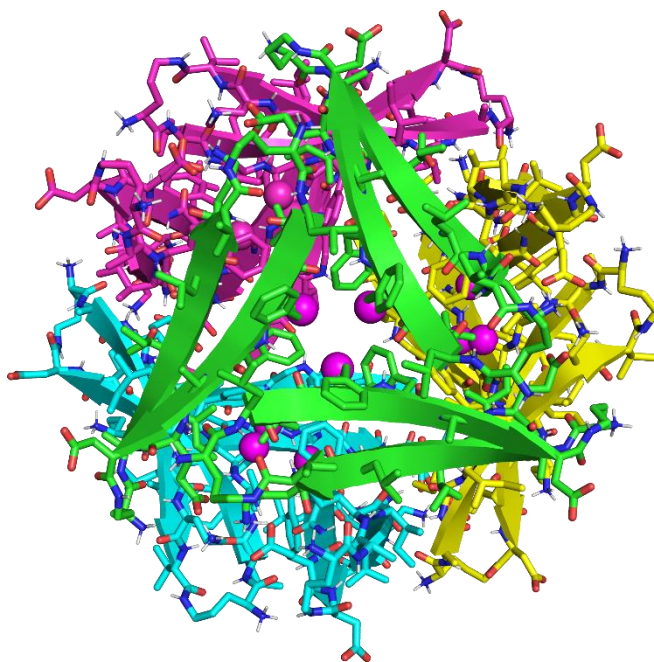


Figure 4.6. X-ray crystallographic structure of the ball-shaped dodecamer formed by peptide **3**.

CONCLUSION

Differences in the assembly of peptides **1–3** reveals that the methyl group is necessary for crystallographic assembly. Replacement of the *N*-methyl blocking group with an α -methyl blocking group prevents uncontrolled aggregation and facilitates the formation of additional intermolecular hydrogen bonds that stabilize and slightly alter the assembly of macrocyclic β -hairpins derived from A β residues 17–22 and 30–36. This replacement allows our model systems to more closely mimic β -hairpins formed by unmodified A β , and possibly better mimic the oligomers they form in the Alzheimer's brain.

REFERENCES

- (1) Dobson, C. M.; Knowles, T. P. J.; Vendruscolo, M. The Amyloid Phenomenon and Its Significance in Biology and Medicine. *Cold Spring Harb. Perspect. Biol.* **2020**, *12* (2), pii: a033878. <https://doi.org/10.1101/cshperspect.a033878>.
- (2) Fauvet, B.; Fares, M. B.; Samuel, F.; Dikiy, I.; Tandon, A.; Eliezer, D.; Lashuel, H. A. Characterization of Semisynthetic and Naturally N α - Acetylated α -Synuclein in Vitro and in Intact Cells: Implications for Aggregation and Cellular Properties of α -Synuclein. *J. Biol. Chem.* **2012**, *287* (34), 28243–28262. <https://doi.org/10.1074/jbc.M112.383711>.
- (3) Kotler, S. A.; Ramamoorthy, A. Preparation of Stable Amyloid- β Oligomers without Perturbative Methods. *Methods Mol. Biol.* **2018**, *1777*, 331–338. https://doi.org/10.1007/978-1-4939-7811-3_21.
- (4) Foley, A. R.; Raskatov, J. A. Assessing Reproducibility in Amyloid β Research: Impact of A β Sources on Experimental Outcomes. *ChemBioChem* **2020**, *21* (17), 2425–2430. <https://doi.org/10.1002/cbic.202000125>.
- (5) Marina, G. B.; Kirkitadze, D.; Lomakin, A.; Vollers, S. S.; Benedek, G. B.; Teplow, D. B. Amyloid β -Protein (A β) Assembly: A β 40 and A β 42 Oligomerize through Distinct Pathways. *Proc. Natl. Acad. Sci. U. S. A.* **2003**, *100* (1), 330–335. <https://doi.org/10.1073/pnas.222681699>.
- (6) Williams, T. L.; Serpell, L. C.; Urbanc, B. Stabilization of Native Amyloid β -Protein Oligomers by Copper and Hydrogen Peroxide Induced Cross-Linking of Unmodified Proteins (CHICUP). *Biochim. Biophys. Acta - Proteins Proteomics* **2016**, *1864* (3), 249–259. <https://doi.org/10.1016/j.bbapap.2015.12.001>.
- (7) Kuhn, A. J.; Abrams, B. S.; Knowlton, S.; Raskatov, J. A. The Alzheimer’s Disease “Non-Amyloidogenic” P3 Peptide Revisited: A Case for Amyloid- α . *ACS Chem. Neurosci.* **2020**. <https://doi.org/10.1021/acchemneuro.0c00160>.
- (8) Cline, E. N.; Das, A.; Bicca, M. A.; Mohammad, S. N.; Schachner, L. F.; Kamel, J. M.; DiNunno, N.; Weng, A.; Paschall, J. D.; Bu, R. Lo; Khan, F. M.; Rollins, M. G.; Ives, A. N.; Shekhawat, G.; Nunes-Tavares, N.; de Mello, F. G.; Compton, P. D.; Kelleher, N. L.; Klein, W. L. A Novel Crosslinking Protocol Stabilizes Amyloid β Oligomers Capable of Inducing Alzheimer’s-Associated Pathologies. *J. Neurochem.* **2019**, *148* (6), 822–836. <https://doi.org/10.1111/jnc.14647>.
- (9) Shi, J. M.; Pei, J.; Liu, E. Q.; Zhang, L. Bis(Sulfosuccinimidyl) Suberate (BS3) Crosslinking Analysis of the Behavior of Amyloid- β Peptide in Solution and in Phospholipid Membranes. *PLoS One* **2017**, *12* (3), 1–13. <https://doi.org/10.1371/journal.pone.0173871>.
- (10) Hoyer, W.; Grönwall, C.; Jonsson, A.; Ståhl, S.; Härd, T. Stabilization of a β -Hairpin in Monomeric Alzheimer’s Amyloid- β Peptide Inhibits Amyloid Formation. *Proc. Natl. Acad. Sci. USA* **2008**, *105* (13), 5099–5104. <https://doi.org/10.1073/pnas.0711731105>.
- (11) Sandberg, A.; Luheshi, L. M.; Söllvander, S.; Pereira de Barros, T.; Macao, B.; Knowles, T. P. J.; Biverstål, H.; Lendel, C.; Ekholm-Petterson, F.; Dubnovitsky, A.; Lannfelt, L.; Dobson, C. M.; Härd, T. Stabilization of Neurotoxic Alzheimer Amyloid- β Oligomers by Protein Engineering. *Proc. Natl. Acad. Sci. U.S.A* **2010**, *107* (35), 15595–15600.

<https://doi.org/10.1073/pnas.1001740107>.

- (12) Lendel, C.; Bjerring, M.; Dubnovitsky, A.; Kelly, R. T.; Filippov, A.; Antzutkin, O. N.; Nielsen, N. C.; Härd, T. A Hexameric Peptide Barrel as Building Block of Amyloid- β Protofibrils. *Angew. Chemie - Int. Ed.* **2014**, *53*, 12756–12760. <https://doi.org/10.1002/anie.201406357>.
- (13) Kreutzer, A. G.; Nowick, J. S. Elucidating the Structures of Amyloid Oligomers with Macrocyclic β -Hairpin Peptides: Insights into Alzheimer's Disease and Other Amyloid Diseases. *Acc. Chem. Res.* **2018**, *51* (3), 706–718. <https://doi.org/10.1021/acs.accounts.7b00554>.
- (14) Yu, L.; Edalji, R.; Harlan, J. E.; Holzman, T. F.; Lopez, A. P.; Labkovsky, B.; Hillen, H.; Barghorn, S.; Ebert, U.; Richardson, P. L.; Miesbauer, L.; Solomon, L.; Bartley, D.; Walter, K.; Johnson, R. W.; Hajduk, P. J.; Olejniczak, E. T. Structural Characterization of a Soluble Amyloid β -Peptide Oligomer. *Biochemistry* **2009**, *48* (9), 1870–1877. <https://doi.org/10.1021/bi802046n>.
- (15) Ciudad, S.; Puig, E.; Botzanowski, T.; Meigooni, M.; Arango, A. S.; Do, J.; Mayzel, M.; Bayoumi, M.; Chaignepain, S.; Maglia, G.; Cianferani, S.; Orekhov, V.; Tajkhorshid, E.; Bardiaux, B.; Carulla, N. A β (1-42) Tetramer and Octamer Structures Reveal Edge Conductivity Pores as a Mechanism for Membrane Damage. *Nat. Commun.* **2020**, *11* (1), 1–14. <https://doi.org/10.1038/s41467-020-16566-1>.
- (16) Leitner, A.; Joachimiak, L. A.; Unverdorben, P.; Walzthoeni, T.; Frydman, J.; Förster, F.; Aebersold, R. Chemical Cross-Linking/Mass Spectrometry Targeting Acidic Residues in Proteins and Protein Complexes. *Proc. Natl. Acad. Sci. U. S. A.* **2014**, *111* (26), 9455–9460. <https://doi.org/10.1073/pnas.1320298111>.
- (17) Kreutzer, A. G.; Nowick, J. S. Elucidating the Structures of Amyloid Oligomers with Macrocyclic β -Hairpin Peptides: Insights into Alzheimer's Disease and Other Amyloid Diseases. *Acc. Chem. Res.* **2018**, *51*, 706–718. <https://doi.org/10.1021/acs.accounts.7b00554>.
- (18) Samdin, T. D.; Kreutzer, A. G.; Nowick, J. S. Exploring Amyloid Oligomers with Peptide Model Systems. *Curr. Opin. Chem. Biol.* **2021**, *64*, 106–115. <https://doi.org/10.1016/j.cbpa.2021.05.004>.
- (19) Spencer, R. K.; Li, H.; Nowick, J. S. X-Ray Crystallographic Structures of Trimers and Higher-Order Oligomeric Assemblies of a Peptide Derived from A β ₁₇₋₃₆. *J. Am. Chem. Soc.* **2014**, *136* (15), 5595–5598. <https://doi.org/10.1021/ja5017409>.
- (20) Kreutzer, A. G.; Hamza, I. L.; Spencer, R. K.; Nowick, J. S. X-Ray Crystallographic Structures of a Trimer, Dodecamer, and Annular Pore Formed by an A β ₁₇₋₃₆ β -Hairpin. *J. Am. Chem. Soc.* **2016**, *138* (13), 4634–4642. <https://doi.org/10.1021/jacs.6b01332>.
- (21) Kreutzer, A. G.; Yoo, S.; Spencer, R. K.; Nowick, J. S. Stabilization, Assembly, and Toxicity of Trimers Derived from A β . *J. Am. Chem. Soc.* **2017**, *139* (2), 966–975. <https://doi.org/10.1021/jacs.6b11748>.
- (22) Kreutzer, A. G.; Spencer, R. K.; McKnelly, K. J.; Yoo, S.; Hamza, I. L.; Salveson, P. J.; Nowick, J. S. A Hexamer of a Peptide Derived from A β ₁₆₋₃₆. *Biochemistry* **2017**, *56* (45), 6061–6071. <https://doi.org/10.1021/acs.biochem.7b00831>.

- (23) Salveson, P. J.; Spencer, R. K.; Kreutzer, A. G.; Nowick, J. S. X-Ray Crystallographic Structure of a Compact Dodecamer from a Peptide Derived from A β _{16–36}. *Org. Lett.* **2017**, *19*, 3465. <https://doi.org/10.1021/acs.orglett.7b01445>.
- (24) Samdin, T. D.; Wierzbicki, M.; Kreutzer, A. G.; Howitz, W. J.; Valenzuela, M.; Smith, A.; Sahrai, V.; Truex, N. L.; Klun, M.; Nowick, J. S. Effects of N-Terminal Residues on the Assembly of Constrained β -Hairpin Peptides Derived from A β . *J. Am. Chem. Soc.* **2020**, *142* (26), 11593–11601. <https://doi.org/10.1021/jacs.0c05186>.
- (25) Haerianardakani, S.; Kreutzer, A. G.; Salveson, P. J.; Samdin, T. D.; Guaglianone, G. E.; Nowick, J. S. Phenylalanine Mutation to Cyclohexylalanine Facilitates Triangular Trimer Formation by β -Hairpins Derived from A β . *J. Am. Chem. Soc.* **2020**, *142*, 20708–20716. <https://doi.org/10.1021/jacs.0c09281>.
- (26) Kreutzer, A. G.; Samdin, T. D.; Guaglianone, G.; Spencer, R. K.; Nowick, J. S. X-Ray Crystallography Reveals Parallel and Antiparallel β -Sheet Dimers of a β -Hairpin Derived from A β _{16–36} That Assemble to Form Different Tetramers X-Ray Crystallography Reveals Parallel and Antiparallel β -Sheet Dimers of a β -Hairpin Derived from A β _{16–36}. **2020**. <https://doi.org/10.1021/acchemneuro.0c00290>.

Supporting information for:

Application of an α -Methyl Amino Acid in Crystallographic Studies of a β -Hairpin Derived from A β

Table of Contents

Supporting Figures and Tables	186
Table S4.1	186
Materials and Methods	187
General information	187
Synthesis of peptides 1–3	188
SDS-PAGE and silver staining	191
Crystallization of peptide 3	192
X-ray crystallographic data collection, data processing, and structure determination of peptide 2a	193
Characterization Data	195
Characterization of peptide 1	195
Characterization of peptide 2	197
Characterization of peptide 3	199

Supporting Figures and Tables

Supplementary Table 4.1. Crystallographic properties, crystallization conditions, data collection, and model refinement statistics for peptide **3**.

peptide	3
Wavelength	0.7293
Resolution range	24.09 -1.001 (1.037 -1.001)
Space group	F 2 3
Unit cell	83.447, 83.447, 83.447 90, 90, 90
Total reflections	1018181 (99256)
Unique reflections	25968 (2555)
Multiplicity	39.2 (38.8)
Completeness (%)	99.72 (97.86)
Mean I/sigma(I)	25.97 (0.75)
Wilson B-factor	13.38
R-merge	0.06135 (6.279)
R-meas	0.0622 (6.361)
R-pim	0.01009 (1.014)
CC1/2	1 (0.297)
CC*	1 (0.677)
Reflections used in refinement	25917 (2519)
Reflections used for R-free	1308 (139)
R-work	0.2034 (0.3619)
R-free	0.2240 (0.3662)
CC(work)	0.951 (0.580)
CC(free)	0.908 (0.496)
RMS(bonds)	0.015
RMS(angles)	1.81
Ramachandran favored (%)	100.00
Ramachandran allowed (%)	0.00
Ramachandran outliers (%)	0.00
Rotamer outliers (%)	0.00
Clashscore	0.00
Average B-factor	16.35
macromolecules	15.47
ligands	17.22
solvent	22.45
Number of TLS groups	20
crystallization conditions	0.1 M HEPES buffer (pH 6.5), 24% (v/v) Jeffamine M-600

Materials and Methods¹

General information

All chemicals were used as received unless otherwise noted. Methylene chloride (CH₂Cl₂) was passed through alumina under nitrogen prior to use. Anhydrous, amine-free *N,N*-dimethylformamide (DMF) was purchased from Alfa Aesar. Deionized water (18 MΩ) was obtained from a Barnstead NANOpure Diamond water purification system. Analytical reverse-phase HPLC was performed on an Agilent 1260 Infinity II instrument equipped with a Phenomenex Aeris PEPTIDE 2.6u XB-C18 column. Preparative reverse-phase HPLC was performed on a Ranin instrument equipped with an Agilent Zorbax SB-C18 column. HPLC grade acetonitrile and deionized water, each containing 0.1% trifluoroacetic acid (TFA), were used for analytical and preparative reverse-phase HPLC. All peptides were prepared and used as the trifluoroacetate salts and were assumed to have one trifluoroacetic acid molecule per amine group on each peptide.

Synthesis of peptides 1–3

a. Loading the resin. 2-Chlorotriptyl chloride resin (300 mg, 1.4 mmol/g) was added to a Bio-RAD Poly-Prep chromatography column (10 mL). Dry CH₂Cl₂ (8 mL) was used to suspend and swell the resin for 30 min with gentle rocking. The solution was drained from the resin and a solution of Boc-Orn-Fmoc-OH (0.78 equiv, 150 mg, 0.33 mmol) in 6% (v/v) 2,4,6-collidine in dry CH₂Cl₂ (8 mL) was added immediately and the suspension was gently rocked for 12 h. The solution was then drained and a mixture of CH₂Cl₂/MeOH/*N,N*-diisopropylethylamine (DIPEA) (17:2:1, 10 mL) was added immediately. The resin was gently rocked for 1 h, to cap the unreacted 2-chlorotriptyl chloride resin sites. The resin was then washed twice with dry CH₂Cl₂ and dried by passing nitrogen through the vessel. This procedure typically yields 0.18 mmol of loaded resin (0.6 mmol/g loading).

b. Manual peptide coupling. The resin loaded with Boc-Orn(Fmoc) was suspended in dry DMF and then transferred to a solid-phase peptide synthesis vessel. Residues 22 through 17 were manually coupled using Fmoc-protected amino acid building blocks. Each manual coupling cycle consisted of *i.* Fmoc-deprotection with of 20% (v/v) piperidine in DMF for 5 min at ambient temperature (5 mL), *ii.* washing with dry DMF (2x, 5 mL), *iii.* coupling of the amino acid (0.44 mmol, 4 equiv) with HCTU (174.0 mg, 0.44 mmol, 4 equiv) in 20% (v/v) 2,4,6-collidine in dry DMF (5 mL) for 30 min, and *iv.* washing the with dry DMF (2x, 5 mL). Residue 19, which follows N-Me-Phe₂₀ in peptide **1**, and residue 18, which follows α-Me-Phe₁₉ in peptide **3**, were double coupled (4 equiv per coupling) using HATU (6 equiv) and HOAt (6 equiv) for 1 hr per coupling to ensure complete reaction. (We have found that coupling after *N*- and α-methyl amino acids is difficult and requires rigorous coupling to minimize incomplete reaction.²)

c. Microwave-assisted coupling of residues 36 through 30. A CEM Liberty Blue Automated Microwave Peptide Synthesizer was used to couple residues 36 to 30. Fmoc-Orn(Dde)-OH

connects residues 17 and 36 in the natural sequence. Each coupling cycle consisted of *i.* Fmoc-deprotection with 20% (v/v) piperidine with 0.1 M Oxyma Pure in DMF for 2 min. at 50 °C, *ii.* washing with DMF (3x), *iii.* coupling of the amino acid (0.75 mmol, 5 equiv) in the presence of HCTU (0.675 mmol, 4.5 equiv) and 20% (v/v) *N*-methylmorpholine (NMM) in DMF for 10 min. at 50 °C, *iv.* washing with DMF (3x).

d. Cleavage of the peptide from resin. The resin was then transferred to a 10-mL Bio-Rad Poly-Prep chromatography column, and washed 3x with dry CH₂Cl₂. The acyclic peptide was cleaved from the resin by rocking the resin for 1 h with a solution of 1,1,1,3,3,3-hexafluoroisopropanol (HFIP) in CH₂Cl₂ (1:4, 8 mL). The suspension was filtered and the filtrate was collected in a 250-mL round-bottomed flask. The resin was washed with additional HFIP in CH₂Cl₂ (1:4, 8 mL). The combined filtrates were concentrated by rotary evaporation to give a white solid. The white solid was further dried by vacuum pump to afford the crude protected linear peptide, which was cyclized without further purification.

e. Cyclization of the acyclic peptide. The crude protected linear peptide was dissolved in dry DMF (150 mL). PyBOP (370 mg, 0.711 mmol, 6 equiv) and *N*-methylmorpholine (NMM) (0.33 mL, 1.8 mmol, 12 equiv) was added to the solution and the mixture was stirred under nitrogen for 48 h. The mixture was concentrated under reduced pressure to afford the crude protected cyclic peptide, a yellow film.

f. Global deprotection of the cyclic peptide. The protected cyclic peptide was dissolved in TFA/triisopropylsilane (TIPS)/H₂O (18:1:1, 10 mL) in a 250-mL round-bottomed flask equipped with a nitrogen-inlet adaptor. The solution was stirred for 1 h under nitrogen. The reaction mixture was then concentrated by rotary evaporation under reduced pressure to afford the crude cyclic peptide. During the 1 h deprotection, two 50-mL conical tubes containing 40-mL of dry ether were chilled on dry ice. The solution was drained and split between the two conical tubes of ether. The

tubes were then centrifuged at 800 x g for 25 mins. The ether supernatant was poured off and the pelleted peptide was dried overnight under vacuum.

g. Reverse-phase HPLC purification. The peptide: DMSO mixture was dissolved in H₂O and acetonitrile (8:2, 5 mL), and the solution was filtered through a 0.2 µm syringe filter and purified by RP-HPLC. The solution of crude peptide was injected at 20% acetonitrile and eluted with a gradient of 20-60% CH₃CN over 90 min. Each peptide eluted between 29-36% CH₃CN. The collected fractions were analyzed by analytical HPLC and MALDI-TOF, and the pure fractions were concentrated by rotary evaporation and lyophilized. Typical syntheses yielded between 48 and 52 mgs of the peptide as the TFA salt.

SDS-PAGE, and silver staining

SDS-PAGE was performed on peptides **1–3** using the reagents, recipes, and procedures for Tricine SDS-PAGE detailed in Schägger, H. *Nat. Protoc.* **2006**, *1*, 16–22. Each peptide was run on a 16% polyacrylamide gel with a 4% stacking polyacrylamide gel at 60 volts. A Spectra™ Multicolor Low Range Protein Ladder (ThermoFischer Scientific, catalog #: 26628) was loaded into the first lane of the gel. The remaining lanes were loaded with 8.0 µL aliquots of each peptide as 50 µM solutions in SDS-PAGE loading buffer, which were prepared as follows: A 10 mg/mL stock solution of each peptide was prepared with deionized water. Aliquots of the 10 mg/mL solutions were then diluted further with deionized water and 6X SDS-PAGE loading buffer (G-Biosciences catalog #: 786-701) to create 100 µM working solutions of each peptide.

Staining with silver nitrate was used to visualize peptides **1–3** in the SDS-PAGE gel. Reagents for silver staining were prepared according to procedures detailed in Simpson, R. J. *Cold Spring Harbor Protocol* **2007**. [We have found it important to prepare sodium thiosulfate, silver nitrate, and developing solutions fresh each time and to use high purity sodium carbonate to prepare the developing solution.] The gel was removed from the casting glass and rocked for 20 min in fixing solution (50% (v/v) methanol and 5% (v/v) acetic acid in deionized water). The fixing solution was then discarded and replaced with 50% (v/v) aqueous methanol for another 10 min of rocking. Next, the 50% methanol was discarded and replaced with deionized water for another 10 min of rocking. Next, the water was discarded and the gel was rocked in 0.02% (w/v) sodium thiosulfate in deionized water for 1 min. The sodium thiosulfate was discarded and the gel was rinsed twice with deionized water for 0.5 min. The gel was then submerged in pre-chilled 0.1% (w/v) silver nitrate in deionized water and rocked at 4 °C for 20 min. The silver nitrate solution was discarded and the gel was rinsed twice with deionized water. The gel was incubated in developing solution (2% (w/v) sodium carbonate, 0.04% (w/v) formaldehyde) until the solution began to brown. The developing solution was then immediately discarded and fresh silver nitrate

solution was added to the gel until the desired intensity of staining was reached. When the desired intensity of staining was reached, the developing solution was discarded and the gel was submerged in 5% aqueous acetic acid.

Crystallization of peptide 3

The hanging-drop vapor-diffusion method was used to determine initial crystallization conditions for peptide **3**. Peptide **3** was screened in 96-well plate format using three crystallization kits (Crystal Screen, Index, and PEG/ION) from Hampton Research. A TTP LabTech Mosquito nanodisperse was used to make three 150 nL hanging drops for each well condition. The three hanging drops differed in the ratio of peptide to well solution for each condition in the 96-well plate. A 10 mg/mL solution of each peptide in deionized water was combined with a well solution in ratios of 1:1, 1:2, and 2:1 peptide:well solution at appropriate volumes to create the three 150 nL hanging drops. Crystals of peptide **3** grew in well conditions of 0.1 M HEPES buffer (pH 6.5), and 24% (v/v) Jeffamine M-600.

Crystallization conditions for each peptide were optimized using a 4x6 matrix Hampton 24-well plate. For peptide **3** the 0.1 M HEPES buffer was varied in each row in increments of 0.5 pH units (6.0, 6.5, 7.0, and 7.5) and the percentage of Jeffamine M-600 was varied in each column in increments of 2% (v/v) (26%, 28%, 30%, 32%, 34%, 36%). Three hanging-drops were prepared on borosilicate glass slides by combining a 10 mg/mL solution of peptide **3** in deionized water with the well solution in the following amounts: 1 μ L:1 μ L, 2 μ L:1 μ L, and 1 μ L:2 μ L. Slides were inverted and pressed firmly against the silicone grease surrounding each well. Crystals were harvested with a nylon loop attached to a copper or steel pin, soaked briefly in MPD, and flash frozen in liquid nitrogen prior to data collection. The optimized crystallization conditions for peptide **3** is summarized Supplementary Table 4.1.

X-ray crystallographic data collection, data processing, and structure determination of peptide 3

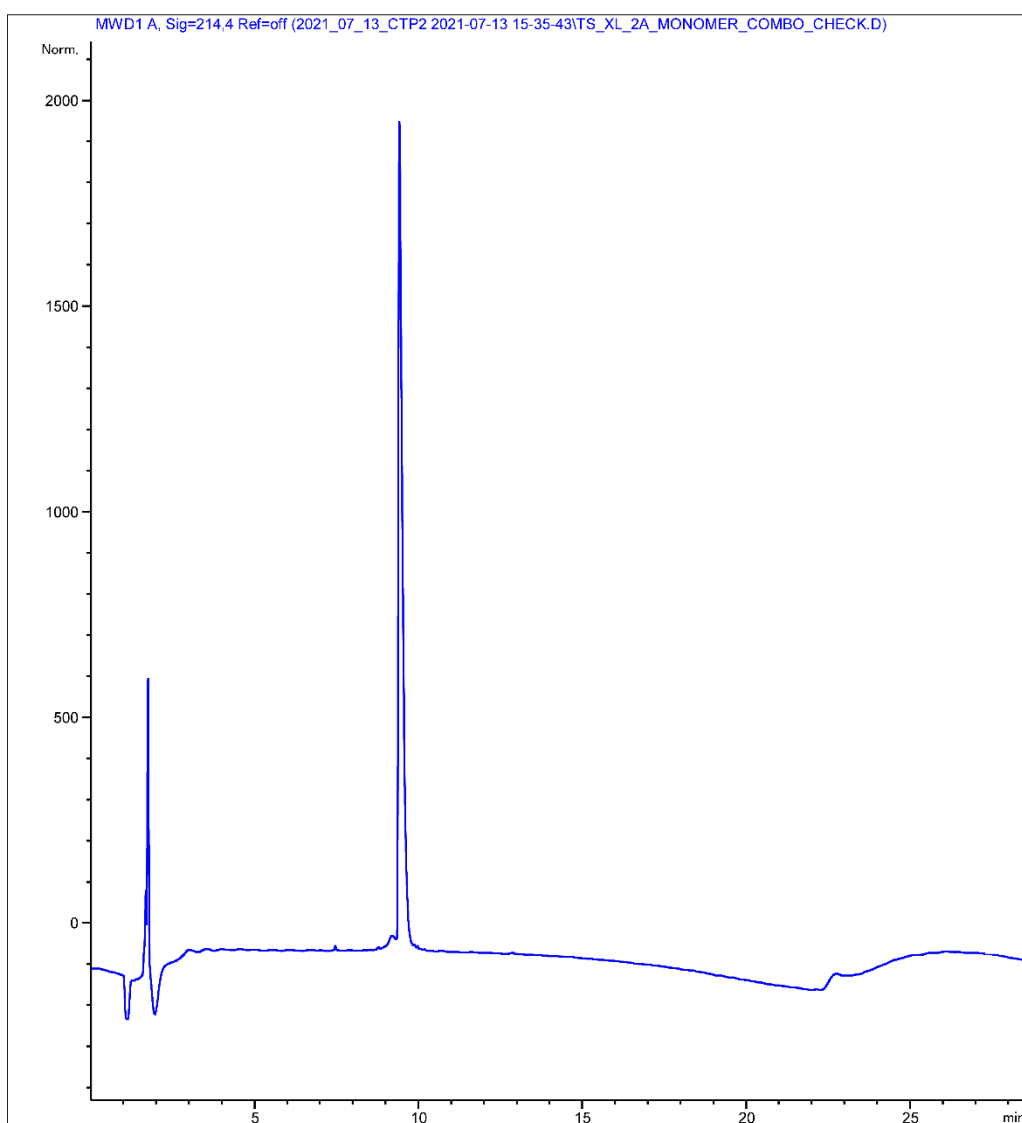
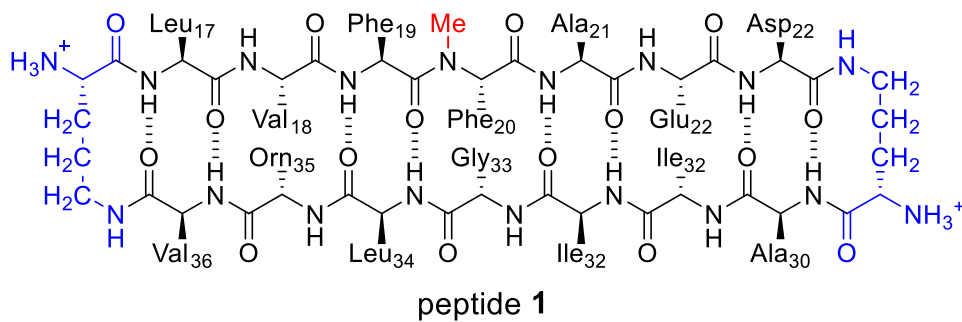
Diffraction data for **3** were collected at the Stanford Synchrotron Radiation Light source, beamline 12.2, at 1.00 Å wavelength. Datasets were indexed and integrated with XDS. Scaling and merging was done with pointless and aimless in CCP4. The structures were solved with molecular replacement in Phaser using a trimer formed by macrocyclic β-hairpin peptide derived from Aβ₁₇₋₃₆ (PDB 5SUR) as the search model. The refinement was done with phenix.refine module of the Phenix suite, with manipulation of the model performed using Coot.

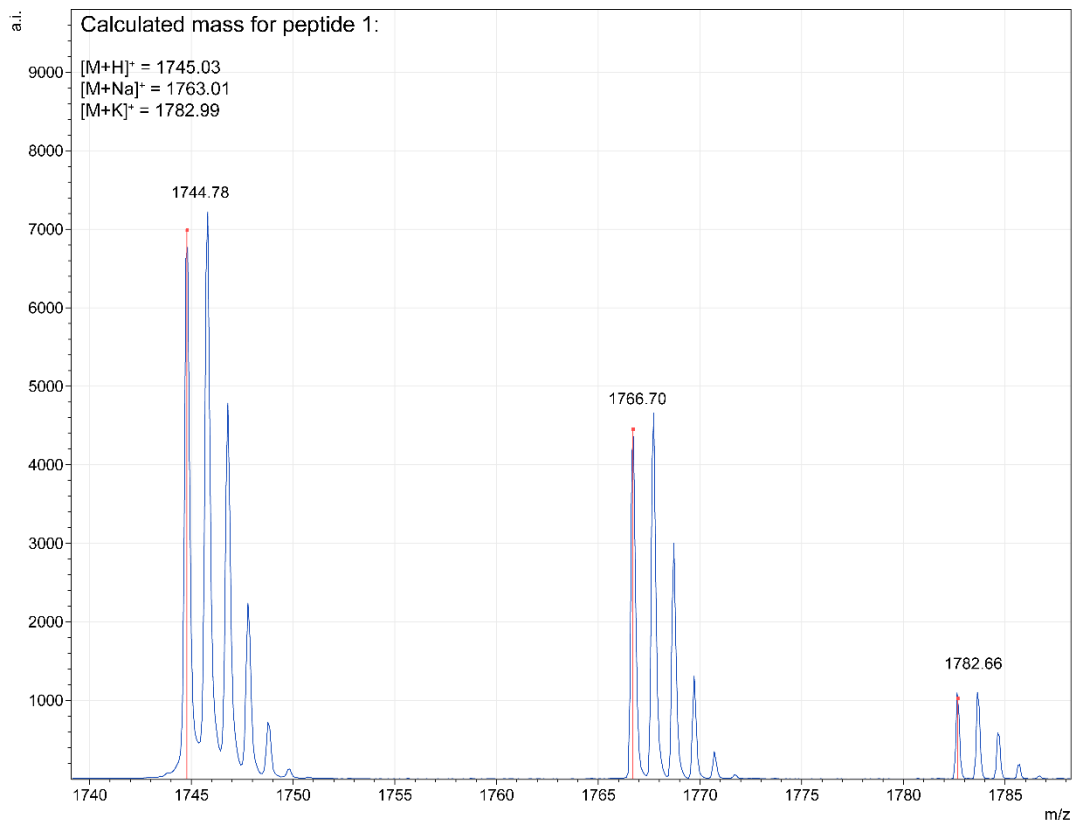
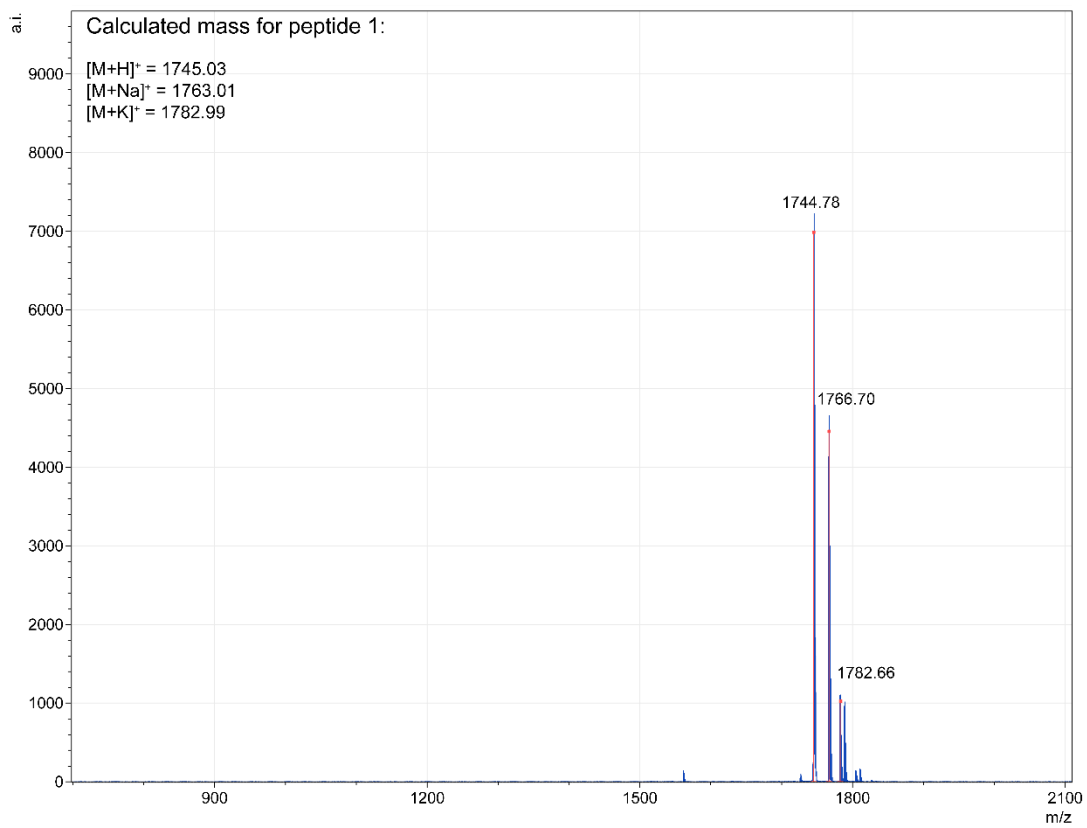
References

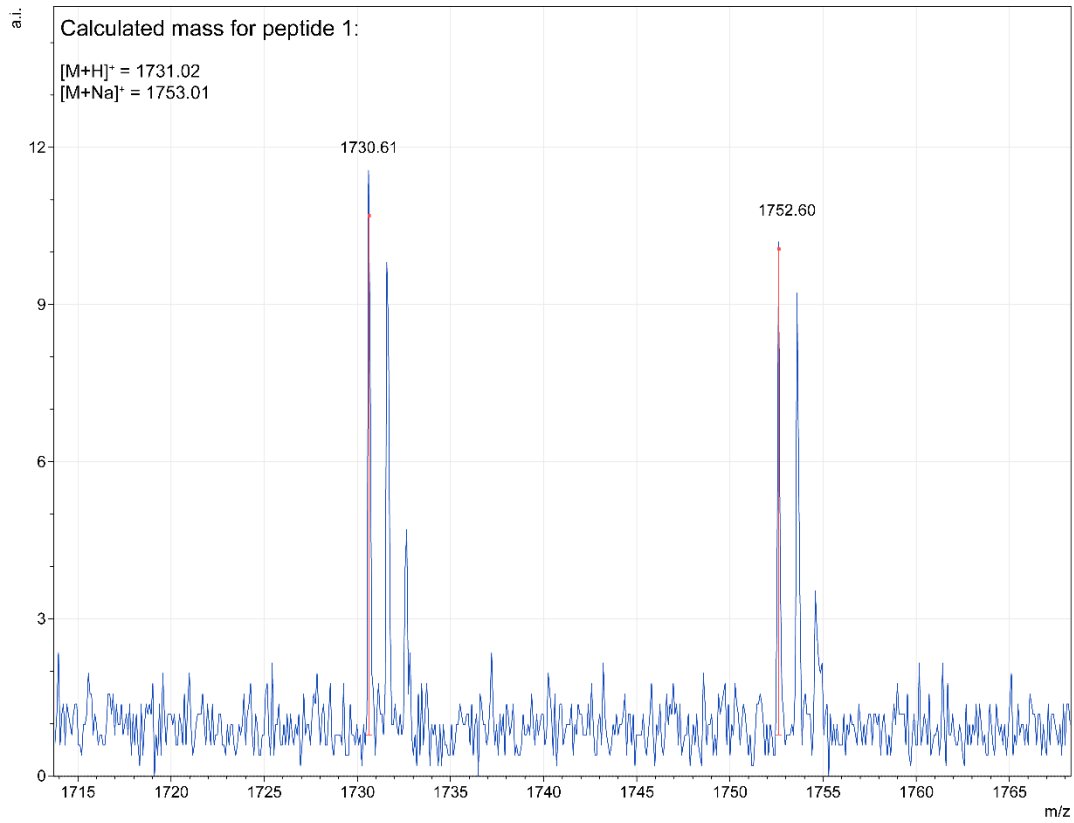
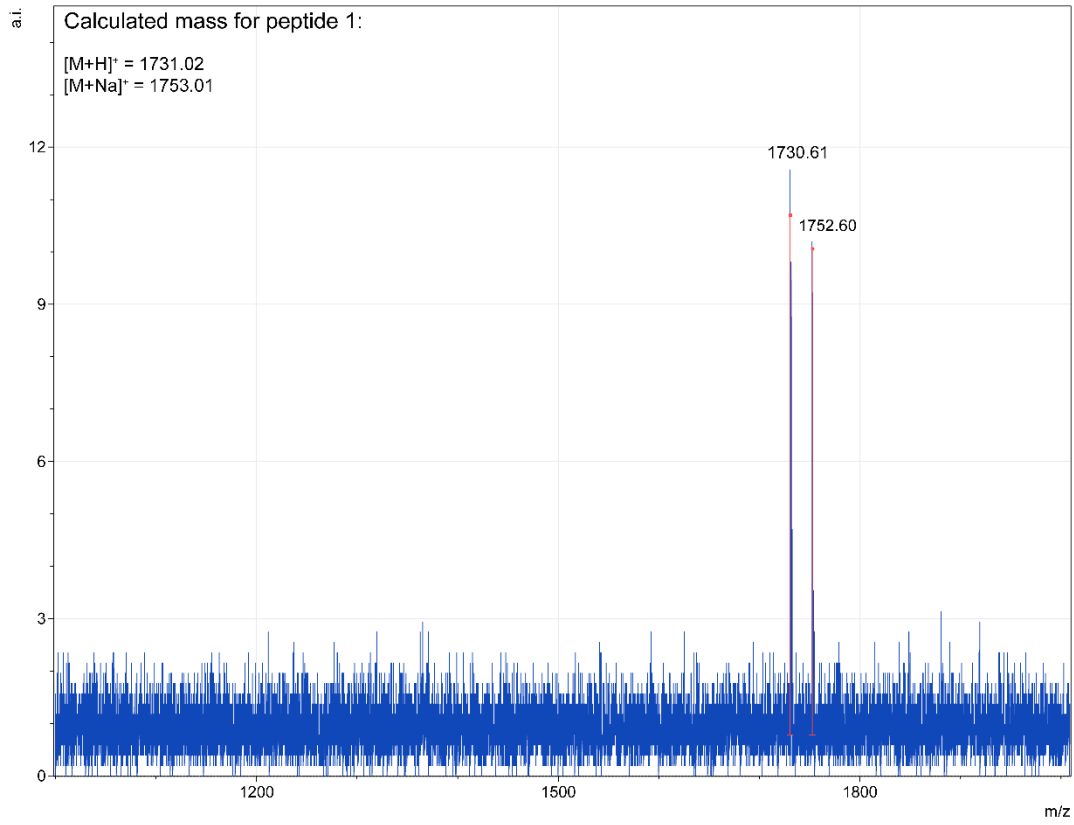
1. These procedures follow closely those that our laboratory has previously published. The procedures in this section are adapted from and in some cases taken verbatim from Kreutzer, A. G.; Hamza, I. L.; Spencer, R. K.; Nowick J. S. *J. Am. Chem. Soc.* **2016**, *138*, 4634–4642, Spencer, R. K.; Kreutzer, A. G.; Salveson, P. J.; Li, H.; Nowick, J. S. *J. Am. Chem. Soc.* **2015**, *137*, 6304–6311, Spencer, R. K.; Li. H.; Nowick, J. S. *J. Am. Chem. Soc.* **2014**, *136*, 5595– 5598, and Kreutzer, A. G.; Yoo, S.; Spencer, R. K.; Nowick, J. S. *J. Am. Chem, Soc.* **2017**, *139*, 966–975, Samdin, T. D.; Wierzbicki, M.; Kreutzer, A. G.; Howitz, W. J.; Valenzuela, M.; Smith, A.; Sahrai, V.; Truex, N. L.; Klun, M.; Nowick, J. S. *J. Am. Chem. Soc.* **2020**, *142*, 11593–11601.

Characterization Data

Characterization of peptide 1







Characterization of peptide 3

